

DIFFERENTIAL CORRECTION AND PRELIMINARY ORBIT
DETERMINATION FOR LUNAR SATELLITE ORBITS

By D.H. Lewis, P.A. Lavoie, and D.S. Ingram

1 December 1965

FACILITY FORM 602

N 66-17 278

(ACCESSION NUMBER)	(THRU)
<u>212</u>	<u>1</u>
(PAGES)	(CODE)
<u>CR-66-135</u>	<u>30</u>
(NASA CR OR TRX OR AD NUMBER)	(CATEGORY)

GPO PRICE \$ _____

CFSTI PRICE(S) \$ _____

Hard copy (HC) 6.00

Microfiche (MF) 1.25

ff 653 July 65

Prepared under Task Order NAS1-4605-2 by

TRW SYSTEMS

ONE SPACE PARK • REDONDO BEACH • CALIFORNIA

for

NATIONAL AERONAUTICS AND SPACE ADMINISTRATION

DIFFERENTIAL CORRECTION AND PRELIMINARY ORBIT
DETERMINATION FOR LUNAR SATELLITE ORBITS

By D.H. Lewis, P.A. Lavoie, and D.S. Ingram

1 December 1965

N66 17278

Distribution of this report is provided in the interest of information exchange. Responsibility for the contents resides in the author or organization that prepared it.

Prepared under Task Order NAS1-4605-2 by

TRW SYSTEMS

ONE SPACE PARK • REDONDO BEACH • CALIFORNIA

for

NATIONAL AERONAUTICS AND SPACE ADMINISTRATION

ABSTRACT

17273

This report describes an investigation into two major areas of orbit determination for lunar satellites.

(1) The convergence properties of the differential correction process are studied. The reasons for convergence difficulties are discussed and a number of possible aids to convergence are analyzed and compared using numerical examples.

(2) Two preliminary orbit determination techniques, that is, techniques which require no prior knowledge of the satellite's state, are analyzed with respect to their ability to determine the satellite's orbit. The effect of data quality, data biases and number of observing stations on the results are discussed and numerical examples are given.

Author

~~R. H. Tolson~~

RHTolson.mbb
Typed 2/2/66

CONTENTS

	<u>Page</u>
1. SUMMARY	11
2. INTRODUCTION	3
3. DIFFERENTIAL CORRECTION OF LUNAR SATELLITE ORBITS.	5
3.1 Convergence Problems in the Differential Correction of Lunar Satellite Orbits	8
3.2 Orbit Selection and Data Simulation	20
3.3 Control of Factors Affecting Convergence.	26
3.4 Convergence of Alternate Lunar Satellite Orbits	66
3.5 Numerical and Statistical Aspects of the Convergence Problem	75
3.6 LRC/TRW Test Case	94
3.7 Relationships Between Differential Correction and Preliminary Orbit Determination	98
4. PRELIMINARY ORBIT DETERMINATION FOR LUNAR SATELLITES	101
4.1 Use of Least Squares Operators in Preliminary Orbit Determination	102
4.2 Numerical Considerations	105
4.3 Orbit Selection and Generation of Data	107
4.4 Position Fix Technique	108
4.5 Range, Range-Rate Technique	145
4.6 Influence of Perturbations Introduced by the Earth and the Moon's Asphericity	153
5. NEW TECHNOLOGY.	158

APPENDIXES

A State Vectors and Classical Elements Defining the Nominal Orbits and Data Sets.	159
B Compendium of Cases Run in Convergence Study	167
C AT-85 Program Description	171
D AT-14 Program Description	177
E Derivation of Closed Form f and g Coefficients	179
F Range, Right Ascension, Declination Orbit Determination Technique.	183
G Range and Range-Rate Orbit Determination Technique.	189
REFERENCES	195
BIBLIOGRAPHY.	197

ILLUSTRATIONS

<u>Figure</u>		<u>Page</u>
1	Lunar Satellite Orbit Geometry	14
2	Doppler Curves of Computed and Observed Orbits	15
3	Computed Range-Rate Residuals	16
4	Periodic Range of Computed and Observed Orbits	18
5	Computed Range Residuals	19
6	Visibility Intervals of Nominal Orbit; DSN Stations	27
7	Effect of Energy Corrected Initial Estimate for Short Arc Fits	31
8	Effect of Energy Corrected Initial Estimate for Long Arc Fits	32
9	Effect of Energy Corrected Initial Estimate for 6σ Observed Orbit	34
10	Effect of Step Fit with 300 Minutes of Data	35
11	Effect of Step Fit with 1000 Minutes of Data	36
12	Approximating Quadric Surface and Bounding Ellipse	40
13	Effect of Bounded Solution on Short Arc Fit.	43
14	Effect of Bounded Solution on Long Arc Fit.	44
15	Effect of Bounded Solution on 6σ Observed Orbit	45
16	Effect of Normal Conditioning Matrix	53
17	Effect of Tracking Span on Position Uncertainties (Two Sensors)	56
18	Effect of Tracking Span on Velocity Uncertainties (Two Sensors)	57
19	Effect of Data Types on Convergence Rate	59
20	Position and Velocity Uncertainties	60
21	Position Uncertainties Using One and Two Sensors for Short Arc Fits	62
22	Velocity Uncertainties Using One and Two Sensors for Short Arc Fits	63
23	Comparison of Velocity Uncertainties for Short Arc Fits	65
24	Convergence Characteristics of B1 Alternate Orbit	67
25	Convergence Characteristics of B2 Alternate Orbit	68
26	Convergence Characteristics of B3 Alternate Orbit	69
27	Convergence Characteristics of B4 Alternate Orbit	70

ILLUSTRATIONS — Continued

<u>Figure</u>		<u>Page</u>
28	Convergence Characteristics of B5 Alternate Orbit	71
29	Convergence Characteristics of B6 Alternate Orbit	72
30	Convergence Characteristics of B7 Alternate Orbit	73
31	Convergence With an Ill-Conditioned Normal Matrix	76
32	TRW/LRC Test Case II Convergence Characteristics of Various Techniques	97
33	Convergence Characteristics of 6σ Energy Perturbed Orbit.	99
34	Convergence Characteristics of 6σ Orientation Perturbed Orbit.	100
35	Semi-Major Axis Estimate Quality Versus Observation Span for Various Angular Data Standard Deviations ($e=0.29$)	114
36	Eccentricity Estimate Quality Versus Observation Span for Various Angular Data Standard Deviations ($e=0.29$) . .	115
37	Inclination Estimate Quality Versus Observation Span for Various Angular Data Standard Deviations ($e=0.29$). . . .	116
38	Nodal Longitude Estimate Quality Versus Observation Span for Various Angular Data Standard Deviations ($e=0.29$) . .	117
39	Argument of Perigee Estimate Quality Versus Observation Span for Various Angular Data Standard Deviations ($e=0.29$).	118
40	Epoch Mean Anomaly Estimate Quality Versus Observation Span for Various Data Standard Deviations ($e=0.29$)	119
41	Semi-Major Axis Estimate Quality Versus Observation Span for Various Angular Data Standard Deviations ($e=0.63$)	120
42	Eccentricity Estimate Quality Versus Observation Span for Various Angular Data Standard Deviations ($e=0.63$) . .	121
43	Inclination Estimate Quality Versus Observation Span for Various Angular Data Standard Deviations ($e=0.63$)	122
44	Nodal Longitude Estimate Quality Versus Observation Span for Various Angular Data Standard Deviations ($e=0.63$) . .	123
45	Argument of Perigee Estimate Quality Versus Observation Span for Various Angular Data Standard Deviations ($e=0.63$)	124
46	Epoch Mean Anomaly Estimate Quality Versus Observation Span for Various Angular Data Standard Deviations ($e=0.63$)	125
47	Semi-Major Axis Estimate Quality Versus Observation Span for Various Angular Data Biases ($e=0.29$)	127
48	Eccentricity Estimate Quality Versus Observation Span for Various Data Biases ($e=0.29$).	128

ILLUSTRATIONS—Concluded

<u>Figure</u>		<u>Page</u>
49	Inclination Estimate Quality Versus Observation Span for Various Angular Data Biases ($e=0.29$)	129
50	Nodal Longitude Estimate Quality Versus Observation Span for Various Angular Data Biases ($e=0.29$)	130
51	Argument of Perigee Estimate Quality Versus Observation Span for Various Angular Data Biases ($e=0.29$)	131
52	Epoch Mean Anomaly Estimate Quality Versus Observation Span for Various Angular Data Biases ($e=0.29$)	132
53	Semi-Major Axis Estimate Quality Versus Observation Span for Various Angular Data Biases ($e=0.63$)	133
54	Eccentricity Estimate Quality Versus Observation Span for Various Angular Data Biases ($e=0.63$)	134
55	Inclination Estimate Quality Versus Observation Span for Various Angular Data Biases ($e=0.63$)	135
56	Nodal Longitude Estimate Quality Versus Observation Span for Various Angular Data Biases ($e=0.63$)	136
57	Argument of Perigee Estimate Quality Versus Observation Span for Various Angular Data Biases ($e=0.63$)	137
58	Epoch Mean Anomaly Estimate Versus Observation Span for Various Angular Data Biases ($e=0.63$)	138
59	Semi-Major Axis Estimate Quality Versus Observation Span for Various Angular Data Biases ($\sigma = 0.005$)	139
60	Eccentricity Estimate Quality Versus Observation Span for Various Angular Data Biases ($\sigma = 0.005$)	140
61	Inclination Estimate Quality Versus Observation Span for Various Angular Data Biases ($\sigma = 0.005$)	141
62	Nodal Longitude Estimate Quality Versus Observation Span for Various Angular Data Biases ($\sigma = 0.005$)	142
63	Argument of Perigee Estimate Quality Versus Observation Span for Various Angular Data Biases ($\sigma = 0.005$)	143
64	Epoch Mean Anomaly Estimate Quality Versus Observation Span for Various Angular Data Biases ($\sigma = 0.005$)	144
65	Inclination Estimate Quality Versus Iteration Number—Range, Range-Rate Program	154
66	Nodal Longitude Estimate Quality Versus Iteration Number—Range, Range-Rate Program	155
67	Argument of Perigee Estimate Quality Versus Iteration Number—Range, Range-Rate Program	156
F1	Block Diagram for Range, Right Ascension, Declination Program	184
G1	Block Diagram for Range and Range-Rate Program	190

TABLES

		<u>Page</u>
I	Classical Elements of Alternate Satellite Orbits	21
II	Tracking Normal Matrix, 3 Minutes Tracking, Two Sensors	50
III	A Priori Normal Matrix	50
IV	The Effect of Angular Data on State Vector Uncertainties. .	61
V	Classical Elements of Alternate Lunar Satellite Orbits. . .	66
VI	Iteration Summary, LRC Test Case I.	95
VII	Iteration Summary, TRW Test Case I	95
VIII	Iteration History for the ρ, α, δ Program With a Poor Initial Estimate.	112
IX	Effect of the Number of Observing Sensors on the Quality of Orbital Element Estimates	146
X	Effect of Data Quantity on the Estimate of Orbital Energy— ρ, α, δ Program	146
XI	Iteration History for the $\rho\dot{\rho}$ Program Assuming Only a Precomputed Semi-Major Axis	151
XII	Effect of Observing Interval on the Quality of the Orientation Element Estimates— $\rho\dot{\rho}$ Program	152
XIII	Effect of Two Body Gravitational Model on the Quality of Element Estimation	158

SYMBOLS

\bar{A}	auxiliary vector, $f\bar{R} + f\dot{\bar{R}}$
A	matrix of derivatives of observations with respect to the state vector
a	semi-major axis, kilometers
a_{ij}	i, j element of the matrix A
\bar{B}	auxiliary vector, $g\bar{R} + g\dot{\bar{R}}$
B	vector of bounds input to control size of differential corrections
C	matrix of observational data weights, $C^T C = W$
E	expectation operator, or eccentric anomaly, degrees
e	eccentricity
f, g	coefficients relating position to epoch position and velocity
i	inclination, degrees
$J_{n,m}$	coefficient in lunar potential harmonic, degree n and order m
l, m, n	direction cosines
M	matrix of components of \bar{A} and \bar{B}
M_0	mean anomaly at epoch
P	period, minutes
\bar{r}	vehicle position vector
S	conditioning matrix
T	time of perifocal passage, Universal Time
u	eigenvector
V	velocity vector magnitude, kilometers/second
W	observational data weight matrix
x	6 x 1 state vector of position and velocity components
δx	variation in state vector
y	vector of observations

δy	variation in observational vector
α	right ascension, degrees
δ	declination, degrees
ϵ	vector of observational noise components
λ	eigenvalue
ρ	range from observer to vehicle, kilometers
Σ	covariance matrix
σ	standard deviation
ϕ	$\partial A / \partial x$
Ω	longitude of the ascending node, degrees
ω	argument of latitude, degrees

Subscripts:

A	actual
c	computed
E	estimate
M	moon
m	measured
mc	measured minus computed
o	observed
P	a priori; primary attractive body
R	reference
T	tracking

Superscripts:

T	transpose
.	(dot) time derivative
\wedge	estimate

DIFFERENTIAL CORRECTION AND PRELIMINARY ORBIT
DETERMINATION FOR LUNAR SATELLITE ORBITS

By D. H. Lewis, P. A. Lavoie, and D. S. Ingram
TRW Systems

1. SUMMARY

This report describes an investigation into the problem of orbit determination for lunar satellites. Two major areas were studied:

- a) The differential correction convergence characteristics for lunar satellite orbits using a large-scale computer program, where an initial estimate of the orbital parameters is needed to start the process and an elaborate mathematical model, including all significant perturbations, is used to compute the orbital path.
- b) The preliminary orbit determination for lunar satellite orbits, where no initial estimate of the orbital parameters is required and a simplified mathematical model is used to compute the orbital path. The technique of preliminary orbit determination is treated here as a prelude to differential correction; i. e., the best possible preliminary estimate of the orbital parameters is computed before attempting to refine the estimate through differential correction.

Observational data for both parts a) and b) were assumed to be taken by the Deep Space Net (DSN) stations at Goldstone, Madrid, and Woomera, with standard deviations of 20 meters in range, 0.02 meter/second in range-rate, $0^{\circ}.06$ in hour angle and declination, and a bias of 40 meters in range.

The lunar satellite orbit used for most of parts a) and b) was the intermediate elliptic orbit for the nominal Lunar Orbiter mission, as defined by the following selenographic osculating orbital elements:
 $a = 2788$ km, $e = 0.2869$, $i = 15^{\circ}$, $\Omega = 25^{\circ}.47$, $\omega = -12^{\circ}.46$,
 $M_0 = 0^{\circ}$. The convergence properties of alternate lunar satellite orbit orientations were considered, with nominal values for a , e , M_0 , and ω ; values of 0° , 30° , 45° , and 60° for i ; and 10° , 90° , and 130° for Ω .

The purpose of part a) was to establish, through operation of the TRW Orbit Determination Program (AT85), the convergence characteristics and to investigate techniques for aiding convergence. Observational data were simulated and noise was added to reflect the DSN sensor performance. Perturbed values of the orbital elements were then selected as initial conditions for starting the AT85 program. The behavior of the program was then observed as various techniques to aid convergence were applied. Techniques considered include:

- 1) Use of short observational data arcs (less than one revolution) before attempting multiple revolution arcs
- 2) Use of bounds on the size of the incremental corrections applied to the orbital elements on each iteration
- 3) Correction of orbital energy
- 4) Use of additional observing sensors

The most effective technique was found to be the use of short arc data spans with observations from two sensors. With this procedure, the TRW Systems AT85 program was found to operate satisfactorily over a wide range of initial condition errors without the use of bounds (or any other convergence aid).

The preliminary orbit determination study (part b) was conducted with the aim of minimizing the time required to compute the preliminary estimate. Two approaches were considered:

- 1) Development of a program to compute an estimate of the orbital elements based on range and angular data (ρ, α, δ). Such a program is potentially capable of computing an estimate using a very short arc of data.
- 2) Development of a program to augment the existing Langley Research Center (LRC) range-rate-only program ($\dot{\rho}$), capable of computing the orientation elements more quickly than may be possible with range-rate-only. The use of high quality range data (ρ , in addition to $\dot{\rho}$), and a redundant data set contribute to the possibility of a reduced computation time.

The ρ, α, δ program gave two or three figures in the orbital elements after 30 minutes of tracking; after 1 hour, four figures were obtained. The objection to the low quality angular data is overcome by the use of a redundant data set and a least squares fit to the observations. No precomputation

based on the doppler curve was required; the only program inputs are the observations.

The ρ , $\dot{\rho}$ program was found to be capable of determining i , Ω , and ω to four figures using data from one revolution of the satellite, when a , e , and M_0 were assumed to have been precomputed by the LRC $\dot{\rho}$ program.

Study of the interface between parts a) and b) revealed that the quality of the initial conditions required to start the differential correction process is much lower than is commonly believed.

The most significant new technology developed under this contract is the position fix preliminary orbit determination technique.

2. INTRODUCTION

The problem of determining an orbit for a lunar satellite differs from that for an earth satellite principally in the geometry involved (reference 1). Because the relative positions of the satellite and the earth-based sensors are limited, some serious computational constraints are imposed on the orbit determination and the subsequent differential correction. The variation in range measurement is small compared to the magnitude of the range vector which is about 60 earth radii. Because the moon subtends an arc of only 0.5° as seen from the earth, angular measurements are low in quality relative to the size of the angle being measured. For the angular data standard deviations of 0.06° used here, the total variation in the quantity being measured is less than 20 times greater than the measurement quality. (for a typical orbit which subtends a total angle of 1° from the earth). Of course, all of the above constraints would vanish if the observer were based on the satellite's primary; however, this is out of the question at the present time.

As a result of the observing geometry, range and range-rate are periodic, permitting a very accurate determination of the orbital energy, i. e., the period. By simply noting the interval of repetition of events, such as zero crossings in the range-rate measurements, the period can be determined to a few minutes accuracy. Accounting for the effects of

the diurnal motion of the observer and the motion of the moon will yield an improved, accurate determination. There is a singularity associated with the periodicity of range and range-rate. If the satellite orbit lies exactly in the plane of the sky (normal to the line of sight of the observer), the range is constant and the range-rate is zero. This is only true if the motion of the moon and the diurnal rotation of the observer is ignored. In fact, for such an orbit orientation, only the diurnal rotation and the moon's motion would permit a non-singular orbit determination.

Differential correction is a process which improves the nominal estimate of an orbit, given tracking observations of the satellite in question. The method of solution involves linearization of a nonlinear regression equation. In essence, an estimate is made which minimizes the sum of squares of the observation residuals in the least squares sense. Residuals are differences between the actual observations and those computed using the initial estimate (which is improved from iteration to iteration).

Before a differential correction can be initiated, an initial estimate of the orbit is required, as mentioned above. The orbit is defined by six associated parameters, such as components of position and velocity. In general, in a preliminary orbit determination, there are more observations than the minimum required for the geometrical determination of the six orbital parameters. Therefore, like in the differential correction process, an overdetermined system of equations is set up and solved in the least squares sense.

The basic differences between the two orbit determination schemes is the precision of the estimate and the starting conditions. The preliminary orbit determination technique requires either no initial estimate or some very pessimistic estimate (like the nearest quadrant for angles), depending on the type of data and orbit in question. Unlike preliminary orbit determinations, a fairly accurate estimate is required to initiate a differential correction. If the estimate is very poor, the assumption of linearity may be strained, resulting in divergent corrections. However, given an appropriate initial estimate, the differential correction process will yield a far more accurate estimate than a preliminary orbit estimate, as the mathematical and physical models for computation are more sophisticated.

For both orbit determination techniques, slant range and slant range-rate observations are available. Angular data, though of poor quality, in either local horizon coordinates (azimuth and elevation) or earth equatorial coordinates (right ascension or hour angle and declination) is also available. Range accuracy is about one part in 10^8 , and range-rate, one in 10^5 . Because of the small angular diameter of the moon, as previously mentioned, angular data is only accurate to one part in 20. Hence the addition of angular data to range and range-rate does not significantly reduce the uncertainty in the tracking estimate.

The primary purpose of preliminary orbit determination techniques is to obtain the orbital elements in a relatively short period of time with no a priori estimate. The accuracy of the elements obtained should be such that their substitution into a differential correction process will permit convergence in a few iterations. Before beginning the study a literature search was conducted; the items of interest that were found are listed in the Bibliography.

The two preliminary orbit determination techniques studied here make use of two different data sets. The first uses range, right ascension, and declination (ρ, α, δ); and the second uses the magnitude of range and the magnitude of range-rate ($\rho, \dot{\rho}$).

3. DIFFERENTIAL CORRECTION OF LUNAR SATELLITE ORBITS

The nominal orbit for this convergence study has an orbital period of 220 minutes. Dispersions of various magnitudes and orientations were added to the nominal components of position and velocity, thus creating observed orbits for the purpose of data simulation. Depending on the convergence technique being evaluated, orbital periods as high as 650 minutes and errors of over 10° in the orientation elements were used as the observed orbit.

The precision orbit determination program used in this study was TRW Systems' AT85 Program. Its primary purpose is to determine satellite orbits using differential correction. The program determines the

elements of a satellite orbit and a covariance matrix of uncertainty in the determination, starting with some initial estimate of these elements and correcting it in accordance with observational data. The program includes a unique collection of mathematical, statistical, and operational techniques to make it operate rapidly and automatically and to produce high precision in the results.

The AT85 Program utilizes a Cowell method of special perturbations, with a Runge-Kutta starter, for propagating the satellite position and velocity. The earth gravitational models provided are of graduated accuracy; the triaxial potential model of the moon is available, and has been utilized in this study.

Since the observations of a trajectory that are made by a tracking system are imperfect, no trajectory fits these observations exactly. Therefore, only an estimate of the actual trajectory can be obtained from the data. Many methods of forming the estimate are possible, but the weighed least squares method is probably the most common and is the method employed by AT85.

AT85 provides a unique automatic control, which enhances the program's ability to converge to correct elements. The differential correction is actually computed subject to a side condition which, in effect, limits the size of the corrections so that the linear approximation is valid. The limits assigned to the differential correction are termed "bounds."

In addition to solving for six orbital elements and two drag parameters, AT85 has the capability to determine and remove biases from observational parameters and topocentric sensor location coordinates. Bias errors in the observations and uncertainty in the locations of the sensors may contribute more error to the orbit element determination than both the mathematical model and computational limitations combined. Furthermore, accurate estimation of the uncertainty in the orbital elements requires that the errors in the observations be unbiased.

AT85 calculates the corrections to the initial estimate in either geocentric or selenocentric coordinates. The latter system permits differential corrections of lunar orbits under special circumstances,

which are otherwise impossible to achieve. The corrections are performed in either Cartesian (xyz) or polar/spherical coordinates. The integration of the trajectory, on option, can be performed using dynamical centers other than the earth, permitting for example, selenocentric integration.

A more detailed description of AT85 is found in the appendix, where the structure and general internal processes of the computer program as well as the mathematical models and techniques employed in the orbit simulation and differential correction process are treated more fully than is permissible here.

The TRW Systems approach for selecting observed state vectors, from which the observations used in differential correction are computed, was to duplicate the "real-world" situation as closely as possible. There are two methods of selecting the reference and observed state vectors, given the dispersions. If the actual state vector, x_A , from which the observations are generated is held constant and the initial estimates, x_R , which are used to start the differential correction, are varied, only one set of simulated observations is required to carry out the study; that is, analyze the effects of various dispersion magnitudes and orientations of the initial estimate from the actual orbit. This would be the least expensive way to conduct the study, since the data simulation requirements are minimized.

However, in a "real-world" mission, the actual state vectors achieved, x_A , would be dispersed about a given preflight nominal, x_R , and each of these state vectors will have its own particular set of observations. The various actual state vectors, x_A , are generated by perturbing the nominal estimate, x_A , in various directions and magnitudes; the observations are then generated from each of these state vectors. Although this latter method involves much more data simulation, it was adopted by TRW Systems because it more nearly reflects what will occur in an actual mission.

The observations corresponding to an observed orbit, which is represented by a state vector, x_A , were generated with TRW Systems' data simulation program, AT-14. From a reference trajectory, which is

specified on an input ephemeris tape, topocentric observations are computed for each radar station desired. The individual noise models, standard deviations, and biases are included in the observations and are computed by means of a random vector generator.

A more detailed description of TRW Systems' AT-14 program is found in the appendixes.

Summarizing the results of this study, the JPL orbit determination program (SPODP) appears to be adequate for the orbit determination of lunar satellites, provided certain operational philosophies are adopted. They are:

- a) Require that at least two sensors be taking simultaneous observations immediately after the lunar deboost.
- b) Use short arc differential corrections with the observations taken in a), and make subsequent fits with the improved estimate of the first as initial conditions.
- c) If the period error is substantial, apply a hand computed energy correction to the initial estimate.

In general, the use of a priori information was not a significant aid to convergence, except for tracking with very few observations. The technique of normal matrix conditioning is not a practical method, especially in real-time considerations. This is because the conditioning normal matrix that will effect convergence is particular to the quantity of tracking data and the tracking geometry.

3.1 CONVERGENCE PROBLEMS IN THE DIFFERENTIAL CORRECTION OF LUNAR SATELLITE ORBITS

3.1.1 Nonlinearities

A trajectory is completely determined by a state vector, q_A , defined at some reference time known as epoch. If a set of observations, z , have been taken from the reference trajectory, the observations are assumed

to be related to the state vector x_A in equation (1). Restricting the discussion to the case where the only source of error is zero mean random noise

$$y = f(x_A) + \epsilon \quad (1)$$

where n is a column matrix ($r \times 1$) of zero mean random noise, y is of order ($r \times 1$), and x_A is of order ($p \times 1$). (The number of solution parameters is p , and the number of observations is r .) Equation (1) is a nonlinear regression equation; the method of solution involves linearizing the equation by expanding f in a truncated Taylor series about an initial estimate, x_o , since the actual value of x_A is unknown. Writing such an expansion and retaining only the linear terms

$$y = y_o + A(x_A - x_o) + \epsilon \quad (2)$$

where

$$y_o = f(x_o)$$

and the elements of the ($r \times p$) matrix A are the partial derivatives of the observations with respect to the state vector. The elements may be written

$$a_{ij} = \frac{\partial y_i}{\partial x_j}$$

By denoting

$$\delta y = y - y_o \quad (3)$$

and

$$\delta x = x_A - x_o \quad (4)$$

equation (2) may be rewritten

$$\delta y = A \delta x_A + \epsilon \quad (5)$$

where δy is the observed minus computed observational residual. The problem is to find a δx_A which, when added to x_o , will yield an improved estimate of x_A . (See equation (4).) This is usually done by finding that x_A , which minimizes the residuals in the least squares sense.

As an example of the least squares criterion, consider the following problem:

Given a set of points (ξ_i, η_i) , $i = 1, 2, \dots, n$, if it is desired to fit a $(p - 1)^{\text{th}}$ order polynomial of the form

$$\eta = \sum_{i=0}^{p-1} b_i \zeta^i$$

a set of coefficients $(b_j, j = 0, 1, \dots, p - 1)$ is determined such that

$$S = \sum_i (\eta_i - \sum_{j=0}^{p-1} b_j \zeta_i^j)^2 \quad (6)$$

is minimized; that is, that the sum of squares of the deviation from the polynomial are minimized. By noting that

$$\eta_i = \sum_{j=0}^{p-1} b_j \zeta_i^j = (1 \zeta_i \zeta_i^2 \dots \zeta_i^{p-1}) \begin{bmatrix} b_0 \\ b_1 \\ b_2 \\ \vdots \\ b_{p-1} \end{bmatrix} \quad (7)$$

is a $(p - 1)^{\text{st}}$ degree polynomial with coefficients b_0, \dots, b_{p-1} evaluated at the point ζ_i , and defining

$$y = \begin{bmatrix} \eta_1 \\ \eta_2 \\ \vdots \\ \eta_n \end{bmatrix}_{n \times 1}, \text{ and } \delta x = \begin{bmatrix} b_0 \\ b_1 \\ \vdots \\ b_{p-1} \end{bmatrix}_{p \times 1}$$

equation (6) may be rewritten

$$S = S(\delta x) = (y - A \delta x)^T (y - A \delta x) \quad (8)$$

Note: In terms of the above definitions, A is a matrix of order $(n \times p)$, and the element a_{ij} is written:

$$a_{ij} = \zeta_i^{j-1} \quad \begin{matrix} i = 1, 2 \dots n \\ j = 1, 2 \dots p \end{matrix}$$

The least squares criterion requires that an \hat{x} be found such that $S(\hat{x})$ is minimized. Expanding equation (8)

$$S(\delta x) = yy^T - 2\delta x^T A^T y + \delta x^T A^T A \delta x \quad (9)$$

$$\begin{aligned} \Delta S(\delta x) &= -2\Delta\delta x^T A^T y + \Delta\delta x^T A^T A \delta x + \delta x^T A^T \Delta\delta x \\ &= -2\Delta\delta x^T A^T y + 2\Delta\delta x^T A^T A \delta x \end{aligned}$$

For the minimum $S(\Delta x)$, $\Delta S = 0$

$$A^T A \delta x - A^T y = 0$$

$$\hat{\delta x} = (A^T A)^{-1} A^T y \quad (10)$$

Equation (10), the required minimization of equations (6) and (8), is called the normal equation.

Rewriting equation (5),

$$\delta y = A \delta x + \epsilon$$

it is obvious that if the observations are not of the same observable (i.e., range, angles, doppler, etc.), then the estimate $\Delta\hat{x}$ is a function of the units. A matrix C is introduced which takes the units into account, and includes a priori knowledge of the variance of the noise and on the observations (See Section 3.4.2). The matrix C is of order $(n \times n)$ and

$$C^T C = W \quad (11)$$

Equation (5) is multiplied by the matrix C

$$Cy = CA \delta x + C\epsilon \quad (12)$$

Letting

$$\delta y' = Cy$$

$$A' = CA$$

$$\epsilon' = C\epsilon$$

equation (12) is transformed

$$\delta y' = A' \delta x + \epsilon' \quad (13)$$

The least squares estimate of δx for this equation, recalling equation (10)

$$\delta \hat{x} = (A'^T A')^{-1} A' \delta y' \quad (14)$$

Eliminating the prime notation and using definition (11)

$$\begin{aligned} \delta \hat{x} &= (A^T C^T C A)^{-1} A^T C \delta y \\ \delta \hat{x} &= (A^T W A)^{-1} A^T \delta y \end{aligned} \quad (15)$$

Since δx minimizes

$$(\delta' y - A' \delta x)^T (\delta' y - A' \delta x) = (\delta y - A \delta x)^T W (\delta y - A \delta x)$$

it is called the weighted least squares estimate corresponding to the original regression equation (equation (5)).

Recalling the constraint under which equation (2) was formulated, (i. e., that only the first-order term in the Taylor series expansion is retained) brings to mind the need for iteration in least squares curve fitting of trajectories. Since a nonlinear system is being solved by linearizing, which is at best a good approximation, the solution is obtained by a succession of linear approximations; i. e., iteration. Closely related to the amount of iteration required is the quality of the initial estimate, x_0 . If the initial estimate is very close to the actual state, x_A , then the linearizing condition is immediately a good approximation, and one or two iterations only are needed to solve the system.

If, on the other hand, the initial estimate is poor (in terms of linearity), it may be difficult or impossible to solve the system because extremely large (and inappropriate) corrections may be called for on the first iteration. The technique of constraining the size of the correction vector is often very helpful in this otherwise hopeless situation. The concept of constraining or bounding the solution to the normal equation is discussed in section 3.3.2.

3.1.2 Consistency of Residuals

A large period error in the initial estimate of a differential correction with greater than one revolution of data gives rise to convergence difficulties. The observed minus computed observations, the residuals, from which the differential corrections to the initial estimate are computed, are inconsistent from one revolution to the next. A numerical example using a 3σ energy perturbed orbit (from the nominal orbit A) illustrates this problem.

To simplify the illustration, assume the observer is on a nonrotating earth and that the moon is stationary. If the orbit is circular and lies in the earth-moon plane, the geometry of figure 1 illustrates the situation. Both range and range-rate are periodic functions of time: for range it is a sinusoidal oscillation about the earth-moon distance, the minimum and the two zero crossings are visible, and the maximum range occurs directly behind the moon; for range-rate the variation is also sinusoidal, there is one zero crossing, and both the maximum and the minimum are visible.

The observed range-rate for a circular orbit of 2800 km, with a period of 220 minutes (the nominal period) is plotted in figure 2. This range-rate history corresponds to the computed observations. On the same graph, the observed range-rate history is plotted. This corresponds to a 3730-km circular orbit with a period of 340 minutes. The "observed minus computed" residuals of the observed range-rate and the computed range rate is plotted in figure 3. These residuals are used to compute corrections to the initial estimate defining the computed orbit.

Three revolutions of the satellite, based on the computed period, have been considered. The second and third revolution residual histories have been redrawn over the first to facilitate comparison. Note that the residuals at the beginning of the first, second, and third revolutions are inconsistent in that they call for changes in the elements (of the nominal orbit, i. e., the computed orbit) which will simultaneously increase, decrease, and leave unchanged the range-rate observations at this point. This example has been computed using a modification of the 3σ energy perturbed orbit; this corresponds to a 90 m/s dispersion in velocity and

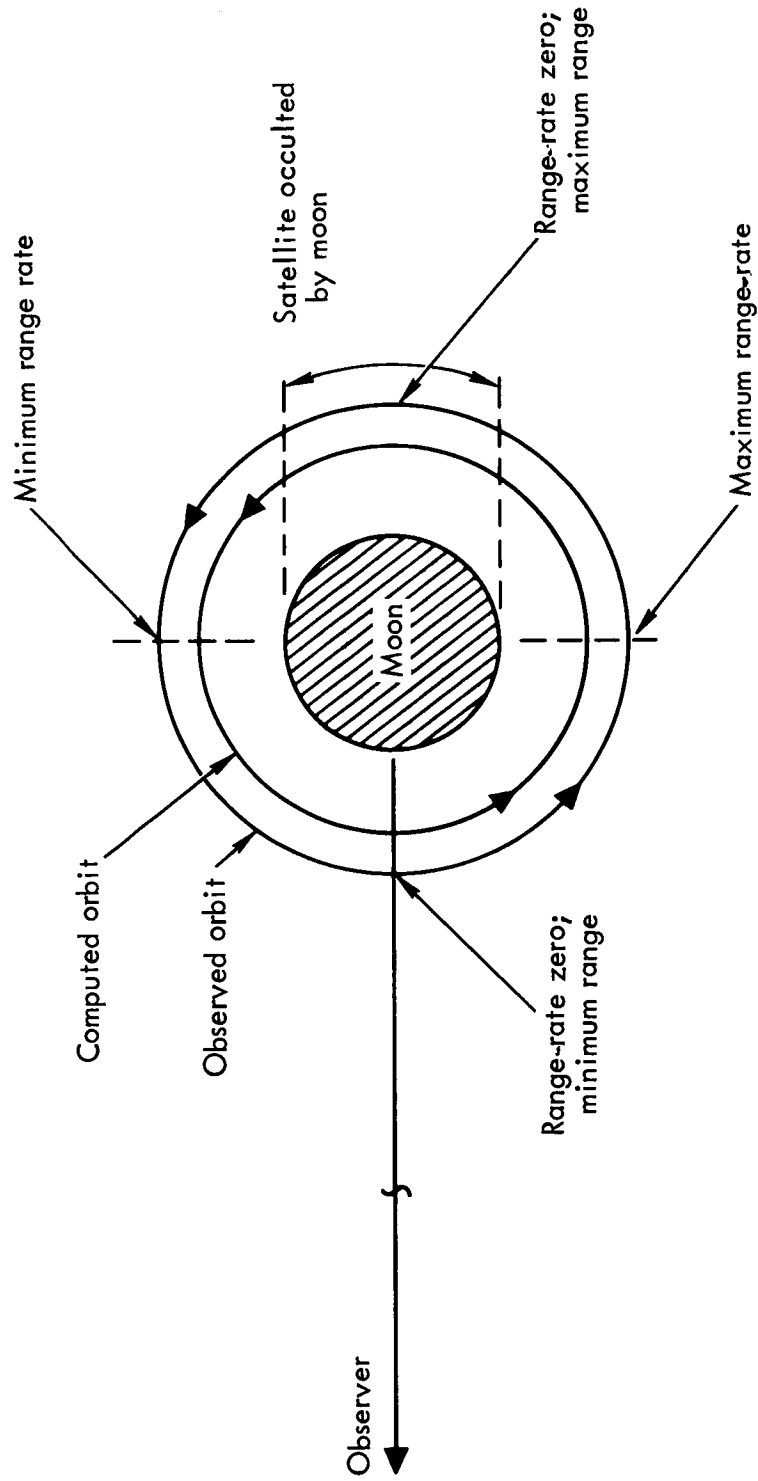


FIGURE 1. — LUNAR SATELLITE ORBIT GEOMETRY

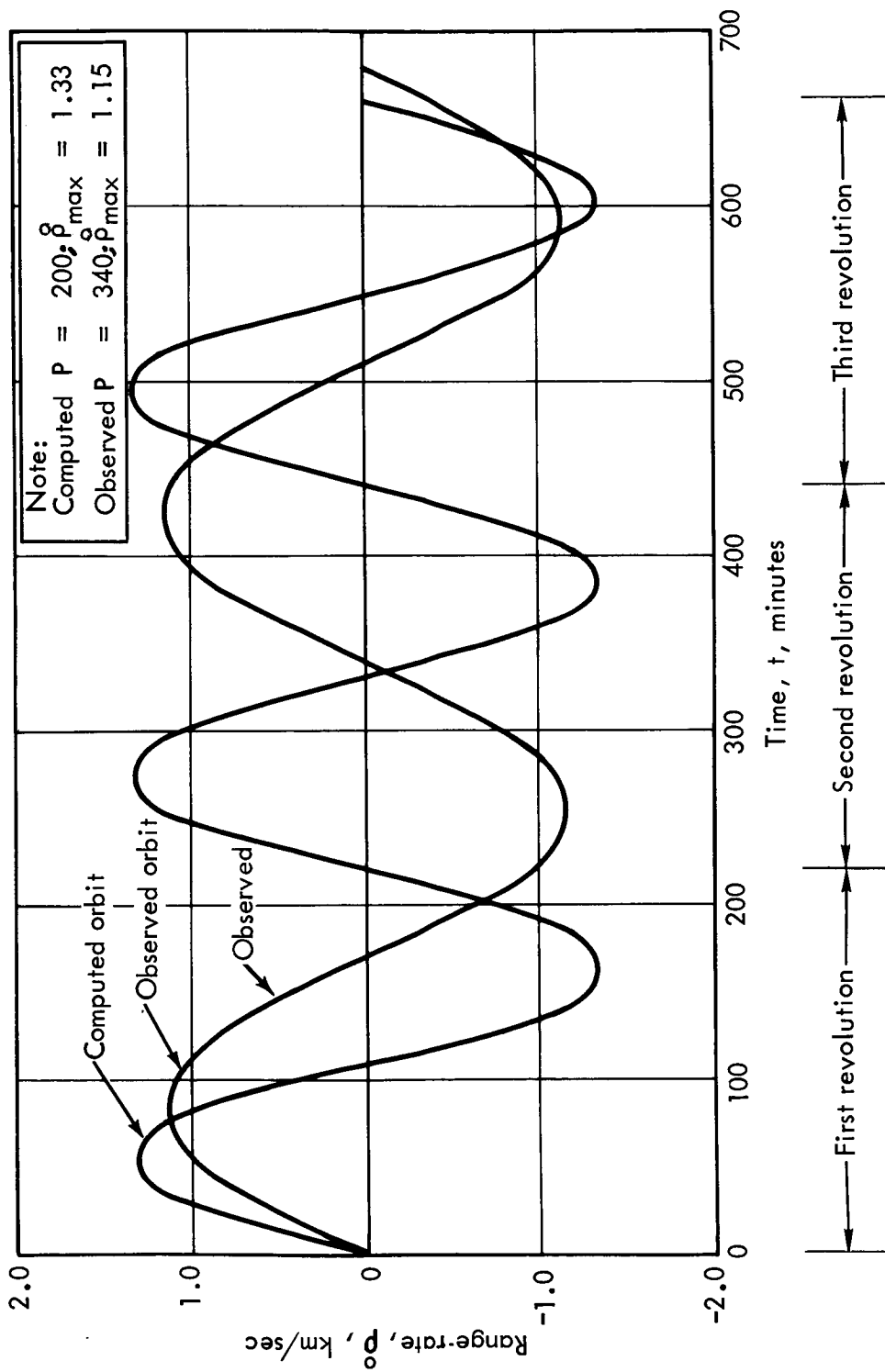


FIGURE 2.—DOPPLER CURVES OF COMPUTED AND OBSERVED ORBITS

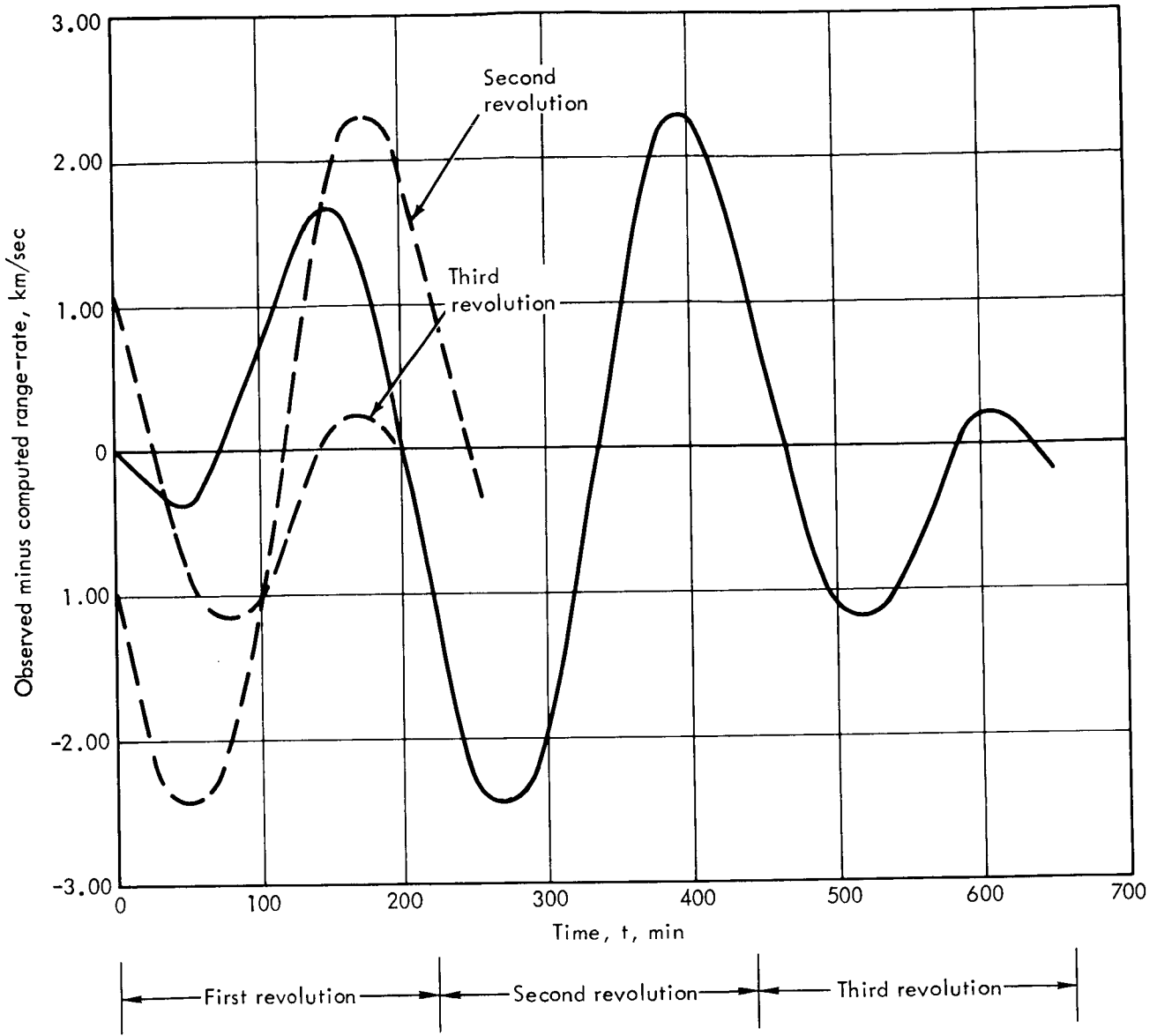


FIGURE 3.—COMPUTED RANGE-RATE RESIDUALS

45 km in position. If the periods of the observed and computed orbits agree, the residuals of this computed example would be the same from one revolution to the next (i. e. , they would be consistent), and their use in a differential correction would lead to an appropriate solution.

The energy correction is a method of adjusting the nominal period to that of the observed one. This technique requires no special programs, but merely a few simple hand computations derived from the observed period of the doppler curve. Since the energy correction is an approximation, there is no point in getting an exact value of the observed period by correcting the doppler curve for the diurnal motion of the observer and the motion of the moon. This subject is treated more fully in section 3.3.1.

After the orbital energy of a nominal estimate has been adjusted to that of the observed orbit, the residual inconsistency from revolution to revolution vanishes; that is, the residuals are in phase. However, if there are appreciable errors (other than orbital period) in the initial estimate, large cyclical residuals could result. Since the orbital energies are equal, the effect may not be very noticeable in the range-rate measurements. However, if these other remaining errors were in the orientation of the orbit with respect to some reference plane, the range residuals would be appreciable. This situation is illustrated in figure 4, where the observed and computed ranges are plotted with the earth-moon distance removed.

The relatively large (phased) range residuals which could be computed from figure 4 would give rise to nonlinearities in the differential correction process. In a nonlinear situation, the range residuals exhibit behavior as illustrated in figure 5, which are computed from figure 4. Therefore, the nature of the convergence problem which is associated with a bad initial estimate can be determined by inspecting the behavior of the computed residuals history; it is preferable to look at the observational residuals of more than one revolution of the nominal estimate, if this data is available to the analyst.

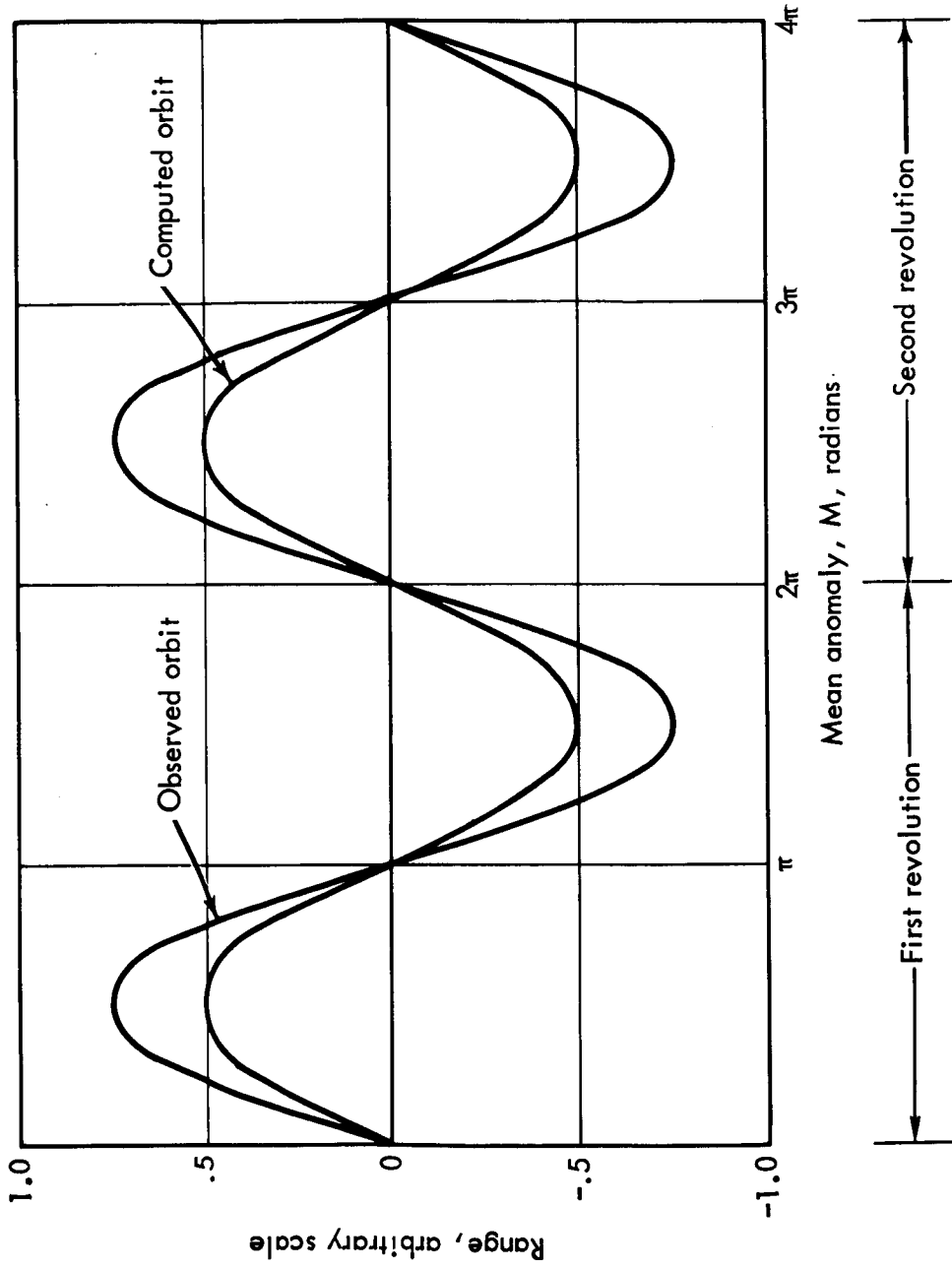


FIGURE 4. — PERIODIC RANGE OF COMPUTED AND OBSERVED ORBITS

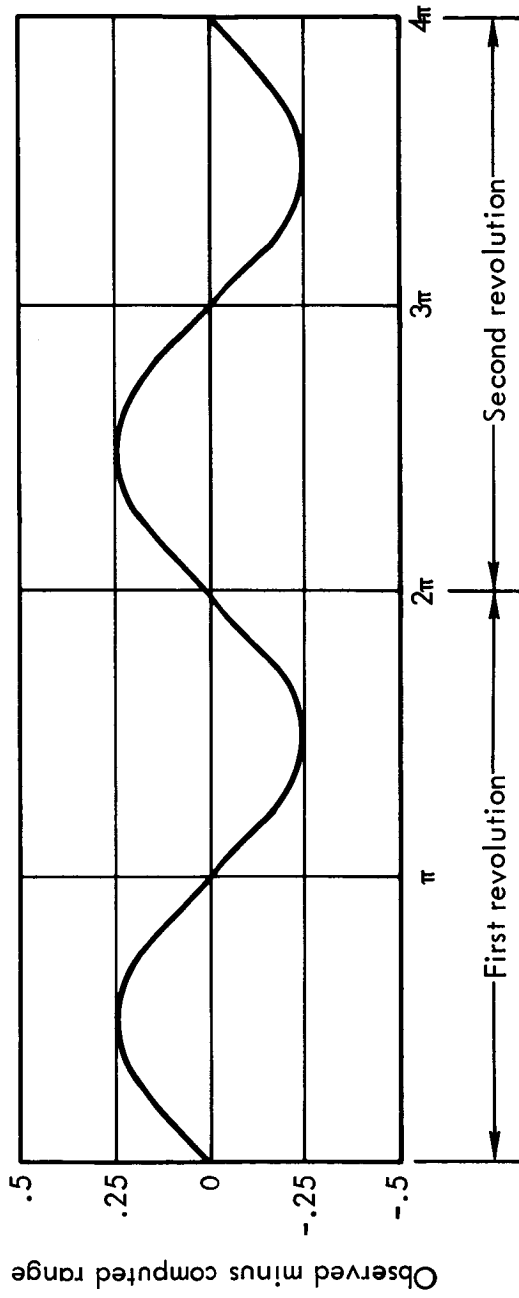


FIGURE 5. — COMPUTED RANGE RESIDUALS

3.2 ORBIT SELECTION AND DATA SIMULATION

3.2.1 Nominal and Alternate Orbits

The nominal lunar satellite orbit used in this study is defined by the following classical selenographic elements:

$$a = 2788 \text{ km}$$

$$e = 0.2869$$

$$i = 15^{\circ}0$$

$$\Omega = 25^{\circ}47$$

$$\omega = -12^{\circ}46$$

$$T = 27 \text{ June } 1966, 4^{\text{h}} 0^{\text{m}} 48^{\text{s}}$$

(Pericyynthion passage)

The equivalent geocentric cartesian elements of this orbit, as well as all other orbits and data sets used in the study, are tabulated in appendix A.

In order to maintain some relationship between the size of the perturbations and the reflected uncertainty of the state vector, perturbations of the state vector were selected using the covariance matrix, Σ_R (supplied by LRC), associated with the above classical elements. These perturbations and the associated data simulation are discussed in the next section.

The nominal orbit has an orbital period of 220 minutes, with pericynthion and apocynthion altitudes of 250 km and 1850 km, respectively. It was the principal orbit used in this convergence study and is referred to as case A.

The study of the convergence characteristics of alternate lunar satellite orientations, the "B" cases, was concerned with the effects of observing the lunar satellite in different orientations. The effect of varying satellite orientations on the differential correction process is evident when one considers an orbit which lies in the plane of the sky. In

such a case, the range is constant, and range-rate is zero, neglecting the motion of the moon. The satellite orbits selected for study are tabulated below for reference.

TABLE I.—CLASSICAL ELEMENTS OF ALTERNATE SATELLITE ORBITS

Orbit code	Classical Elements					
	a	e	i	Ω	ω	M
B1	2788	0.2869	0°	25° 47	-12° 46	0
B2	2788	0.2869	30°	25° 47	-12° 46	0
B3	2788	0.2869	45°	25° 47	-12° 46	0
B4	2788	0.2869	60°	25° 47	-12° 46	0
B5	2788	0.2869	15°	10°	-12° 46	0
B6	2788	0.2869	15°	90°	-12° 46	0
B7	2788	0.2869	15°	130°	-12° 56	0

T = 27 June 1966, 4^h 0^m 48^s

The orbital period, the pericyynthion altitude, and the apocynthion altitudes are unchanged from the nominal orbit.

3.2.2 Data Simulation

The purpose of the data simulation is to provide computed observations, which would be taken by tracking stations of interest. The computed observations are then used to initiate a differential correction procedure using a nominal estimate, x_N , which is perturbed from the actual state vector, x_A .

In the real-world situation, the actual state vectors, x_A , achieved after the main lunar deboost will be dispersed about the nominal aim point, and each of these state vectors will have its own particular observational

time history. Since there is only one preflight nominal state vector x_R , the computed observations are based on an actual state vector x_A , which is perturbed in some way from the preflight nominal. Hence, this approach requires a data set for each actual state vector, x_A , which is selected for study.

A systematic method of calculating the state vector x_A is needed in order to keep the number of data sets small. As previously inferred, the actual state vector, x_A , is related to the preflight nominal state vector, x_R , by the equation

$$x_A = x_R + f(\Sigma_R)$$

where Σ_R is the a priori covariance matrix reflecting the uncertainties in x_R . It is assumed that the uncertainties in position and velocity components are each spherically distributed, and that (for the moment) \bar{r} and \bar{v} are uncorrelated. The probabilities that the magnitudes of the perturbations lies within the 1, 2, and 3 σ spheres are 0.20, 0.74, and 0.97, respectively. The 1 σ values of position and velocity derived from Σ_R (see Appendix A) are 15 km and 30 meters/second, respectively.

The orientation of the perturbations to the nominal state vector, x_R , were applied in the directions described below:

- a) 1, 2, and 3 perturbations in the direction of the nominal position and velocity vectors. That is, to maximize the error in orbital energy, $|\Delta r|$ and $|\Delta v|$ multiplied by their respective direction cosines will yield the appropriate vector components.
- b) 1, 2, and 3 σ perturbations in the direction normal to the orbital plane; i. e., normal to the plane of \bar{r} and \bar{v} . This maximizes the perturbations in the orientation elements, Ω and i . Since this perturbation results in a relatively small change in the magnitudes of the position and velocity vectors, the accompanying energy change is very small.

The energy perturbed state vector is calculated as follows:

l, m, n = direction cosines of position
or velocity vectors

$$x_A = x_R + f(\Sigma_R)$$

$$x_A = \begin{bmatrix} x \\ y \\ z \\ \dot{x} \\ \dot{y} \\ \dot{z} \end{bmatrix} + \begin{bmatrix} 1 \\ m \\ n \\ 0 \\ 0 \\ 0 \end{bmatrix}_p [r] n\sigma + \begin{bmatrix} 0 \\ 0 \\ 0 \\ 1 \\ m \\ n \end{bmatrix}_v [v] n\sigma$$

The orientation perturbed state vector is calculated as shown below:

$$x_A = x_R + f(\Sigma_R)$$

$$\frac{\vec{r} \times \vec{v}}{|\vec{r} \times \vec{v}|} = \begin{bmatrix} h_x \\ h_y \\ h_z \end{bmatrix} = \text{direction cosines of angular momentum vector}$$

$$x_A = \begin{bmatrix} x \\ y \\ z \\ \dot{x} \\ \dot{y} \\ \dot{z} \end{bmatrix} + \begin{bmatrix} h_x \\ h_y \\ h_z \\ 0 \\ 0 \\ 0 \end{bmatrix} [r] n\sigma + \begin{bmatrix} 0 \\ 0 \\ 0 \\ h_x \\ h_y \\ h_z \end{bmatrix} [v] n\sigma$$

A system of abbreviations has been adopted to allow compact specification of the actual state vectors, x_A , representing a real-world satellite (dispersed about a given nominal state, x_R)

OPn - Orientation perturbed; $n\sigma$ dispersion magnitudes

EPn - Orbital energy perturbed; $n\sigma$ dispersion magnitudes

Example:

B3OP3 - Reference orbit B3 with 3σ orientation perturbations

AEP2 - Reference orbit A with 2σ orbital energy perturbations

Since the computed observations are generated from a trajectory which was propagated from a state vector, the abbreviations introduced above are applicable to a set of observations.

Hence, AEP3 data was computed from a trajectory which was generated by the state vector, AEP3 (nominal state vector A, energy perturbed, 3σ).

The perturbations described permit two different types of initial conditions for the start of a differential correction: 1) an energy perturbation, and 2) an orientation perturbation. A third type of perturbed initial condition, the epoch perturbation, can be achieved by simply shifting the epoch time. This technique results in essentially an in-plane error. However, the epoch perturbation has a unique constraint among the three types of perturbations; the initial conditions for the differential correction must be selenocentric. If initial conditions were input in geocentric coordinates, the effective perturbation on the initial conditions would be equal to the change in position and velocity of the moon during the epoch shift interval.

The first step in the process of simulating observations is to calculate perturbed state vectors, dispersed from the nominal state vector by a function of the a priori covariance estimate of the nominal state vector. Orbital energy and orientation perturbations of varying magnitudes ($n\sigma$) were added to the nominal state vectors, resulting in the appropriate perturbed initial conditions. There were eight nominal state vectors; the first is referred to as the "A" vector, which was used to implement most of the convergence study; the remaining seven state vectors, B1 thru B7, represent the alternate lunar satellite orbits. (Listed in the previous section and in the appendix).

The perturbed state vectors were the initial conditions for generating a trajectory; the duration of the trajectory was equal to the longest simulated tracking interval anticipated. The physical model consisted of the moon as the dynamic center with a triaxial potential representation, and with the sun and the earth as perturbing bodies. The initial position

and velocity were in earth-centered inertial (ECI) coordinates; however, the state vector was "phase shifted" to selenocentric coordinates immediately, thereby making the moon the dynamical center.

The geocentric cartesian position and velocity of the vehicle were written on an (ephemeris) output tape at a 1-minute interval. The output tape representing the trajectory of the vehicle in a perturbed trajectory was then used as an input tape to the TRW Systems data generation program, AT-14. (See appendix D.) Given the geographical coordinates of the stations of interest, the noise model for each, and an ephemeris tape, the AT-14 program generates the topocentric observations of range, range-rate, right ascension, and declination on punched cards in suitable format for input to the AT-85 program as observations.

The station locations of the three sensors used in the simulation are tabulated below:

<u>Station ID</u>	<u>Latitude</u>	<u>Longitude</u>	<u>Height (m)</u>	<u>Name</u>
01	35.2060	243.1500	1040	Goldstone
02	-31.2100	136.8850	151	Woomera
03	40.4370	- 3.7650	50	Madrid

The following data qualities for the three Deep Space Net (DSN) stations which are appropriate to a 1-minute data rate are listed below.

Range	$\sigma = 20 \text{ m}$	Bias = 40 m
Range rate	$\sigma = 0.02 \text{ m/s}$	Bias = 0
Right ascension	$\sigma = 0^{\circ}06$	Bias = 0
Declination	$\sigma = 0^{\circ}06$	Bias = 0

The AT-14 program generates observations at a specified data rate but does not check for lunar occultation. However, the AT-4 Tracking Program has a radar steering option which specifies the lunar occultation intervals as seen from a given radar station on earth for any given orbit about the moon. This made it possible to delete the appropriate "occultation spans" from the unedited output of AT-14.

The importance of deleting the unobservable data becomes apparent in some of the alternate lunar satellite orbits when the vehicle goes behind the moon a few minutes after the beginning of the tracking epoch.

Figure 6 is a chart of the rise and set times of the lunar satellite for the three DSN stations. The lunar occultation times for the entire 24-hour span are also indicated.

3.3 CONTROL OF FACTORS AFFECTING CONVERGENCE

3.3.1 Techniques for Obtaining Consistent Residuals

Initial estimate.— The best method of avoiding inconsistent residuals is to have the best possible nominal estimate. Although the mission nominal may reflect small uncertainties, the 1σ energy error for the missions under consideration is about 15 percent. An estimate obtained from a preliminary orbit determination technique is far better than a mission nominal, and using such an estimate would obviate any technique which is designed to cope with the inconsistent residuals problem.

Energy correction.— The solution to the problem of inconsistent residuals is an energy adjustment. Since both range (with the earth-moon distance removed) and range-rate are periodic, the orbital period, and hence the energy, are readily calculable. The period of the orbit can be approximated by noting the elapsed time between two successive zero crossings of the range-rate observations.

It should be noted that the period obtained in this fashion is uncorrected for the observer's diurnal motion and the motion of the moon. To correct for these two effects, certain quantities are computed, given the following information:

$$\dot{\bar{r}}_E = \text{observer's geocentric velocity}$$

$$\bar{r}_M = \text{geocentric range of moon}$$

$$\dot{\bar{r}}_M = \text{geocentric velocity of moon}$$

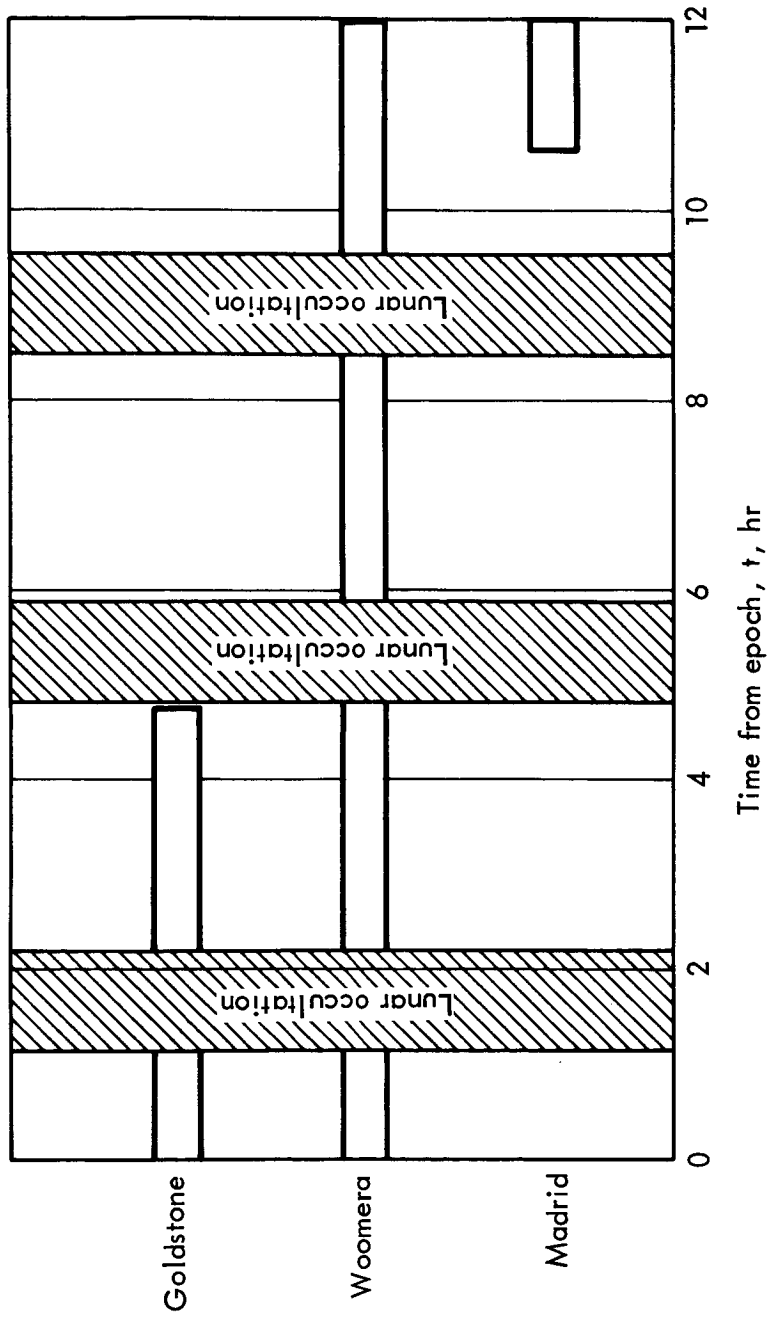


FIGURE 6. — VISIBILITY INTERVALS OF NOMINAL ORBIT; DSN STATIONS

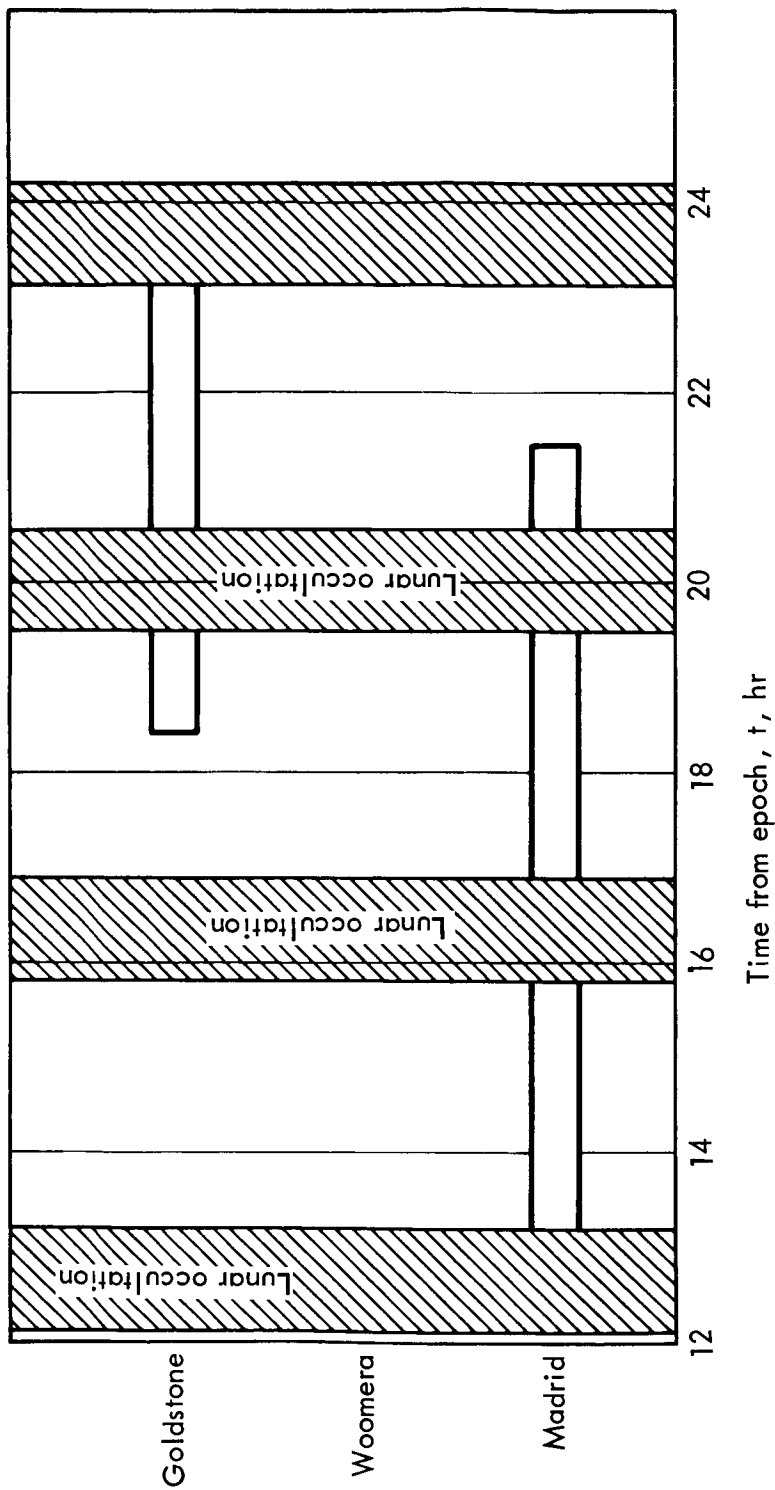


FIGURE 6. — Concluded

$$\dot{\rho}' = \dot{\rho} - \frac{\dot{\vec{r}}_E \cdot \vec{r}_M}{|\vec{r}_m|} - \frac{\dot{\vec{r}}_M \cdot \vec{r}_M}{|\vec{r}_M|}$$

= range-rate corrected

The quantity $\dot{\rho}$, the range of the satellite with respect to the observer, should be used instead of $\dot{\vec{r}}_M$, but since the former quantity is not known accurately, the approximation is made. As will be shown later, these corrections are not critical to the energy correction method.

The energy correction is applied by improving the initial estimate of the velocity vector. The difference between the observed and computed periods can be equated to a difference in semimajor axis; this difference, in turn, is equated to a change in velocity. The radius vector remains unchanged. Note that this is only one of many ways of correcting the energy; since we have no a priori knowledge as to how the correction should be applied, the most convenient is selected.

The foregoing formulation is valid for relatively small differences (<10%) in period. Using a canonical set of units,

$$P^2 = a^3$$

$$2P\Delta P = 3a^2\Delta a$$

$$\Delta P = \frac{3}{2}\Delta a \sqrt{a} = P_{\text{observed}} - P_{\text{computed}}$$

$$V^2 = \frac{2}{r} - \frac{1}{a}$$

$$\Delta V = \frac{\Delta a}{2Va}$$

This ΔV correction, when applied to the initial velocity estimate, will equate the observed period to the computed period.

When the difference between the two periods is large (>10%) the differential formulas given above become inadequate. The ΔV is then computed without using differentials.

$$V' = \frac{2}{r_{\text{initial}}} - \frac{1}{a_{\text{observed}}} \quad (\text{scalar})$$

$$\Delta V = V' - V_{\text{initial}} \quad (\text{scalar})$$

The energy corrected velocity vector is then computed

$$\vec{V}_{\text{EC}} = \vec{V}_{\text{initial}} + \begin{bmatrix} l \\ m \\ n \end{bmatrix} |\Delta V|$$

where $\begin{bmatrix} l \\ m \\ n \end{bmatrix}$ are the direction cosines of the initial velocity vector.

Since the energy correction matches the periods by a velocity adjustment only, it is at best a partial improvement to the initial state vector. And, because it is only an approximation (the tendency is to over-correct the velocity), it is not critical that the estimated period, presumably from a Doppler curve, be corrected for the motion of the moon and the diurnal motion of the observer.

It should be noted that all test cases, unless discussed in the following sections, have simulated tracking from two sensors. Also, all test cases use AEP3 data, which is 3σ -energy perturbed from the nominal orbit. The AEP3 observed period is 340 minutes; the nominal period is 220 minutes.

The energy correction technique was tested extensively. It was used in many of the "A" cases; that is, with the nominal orbit. Using AEP3 data (3σ , energy perturbed) the energy corrected initial estimate proved to be an effective convergence aid for data spans of up to 1000 minutes. For the relatively short data spans, (60 minutes), the nominal (not-energy corrected) achieved convergence, although the energy correction has a higher convergence rate. This is illustrated in figure 7. The energy correction becomes essential for convergence if there is more than one revolution of data. Figure 8 illustrates the convergence of an energy corrected curve fit and the divergence of the nonenergy corrected fit. This test case had 680 minutes (2 revolutions) of tracking. These remarks apply only to 3σ energy perturbations.

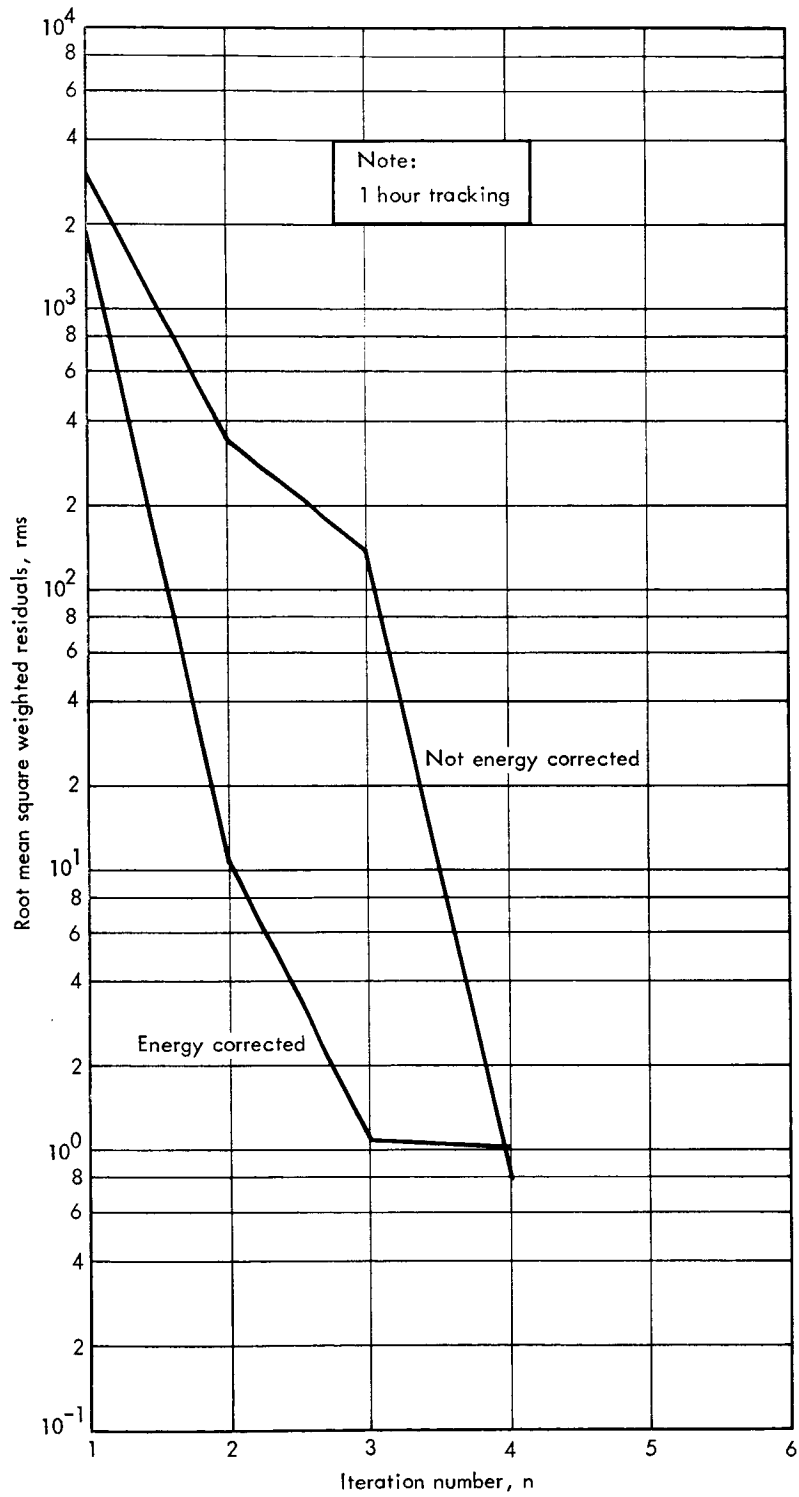


FIGURE 7. — EFFECT OF ENERGY CORRECTED INITIAL ESTIMATE FOR SHORT ARC FITS

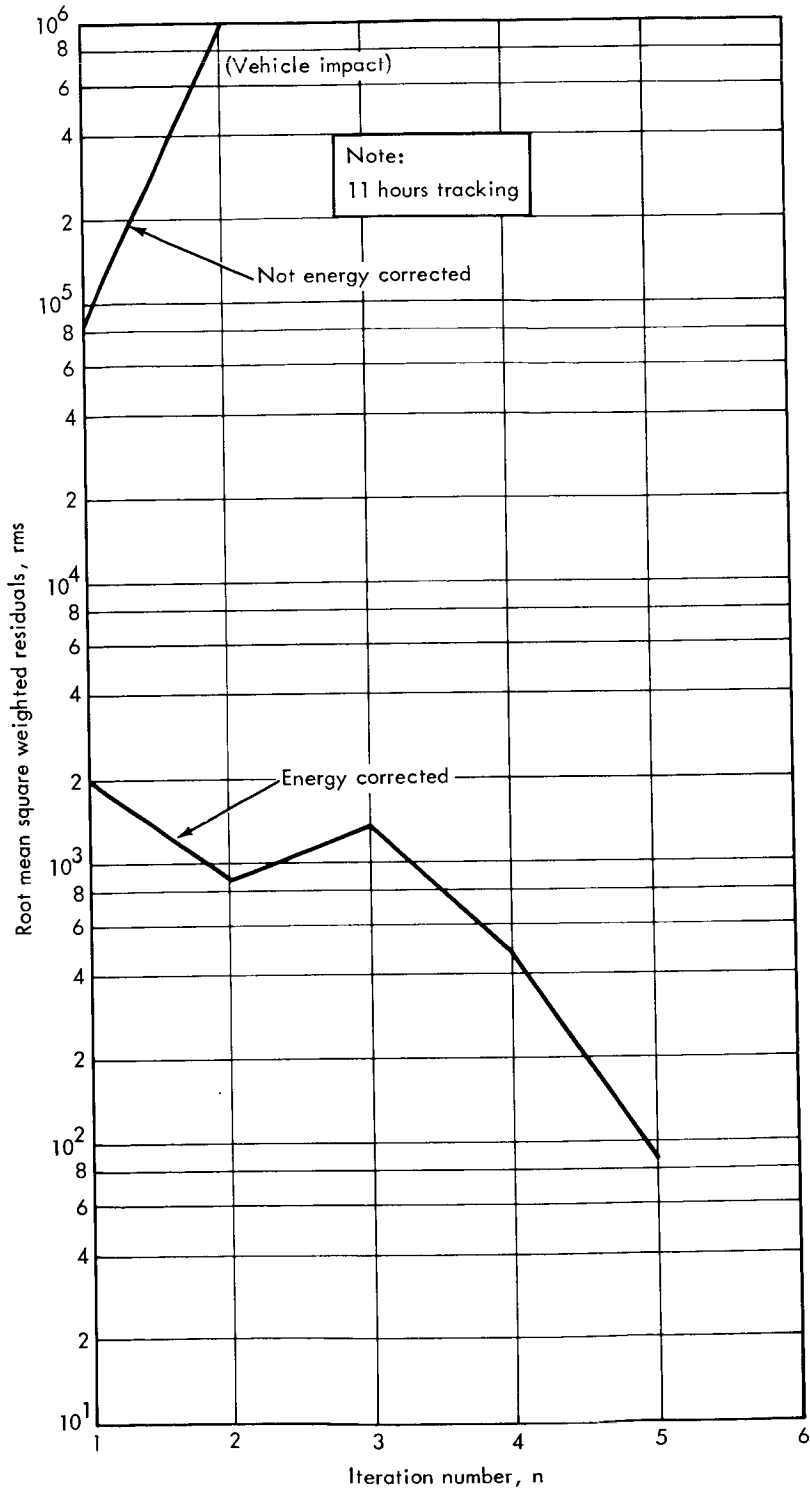


FIGURE 8. — EFFECT OF ENERGY CORRECTED INITIAL ESTIMATE FOR LONG ARC FITS

The effectiveness of the energy correction was demonstrated when a 45-minute data arc required an energy correction to converge. The data was 6σ energy perturbed (AEP6); the period was 650 minutes, nearly three times the nominal value. Figure 9 illustrates this case.

The energy correction for a short arc fit may be of academic interest only, since at least one complete revolution of data is required before the period (and hence, energy) can be estimated. However, if the period error is very large, say greater than 100 percent, an energy correction is needed, even for a relatively short arc. (See Figure 9)

Stepwise fits.—The technique of stepwise fits refers to a series of differential corrections, beginning with short data arcs, and progressively adding more data, each time using as initial conditions the converged state vector from the previous fit. This method can be considered as an alternative to the energy correction, since the converged state vectors from short arc fits already have an improved energy estimate. The method is practical for real-time data operation, since data can be used as it becomes available.

The stepwise fit technique is an effective means of achieving convergence with large amounts of data, and does not require an energy correction. Figure 10 illustrates the convergence rates of 300-minute data arc differential corrections. Figure 11 illustrates the convergence rates for 1000 minutes of tracking. The nominal curve is an energy corrected fit. (Such a long data span would not converge, were it not energy corrected.) The step fit used the converged state vector of a 45-minute tracking arc as in Figure 10 as its initial estimate. The effectiveness of the energy correction shows up in the low initial RMS when compared to the nonstep fits.

In-Plane correction.— The convergence study has been based on the recovery of state vectors which were dispersed in orbital energy or orientation from the nominal estimate. A third type of dispersion, an in-plane error, can be simulated by simply shifting the time associated with the initial estimate.

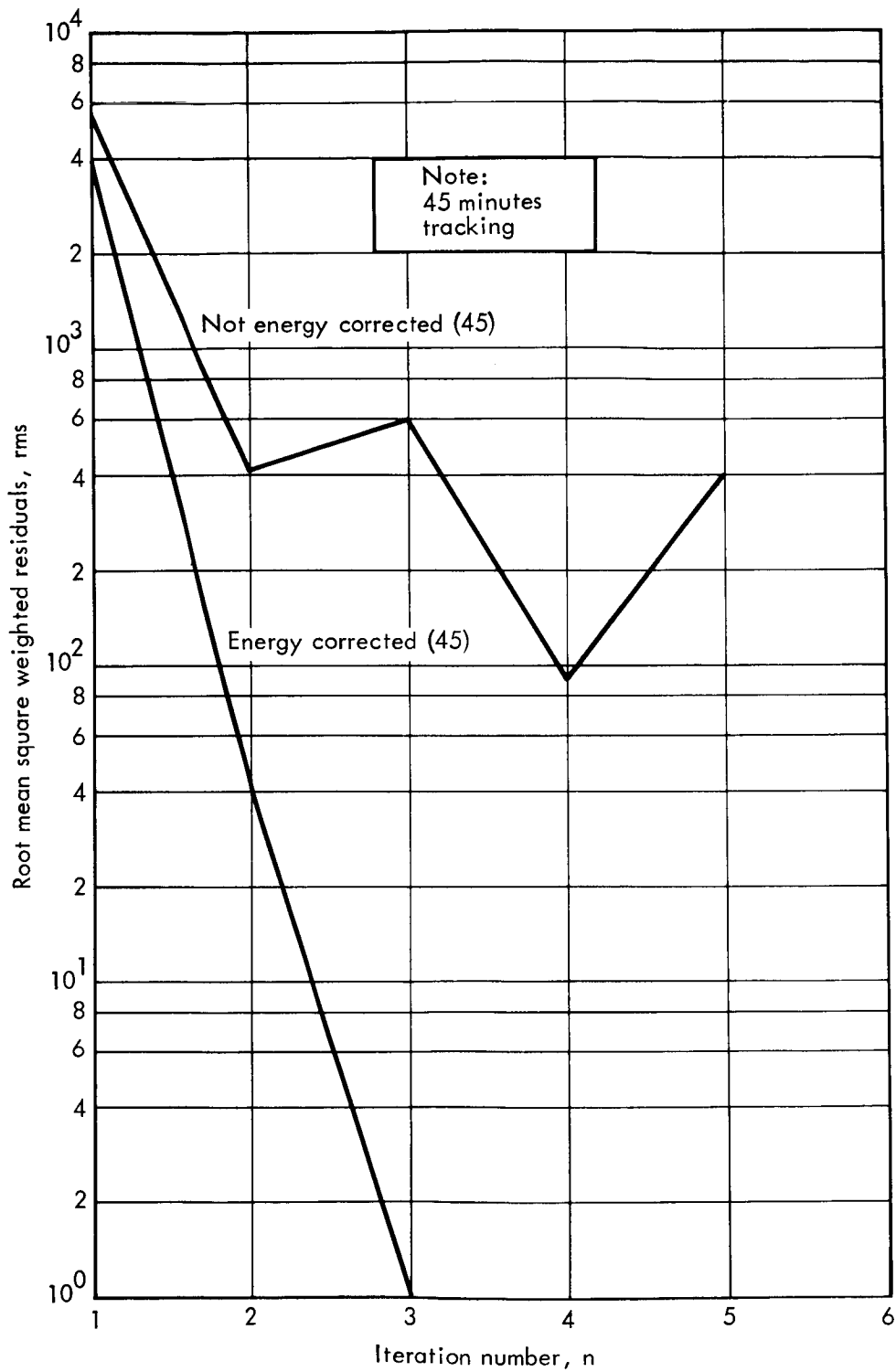


FIGURE 9. — EFFECT OF ENERGY CORRECTED INITIAL ESTIMATE FOR 6σ OBSERVED ORBIT

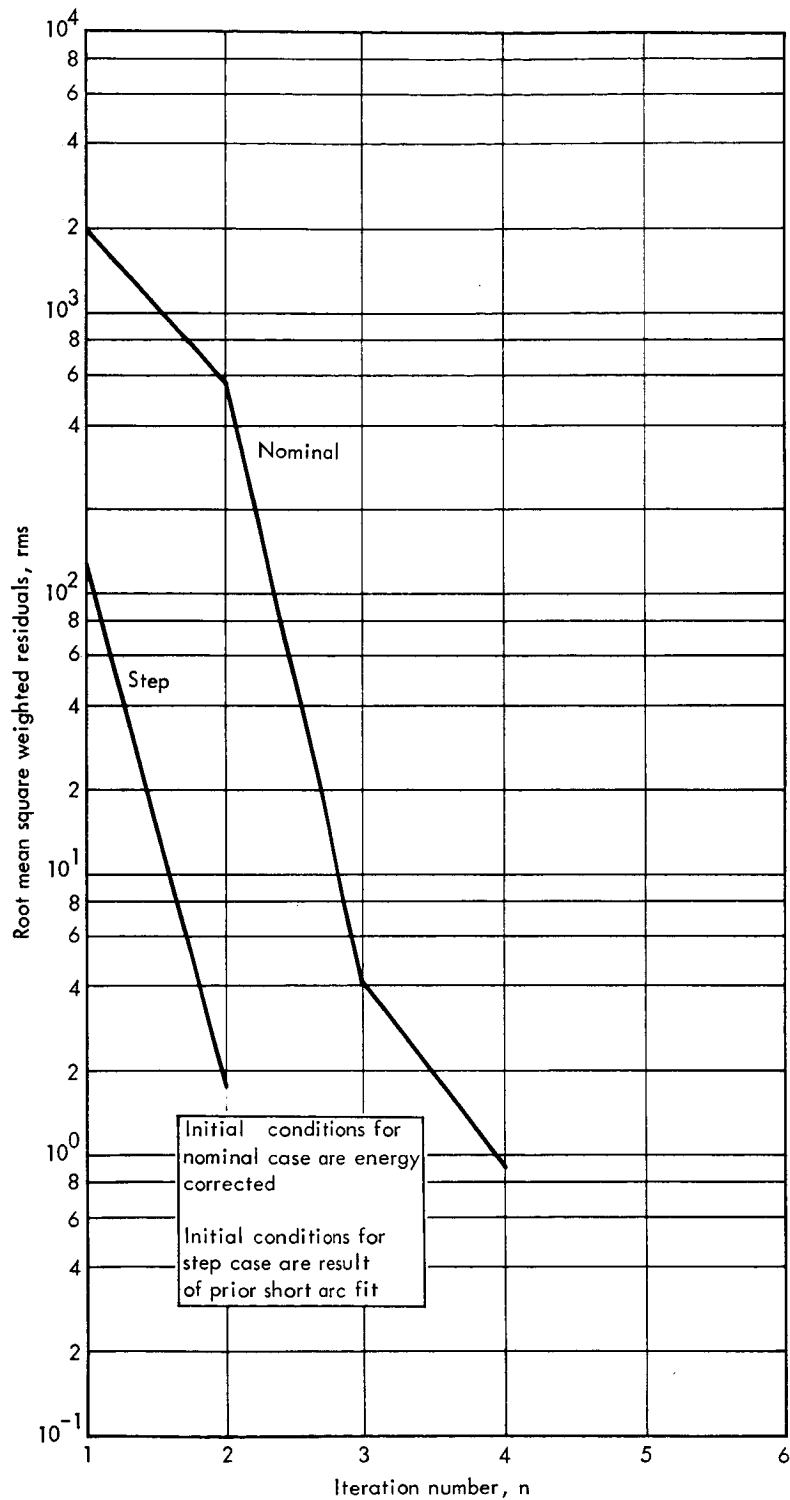


FIGURE 10. — EFFECT OF STEP FIT WITH 300 MINUTES OF DATA

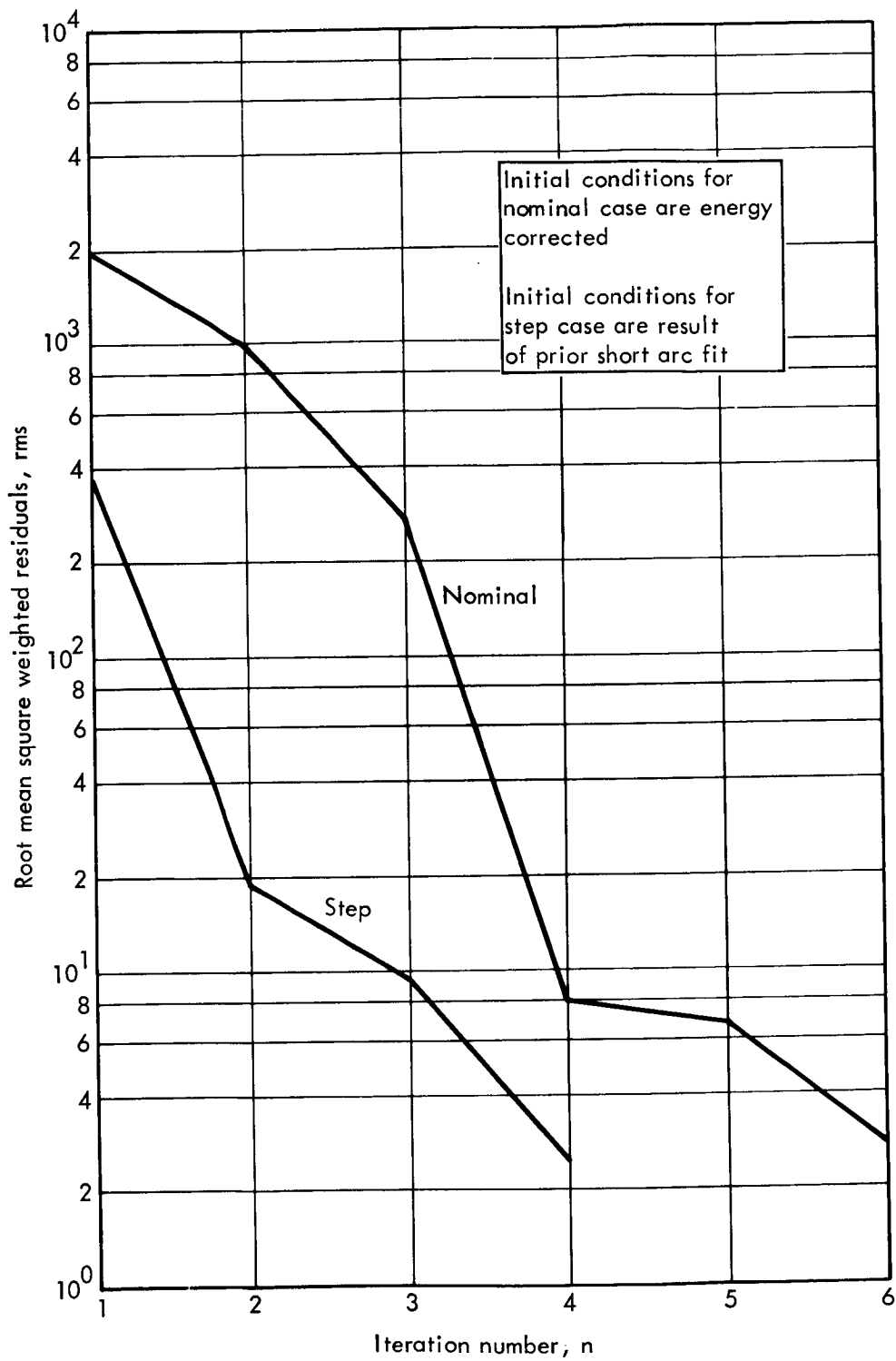


FIGURE 11. — EFFECT OF STEP FIT WITH 1000 MINUTES OF DATA

It is imperative that the state vector be in a selenocentric coordinate system when an epoch shift is initiated. If the geocentric state vector with a perturbed time tag is input as initial conditions, the motion of the moon during this interval is unaccounted for, thereby shifting the position of the satellite (with respect to the moon) by a vector equal to the difference of the two position vectors of the moon at the initial time and the perturbed epoch time.

By shifting the epoch time 10 minutes, and stating the initial conditions in selenocentric coordinates, a 30° in-plane error was simulated. Since the selenocentric position and velocity vectors of the satellite (in a 340 minute orbit) change rapidly with time, it was necessary to constrain, i. e., bound, the size of the solution vector. Since the position and velocity vectors are nonlinear over such a time interval, the unrestrained solution was divergent. However, the bounded correction vector eventually (10 iterations) changed the initial estimate to the position and velocity of the perturbed epoch time (10-minute shift).

This technique can be extended to a situation where the satellite goes behind the moon before acquisition. When the satellite becomes visible again, the residuals due to a poor initial period estimate could be very large. As will be shown in a later section, a poor initial period estimate is best recovered by using a short arc of tracking immediately after injection into a lunar orbit. However, if the satellite is occulted before any data is acquired, either because the satellite becomes occulted almost immediately after deboost or a tracking malfunction prevents acquisition at the critical time, this critical data near the deboost point is missing. The situation is not hopeless, however.

When the satellite comes back on the visible side of the moon, the time at which the range-rate is zero, and/or when the range is minimum, can be noted. When this time is compared to the computed time (from the initial estimate) of zero range-rate crossing time and minimum range, a period difference is obtained. By updating the computed time to the observed time, that is increasing the reference time by the observed period, the large residuals which would have occurred will be avoided. A short tracking arc as the satellite passes near the epoch should yield the actual state vector. As in the test mentioned, it may be necessary to bound the solution, as large nonlinearities are encountered in this type of differential correction.

3.3.2 Techniques for Handling Nonlinearity Problems

Bounded solutions to the normal equation. - The differential correction process depends upon the appropriateness of a linear approximation to a nonlinear function. In the event that computed corrections from the linear approximations are too large, the correction may be a divergent one. It is the function of the bounds to limit the size of the correction so that the linear approximation is valid. (See References 2 and 3.)

The basic problem of orbit determination is to find values for the parameters x such that the weighted residuals $\delta y, = y_m - y_c(x)$ are minimized in the least squares sense. $z_m =$ observed data, $y_c =$ computed data based on initial estimate. The problem of minimizing $f(x) = \|y_m - y_c(x)\|^2$ is nonlinear in x and is approximated by a linear problem. That is, finding a δx such that

$$f_1(\delta x) = \|y_m - y_c(x_0) - A \cdot \delta x\|^2 \quad (16)$$

or

$$f_1(x) = \|A \cdot x - y_{mc}\|^2 \quad (17)$$

is a minimum. As in the notation of section 3.1.1, A is the matrix of partial derivatives of observations with respect to the state vector parameters, x .

In the development which follows, only two parameters will be considered in order to permit graphical interpretation.

That is,

$$\delta x = \begin{pmatrix} x_1 \\ x_2 \end{pmatrix} = \begin{pmatrix} x \\ y \end{pmatrix} \quad (18)$$

The surface f will be represented above the $x_1 - x_2$ plane by its contour lines. The contour lines of $f_1(\delta x)$ are ellipses, and to the extent that the residuals, δy , are linear in x , the true surface $f(x)$ exhibits the same property.

When, as is usually the case, the residuals are not linear in δx , the surface

$$\delta y(x) = \|y_m - y_c(x_0 + \delta x)\|^2 \quad (19)$$

is not quadratic. In such a case, the orbit determination process is executed in the following sequence (iteratively):

- (a) Accumulate the $A^T A$, $A^T b$, and $b^T b$ matrices; b is the column vector of residuals. The $A^T A$ matrix represents the shape of the quadratic surface; $A^T b$, the direction of its gradient; and $b^T b$, the contour level of the point x_0 .
- (b) The $A^T A$ matrix is then used to approximate the quadratic surface, and its minimum point, x , is taken as the next approximation to the minimum point of the true surface, $f(\delta x)$.
- (c) The predicted height of the estimate x' is compared with $\|\delta y\|^2$. If the difference is insignificant, the process is said to be converged; otherwise, the procedure (a), (b), (c) is repeated.

Repeating the process is no assurance that the next (nth) iteration will be a converging one. If the following (n+1) iteration is converging, the intervening divergence is ignored. This is not likely to happen, since the diverging solution is not as good (not as high a contour level) as the previous solution. It is best to go back to the best previous estimate, and constrain the correction $\delta x'$ such as to assure convergence.

To restrict the size of the correction, an ellipse is drawn in the parameter space ($x_1 - x_2$ plane) with specified axes in the coordinate directions. (See figure 12.) The dimensions of the ellipse are specified on input by the analyst. The minimum of the approximating quadratic surface, $f_1(\delta x)$, is found along the bounding ellipse. This point, x' , is also the minimum point on $f_1(\delta x)$ within the bounding ellipse.

Mathematically, the problem is to minimize

$$f_1(\delta x) = \|A \cdot \delta x - \delta y\|^2 \quad (20)$$

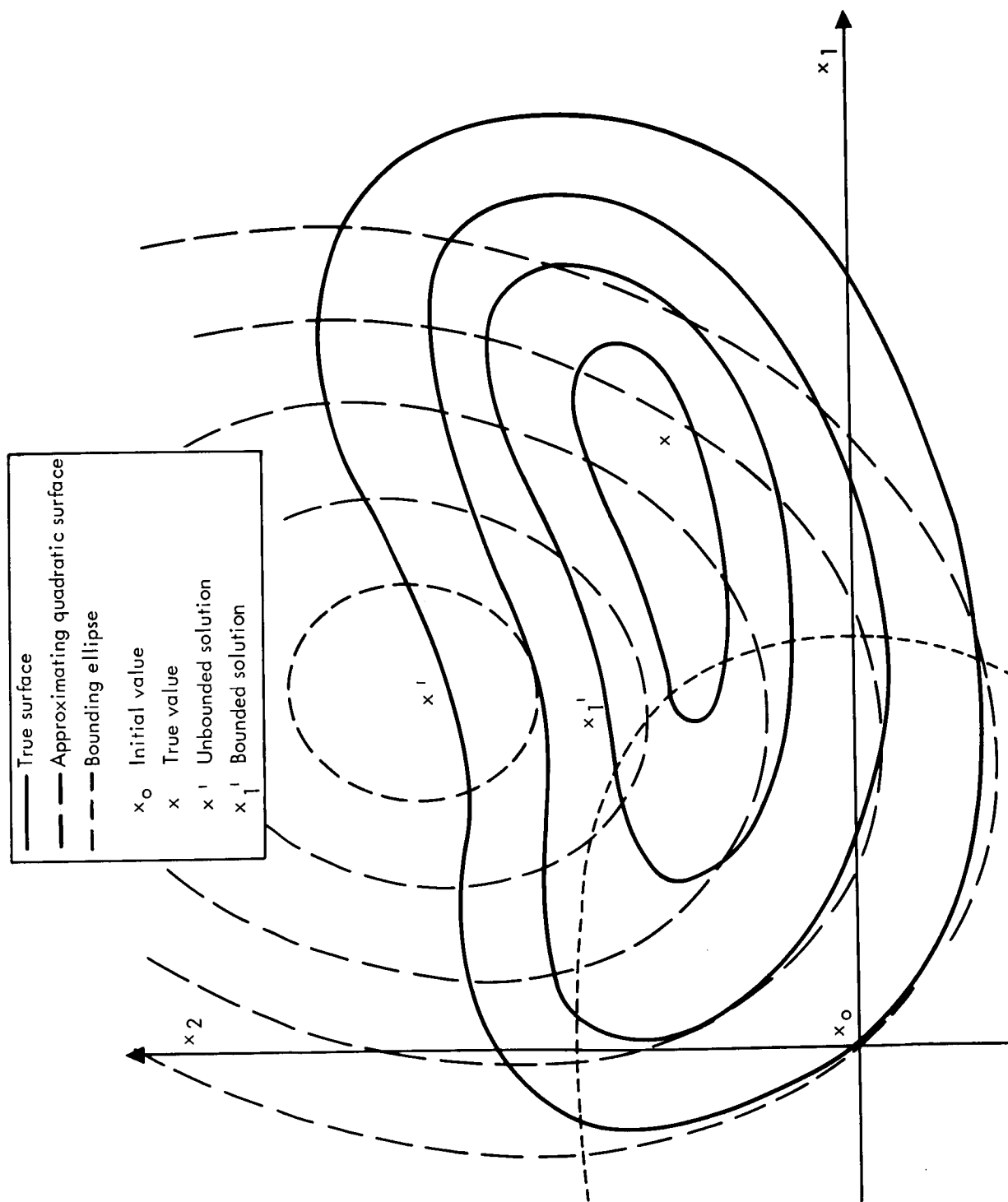


FIGURE 12. — APPROXIMATING QUADRIC SURFACE AND BOUNDING ELLIPSE

such that

$$\| B \cdot \delta x \|^2 \leq 1 \quad (21)$$

where B is a diagonal matrix whose elements b_{ii} is the bound (input) on the i^{th} variable and the semiaxis of the ellipse. Actually, an estimate, $\delta x'$ is first computed which locates the minimum of the approximating quadratic surface, i. e. ,

$$\delta x' = (A^T A)^{-1} A^T b \quad (22)$$

If the condition of equation (20) is met, the minimum point already lies within the bounding region. If the condition is not met ($\|B \cdot \delta x'\|^2 > 1$), a new function,

$$F(\delta x) = f_1(\delta x) + d \|B \cdot \delta x\|^2 \quad (23)$$

equation (23), is minimized. As the value of d increases, the minimization of F requires smaller and smaller values of δx , the correction. By iteration, a value of d is found such that $\|B \cdot \delta x\|^2 = 1$. The minimization of F is then

$$F = f_1(\delta x) + d \|B \cdot \delta x\|^2 = f_1(\delta x) + d \quad (24)$$

which is equivalent to minimizing f, since they differ only by a constant, d. Therefore the point x_1' ,

$$x_1' = x_0 + \delta x_1' \quad (25)$$

minimizes $f_1(\delta x)$ along the bounding ellipse $\|B \cdot \delta x\| = 1$. It can be shown that x_1' minimizes $f_1(\delta x)$ within the ellipse also.

In actual practice, the bounds are automatically adjusted to compensate for divergence and for convergent steps which are "too slow"; that is, not permitting large enough steps while still preserving the linearity assumptions. In the AT85 Program, the bounds are halved if an iteration yields a larger sum of squares of weighted residuals. If this fails, the bounds are halved again, until the solution is constrained to a linear region. The process stops when one-eighth bounds are reached and the iteration is still divergent. On the other hand, if the new sum of

squares is less than the previous iteration and within a certain range of the predicted sum of squares, the bounds are doubled to permit larger corrections. There is a test criterion for doubling bounds which involves comparing the predicted sum of squares with the actual sum of squares. This is covered in the appendix.

Figures 13 and 14 depict the convergence rates for 60- and 300-minute differential corrections — bounded and unrestrained. All initial conditions are energy corrected. For both data arcs, the unrestrained solution converges in fewer iterations than the bounded solution.

Most of the short arc fits did not require a bounded solution. In fact, bounding the solution tended to retard convergence, though it did not prevent convergence. In some special situations which would tend to be divergent, such as one-station-only differential corrections, the bounds prevented large divergent steps from which the program could not have recovered. For very long data arcs (greater than two revolutions) initial conditions that are energy corrected only should have a restricted solution. No generalization can be made concerning the convergence of an unrestrained solution. Some cases converged nicely, while others impacted the moon, etc. Restricting the solution vector of these divergent cases achieved convergent iterations, although many iterations are needed to achieve final convergence. As shown previously, long data arcs should be handled with the step fit technique, which does not require a bounded solution.

As a final illustration of the use of a bounded solution, an AOP6 data arc curve fit is considered. The 6σ perturbations in inclination and node (5° , 12° respectively) are much larger than normal corrections to these elements in a differential correction. As can be seen in figure 15, a 45-minute data arc diverges if the solution is unrestrained but converges with a bounded solution. The convergence rate is lower than the unrestrained case; however, the smaller corrections lead to a successful conclusion, whereas the unrestrained solution is divergent.

A priori statistical information. — The distinction between the use of a priori information as a statistically independent estimate of the state

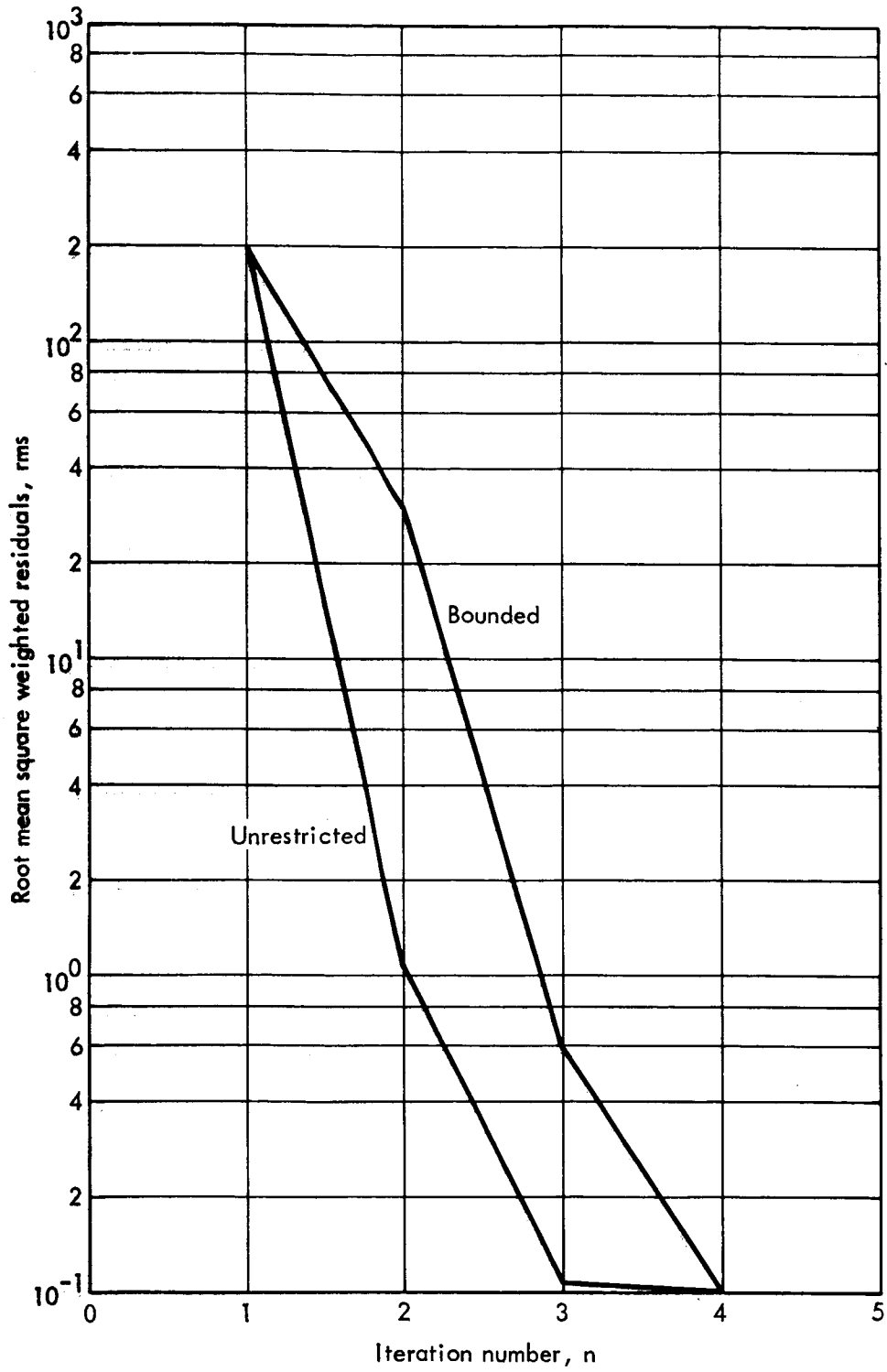


FIGURE 13. — EFFECT OF BOUNDED SOLUTION ON SHORT ARC FIT

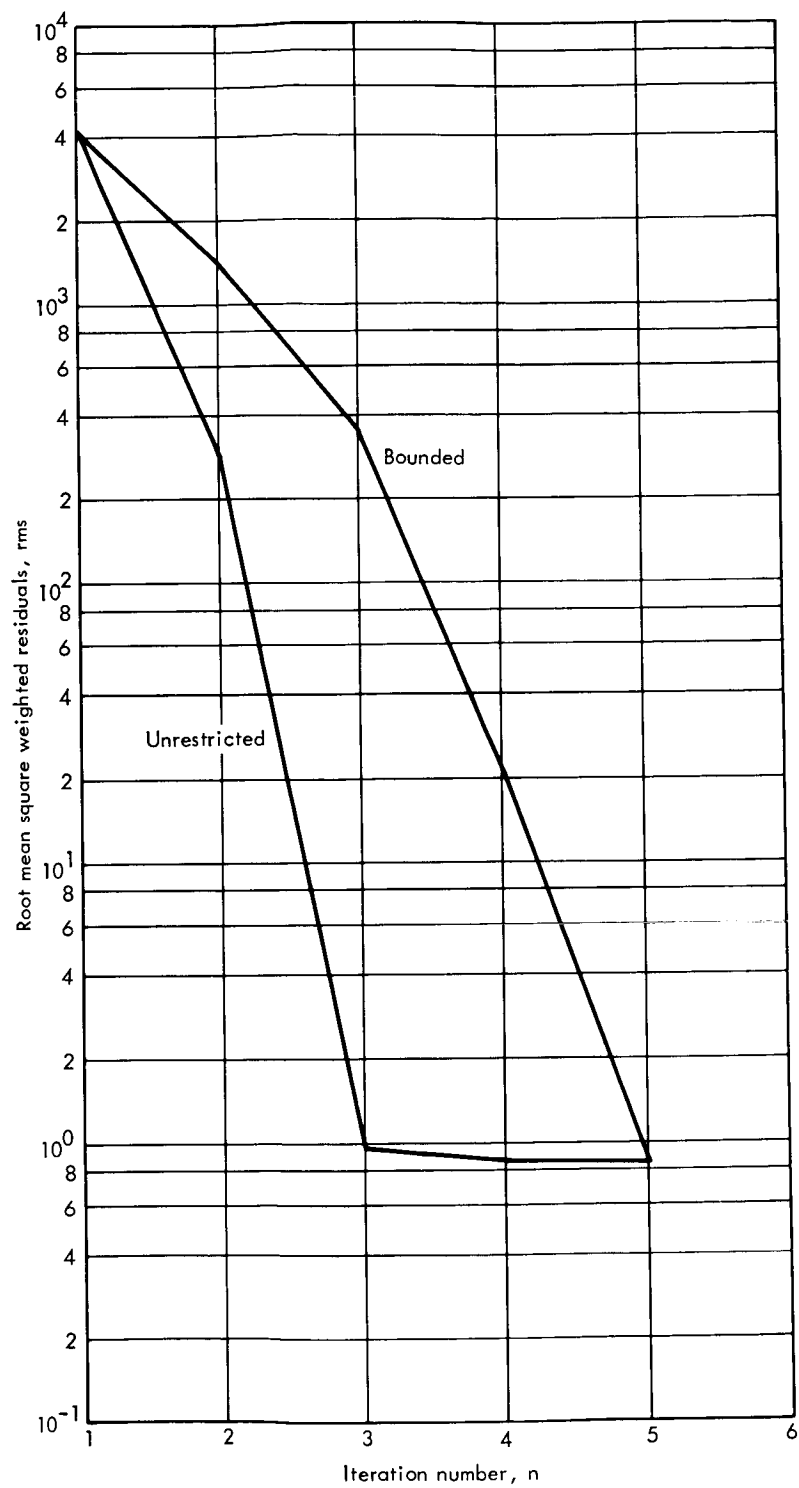


FIGURE 14. — EFFECT OF BOUNDED SOLUTION ON LONG ARC FIT

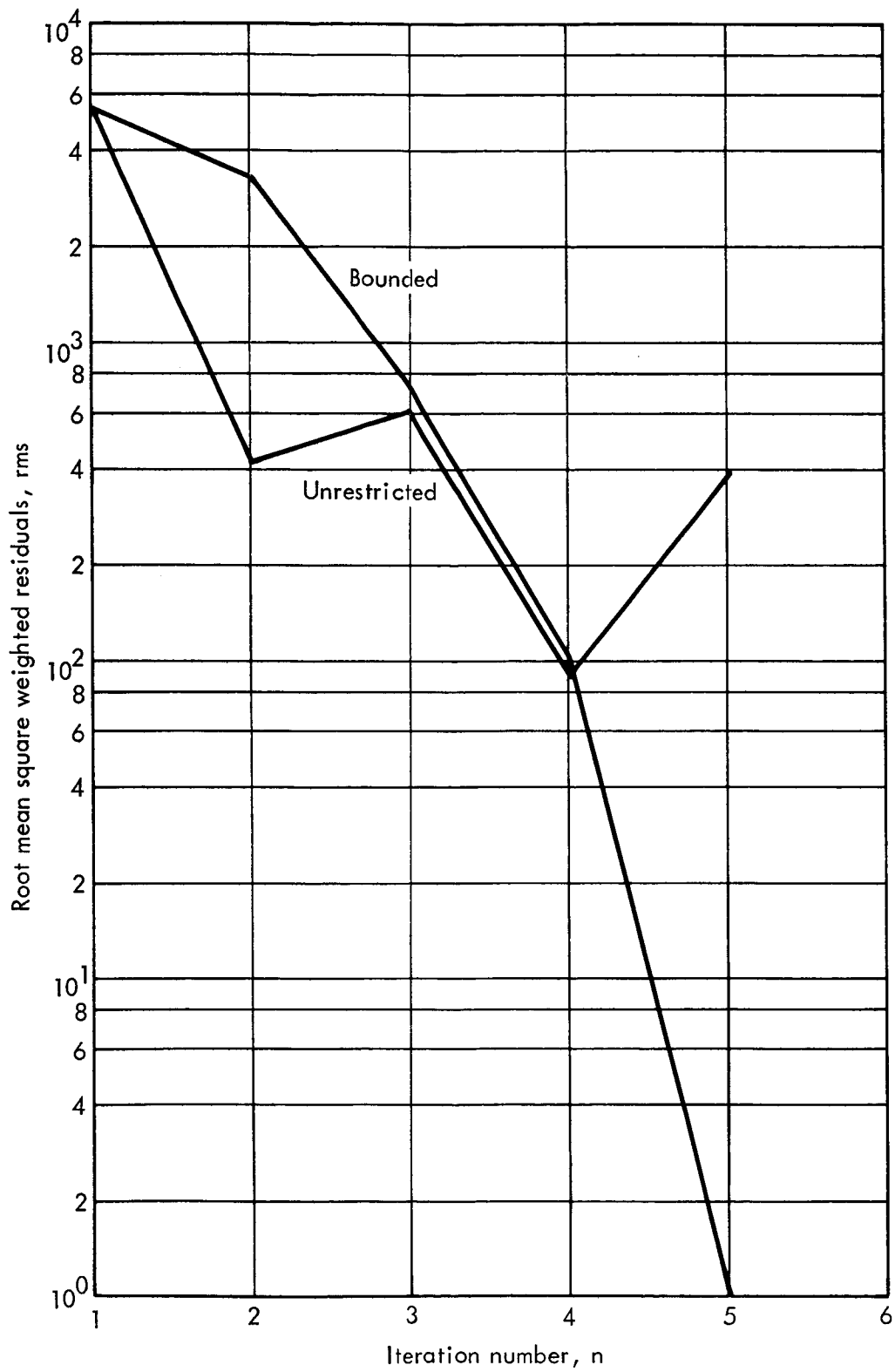


FIGURE 15. — EFFECT OF BOUNDED SOLUTION ON 6σ OBSERVED ORBIT

vector and as a technique to limit the solution vector needs to be clearly made. The handling of the a priori, and indeed the normal equation, are different in these two applications. Unfortunately, the same name is used to describe both applications. In the first application, the a priori information matrix reflects the confidence to be placed in the a priori state vector estimate, while in the second application an arbitrary matrix of numbers (of the appropriate dimension) is added, with no particular physical interpretation, to the normal matrix to make the corrections smaller. In the former case, the answer is the combined estimate, including contributions from both tracking performance and a priori knowledge. When the added matrix is used in a conditioning device, as described in the second application, the final answer is not affected.

Suppose it is desired to estimate a parameter x , given two other estimates of x , x_1 , and x_2 with associated covariance matrices Σ_1 and Σ_2 . The minimum variance unbiased estimate formed by a linear combination of x_1 and x_2 can be found by a simple construction.

More specifically, the problem is that of combining an a priori estimate of the state vector, x_P , with the a priori covariance matrix, Σ_P , with a state vector estimate and covariance matrix obtained from tracking information, x_T and Σ_T . The handling of the a priori knowledge from iteration to iteration, as the tracking estimate changes, must also be considered.

Differential correction is based on a linearized equation relating the first order differentials in the observations to the solution parameter corrections,

$$\delta y = A (x - x_R) + \epsilon \quad (26)$$

where y represents the observed minus computed residual, x_R is the state vector which is the basis for the linearization, x is the current state vector estimate, and A is equal to the matrix of derivatives of observations with respect to the orbital parameters. The weighted least squares estimate, $(\hat{x} - x_R)$, of $(x - x_R)$ is then

$$\hat{x} - x_R = A^T W A^{-1} A^T W \delta y \quad (27)$$

This is also the minimum variance unbiased linear estimate when the radar noise vector, n , has normally distributed, zero mean components, and the weighting matrix, W , is equal to the inverse of the noise covariance matrix; that is,

$$W = \Sigma_{\epsilon}^{-1} \quad (28)$$

The combined estimate may be calculated from equation (26), given the unbiased estimates and covariances matrices from a priori knowledge, q_p and Σ_p , respectively, and x_T and Σ_T from tracking. For this purpose, the observable becomes the state vector itself, and the residual becomes the difference in the state vectors,

$$\delta y = \begin{bmatrix} x_P - x_R \\ \text{-----} \\ x_T - x_R \end{bmatrix} \text{ and } A = \begin{bmatrix} I \\ \text{-----} \\ I \end{bmatrix}$$

Hence, rewriting equation (26), in terms of the combined estimate,

$$\begin{bmatrix} x_P - x_R \\ \text{-----} \\ x_T - x_R \end{bmatrix} = \begin{bmatrix} I \\ \text{-----} \\ I \end{bmatrix} (x - x_R) + \begin{bmatrix} \epsilon_P \\ \text{-----} \\ \epsilon_T \end{bmatrix} \quad (29)$$

where n_P and n_T are column vectors reflecting the errors in the a priori and tracking estimates, respectively. From the definition of the covariance matrix of a vector, the combined noise covariance matrix is written,

$$\begin{aligned} \Sigma_{\epsilon} &= E \begin{bmatrix} \epsilon_P \\ \text{-----} \\ \epsilon_T \end{bmatrix} \begin{bmatrix} \epsilon_P^T & \epsilon_T^T \end{bmatrix} \\ &= \begin{bmatrix} \Sigma_P & \Sigma_{PT} \\ \text{-----} & \text{-----} \\ \Sigma_{TP} & \Sigma_T \end{bmatrix} \end{aligned} \quad (30)$$

$$\hat{x} - x_R = \left\{ \begin{bmatrix} I & I \end{bmatrix} \begin{bmatrix} \Sigma_P & \Sigma_{PT} \\ \text{-----} & \text{-----} \\ \Sigma_{TP} & \Sigma_T \end{bmatrix}^{-1} \begin{bmatrix} I \\ \text{-----} \\ I \end{bmatrix} \right\}^{-1} \begin{bmatrix} I & I \end{bmatrix} \begin{bmatrix} \Sigma_P & \Sigma_{PT} \\ \text{-----} & \text{-----} \\ \Sigma_{TP} & \Sigma_T \end{bmatrix}^{-1} \begin{bmatrix} x_P - x_R \\ \text{-----} \\ x_T - x_R \end{bmatrix} \quad (31)$$

Assuming that the a priori estimate and the tracking estimate are uncorrelated,

$$\Sigma_{PT} = \Sigma_{TP} = 0$$

equation (31) simplifies to

$$\hat{x} - x_R = \left[\Sigma_P^{-1} \right]^{-1} \left[\Sigma_P^{-1} (x_P - x_R) + \Sigma_T^{-1} (x_T - x_R) \right] \quad (32)$$

Using the following equivalences from the normal equation which is accumulated to compute the tracking estimate

$$1) \quad \Sigma_T^{-1} = A^T W A$$

and $2) \quad \Sigma_T^{-1} (x_T - x_R) = A^T W \delta y$

We may rewrite (32) as

$$\hat{x} - x_R = \left[A^T W A + \Sigma_P^{-1} \right]^{-1} \left[A^T W \delta y + \Sigma_P^{-1} (x_P - x_R) \right] \quad (33)$$

Since the above equation is to hold on each of several iterations during which the reference state vector, x_R , and the tracking normal matrix Σ_T^{-1} , or $A^T W A$, will be changing, a subscript notation is introduced to indicate which iteration through the data was used to generate the estimate. Equation (33) becomes,

$$\hat{x}_i - x_{R_i} = \left[(A^T W A)_i + \Sigma_P^{-1} \right]^{-1} \left[(A^T W \delta y)_i + \Sigma_P^{-1} (x_P - x_{R_i}) \right] \quad (34)$$

For the first iteration, $i = 1$, the reference state vector is set equal to the a priori estimate.

$$x_{R1} = x_P \quad (35)$$

Substituting into equation (34)

$$\hat{\mathbf{x}} - \mathbf{x}_{R1} = \left[(\mathbf{A}^T \mathbf{W} \mathbf{A})_1 + \Sigma_P^{-1} \right] \left[(\mathbf{A}^T \mathbf{W} \delta \mathbf{y})_1 \right] \quad (36)$$

For all subsequent iterations, the estimates are combined as in equation (34).

Statistical interpretation of the a priori covariance matrix. — Some authors (reference (4)) raise objections to using an a priori covariance matrix based on a guidance error analysis. The objection stems from the definition or meaning of an error or standard deviation on a guidance system component. Empirical estimates of an error on a particular component are obtained by simulating flight conditions from which the probability function is determined. Therefore the covariance matrix, Σ_P , reflects estimates of the variances and covariances, i. e., a statistical average of all flights designed to achieve given nominal injection conditions.

In order to weigh the covariance matrix properly, it should be influenced by the particular flight at hand. Hence, any in-flight data (prior to nominal injection) from the guidance system should be weighed heavily in evaluating the a priori state vector and covariance matrix, \mathbf{x}_P and Σ_P . If a component failed, the a priori estimates could be considerably different from the designed values.

Therefore, the use and validity of a priori estimates seems limited to the early orbit determination of a space probe. Usually a very large (pessimistic) covariance matrix, Σ_P is assumed, thereby reflecting an initial solution which is unrestrained.

Many test cases were set up to determine the effects of an a priori covariance matrix on convergence. The test cases were matched with respect to the tracking situation, and were run in tandem — one with a priori information, and the other without.

A priori information, the covariance matrix listed in appendix A, did not affect the convergence rate or the quality of the tracking estimate. Inspection of the tracking normal matrix and the inverse of the a priori

covariance matrix explains why the latter did not affect the solution. Referring to equation (32), it can be seen that these two normal matrices are added ($\Sigma_P^{-1} = 0$, if there is no a priori covariance estimate). The tracking normal matrix and the a priori normal matrix are tabulated in table II and table III, respectively. When these two matrices are added, the tracking normal matrix is unaffected to at least six decimal places. The normal matrix for 3 minutes of tracking was included for comparison purposes, as it was the smallest (in terms of the elements) available. Because of the large uncertainties associated with only 3 minutes of tracking, a much longer tracking arc is required for a solution with acceptable uncertainties. A minimal tracking interval of 15 minutes, with two sensors as determined in the aforementioned section, has a normal matrix with elements which are nearly an order of magnitude larger. Hence, under these conditions, the accumulated normal matrix is unaffected for at least seven leading digits by the a priori matrix. This explains the negligible effect of a priori information on the convergence tests.

TABLE II.—TRACKING NORMAL MATRIX, 3 MINUTES TRACKING, TWO SENSORS

1. 13733E-3	5. 35534E-4	1. 71139E-4	1. 37027E-1	6. 42346E-2	2. 04928E-2
	2. 53320E-4	8. 08864E-5	8. 91175E-2	4. 18096E-2	1. 33252E-2
		2. 60732E-5	3. 06943E-2	1. 43980E-2	4. 59554E-3
			1. 13705E3	5. 32808E2	1. 69991E2
				2. 49807E2	7. 95205E1
					2. 55474E1

SYMMETRIC

TABLE III.—A PRIORI NORMAL MATRIX

2. 64890E-10	-1. 58197E-10	-1. 36559E-10	3. 23647E-8	2. 60865E-8	3. 05697E-8
	2. 51607E-10	-1. 51674E-10	2. 60865E-8	2. 10263E-8	2. 46398E-8
		2. 40516E-10	3. 05697E-8	2. 46398E-8	2. 88744E-8
			7. 37806E-5	-4. 40631E-5	-3. 80362E-5
				7. 00810E-5	-4. 22463E-5
					6. 69915E-5

SYMMETRIC

The effect of very optimistic a priori knowledge was simulated by arbitrarily multiplying the elements of the a priori matrix by 10^4 . The tracking normal matrix was no longer insensitive to the addition of the a priori matrix; however, since the modified a priori normal matrix reflected very optimistic (and unwarranted) confidence in the initial estimate, the differential correction converged to an erroneous state vector. The associated covariance matrix reflected very small uncertainties; as expected. Although the differential correction was convergent and the a priori matrix was sensed in the normal equation, the technique is statistically invalid. In fact, if the a priori covariance matrix is sufficiently small, the program will ignore the tracking data, and return the a priori estimate.

As was pointed out earlier, injection or deboost a priori information has limited use unless it can be increased by, for example, tracking during the deboost maneuver. The above results suggest that the use of the existing pessimistic a priori knowledge amounts to relying on the tracking for orbital improvement.

Normal matrix conditioning.—The use of an arbitrary matrix to control the size of the corrections on each iteration is termed normal matrix conditioning. The normal equation has the form

$$\mathbf{x} - \mathbf{x}_R = \left[\mathbf{A}^T \mathbf{W} \mathbf{A} + \Sigma_P^{-1} \right]^{-1} (\mathbf{A}^T \mathbf{W} \delta \mathbf{y}) \quad (37)$$

This is identical to the normal equation on the first iteration when using a priori knowledge. With proper selection of Σ_P^{-1} , the size of the correction can be limited, thus avoiding nonlinearities. However, this arbitrary selection of the conditioning matrix destroys the statistical significance of the covariance estimate. The conditioning matrix has to be selected by hand, as the solution is sensitive to the size of the elements (normally diagonal). This constraint makes it undesirable to use in a real-time operation. Appropriate conditioning matrices would have to be found for all possible tracking situations; that is, for all orbital geometries, data types, tracking intervals, etc. The bounds technique used in the AT85 Orbit Determination Program is essentially an automated and refined version of this procedure.

At convergence, the gradient of the approximating quadratic surface,

$$\begin{aligned}
 \text{Grad } (\delta y - A\delta x)^T (\delta y - A\delta x) &= 0 \\
 &= \frac{\partial}{\partial \delta x} (\delta y^T \delta y + 2\delta x^T A^T \delta y + 2\delta x^T A^T A \delta x) \Big|_{\delta x} = 0 \\
 &= A^T A \delta x - 2A^T \delta y \Big|_{\delta x} = 0 \\
 &= -2A^T y = 0
 \end{aligned}$$

Thus, it can be seen that equation (37), when used in a series of iterations, will give the same answer regardless of the value of Σ_P^{-1} , since, at convergence, (i. e., when the sum of squares of the residuals has been minimized)

$$A^T W \delta y \equiv 0 \quad (38)$$

Hence, the value of the coefficient $(A^T W A + \Sigma_P^{-1})$ is irrelevant. Although the converged value of the state vector is independent of Σ_P^{-1} , as shown above, the path to the solution is influenced by Σ_P^{-1} , the arbitrary conditioning matrix. The sum of the corrections may be written,

$$\sum_{i=1}^n \delta x_i = \text{constant} \quad (39)$$

where n is the number of iterations and

$$\delta x_i = x_i - x_{Ri} \quad (40)$$

Therefore, from equation (39), it can be seen that the number of iterations, n , required for convergence is not constant, but influenced by the choice of Σ_P^{-1} .

To illustrate the sensitivity of the solution of the normal equation to various conditioning matrices, the convergence rates of a differential correction with varying Σ_P^{-1} matrices are plotted versus iteration number in figure 16. The control case ($n = 0$) had no conditioning matrix;

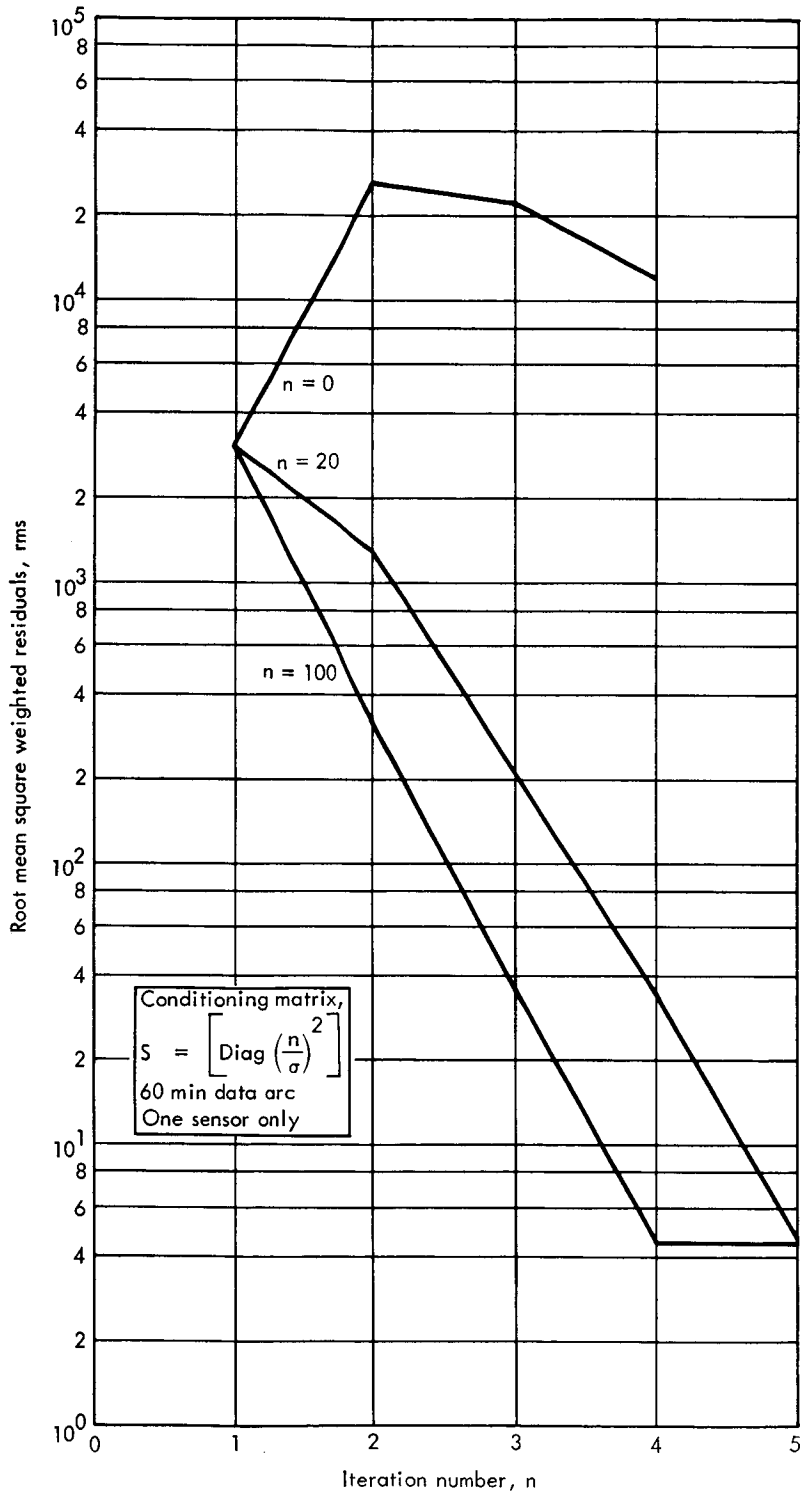


FIGURE 16.— EFFECT OF NORMAL CONDITIONING MATRIX

the tracking situation; one sensor tracking for 60 minutes; the solution is unrestrained. The elements of the diagonal matrix Σ_P , the inverse of the normal conditioning matrix (Σ_P^{-1}), are indicated on the graph. Note that the conditioning matrices cause an otherwise divergent situation to converge, and at a rate depending upon the size of the elements.

3.3.3 Selection of Observational Parameters

Length of data arc. - The length of the tracking span is an important variable in a convergence study, with respect to the quality of the initial estimate, and also to the uncertainty of the converged estimate.

As can be seen from other sections of this report, the tracking span strongly influences the convergence and convergence rates, other observational parameters being equal. The effect of varying the tracking span as it applies to the various other factors affecting convergence is treated in the respective sections of the report.

One of the important characteristics of the differential correction is the uncertainty associated with the tracking estimate or a combination of the a priori estimate and the tracking estimate, as the case may be. The covariance matrix of the unbiased weighted least squares estimate is $(A^T W A)^{-1}$. Referring to equation (33) of section 3.3.2, it can be shown from the definition of the covariance matrix, i. e. ,

$$\Sigma_x \triangleq E \left(\hat{x} - x_R \right) \left(\hat{x} - x_R \right)^T = (A^T W A)^{-1} \quad (41)$$

that the covariance matrix of the combined estimate, a priori information and tracking, is equal to

$$\Sigma_x = \left[A^T W A + \Sigma_P^{-1} \right]^{-1} \quad (42)$$

where $A^T W A$ is the accumulated normal matrix from tracking and Σ_P is the covariance matrix of the a priori estimate.

The interpretation of the covariance matrix is treated in section 3.4.2. As a relative measure of quality of the estimate derived from tracking and/or a priori information, the standard deviation, i.e., the square root of the variance, of the components of position and velocity are plotted as a function of the tracking situation.

The 1σ uncertainties in position and velocity (by components) as a function of tracking span are presented in figures 17 and 18, respectively. The definition of tracking span as it relates to the number of observing sensors should be pointed out.

The visibility span of a lunar satellite for a particular sensor is essentially equal to the time span during which the moon is above the horizon at the particular sensor's location on the topos. Lunar occultation and the slight angular separation of the satellite from the moon's disk are the two effects which will slightly influence the validity of the previous statement.

Therefore, for a particular day, regardless of the lunar satellite orbit orientation, the rise and set times for a given sensor of the satellite are invariant. For the particular day in question, 27 June 1966, the visibility times, by station are as follows:

Station	Acquisition	Set	Tracking Span (Minutes)
Goldstone	4 ^h 0 ^m	8 ^h 45 ^m	285
Woomera	4 ^h 0 ^m	16 ^h 57 ^m	777
Madrid	14 ^h 40 ^m		

Therefore, when comparing the relative state vector uncertainties in figures 17 and 18, it should be kept in mind that there are two sensors tracking simultaneously for the first 285 minutes only. Thereafter, only Woomera can track the satellite until acquisition by Madrid at 14^h 40^m.

For example, with all three DSN sensors tracking, given the first 1000 minutes of data, there are two sensors for the first 285 minutes and only one sensor for the rest of the span. Lunar occultation must also be

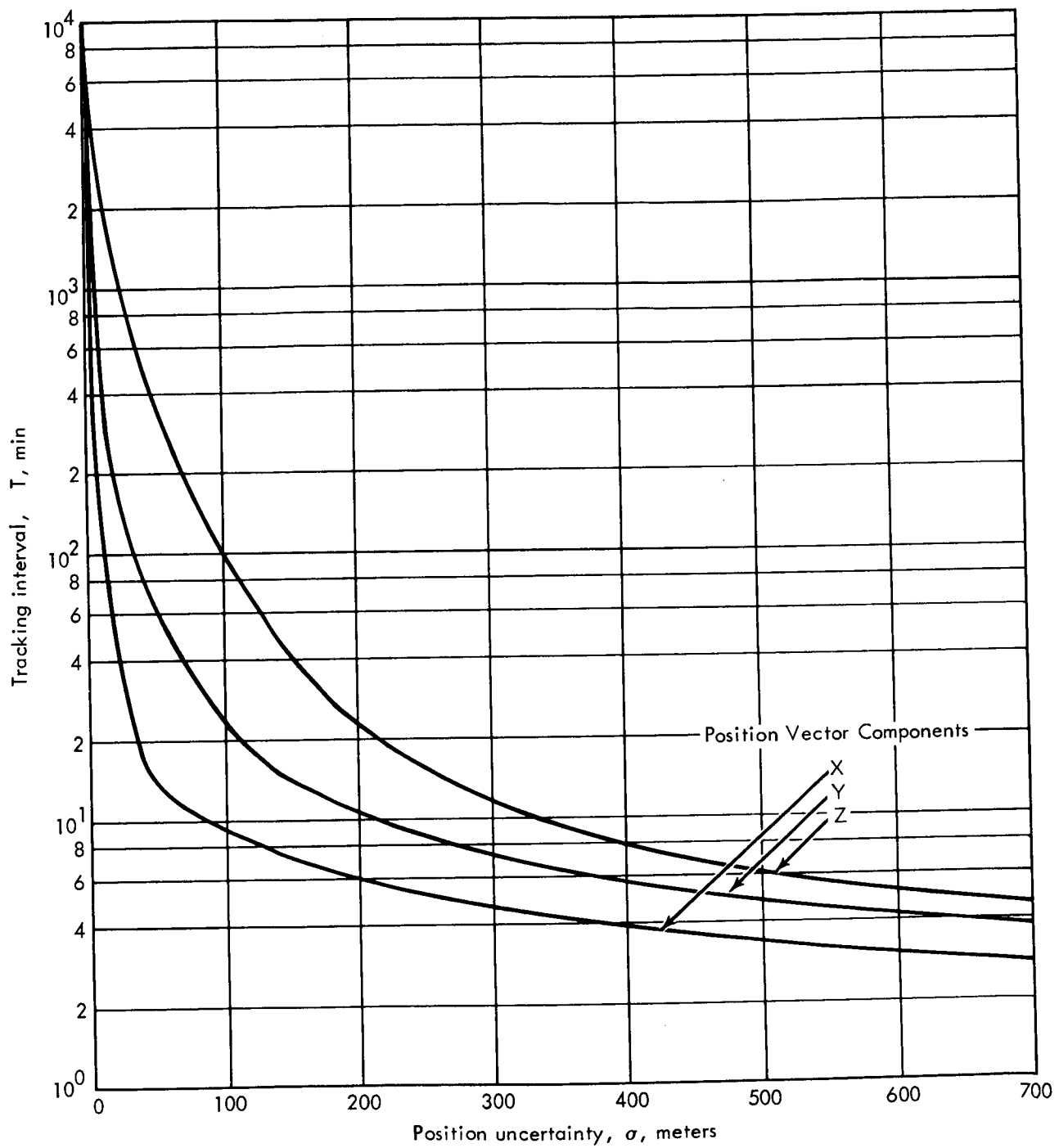


FIGURE 17. — EFFECT OF TRACKING SPAN ON POSITION UNCERTAINTIES (TWO SENSORS)

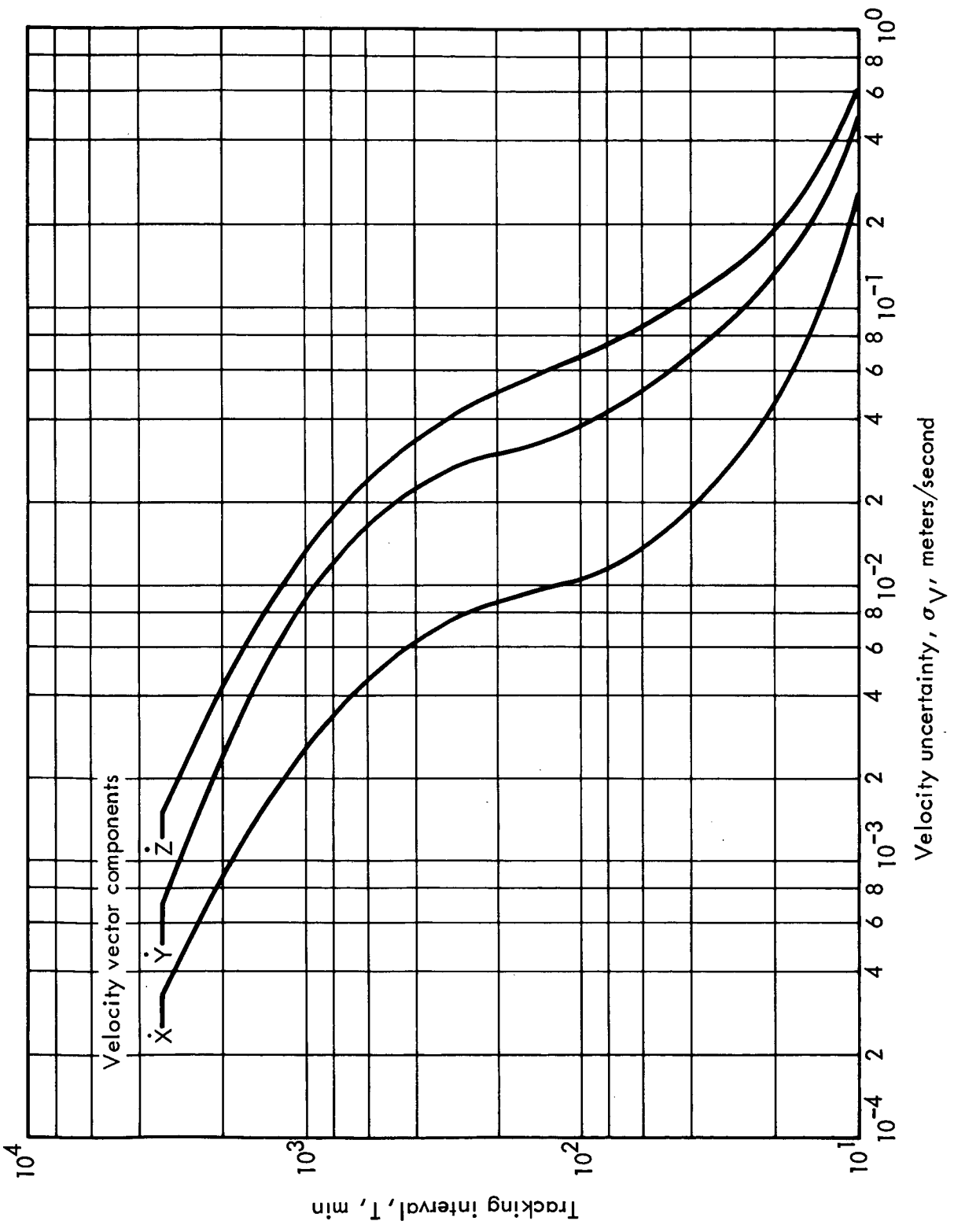


FIGURE 18.— EFFECT OF TRACKING SPAN ON VELOCITY UNCERTAINTIES (TWO SENSORS)

considered. Therefore, the length of the data arc is not proportional to the amount of data, unless there is less than 100 minutes of tracking (from epoch), at which time the satellite is occulted by the moon.

Figure 17 clearly shows that the position uncertainties become quite large with less than 15 minutes of tracking. The velocity uncertainties are about 0.1 m/s for 20 minutes of tracking as seen in figure 18. There is some variation in the locus of the curves of figures 17 and 18 for the alternate lunar satellite orientations. However, the curves included here represent typical values.

Data type.—The effect of data types on differential corrections is not very significant, when compared to the other factors affecting convergence. Figure 19 illustrates the convergence history by iteration of four data type configurations: 1) range-rate only; 2) range only; 3) range and range-rate; and 4) range, range-rate, and angles (right ascension and declination). The convergence rates are about equal, requiring four iterations to achieve convergence.

The 1σ uncertainties in position and velocity by components for the four data type configurations is illustrated in figure 20. The range-rate-only configuration is the only one which suffers any significant accuracy when compared to the other data types. It should be noted that adding angular data to range, range-rate data does not affect the convergence rate nor the quality of the tracking estimate.

The next section is concerned with the number of observing sensors. Since one sensor only has been shown to be inadequate (using range, range-rate data), angles were added to determine if it would improve the differential correction to relatively acceptable (i. e., two sensor) standards. As in the two sensor situation, the convergence rate was unaffected. Similarly, the 1σ uncertainties were virtually unaffected, the addition of angular data improving the tracking estimate negligibly. The uncertainties are tabulated in Table IV.

Number of observing sensors.—From the point of view of geometry, orbital improvement of a lunar satellite orbit by means of a differential correction can become ineffective. During the relatively brief period of

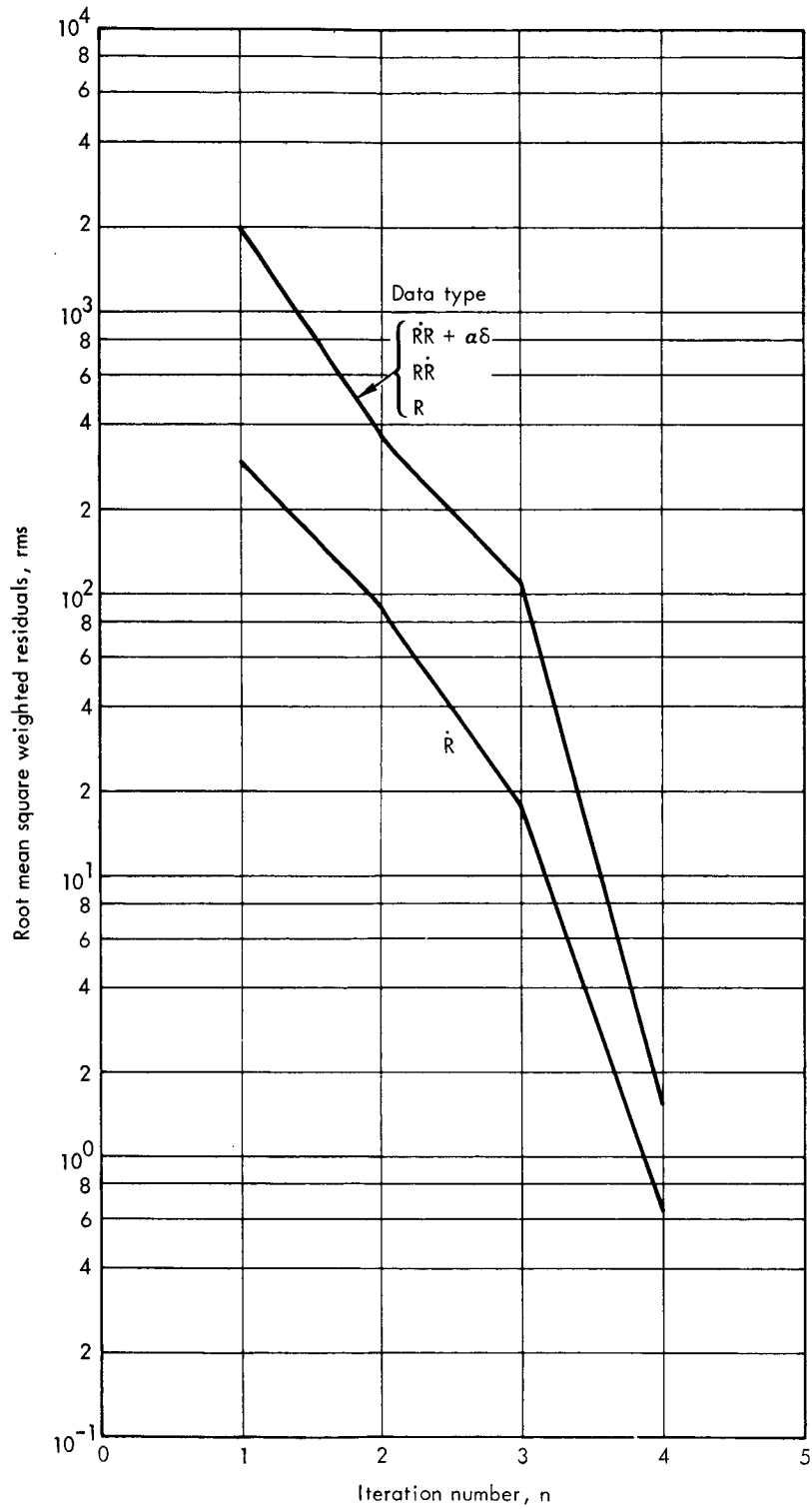


FIGURE 19. — EFFECT OF DATA TYPES ON CONVERGENCE RATE

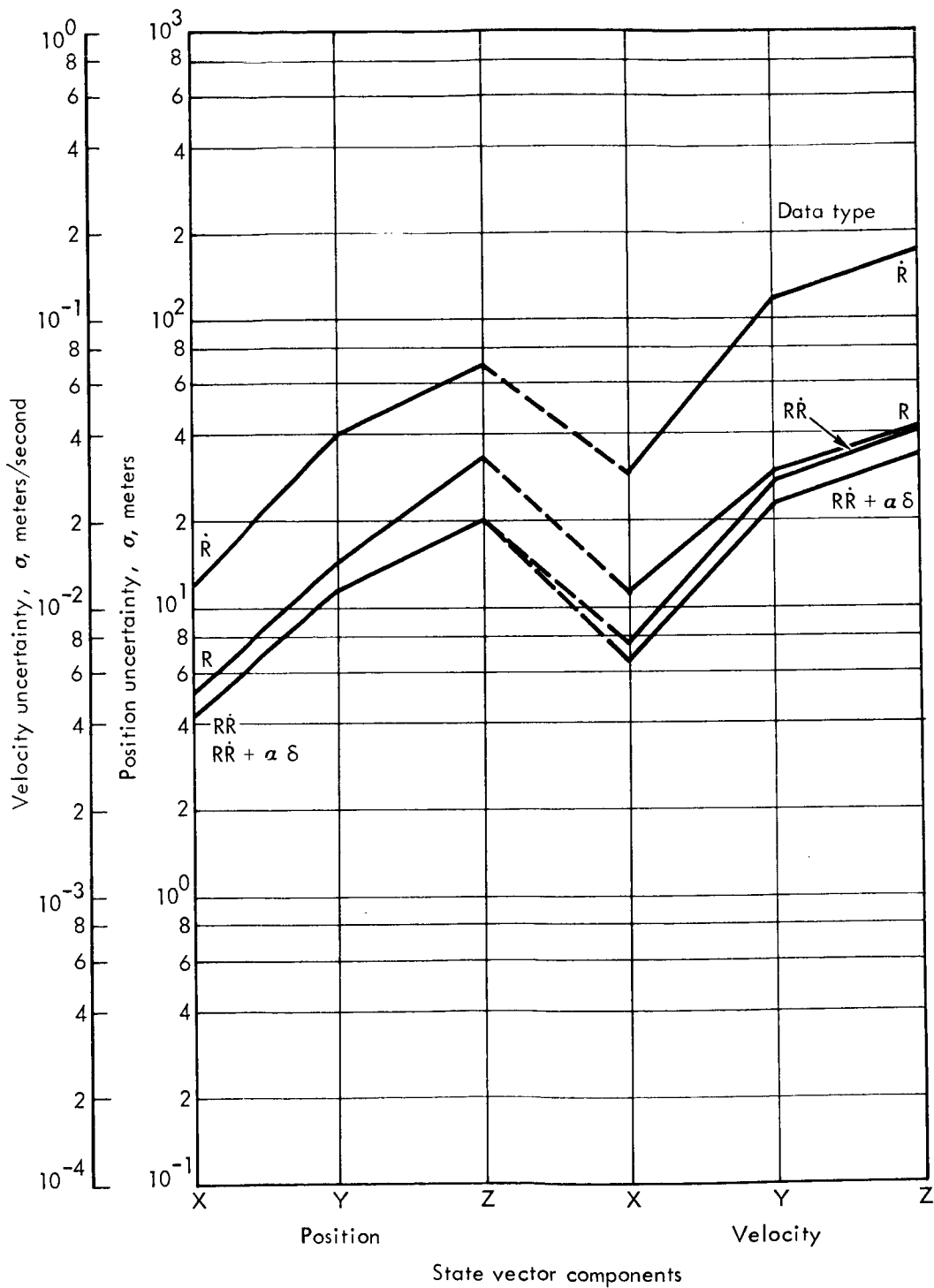


FIGURE 20.— POSITION AND VELOCITY UNCERTAINTIES FOR VARIOUS DATA SET TYPES

TABLE IV.—THE EFFECT OF ANGULAR DATA ON STATE VECTOR UNCERTAINTIES

State Vector Component	Data Set	
	R, \dot{R}	R, \dot{R} plus α, δ
X	18.873	18.861
Y	81.638	81.598
Z	133.710	133.670
\dot{X}	.01351	.01350
\dot{Y}	.05095	.05094
\dot{Z}	.07504	.07503

tracking the satellite before it goes behind the moon, the relative positions of an earth-based sensor and a lunar satellite, at a distance of about 60 earth-radii, are limited. This single sensor geometry restriction gives rise to conditions in which the orbit is difficult to establish; the orbital path is not well determined, geometrically.

The addition of a second sensor to the tracking network greatly enhances the geometry of the situation. In a sense, the two sensors provide the basis for a triangulation determination. Maximum sensor separation provides the best geometric determination, but there is a simultaneous tracking constraint which must be considered. However, since a few hours of simultaneous tracking is adequate to perform a convergent differential correction with small uncertainties, a relatively large sensor separation is possible, thus permitting a mathematically determinate sensor-satellite triangulation.

Geometric indeterminacy is reflected in the uncertainties in the estimate as described by the tracking covariance matrix. The uncertainties in the components of position and velocity for short tracking intervals is presented in figures 21 and 22. Especially significant (figure 22) are the relative velocity uncertainties for the one sensor determination and

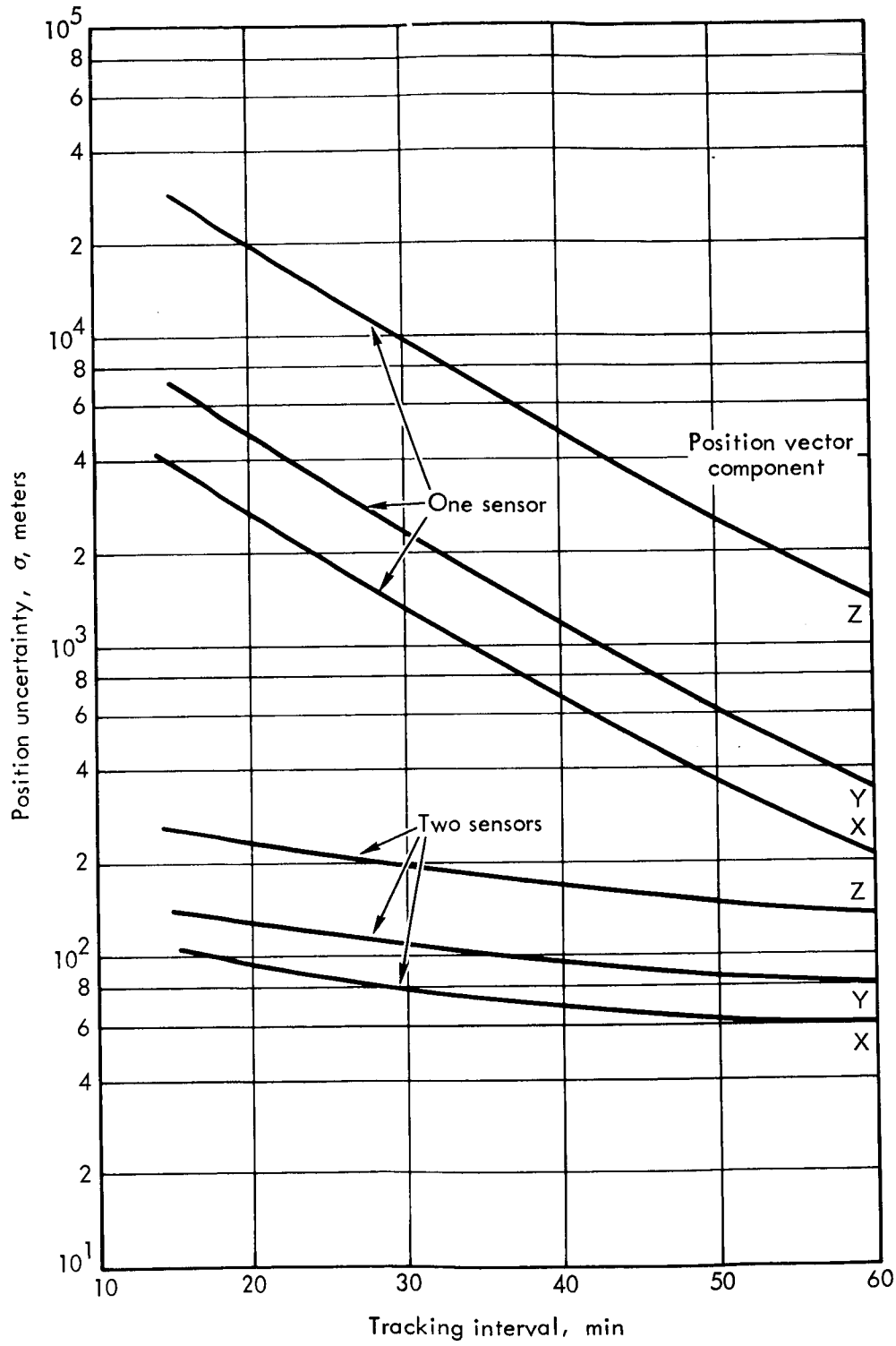


FIGURE 21.— POSITION UNCERTAINTIES USING ONE AND TWO SENSORS FOR SHORT ARC FITS

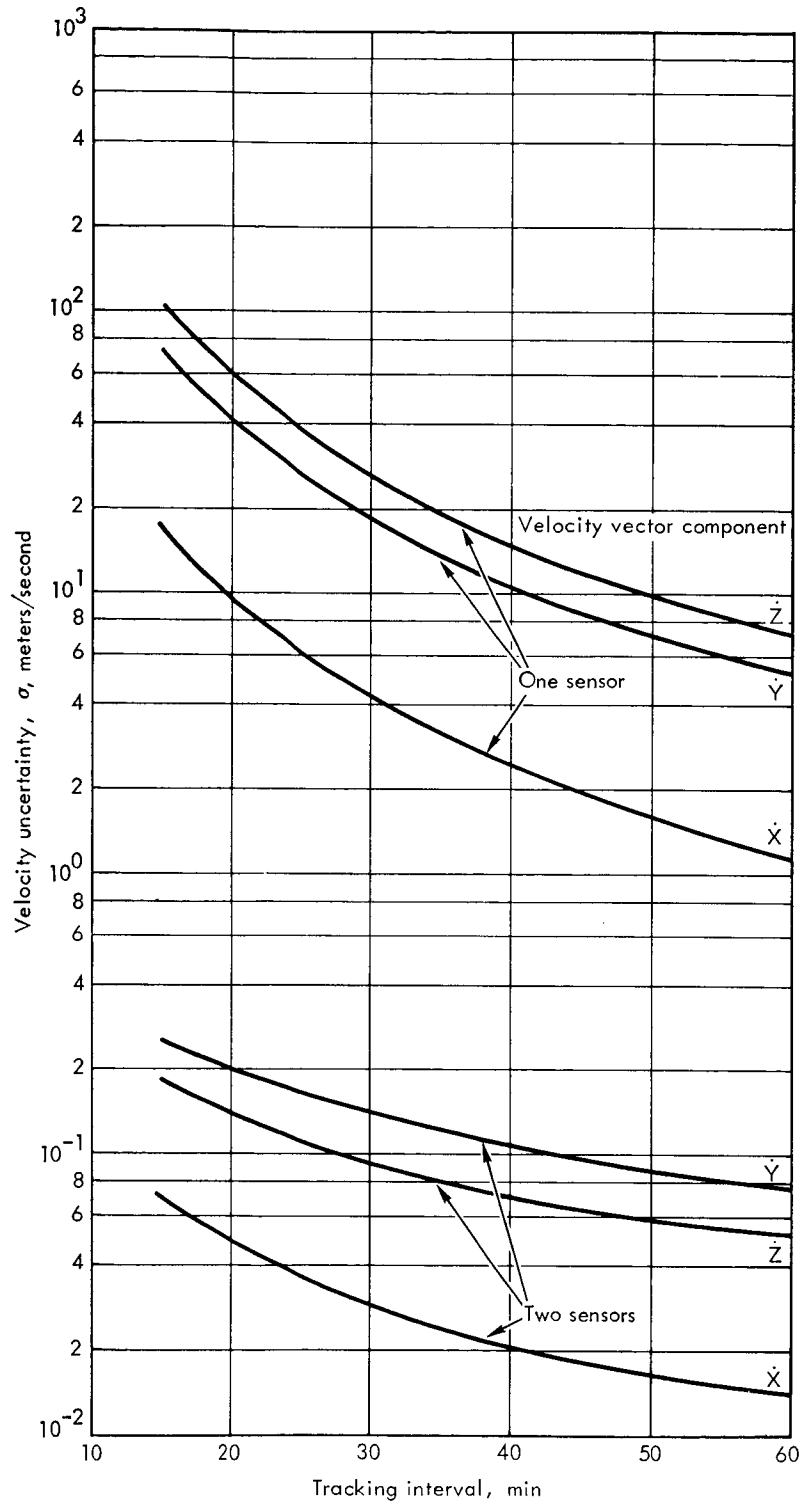


FIGURE 22.— VELOCITY UNCERTAINTIES USING ONE AND TWO SENSORS FOR SHORT ARC FITS

the two sensor configuration. The single sensor uncertainties are approximately two orders of magnitude larger.

Equal total amounts of data from one sensor and two does not result in equally determinate systems. In figure 23, one sensor uncertainties for 30 minutes and 60 minutes of tracking are compared to 15 minutes and 30 minutes of tracking with two sensors. There are equal amounts of data in the determination of each situation. However, the triangulation aspect is missing in the single sensor configuration. Adding angular data, right ascension, and declination to range and range-rate information in a single sensor configuration hardly affects the tracking estimate uncertainties, as can be seen in table IV of section 3.3.3.

The mathematical indeterminacy of the single sensor configuration results in the ill conditioning of the normal matrix. There are several ways of measuring ill conditioning of matrices. One method is to compare the right inverse with the left inverse, or the double inverse. The correlation matrix is printed with each iteration summary in TRW System's AT85 Orbit Determination Program. The correlation matrix is simply a triangular matrix of correlations, derived from the tracking covariance matrix, $(A^TWA)^{-1}$. Correlations greater than ± 1 are indicative of an ill-conditioned matrix. When all observations are confined to information in a single line or plane due to observing geometry, the result is the inability to solve for certain linear combinations of the data. This results in an ill conditioned normal matrix, which in turn is reflected in its inverse, the covariance matrix, from which the correlations are derived. Many one sensor test cases had ill conditioned matrices, which, as pointed out above, is indicative of indeterminate tracking geometry.

In summary, simultaneous tracking from two stations is required in a differential correction of a lunar satellite. This is especially critical when performing the first differential correction after deboost into lunar orbit. The one sensor tracking configuration is geometrically indeterminate in terms of expected uncertainties when performing a differential correction.

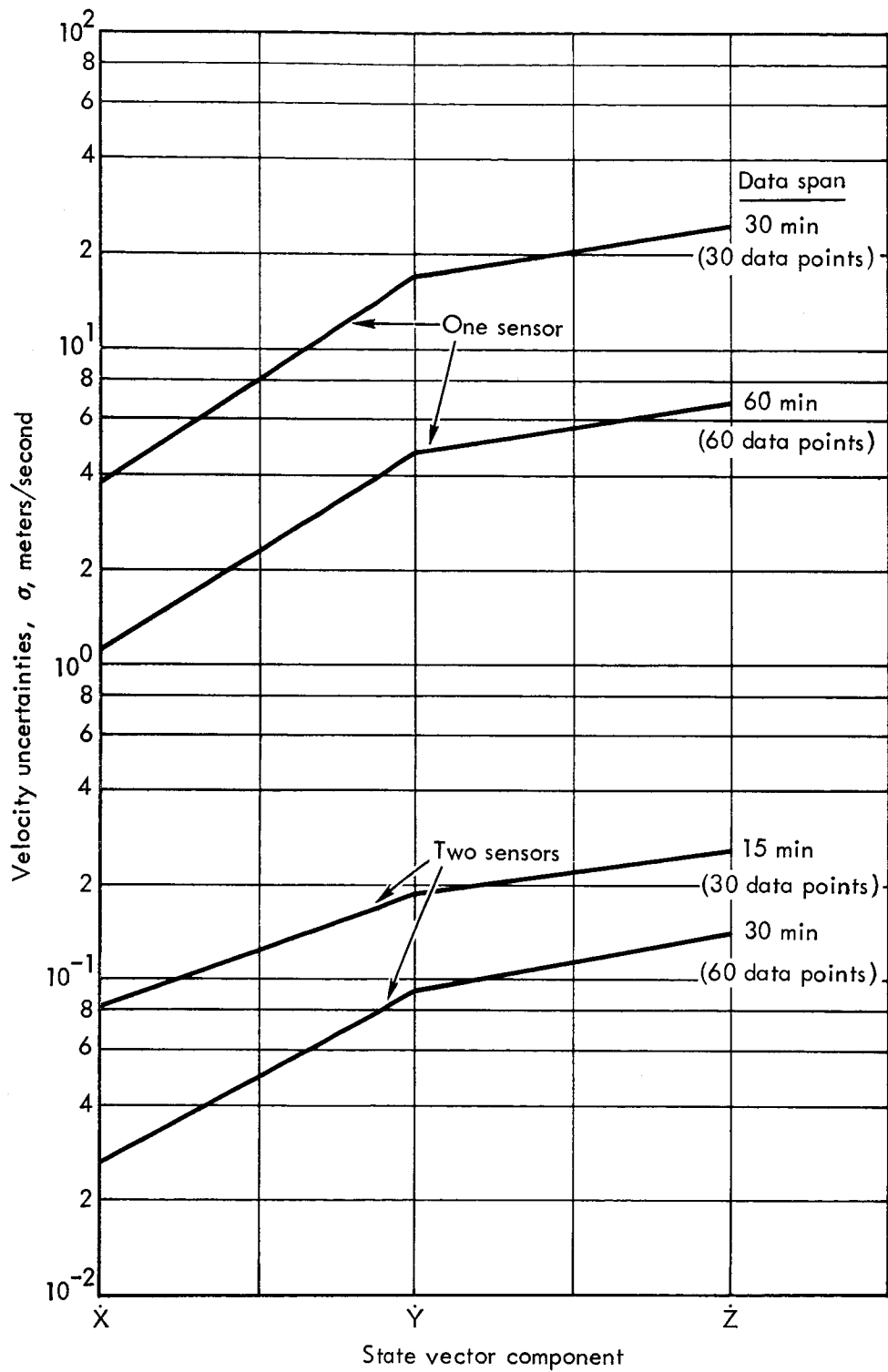


FIGURE 23. — COMPARISON OF VELOCITY UNCERTAINTIES FOR SHORT ARC FITS

3.4 CONVERGENCE OF ALTERNATE LUNAR SATELLITE ORBITS

This portion of the study is concerned with the effects of observing the lunar satellite orbit in different orientations; that is, with different inclinations and longitudes of the ascending node. The alternate lunar satellite orbits are listed below for convenient reference.

TABLE V. CLASSICAL ELEMENTS OF ALTERNATE
LUNAR SATELLITE ORBITS

Orbit code	a	e	i	Ω	ω	M
B1	2788	0.2869	0°	25.°47	-12.°46	0.0
B2	2788	0.2869	30°	25.°47	-12.°46	0
B3	2788	0.2869	45°	25.°47	-12.°46	0
B4	2788	0.2869	60°	25.°47	-12.°46	0
B5	2788	0.2869	15°	10.°	-12.°46	0
B6	2788	0.2869	15°	90.°	-12.°46	0
B7	2788	0.2869	15°	130.°	-12.°46	0

$$T_0 = 27 \text{ June } 1966, 4^{\text{h}} 0^{\text{m}} 48.5^{\text{s}}$$

The classical elements listed in table V served as the initial conditions for the differential corrections. Observational data was simulated for a 3σ energy perturbed orbit and for a 3σ orientation perturbed orbit. Since this was the final phase of the convergence study, and considering the large number of different orbits, many of the convergence techniques which proved successful in the main portion of this study were used in order to maximize the convergence probability. Energy corrected initial conditions were used for the energy perturbed cases, and a bounded solution constraint was imposed on the orientation perturbed cases. All cases had simulated data for 60 minutes from two sensors tracking simultaneously. Each graph in the following sequence (figures 24 through 30) is a convergence summary of two cases; representative of a particular lunar satellite orbit orientation. The two cases consist of (1) observing an energy perturbed orbit (3σ) and having energy corrected initial conditions;

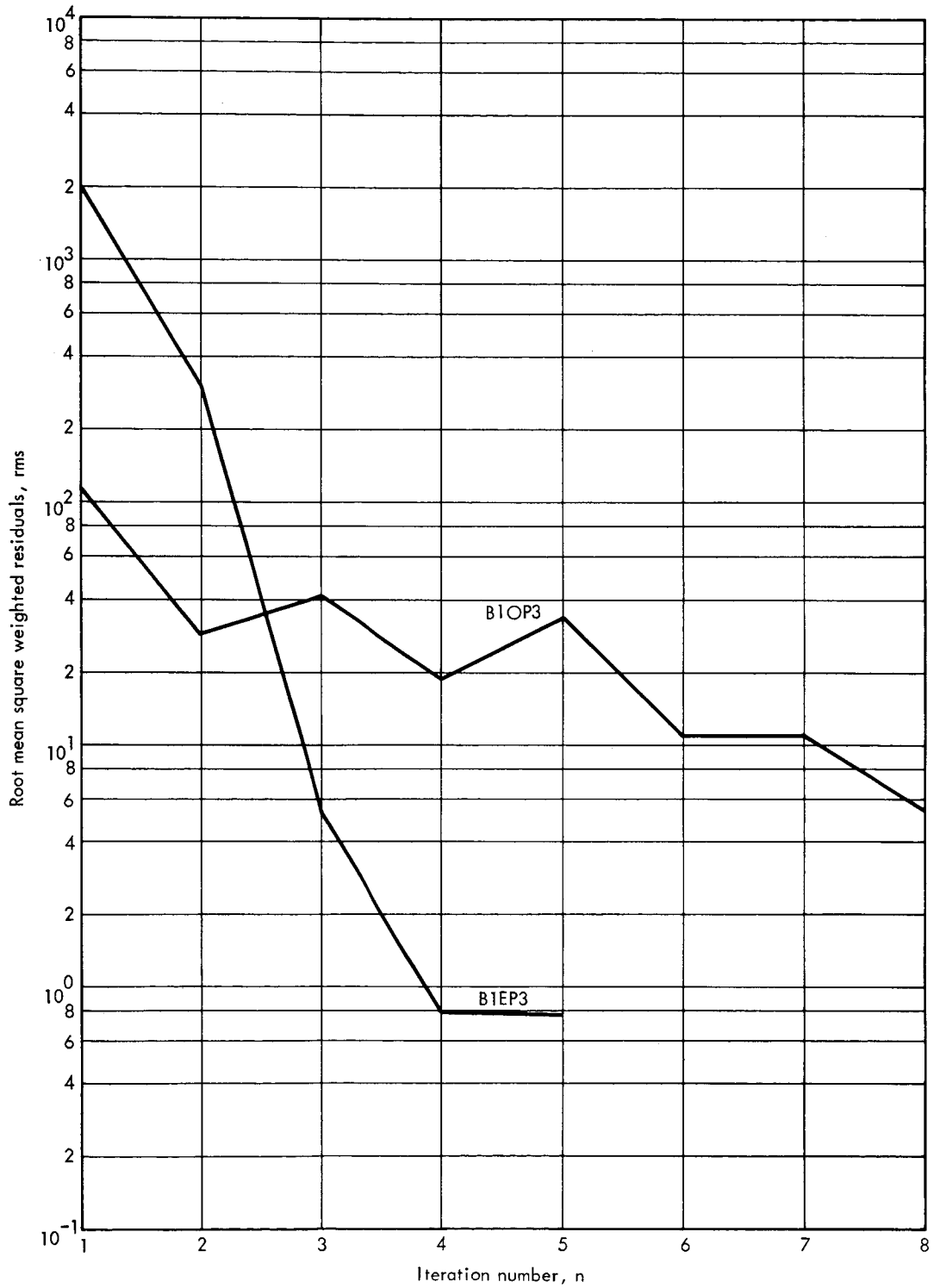


FIGURE 24. — CONVERGENCE CHARACTERISTICS OF B1 ALTERNATE ORBIT

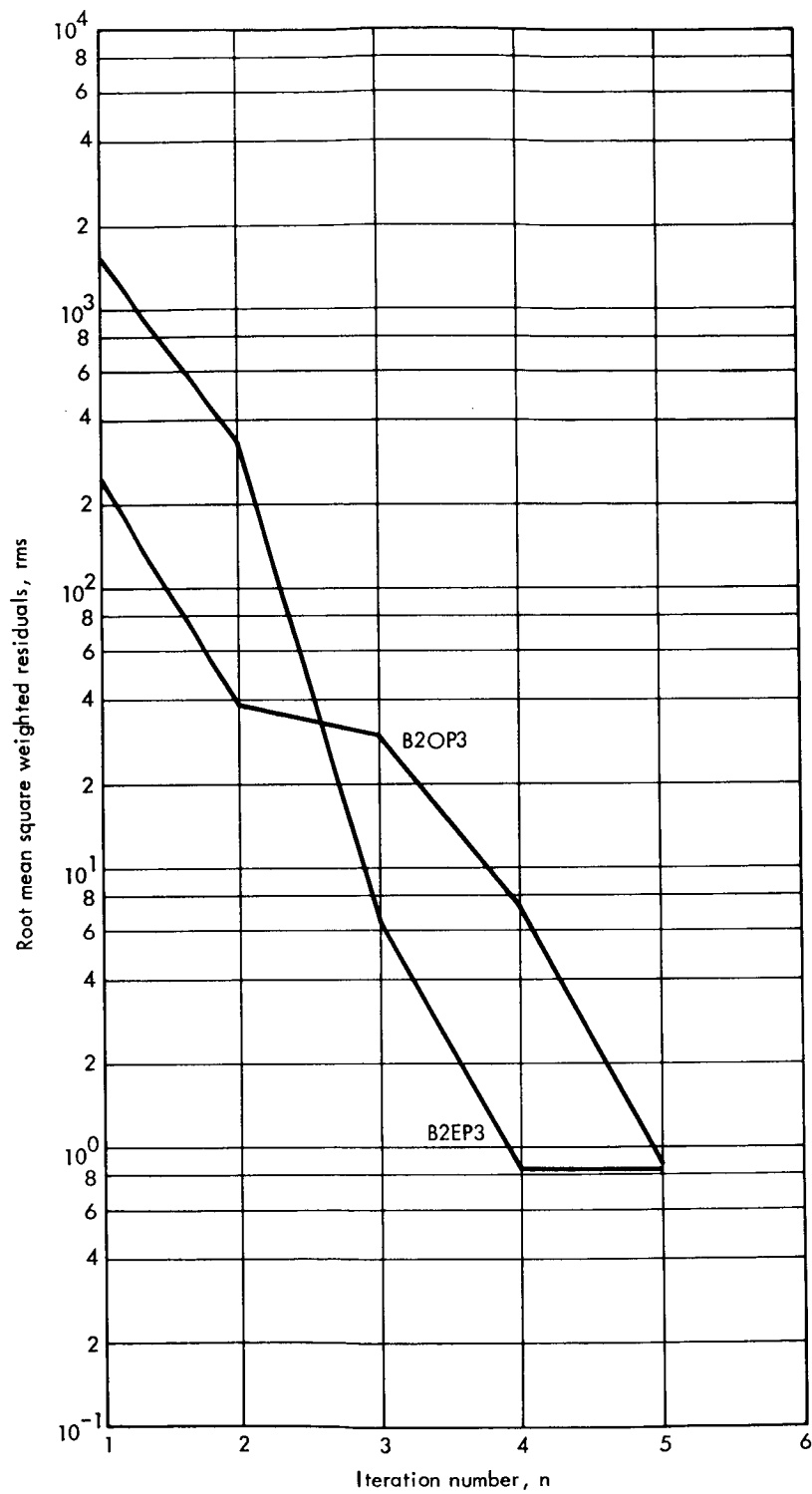


FIGURE 25. — CONVERGENCE CHARACTERISTICS OF B2 ALTERNATE ORBIT

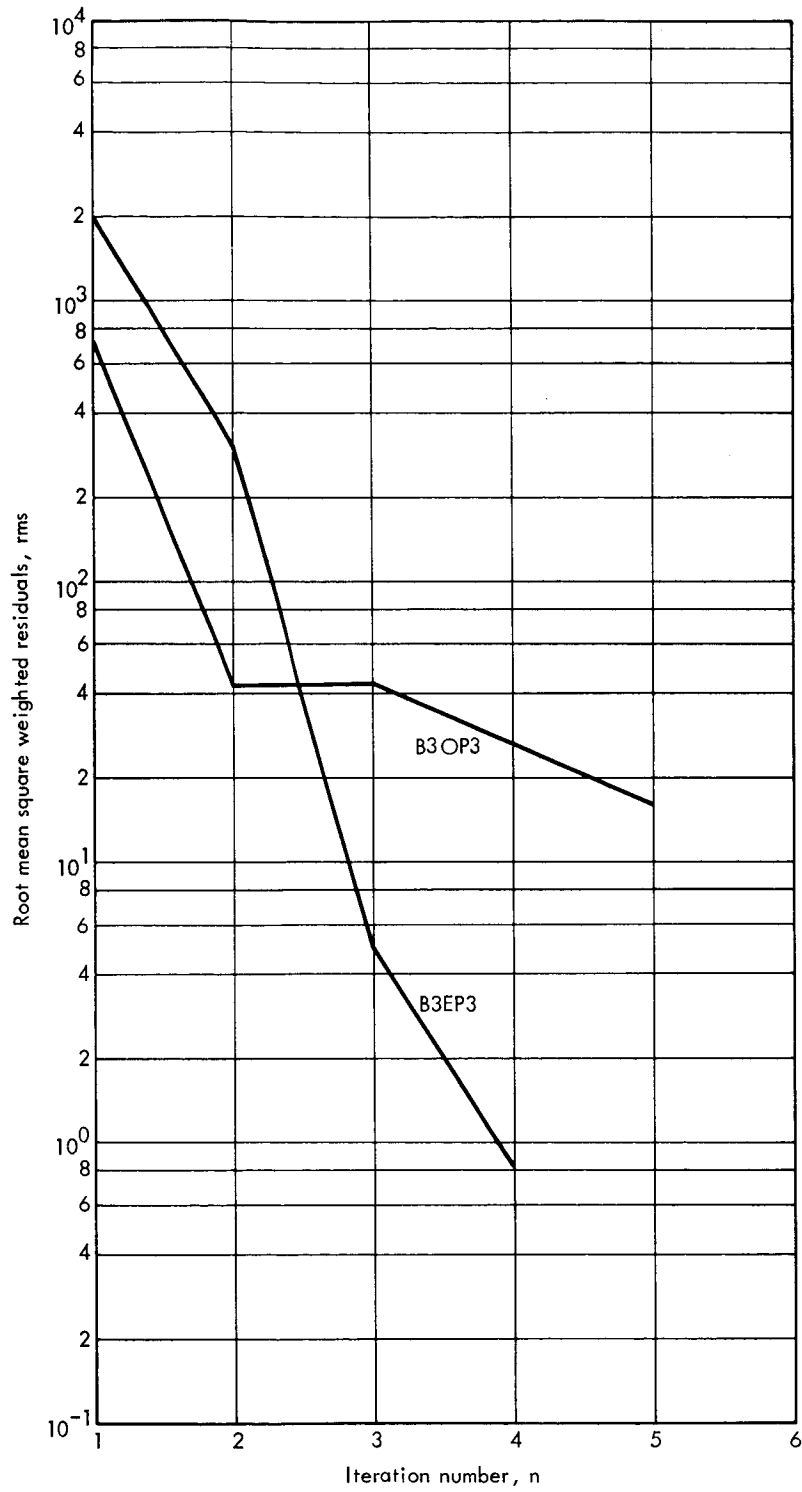


FIGURE 26.— CONVERGENCE CHARACTERISTICS OF B3 ALTERNATE ORBIT

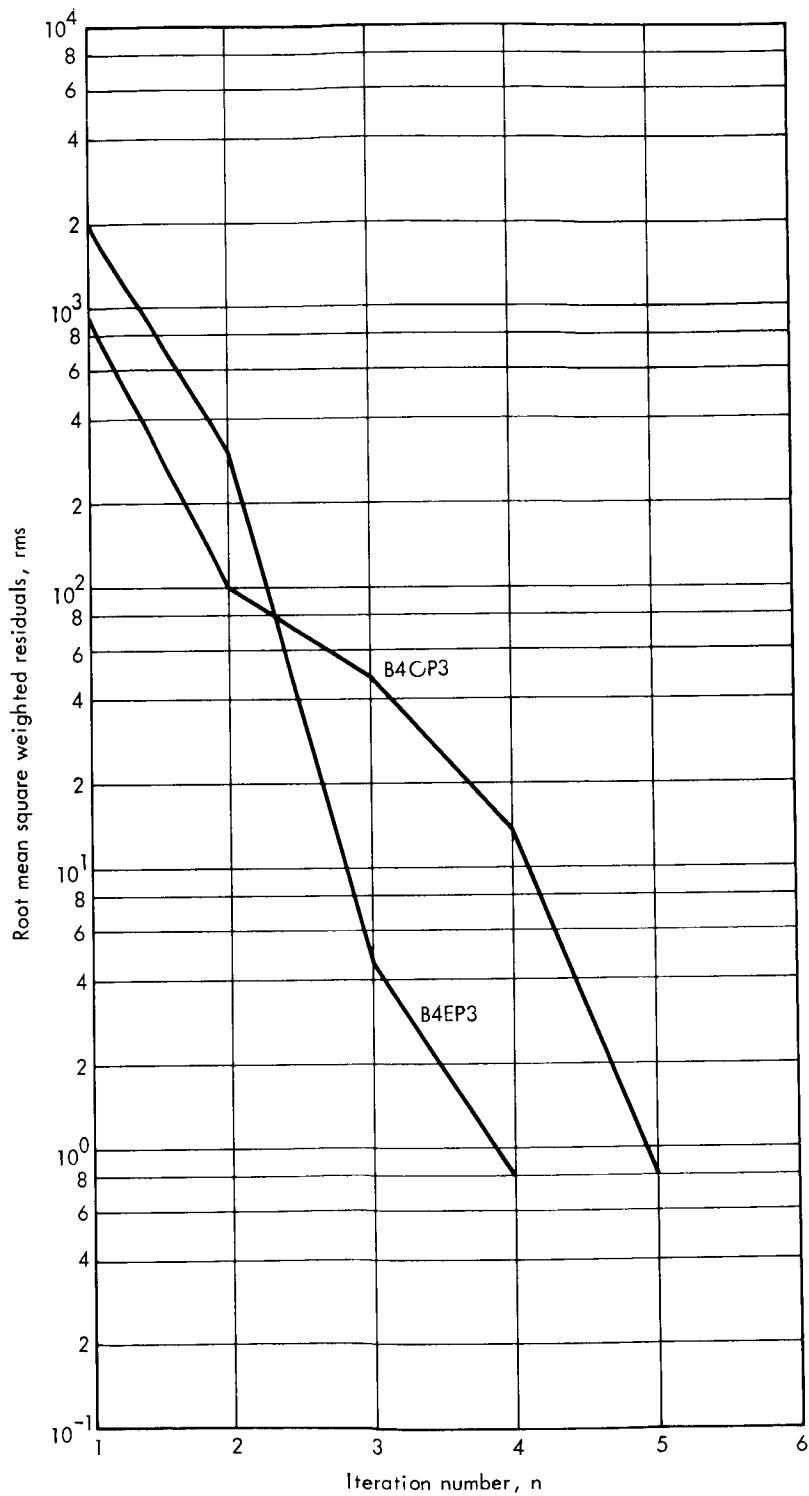


FIGURE 27. — CONVERGENCE CHARACTERISTICS OF B4 ALTERNATE ORBIT

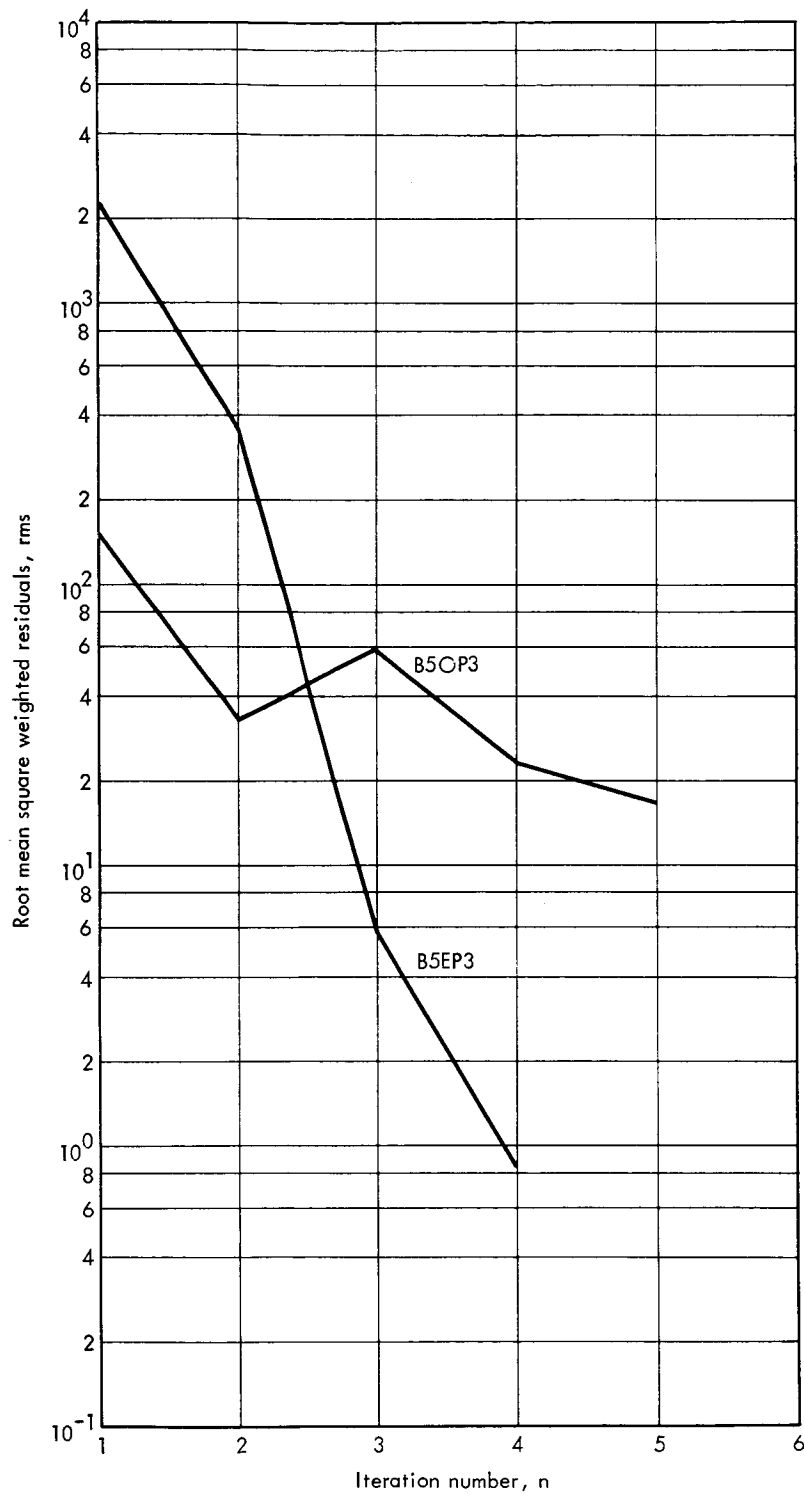


FIGURE 28. — CONVERGENCE CHARACTERISTICS OF B5 ALTERNATE ORBIT

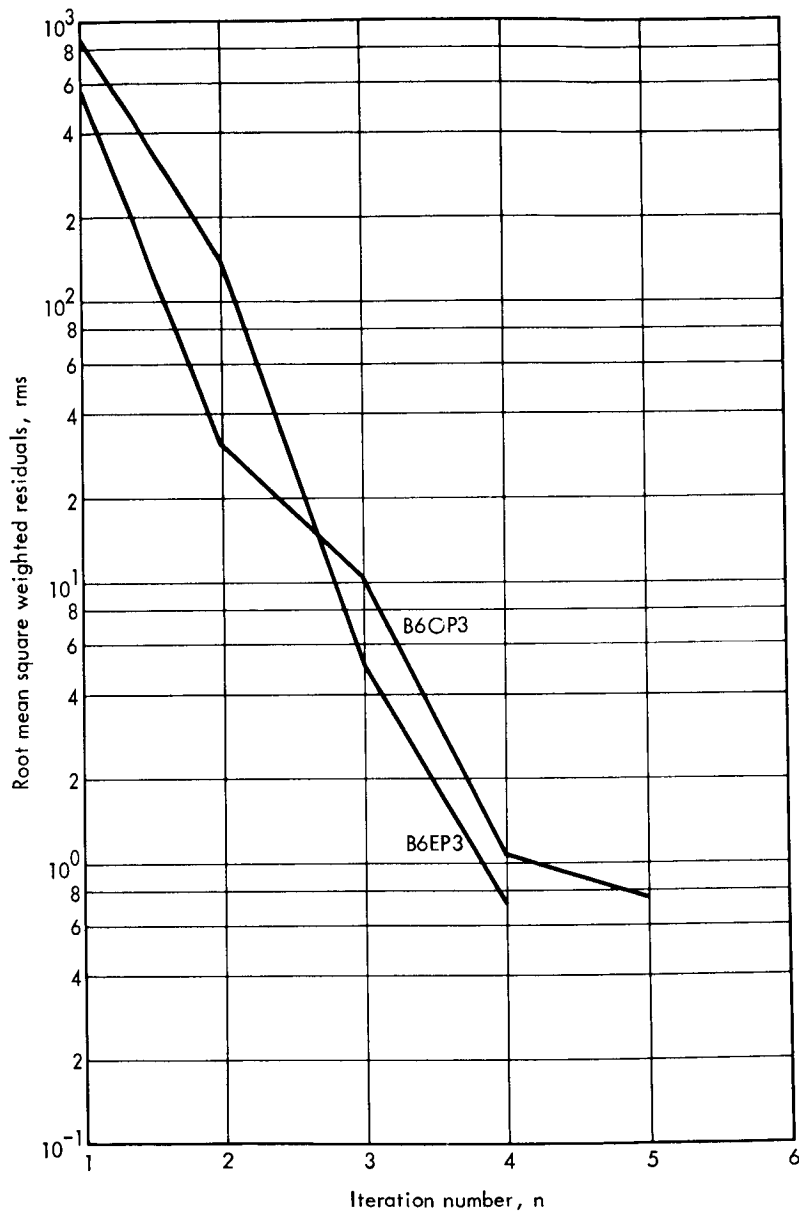


FIGURE 29.— CONVERGENCE CHARACTERISTICS OF B6 ALTERNATE ORBIT

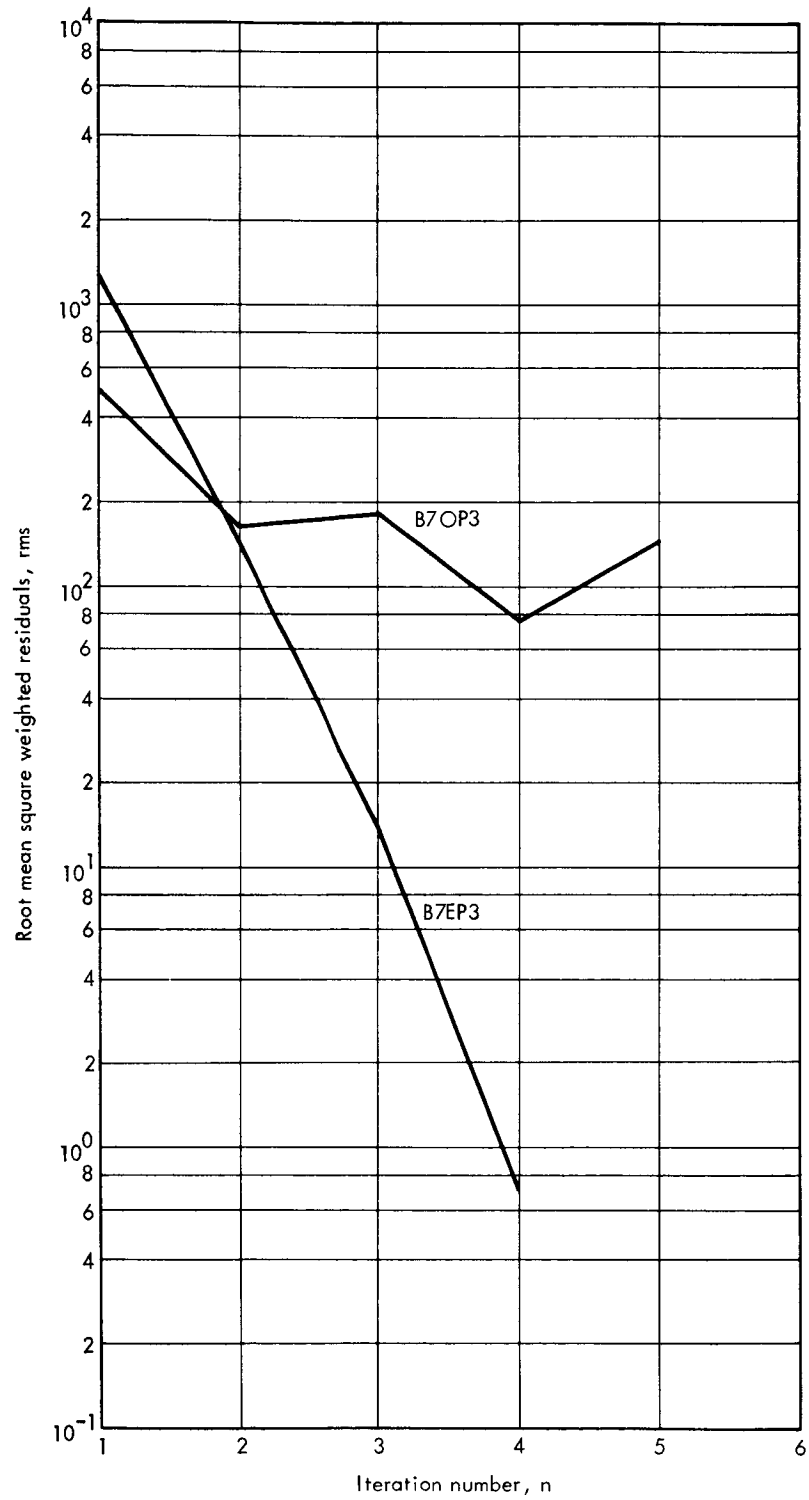


FIGURE 30.—CONVERGENCE CHARACTERISTICS OF B7 ALTERNATE ORBIT

and (2) observing an orientation perturbed orbit (3σ) and starting with nominal (unperturbed) initial conditions. The energy perturbed orbit has a period of 340 minutes (nominal is 220 minutes), although this error is removed with the energy correction. The orientation perturbed orbit has an average error of 2.05 in inclination, 7° in longitude of the ascending node, and virtually no energy error.

The orbital data code on the graph consists of nominal orbit code, type of perturbation and magnitude of perturbation. For example, B3OP3 is interpreted:

B3 = nominal orbit, B3

OP = orientation perturbed (EP = energy perturbed)

3 = magnitude of perturbation, 3σ

For all lunar satellite orbit orientations, the differential correction of the orientation perturbed orbits did not converge as rapidly or as easily as the energy perturbed orbits. This can be attributed to the fact that the energy perturbed cases have an improved (over the nominal) initial estimate, whereas the orientation perturbed cases have no equivalent "orientation correction" to the nominal estimate.

All lunar orbit orientations converged successfully with the exception of the B7OP3 orbit, figure 28. This exception can be attributed to the fact that the satellite was occulted by the moon for 45 minutes of the 60 minutes of data, beginning two minutes after tracking began. The identical case with 300 minutes of tracking converged successfully. Since all the lunar satellite orientations covered presented no difficulties with 60 minutes of tracking, the step fit technique could be used to incorporate any additional data. In fact, subsequent differential corrections starting with the converged state vector of a 60 minute data fit would require relatively few iterations, as the uncertainties in the 60 minute fit (with two sensors tracking) are very small. See section 3.3.3.1.

3.5 NUMERICAL AND STATISTICAL ASPECTS OF THE CONVERGENCE PROBLEM

3.5.1 Conditioning of the Normal Matrix

There are three major sources for poor numerical conditioning:

1. All observations restricted to either a linear or planar geometry (because of the observing situation).
2. The accumulation of a large number of partials in single precision.
3. High correlations between the separate elements of the state vector because of secondary dependence on some well determined implicit parameter such as period.

The first and third sources arise from physical considerations; the second, from numerical limitations in the computer.

The first source, the restricted observing geometry, has been the most common source of poor numerical conditioning in this study. Some authorities (reference 5) have shown that iterations can converge in the presence of computation and round-off errors even if the inverse of the normal matrix has less than one significant figure; this is derived under the assumption that the iterations converge rapidly when calculated in "infinite precision."

Several examples of convergent iterations despite poor numerical conditioning were encountered in this study. In general, a one-sensor-only tracking configuration with a bounded solution vector produced convergent iterations, though the inverse of the normal matrix had correlations greater than ± 1 and negative variances. Figure 31 illustrates the successively convergent iterations of a one-sensor-only fit which had poor numerical conditioning in every iteration.

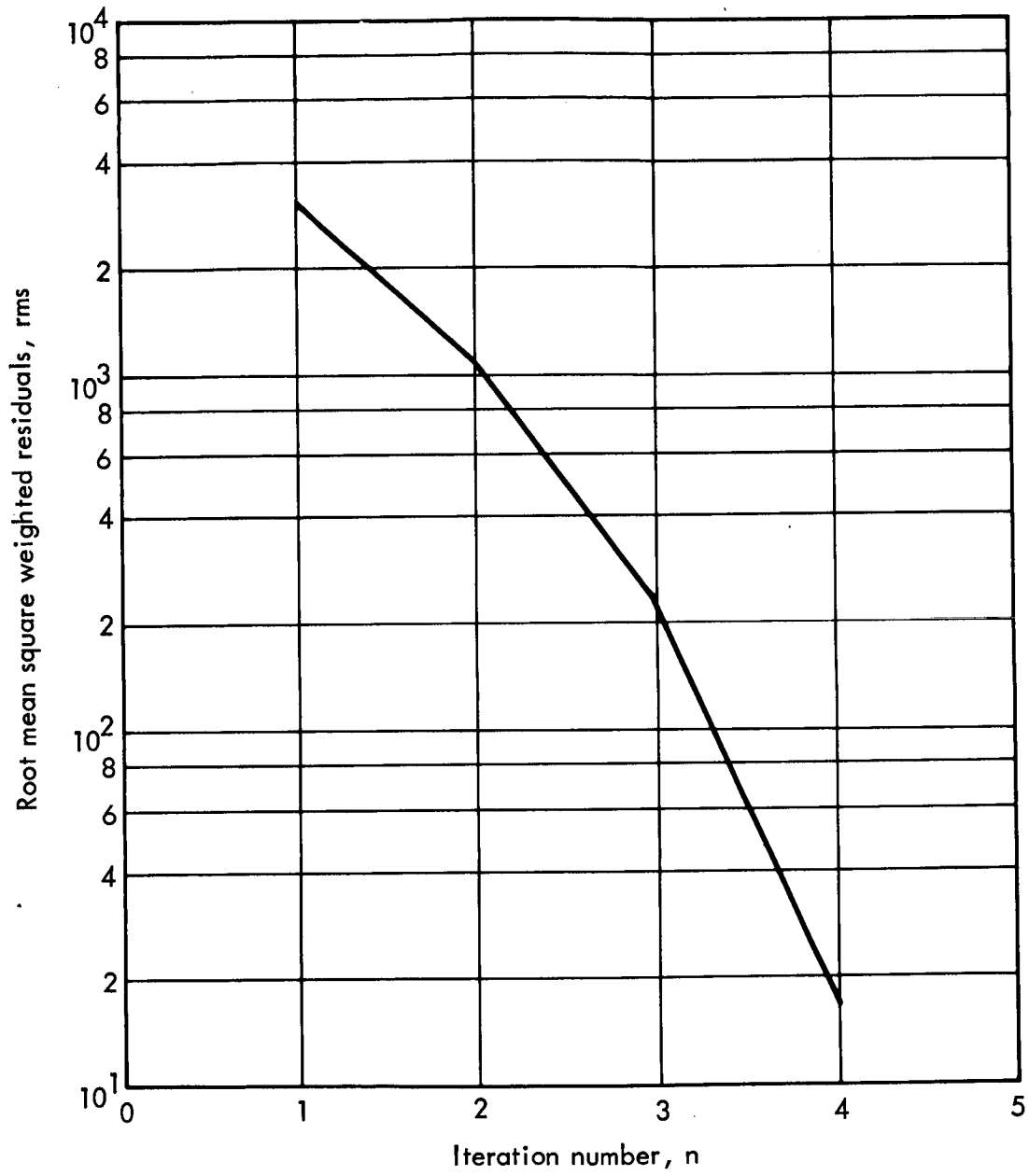


FIGURE 31. — CONVERGENCE WITH AN ILL-CONDITIONED NORMAL MATRIX

An illustration of poor numerical conditioning because of the accumulation of a large number of observations was encountered when a differential correction, with no error in the initial estimate, was attempted using 10 revolutions of data (55 hours of tracking with the three DSN sensors). The solution vector was appropriately small (negligible when added to the initial estimate), although the inverse of the normal matrix had negative variances and correlation coefficient greater than ± 1 .

3.5.2 Statistical Interpretation of the Inverse of the Normal Matrix

The orbit determination problem as posed and solved by the method of least squares, for any given set of tracking data, converges after iterating to a unique estimate of the orbital parameters. But the original tracking data contains random noise, biases, systematic errors, and miscellaneous anomalies which most certainly cause the estimate to differ from the "true value", a value which unfortunately can never be obtained. The estimate is a single sample drawn from the population of solutions which would arise if the error sources at the measuring instruments (i. e., tracking radars) could somehow be allowed randomly to fluctuate through their physically permissible ranges. But, since a satellite only goes by once per pass, the errors which arise on that pass are a unique set, a single sample from an experiment that cannot be repeated.

For planning or operational purposes, we would like to have an idea of the uncertainty in our estimate, that is, we would like to have a statistical description of the solution. The standard form for multivariate normal distributions, standard deviations and correlations for the estimated parameters may be obtained when certain conditions are satisfied. Briefly, the restrictions are that the errors in the tracking data must be normally distributed with mean zero and have a known standard deviation. (For most practical orbit determination programs, the errors must also be uncorrelated.) Biases in the tracking data must not exist, or else be solved for. The acceleration and perturbation models affecting the spacecraft motion either must be perfectly known, or else the unknown parameters in the acceleration model must also be solved in the least

squares solution. Within these restrictions, the covariance matrix may be derived by applying the expectation operator to the least squares estimating equation.

The weighted least squares estimate of the state vector may be written

$$\delta x_E = (A^T W A)^{-1} A^T W \delta y \quad (43)$$

where the residual vector

$$\delta y = A \delta x_A + n \quad (44)$$

Using the equation for the residual vector (equation 44),

$$\begin{aligned} \delta x_E &= (A^T W A)^{-1} A^T W (A \delta x_A + n) \\ &= \delta x_A + (A^T W A)^{-1} A^T W n \end{aligned}$$

The mean of the error in the estimate is the expected value of $\delta x_E - \delta x_A$, i. e.,

$$E(\delta x_E - \delta x_A) = (A^T W A)^{-1} A^T W E_n \quad (45)$$

If we assume zero mean observational noise, i. e.,

$$E_n = 0$$

equation (45) becomes

$$E(\delta x_E - \delta x_A) = 0$$

Thus the weighted least squares estimate is an unbiased estimate.

The covariance matrix of the estimate may be written (again using the expectation operator),

$$E(\delta x_E - \delta x_A) - E(\delta x_E - \delta x_A) (\delta x_E - \delta x_A) - E(\delta x_E - \delta x_A)^T$$

or, since the error in the estimate has zero mean,

$$E(\delta x_E - \delta x_A)(\delta x_E - \delta x_A)^T = (A^T W A)^{-1} A^T W E_{nn}^T W A (A^T W A)^{-1} \quad (46)$$

The matrix $E(nn^T)$ is the covariance matrix of the observational noise. If we now make the assumption that the least squares weighting matrix is equal to the inverse of the noise covariance matrix,

$$W^{-1} = E(nn^T)$$

equation (46) becomes,

$$E(\delta x_E - \delta x_A)(\delta x_E - \delta x_A)^T = (A^T W A)^{-1} \quad (47)$$

Thus, under certain assumptions, the diagonal elements, a_{ii} , of $(A^T W A)^{-1}$ are the variances of the corresponding elements of the solution vector, δx_E^i , and the off-diagonal elements, a_{ij} , are the covariances of the corresponding solution vector elements, δx_E^i and δx_E^j .

For a two dimensional solution vector, the covariance matrix would have the form

$$(A^T W A)^{-1} = \begin{bmatrix} \sigma_1^2 & \rho_{12} \sigma_1 \sigma_2 \\ \rho_{12} \sigma_1 \sigma_2 & \sigma_2^2 \end{bmatrix}$$

where σ_i^2 is the variance in δx_E^i (the i^{th} component of the solution vector) whose true value is δx_A^i , i. e., $\sigma_i^2 = E(\delta x_E^i - \delta x_A^i)^2$, $\rho_{ij} \sigma_i \sigma_j = E(\delta x_E^i - \delta x_A^i)(\delta x_E^j - \delta x_A^j)$ is the covariance between δx_E^i and δx_E^j . The coefficient ρ_{ij} is called the correlation coefficient between δx_E^i and δx_E^j .

The criteria which must be satisfied in order that this be true are:

- a) The observational noise is unbiased, or else the non-zero biases are included in the solution vector. This is the assumption which allowed writing the covariance matrix in the form in equation (46).

- b) The observational noise is uncorrelated and the variances of the observations are known a priori and are used in the weighting matrix. This requirement arises from the computer implementation of the program, rather than from any assumptions made in the theory; recall that in deriving equation (47) we required only that $E(nn^T) = W^{-1}$. In case the observational errors are correlated, an "equivalent-or-worse" variance may be used in weighting observations, resulting in a value for $(A^TWA)^{-1}$ which is an upper bound on the actual covariance matrix (see reference 6).
- c) The mathematical model of the orbit and the observations is correct, and all parameters (biases, station locations, physical constants, etc.) which do not appear in the solution vector are known exactly.

When these criteria are met, the weighted least squares solution is also the minimum variance unbiased estimate of the parameters to be solved for. Obviously, these criteria can never be met exactly in any real tracking problem. When they are not met, $(A^TWA)^{-1}$ is to that extent an incorrect estimate of the actual covariance matrix.

Perhaps the most common departure from the criteria listed above occurs under item c, where uncertainties in the knowledge of the mathematical model (systematic errors) destroy the statistical significance of the inverse of the normal matrix.

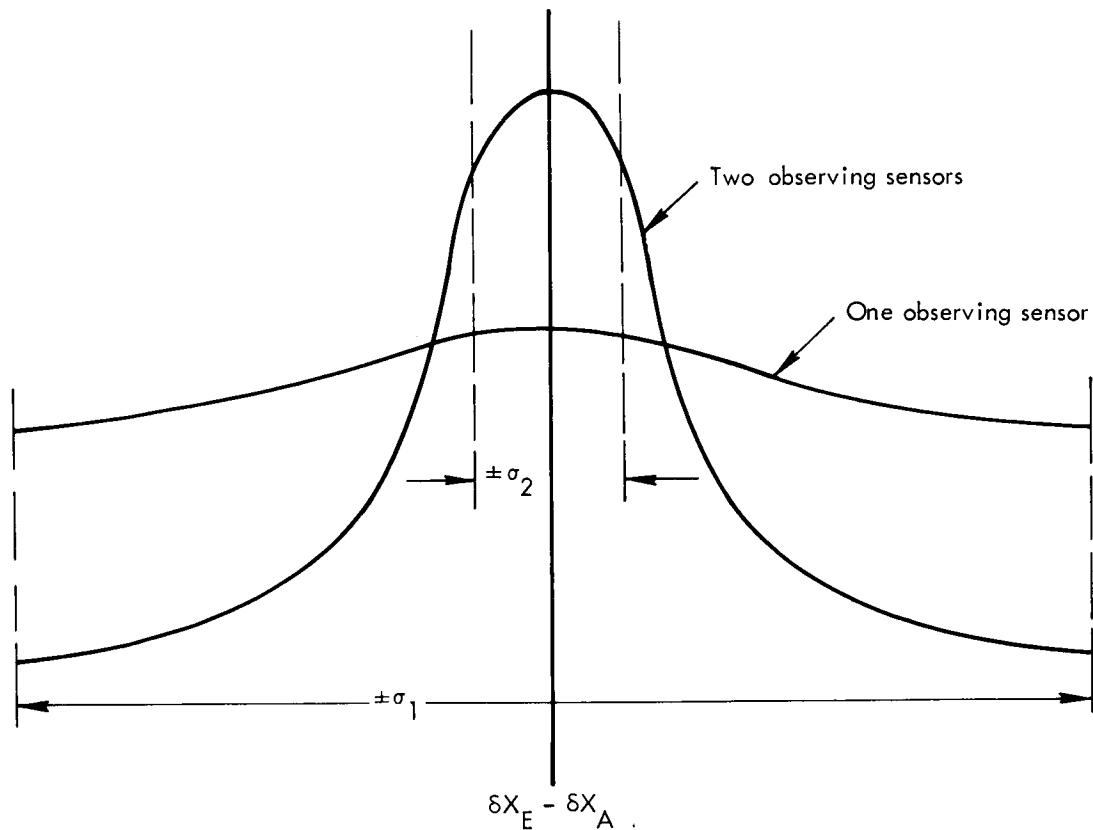
These systematic errors (as opposed to random radar observational errors), if not accounted for, may lead to unrealistic results. Examples of important systematic errors are observing station location uncertainties, data biases, and uncertainties in the constants which define the atmospheric and gravitational models. The effects of systematic errors may be accounted for by either a) increasing the dimensions of the solution vector to include the systematic errors (i. e., solve for the errors) or b) maintain the dimensions of the fit (solve only for position and the velocity) but include the degrading effect of systematic errors on the position and velocity covariance matrix (i. e., consider the effects of the errors). It can be shown that the covariance matrices,

$$\Sigma_{\text{random}} \leq \Sigma_{\text{solve}} \leq \Sigma_{\text{consider}}$$

i. e., that the "solve" case is bounded by the random and consider covariance matrices. In the consider case, of course, the estimate itself is not changed from the value that would be obtained from a random only fit. Only the covariance matrix of position and velocity is degraded to reflect increased uncertainties. It has been found that if the presence of systematic errors is recognized, but their effects are not accounted for (by not solving for them), the solution for the parameters of the orbit can have large errors in comparison to the case where these systematic errors are solved for. Consequently, portions of this study should be repeated with an expanded state vector to study the effects of the lunar gravitational parameters on the quality of the estimate of the orbital elements.

However, the covariance matrix can serve as an indication of the relative quality of two similar least square fits, even in the presence of systematic errors; in this case the matrix should not be interpreted as a statistical description of the state vector.

In the situation where there is sufficient confidence that the assumptions listed above have not been seriously violated, the covariance matrix will give an indication of the confidence to be placed in the estimate. That is, the estimate itself is a random variable (since it is computed from observations containing random errors) with zero mean, and its quality will be proportional to the variance. Various tracking situations can be evaluated by noting the variances in the estimates of the solution vector components. A good example of this comparative use of the inverse of the normal matrix is provided by the study of one versus two station tracking (section 3.3.3). The two station differential corrections have small variances, and have a high probability of giving an estimate very close to the actual state vector. The one station fits, on the other hand, have large variances, and may converge to solutions with large errors compared to the actual state vector. For example, if the solution vector had only a single component, the variances could be interpreted as shown in the sketch on the following page. For this hypothetical one-dimensional differential correction, 67 percent of the estimates for each of the tracking situations will lie with $\pm 1\sigma$ of the mean. Since $\sigma_2 \ll \sigma_1$, the



probability that the estimate will be within a given distance from the mean (which is the correct answer under the assumptions detailed above) is much greater for the two station case. When designing a tracking pattern, the aim is to make these distributions as "sharp" as possible, i.e., decrease the variances in the estimate of the state vector. Note that increasing the precision of the computation is not going to significantly improve the quality of the estimate from the one station differential correction.

There may be small changes in the magnitudes of the variances as information which may have been lost in roundoff noise is brought into the problem, but the basic "flatness" characteristic of the estimation (the least squares operator) remains. That is, the estimate will still be a random variable with a large variance, and may consequently give a poor answer, i.e., an answer which minimizes the sum of squares, but possibly far from the actual state vector. Although not a contributing factor in the

current study, a special case to beware of appropriate to this heading is when the solution vector is less than the full position-velocity state vector. For example, it is feasible to solve for velocity change only at the time of a burn to estimate the velocity gained during the burn. This assumes that both position and preburn velocity are known from tracking data prior to the burn, and that tracking data after the burn have also become available. Then an abridged solution vector can get the best estimate of the velocity gained solved from postburn data, but will not include the uncertainty in velocity due to the uncertainty in the original position.

The orientation of the reference axes. — The solution vector has been taken to be the position and velocity of the spacecraft represented in a particular cartesian coordinate system. The full covariance matrix accordingly is as follows:

$$\begin{bmatrix}
 \sigma_x^2 & \sigma_{xy} & \sigma_{xz} & \sigma_{x\dot{x}} & \sigma_{x\dot{y}} & \sigma_{x\dot{z}} \\
 & \sigma_y^2 & \sigma_{yz} & \sigma_{y\dot{x}} & \sigma_{y\dot{y}} & \sigma_{y\dot{z}} \\
 & & \sigma_z^2 & \sigma_{z\dot{x}} & \sigma_{z\dot{y}} & \sigma_{z\dot{z}} \\
 \text{SYMMETRIC} & & & \sigma_{\dot{x}}^2 & \sigma_{\dot{x}\dot{y}} & \sigma_{\dot{x}\dot{z}} \\
 & & & & \sigma_{\dot{y}} & \sigma_{\dot{y}\dot{z}} \\
 & & & & & \sigma_{\dot{z}}^2
 \end{bmatrix}$$

The orientation of the cartesian axes is usually accidental with regard to how "interesting" the resulting positional uncertainties might be. For example, the cartesian z axis is typically aligned with the earth's axis, and the x axis is oriented in the direction of the vernal equinox. By contrast, the radar sees range and range-rate, the high accuracy measurements, in the direction of the moon, and its low accuracy angular measurements normal to the earth-moon line. Correspondingly, if we were tracking a short arc of data across the face of the moon, we could estimate the uncertainties we might expect to see in the radar coordinate

system, i. e., that which is natural to the observations. But without a special rotation we would not be able to estimate the uncertainties we might expect in the accidental cartesian frame.

To put the covariance matrix to convenient use, it is often desirable to consider the uncertainties in a coordinate system different from the original coordinate system. The new system may be either a differently oriented cartesian system, or an entirely different reference such as the classical elements or the polar-spherical position and velocity. In any of these cases, the covariance matrix may be directly transformed by pre-multiplying by the transform matrix that carries the original coordinates into the new coordinates, and post multiplying by the transform of that matrix. This is shown by referring back in section 1 above, equation (47).

$$E(\delta x_E - \delta x_A)(\delta x_E - \delta x_A)^T = (A^T W A)^{-1}$$

Let the matrix which carries δx_E to δy_E be B, i. e.,

$$\delta y_E = B \delta x_E$$

$$\delta y_A = B \delta x_A$$

Then the expectation referred to the new coordinate is E_Y

$$\begin{aligned} E_Y &= E(\delta y_E - \delta y_A)(\delta y_E - \delta y_A)^T \\ &= E(\delta B x_E - \delta B x_A)(\delta B x_E - \delta B x_A)^T \\ &= E\left(B(\delta x_E - \delta x_A)(\delta x_E - \delta x_A)^T B^T\right) \\ &= B(A^T W A)^{-1} B^T \end{aligned}$$

Thus as long as B is a linear operator, this rotation may be made.

The following coordinates have been occasionally used to reference the uncertainty of the position and velocity determinations:

- 1) Vehicle centered cartesian: axes oriented with the earth's axis and the line to the vernal equinox (x y z)
- 2) Vehicle centered cartesian: axes oriented with the spacecraft velocity vector and the line normal to the orbit plane (STW)
- 3) Vehicle centered cartesian: axes oriented with the line to the central body and the line normal to the orbit plane (UVW)
- 4) Classical osculating elements (a e i ω Ω M)
- 5) Central body centered polar (velocity - spherical (position) coordinates (Azimuth angle, flight path angle, and magnitude of velocity vector; right ascension, declination, and magnitude of position vector)

It is also possible to examine the uncertainty in single parameters, such as pericyynthion distance, velocity at some latitude crossing, etc. If this is desirable, the rotation to these single components may be made.

Partitions of the covariance matrix. — The covariance matrix shows the covariances between position and velocity elements. These "phase-space" correlations reflect the important orbit determination phenomenon that the energy of an orbit is as well determined as the period (assuming perfect knowledge of the mass of the central body). Since the energy is related only to the position (potential) and velocity (kinetic), if energy is well known, then position and velocity are strongly correlated. As a vehicle revolves on its orbit, the uncertainty is exchanged back and forth between position and velocity. The greater uncertainty rests with the relatively larger component, i. e., at pericentron velocity (with respect to the central body) and velocity uncertainty are highest and at apocentron position (from the central body) and position uncertainty are highest. Thus the interpretation of magnitudes of position and velocity uncertainty must be tempered by knowledge of the vehicle's position on its orbit.

The correlations between position and velocity may be disregarded and the full 6 x 6 covariance matrix may be examined as a pair of smaller 3 x 3 covariance matrices in position and velocity respectively. Aside

from the consideration of the foregoing paragraph this is always valid. The isolated smaller matrices may be rotated and examined for all purposes as long as they are not propagated to a different position (or time) along the orbit.

The smaller matrices obtained by simple partitioning are to be interpreted as the uncertainties and covariances which would be obtained when the complementary part is left unrestricted. For example, the partitioned off position 3 x 3 submatrix is the set of uncertainties obtained as velocity takes on all possible values; it must not be interpreted as that set of position uncertainties obtained for velocity limited only to the value appearing in the solution. The position uncertainties obtained by partitioning the full 6 x 6 matrix are typically greater than those obtained by omitting velocity from the solution vector and thereby obtaining the position uncertainties associated with a fixed velocity. This paragraph is referring in general to the distinction between conditional and marginal distributions; this topic will be discussed further in section 8 below.

Interpretation of the covariance matrix as an ellipsoid. — A homogeneous expression of the second degree, of the form

$$F = a_{11} x_1^2 + a_{22} x_2^2 + \dots + a_{nn} x_n^2 + 2a_{12} x_1 x_2 + 2a_{13} x_1 x_3 + \dots + 2a_{n-1, n} x_{n-1} x_n \quad (48)$$

is called a quadratic form in x_1, x_2, \dots, x_n . In two-dimensional space, the equation $F = \text{constant}$ represents a general second-degree curve (conic) with center at the origin. For example, in the analytic geometry of conic sections, the equation of an ellipse is usually given in the form

$$\frac{u_1^2}{b_1^2} + \frac{u_2^2}{b_2^2} = 1 \quad b_1, b_2 \text{ real.}$$

If the coordinates are rotated by an angle γ so that

$$u_1 = x_1 \cos \gamma - x_2 \sin \gamma$$

$$u_2 = x_1 \sin \gamma + x_2 \cos \gamma$$

then

$$\begin{aligned} 1 = & \left(\frac{\cos^2 \gamma}{b_1^2} + \frac{\sin^2 \gamma}{b_2^2} \right) x_1^2 + \\ & + 2 \left(\frac{1}{b_1^2} + \frac{1}{b_2^2} \right) \sin \gamma \cos \gamma x_1 x_2 + \\ & + \left(\frac{\sin^2 \gamma}{b_1^2} + \frac{\cos^2 \gamma}{b_1^2} \right) x_2^2 \end{aligned}$$

and simple functions of γ , b_1 and b_2 may be identified with a_{11} , a_{12} , and a_{22} . Under certain restrictions on the quadratic form, it is always possible to rotate to the axes where the standard form of the ellipse is evident.

In three dimensional space the equation $F = \text{constant}$ represents a general quadric surface with center at the origin. Taking an example from solid analytic geometry, the equation of an ellipsoid is generally written

$$\frac{x^2}{a^2} + \frac{y^2}{b^2} + \frac{z^2}{c^2} = 1 \quad a, b, c \text{ real} \quad (49)$$

A similar rotation principal applies.

This equation can be easily generalized to an arbitrary number of coordinate directions

$$\lambda_1 x_1^2 + \lambda_2 x_2^2 + \lambda_3 x_3^2 + \dots + \lambda_n x_n^2 = 1 \quad (50)$$

$$\lambda_i > 0$$

where the different letters x, y, z have been replaced by x_1, x_2, \dots, x_n , and the constants a^2, b^2, c^2, \dots have been replaced by $1/\lambda_1, 1/\lambda_2, \dots, 1/\lambda_n$.

Equation (50) can be thought of as an ellipsoid in n -dimensions; the fact that n is now greater than three, and the ellipsoid has lost a realistic physical interpretation is of no consequence, since the rule for writing the equation is well known and a simple analog to the realizable case.

The correspondence between algebraic quadratic forms and an equivalent matrix-vector notation can be shown. If x is an n -dimensional column vector, and

$$A = A^T = \begin{bmatrix} a_{11} & a_{12} & a_{1n} \\ & a_{22} & \vdots \\ \text{symmetric} & & a_{nn} \end{bmatrix}$$

the quadratic form of Equation (48) can be written

$$F = x^T A x \tag{51}$$

If the matrix A satisfies the criterion that it be positive definite, i. e., that $|A| > 0$, then the quadric surface defined by A is an ellipsoid. In the theory of covariance matrices $(A^T W A)^{-1}$ the inverse of the covariance matrix, the so-called information matrix or normal matrix $A^T W A$ has precisely the necessary properties (except in ill-conditioned situations). It is identified with the A of the immediately preceding development. Thus, the quadratic form

$$x^T A^T W A x = C^2$$

defines an ellipsoid whose shape is determined by $A^T W A$ and whose scaling, or size, is determined by C^2 .

Eigenvalues of the ellipsoid. — If one is interested in studying the properties of an ellipsoid, it is reasonable to immediately select a coordinate system in which they are most efficiently displayed. A natural choice here would be to align the axes of the coordinate system with those of the

ellipsoid. However, in most engineering problems the problem of an ellipse or ellipsoid is not encountered in this manner. We normally have a coordinate system selected by some other considerations (the usual choice in orbit determination is the equatorial plane-vernal equinox system), and the ellipsoid when it appears in this reference frame will be rotated to some arbitrary orientation. The properties of the ellipsoid in this system may be observed. In the equations (49) and (50) above, this skewness would be indicated by cross terms of the form xy , yz , xz , so that in three dimensions the equation for the ellipsoid would have six terms instead of three.

Given that the properties of the ellipsoid are of interest, the problem becomes one of determining the principal axis of this quadric surface. If the equation for the surface is already in the form of equation (60), then the principal axes will be in the coordinate directions x_1, x_2, \dots, x_n , i. e., we are very fortunate in that our coordinate system axes already coincide with the principal axis of the surface. Normally, however, this is not the case and we must compute the principal axes.

It is instructive to consider the meaning of the term principal as it modifies axis. Construct at every point on the surface a normal vector, i. e., a vector which is orthogonal to the plane tangent to the surface at that point. A vector from the origin of the coordinate system to this arbitrary point will not generally be parallel to the normal. Only in special directions, namely in those directions in which the ellipsoidal equations are simplest (i. e., contain no cross terms), does it happen that r and n are parallel. These special directions are called the principal directions and form the basis for the principal axes. Alternately the principal axes are the line intersections of the planes of symmetry of the ellipsoid.

An algebraic definition of the principal axes describes them as those vectors u_i which, when premultiplied by the matrix A (associated with the quadric surface), generates a new vector b which is parallel to the original vectors u_i . That is,

$$A u_i = b_i = \lambda u_i \tag{52}$$

where λ is a scalar constant.

If Equation (52) is rewritten as a homogeneous equation, i. e., with zero on the right hand side,

$$(A - \lambda) u_i = 0 \quad (53)$$

or, written out in components (letting u_i consist of the components $u_{i1}, u_{i2}, \dots, u_{in}$),

$$\begin{aligned} (a_{11} - \lambda) u_{11} + a_{12} u_{12} + \dots + a_{1n} u_{1n} &= 0 \\ a_{21} u_{21} + (a_{22} - \lambda) u_{22} + \dots + a_{2n} u_{2n} &= 0 \\ \vdots & \\ a_{n1} u_{n1} + a_{n2} u_{n2} + \dots + (a_{nn} - \lambda) u_{nn} &= 0 \end{aligned}$$

A nontrivial solution (i. e., the only solution other than the vanishing of all x 's) to this set of n homogeneous linear equations in n unknowns exists only if the determinant

$$|A| = \begin{vmatrix} a_{11} - \lambda & a_{12} & \dots & a_{1n} \\ a_{21} & a_{22} - \lambda & \dots & a_{2n} \\ \vdots & \vdots & \ddots & \vdots \\ a_{n1} & a_{n2} & \dots & a_{nn} - \lambda \end{vmatrix} = 0$$

Expanding this determinant gives the characteristic polynomial of A ,

$$\lambda^n + C_{n-1} \lambda^{n-1} + C_{n-2} \lambda^{n-2} + \dots + C_0 = 0$$

This n^{th} order polynomial has n roots $\lambda_1, \lambda_2, \dots, \lambda_n$, and it can be shown that for a real symmetric matrix (such as a covariance matrix) the roots are all real. To every possible $\lambda = \lambda_i$, a solution to the homogeneous set, equation (53) can be found. These define the u_i 's, called eigenvectors and represent the n distinct directions in space described above, i. e., the principal directions. The λ_i associated with u_i is called the eigenvalue.

The geometrical significance of the eigenvalues of the covariance matrix can be found through a simple analysis.

Returning to the fundamental equation of eigenvalue analysis

$$Ax = \lambda x \quad (54)$$

and recalling that the quadric surface, F , can be represented by

$$x^T Ax = 1$$

we can write (multiply equation (54) by x),

$$x^T Ax = \lambda x^2 = 1$$

and

$$x^2 = \frac{1}{\lambda}$$

Since

$$x^2 = x_1^2 + x_2^2 + \dots + x_n^2 = r^2$$

is the square of the distance to the point where the principal axis intersects the surface, the eigenvalue λ_1 may be interpreted as the reciprocal of the square of the distance from the center to the surface at the point where the corresponding principal axis penetrates the surface.

A large eigenvalue means that in the direction of the associated eigenvector (principal axis) the quadratic surface comes near to the center. A small eigenvalue means that in the direction of the associated eigenvector, the surface stays far from the center.

Since the surface of interest here is represented by the quadratic form of equation (51), in which the matrix A has been replaced by \mathcal{A}^{-1} , the distance of approach of the surface to the origin along any principal direction is directly proportional to the square root of the eigenvalue of \mathcal{A} for that direction.

Probability density function interpretation of an error ellipsoid. — The least squares estimation in the differential correction procedure results in an estimate of the mean correction δx_E to be applied to the already available estimate of a spacecraft state vector x_D . The foregoing discussions show how the $(A^T W A)^{-1}$ matrix may be identified (with reservations) with the covariance matrix Φ of this estimate. Another application of these parameters is to estimate the probability one has that the "true value" of the state vector lies within some volume of phase space in the vicinity of the newly estimated position. The probability is derived from the multivariate normal probability density function which is closely related to the error ellipsoid. This multivariate pdf is given by

$$f(\delta x_A) = \left[(2\pi)^n |\Sigma| \right]^{-1/2} e^{-1/2 (\delta x_A - \delta x_E)^T \Phi^{-1} (\delta x_A - \delta x_E)}$$

$$\delta x_A = \text{col}(\delta x_{A1}, \delta x_{A2}, \dots, \delta x_{An})$$

If the estimated correction δx_E is applied to the available estimate x_D , then the dispersion of the actual correction about the estimated correction becomes the same as the dispersion of the actual state vector about the newly computed best available estimate $x_E = x_D + \delta x_E$. Hence the pdf for $x_{\text{Actual}} = x_A = x_E + x$

$$f(x_A - x_E) = \left[(2\pi)^n |\Sigma| \right]^{-1/2} e^{-1/2 (x_A - x_E)^T \Sigma^{-1} (x_A - x_E)}$$

or

$$f(x) = \left[(2\pi)^n |\Sigma| \right]^{-1/2} e^{-1/2 x^T \Sigma^{-1} x}$$

The integral of the pdf over all of n-space is unity. The integral of the pdf over any finite (or semi finite) region of n-space is the probability that the spacecraft is located within that region situated relative to the estimated position x_E . It is exceedingly difficult to integrate this pdf over arbitrary volumes of 6-space, and tabular methods such as may be used in the one or two dimensional cases are not generally available. An abridged but fairly useful 3-space tabular approach has been published

(reference 7), but higher dimensional aids are not known to the authors. However, with the partitioning between position and velocity permitted, it is not necessary to consider more than three dimensions at once.

Partitioning leads to the separate questions: 1) How well is velocity known if position is disregarded? and 2) How well is position known if velocity is disregarded? By disregarded is meant that the parameter takes on all possible values. We cannot, with the partitioning approach, ask the question "What is the probability that velocity is within this much of estimated value, provided also (= conditional upon) that position within certain boundaries has been achieved. In critical cases this may be a valid question, but present practice is not adequate for quick correct answers.

A request is often made to examine the 1, 2, or 3 σ ellipsoid. This is on the surface a legitimate request, but the 1 σ ellipsoid can be mistakenly interpreted if the dimension of the solution vector is not considered. As the number of elements in the solution vector and the dimension of the corresponding error ellipsoid increase, the probability that all components simultaneously be within one standard deviation of the estimated state vector decreases sharply. The problem is further complicated (but less aggravated) by high correlations between the solution parameters. Most engineers have a feeling for the statistics of one variable, where 1 σ means 68% probability, 2 σ means 95% probability, and 3 σ means 99+% probability. This rule does not apply to cases where there are more than one variable. The following table compares 1, 2, and 3 dimensions.

Probability that all variables are within $n\sigma$ from the estimate (assuming independent variables).

<u>n</u> <u>No. of σ's</u>	<u>1 variable</u>	<u>2 variables</u>	<u>3 variables</u>
1 σ	0.68	0.48	0.20
2 σ	0.95	0.85	0.75
3 σ	0.99+	0.99	0.97

The confidence interval concept can also be applied to higher dimensions. The following table summarizes its application up to dimension 3.

Confidence Limits in C Standard Deviations

The probability is P that all n variables are less than c σ 's from the estimate.

<u>P</u>	<u>1 variable</u>	<u>2 variables</u>	<u>3 variables</u>
0.25	0.3	0.76	1.1
0.50	0.7	1.2	1.5
0.75	1.2	1.7	2.0
0.90	1.7	2.1	2.5
0.95	1.9	2.4	2.8
0.99	2.6	3.0	3.4

3.6 LRC/TRW TEST CASES

Langley Research Center (LRC) supplied TRW Systems with four (4) test cases which were run on Jet Propulsion Laboratories' Single Precision Orbit Determination Program, (SPODP). Cases I and II were run

on TRW Systems AT85 Program. Case III was not run as the tracking data was f_{c3} , coherent three-way integrated doppler frequency, an observation format which is not acceptable in the AT85 Program. Case IV was identical to Case II.

Case I

The pertinent input information to this case is as follows:

1. Epoch Time: 27 June 1966, 4^h 59^m 49.583^s
2. Initial Conditions: See iteration summary
3. Tracking: One sensor (Goldstone) for 31 minutes;
Range and range-rate data
 $\sigma_R = 20$ m. bias = 40 m
 $\sigma_{\dot{R}} = 0.02$ m/s
4. Solution Vector: Q, 6 x 1 vector of Cartesian components of position and velocity: x, y, z, \dot{x} , \dot{y} , \dot{z}

5. Other: Pessimistic a priori covariance matrix
 Unrestrained Solution (No bounds)
 One iteration

TABLE VI. ITERATION SUMMARY, LRC TEST CASE I

<u>Q</u>	<u>Delta Q</u>	<u>Old Q</u>	<u>New Q</u>
x	-0.55958147 E 02	-0.33309137 E 06	-0.33314732 E 06
y	0.57432841 E 02	-0.15951624 E 06	-0.15945880 E 06
z	0.17323176 E 03	-0.51329038 E 05	-0.51155806 E 05
\dot{x}	-0.10354523 E 00	-0.37497834 E-01	-0.14104306 E 00
\dot{y}	0.33810762 E 00	0.85750411 E-01	0.42385804 E 00
\dot{z}	-0.33123248 E 00	0.63568708 E 00	0.30445459 E 00

TABLE VII. ITERATION SUMMARY, TRW TEST CASE I

<u>Q</u>	<u>Delta Q*</u>	<u>Old Q</u>	<u>New Q</u>
x	-0.33707289 E 00	-0.33309137 E 06	-0.33309169 E 06
y	0.37816917 E 00	-0.15951624 E 06	-0.15951585 E 06
z	0.69214746 E 00	-0.51329038 E 05	-0.51328341 E 05
\dot{x}	-0.34459841 E-03	-0.37497834 E-01	-0.37844620 E-01
\dot{y}	0.11340711 E-02	0.85750411 E-01	0.86883255 E-01
\dot{z}	0.12165384 E-02	0.63568708 E 00	0.63446997 E 00

*Delta Q, which is the correction to the state vector, Q, called for by the solution to the normal equation, is in mean of 1950.0 coordinates.

The results of the test case are summarized in table VI (LRC version) and table VII (TRW version). Since there was no error in the initial estimate, the corrections (Delta Q vector) should be negligible, or zero. The SPODP version made corrections of over 100 km in position and 500 m/sec in velocity. The TRW Systems AT85 Program made small corrections of 1.0 km and 1.0 m/sec. Nevertheless, the uncertainties of the tracking covariance matrix were of the order of 25 km in position and 50 m/sec in velocity. Because of the poor tracking geometry, (one sensor only) the normal matrix was ill conditioned; this was reflected in the correlation state vector component correlations, which are computed from the inverse of the normal matrix. Using tracking data from two sensors would reduce the large uncertainties in the corrections and

improve the conditioning of the normal matrix; this technique would probably result in a convergent step if used on the SPODP. However, regardless of the poor tracking geometry and its numerical consequences, given no error in the initial estimate, the correction to the initial estimate should be negligible.

Case II

The input conditions are as follows:

1. Epoch time: 27 June 1966, 4^h 59^m 49.583^s
2. Initial Conditions: $\Delta 15$ Km error in position
 $\Delta 45$ m/s error in velocity
3. Tracking: One sensor (Goldstone) for 135 minutes
Range and range-rate data
 $\sigma_R = 20$ m bias = 40 m
 $\sigma_{\dot{R}} = 0.02$ m/s
4. Solution vector: 6×1 ; $x, y, z, \dot{x}, \dot{y}, \dot{z}$
5. Other: A priori covariance matrix
Diagonal $(3\Delta X)^2, (3\Delta Y)^2$
Unrestrained solution

The LRC test case (using SPODP) and the TRW Systems case (using AT85), with inputs as specified above, both diverged. Since this was a one sensor tracking configuration, the normal matrix was ill conditioned. This was reflected in the correlations derived from the inverse of the normal matrix. As mentioned in section 3.5.1, the ill conditioning of the normal matrix does not prevent convergence altogether; however, it is a factor in divergence, along with nonlinearity and residual inconsistency. Hence, the best way to rectify this test case is to resolve the ill conditioning of the normal matrix, i. e., use two sensors.

There are a few convergence techniques which, when applied to this case, result in convergence, despite the one sensor tracking configuration. One method slows down the convergence process; however, the iterations yield appropriate corrections. A second method is to employ the energy correction as discussed in previous sections. A convergence summary of these techniques when applied to this test case (case II) are illustrated in figure 32. Because of the large uncertainties associated with one sensor only determination, this test case, as all differential corrections of lunar orbiters, should have a two sensor tracking data set.

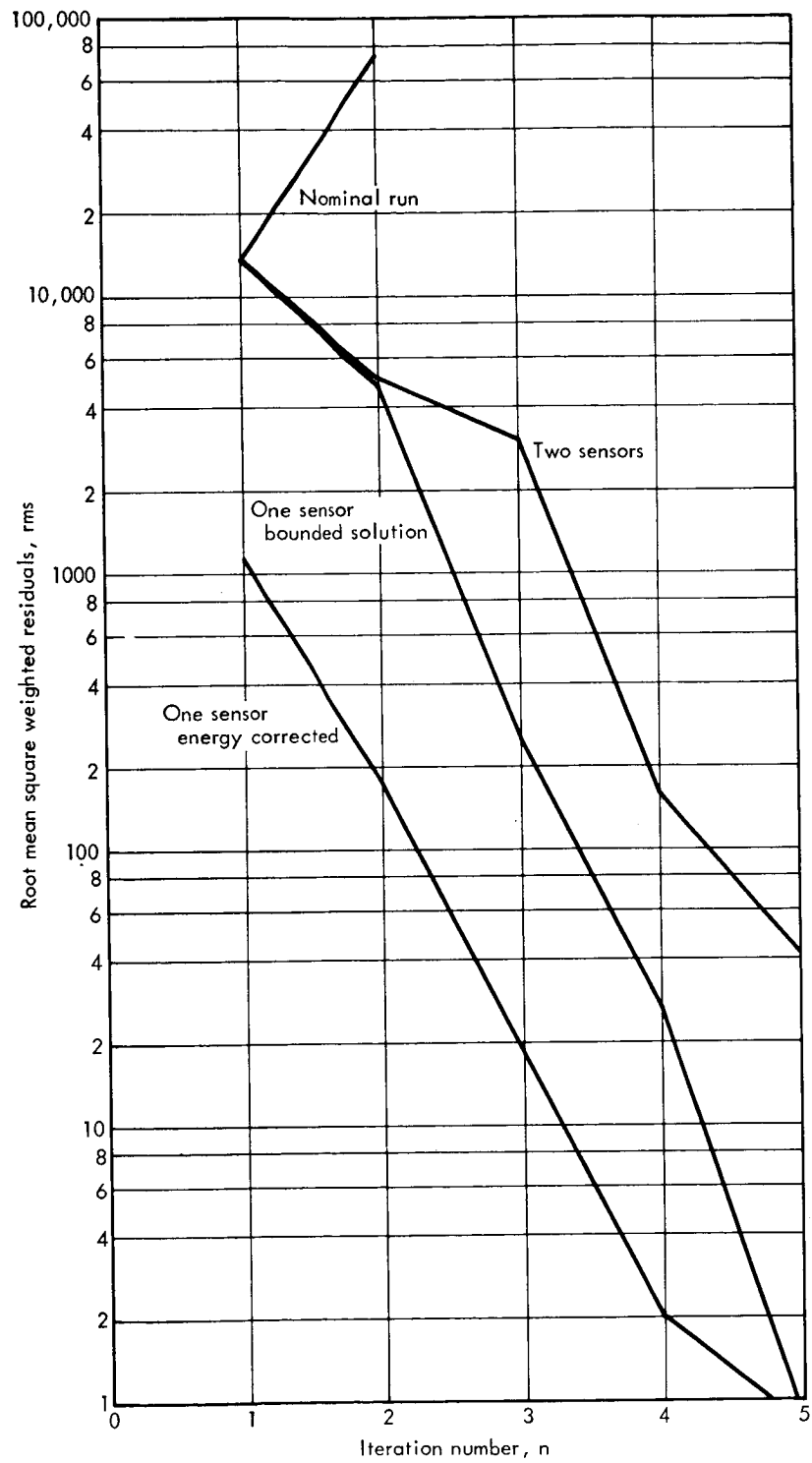


FIGURE 32.—TRW/LRC TEST CASE II CONVERGENCE CHARACTERISTICS OF VARIOUS TECHNIQUES

3.7 RELATIONSHIPS BETWEEN DIFFERENTIAL CORRECTION AND PRELIMINARY ORBIT DETERMINATION

In an effort to investigate the need for a preliminary orbit determination program estimate to initiate a differential correction, very large dispersions (6σ) from the nominal estimate were used to generate AEP6 and AOP6 orbits.

The AEP6 orbit has a period of 647 minutes, nearly three times the nominal estimate, and an eccentricity of 0.64. Figure 33 illustrates the convergence behavior when 15, 30, and 45 minutes of tracking data (two sensors) are used. It should be emphasized that the initial conditions are not energy corrected, and that the solution vector is unrestrained. For the 15 and 30 minutes of data, the AEP6 state vector was recovered. Longer data arcs require either a bounded solution or an energy corrected initial estimate. Nevertheless, an orbit with 6σ dispersions in energy does not require a preliminary orbit determination program estimate to establish the correct state vector.

The AOP6 orbit has a period of 227 minutes, very close to the nominal value of 220 minutes. However, the error in inclination is 5.5 deg., and in longitude of the ascending node, 12 deg. Figure 34 illustrates the convergence rates for short arc fits, using data from two sensors. The AOP6 state vector describing the 6σ perturbed orientation orbit was established in three iterations, with an unrestrained normal solution. The trend of the convergence rate in the first few iterations indicate that 45 minutes of data is near the limit of convergence, if the solution is to remain unrestrained. The technique of step fitting could be used when more than 45 minutes of data are available.

The errors in the elements of the lunar satellite are unlikely to be as large as 6σ dispersions, especially in the orientation elements of i and Ω . The judicious selection of the initial tracking arc and subsequent step fit technique should insure an adequate correct orbit determination for a lunar satellite. In a sense, the first short arc fit could be considered a

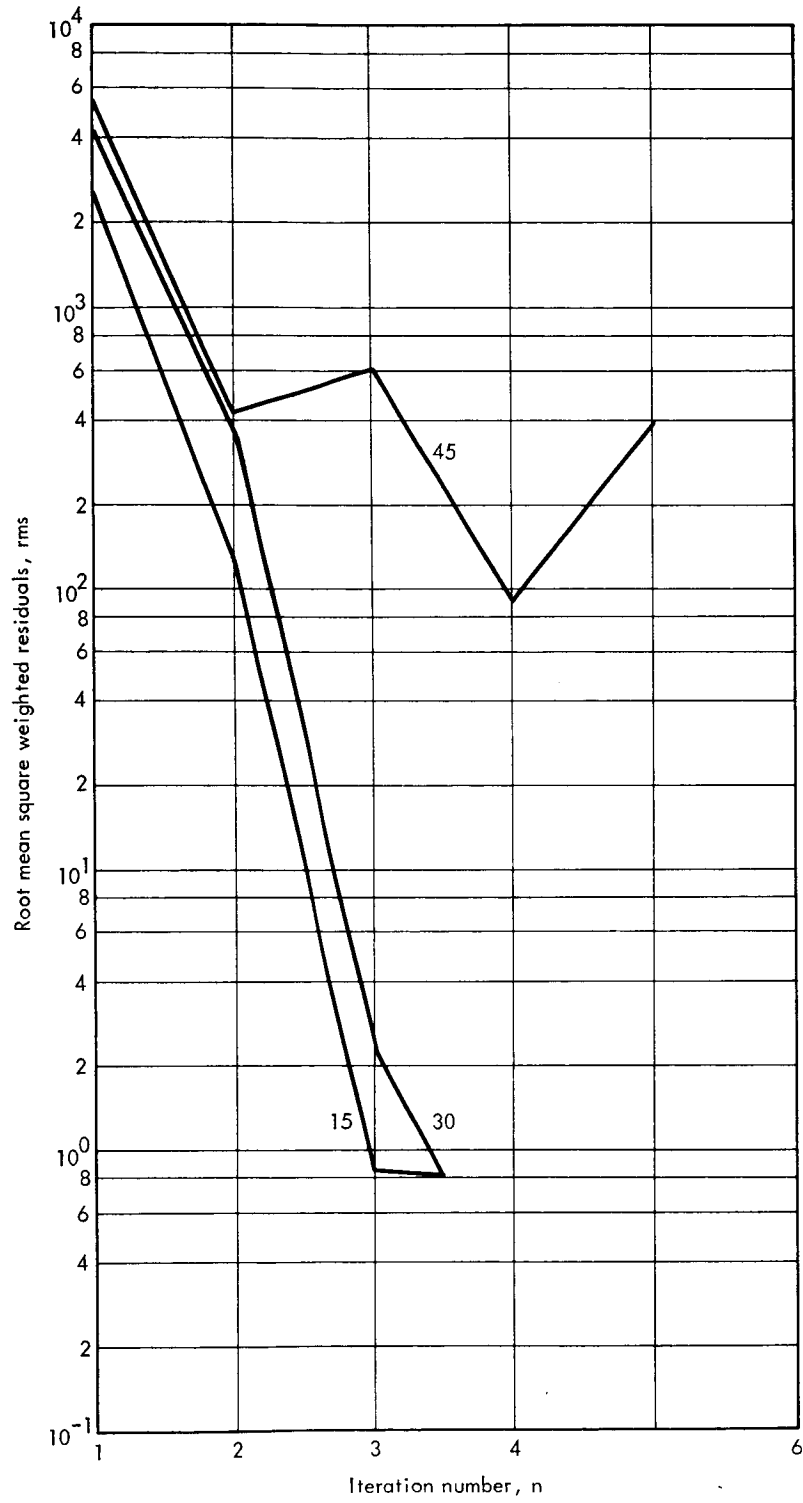


FIGURE 33. — CONVERGENCE CHARACTERISTICS OF 6σ ENERGY PERTURBED ORBIT

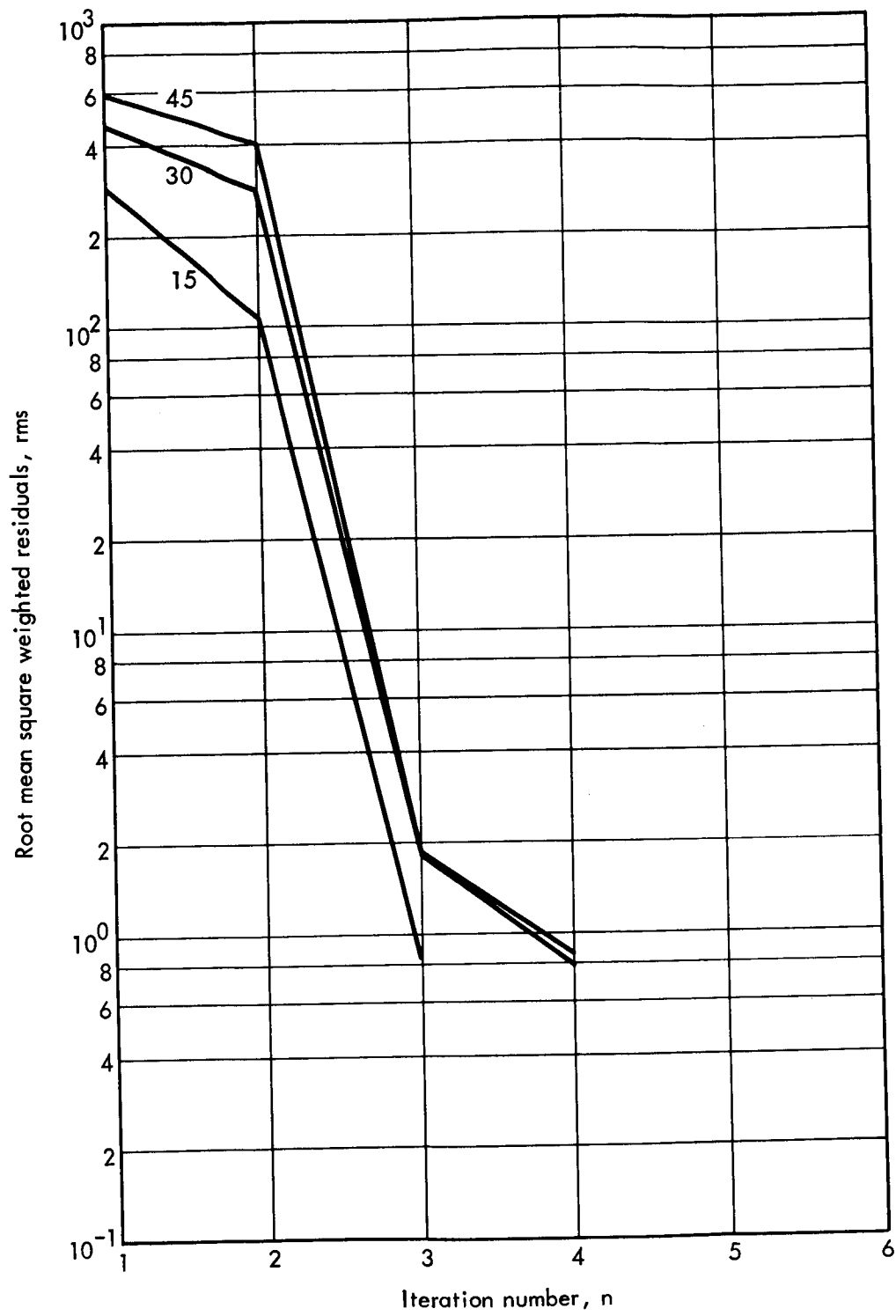


FIGURE 34.— CONVERGENCE CHARACTERISTICS OF 6σ ORIENTATION PERTURBED ORBIT

preliminary orbit determination, considering that orbital periods in error by a factor of three (3), a 5° inclination error, and over 10° in ascending node error can be handled with an ordinary tracking program.

4. PRELIMINARY ORBIT DETERMINATION FOR LUNAR SATELLITES

The advantage of the range and angles technique is that the data give a complete position fix and consequently define the plane of the orbit. The primary disadvantage is that the noise on the angular data produces inaccuracies in the selenocentric position vectors, resulting in a scattering of the Cartesian components. A significant problem that must be solved is the smoothing of the observations and elimination of the scattering. The smoothing is accomplished by use of a least squares solution. Numerical evaluation of the technique has shown it is possible to obtain a good estimate of the orbit elements in a 1 hour observation span using data with the nominal data noise components of 0.06° in angles and 20 meters in range. In an operational sense, this technique would work satisfactorily in determining an orbit using data from the end of main deboost to the first occultation by the moon. Extensive numerical results are presented in section 4.4.2.

An advantage of the range, range-rate technique is that the quality of the observations for ρ and $\dot{\rho}$ is very high. The disadvantage of this technique is that in order to determine all six elements it is necessary to invert a matrix which may be ill conditioned. The difficulty of inverting the matrix can be overcome either by observing for a long time period or by using more than the minimum set of six independent observations which are required to define a conic section (the minimal data set) and a least squares solution.

The $\rho, \dot{\rho}$ program was designed to augment the existing LRC $\dot{\rho}$ (binary star) program by allowing computation of $i, \Omega,$ and ω (the orientation elements) sooner than would be possible using $\dot{\rho}$ only. The possibility of a quicker recovery of the orientation elements is due to the use of high quality ρ data (in addition to $\dot{\rho}$), and a redundant data set.

Using a time history of ρ and $\dot{\rho}$, it is possible to obtain the inplane orbital elements a , e , and M_0 , by use of the classical binary star technique, although it is necessary to remove the effect of the observer's diurnal motion before a , e and M_0 can be determined. This can be accomplished by subtracting $\dot{\bar{r}}_T \cdot \bar{r}_P / |\bar{r}_P|$ from the Doppler curve, where $\dot{\bar{r}}_T$ is the observer's geocentric velocity and \bar{r}_P is the geocentric position of the primary body. This is the function of the LRC $\dot{\rho}$ program.

It has been demonstrated that if a , e and M_0 are obtained from Doppler data that the remaining orbital elements, i , Ω and ω can be determined using ρ and $\dot{\rho}$ data from one revolution of the satellite. It is possible to perturb the initial estimate of the orientation elements by $\pm 80^\circ$ and recover a satisfactory orbit. Extensive numerical results are presented in section 4.5.2.

In summary, both techniques solve for that orbit which, in the least squares sense, best fits a set of tracking data. It has been demonstrated that an orbit can be recovered in one hour, using ρ , α , δ data, with no prior knowledge of the orbital elements, or in one revolution using ρ and $\dot{\rho}$ data, when a , e and M_0 have been precomputed.

4.1 USE OF LEAST SQUARES OPERATORS IN PRELIMINARY ORBIT DETERMINATION

In the ρ , α , δ preliminary orbit determination technique it is necessary to obtain selenocentric position vectors. The effect of the angular data is such that an error of 0.06 in α or δ produces an error of 0.4×10^5 meters in any coordinate of the selenocentric position vector. Since the angular error is assumed to have a normal or gaussian distribution with a standard deviation of 0.06 , the problem is to determine a technique which will smooth the data. The quality of the solution obtained is a function of the number of triads of ρ , α , δ that are used in the orbit determination process; the use of a minimal data set can produce serious errors, since it is possible to have angular observations such that one has a maximum positive deviation and the other has a maximum negative

deviation, resulting in serious orientation element errors. The use of a least squares operator averages out the effect of these large angular errors.

The least squares criterion requires that we minimize the sum of squares of the difference between the measured and computed observations, i. e. ,

$$\min \left\| y_m - y_c \right\|^2$$

where y_m is the vector of measured observations and y_c is the vector of computed observations. If we let x be the state vector which achieves this minimum, and x_0 some initial estimate of the state vector, the computed observation vector corresponding to x , $y_c(x)$, may be expanded in a first order Taylor series about x_0 ,

$$\begin{aligned} y_c(x) &= y_c(x_0) + \left. \frac{\partial y_c}{\partial x} \right|_{x = x_0} (x - x_0) + \dots + \\ &= A(x_0) x_0 + \left. \frac{\partial y_c}{\partial x} \right|_{x = x_0} (x - x_0) + \dots + \end{aligned}$$

where we have assumed a linear relationship between the observation and the state,

$$y_c(x) = A(x) x$$

The least squares criterion becomes

$$\min \left\| y_m - A(x_0) x_0 - \left. \frac{\partial y_c}{\partial x} \right|_{x = x_0} (x - x_0) \right\|^2$$

Since

$$\begin{aligned}\frac{\partial y_c}{\partial x_o} &= \frac{\partial}{\partial x_o} (A(x_o)x_o) \\ &= A(x_o) + \frac{\partial A}{\partial x} x_o \\ &= A + \phi\end{aligned}$$

$$\begin{aligned}\min_{x = x_o} \left\| y_m - A(x_o)x_o - \frac{\partial y_c}{\partial x} (x - x_o) \right\|^2 &= \min \left\| y_m - A x_o - (A + \phi)(x - x_o) \right\|^2 \\ &= \min \left\| y_m - A x - \phi(x - x_o) \right\|^2\end{aligned}$$

The matrix ϕ , whose ϵ_{kp} element,

$$\epsilon_{kp} = \sum_j \frac{\partial a_{kj}}{\partial x_p} x_j^o$$

where x_p^o and x_j^o are components of x_o , a_{kj} are the elements of the matrix A , and the summation is over the components of x_o , should be small over short time spans, since it represents the sensitivity of the f and g coefficients to perturbations in the local state vector. The contribution of the term including ϕ is further reduced when the coefficient, $(x - x_o)$, is small, i. e., when we are near the solution.

Ignoring the term $\phi(x - x_o)$,

$$\min \left\| y_m - A x \right\|^2 = \min (y_m - A x)^T (y_m - A x)$$

The minimum of this quadratic surface can be found by setting its gradient with respect to x equal to zero, i. e.

$$\begin{aligned} \nabla_x (y_m^T y_m - x^T A^T y_m - y_m^T A x + x^T A^T A x) &= 0 \\ -2y_m^T A + 2x^T A^T A &= 0 \end{aligned}$$

Solving for x ,

$$x = (A^T A)^{-1} A^T y_m$$

This is the least squares operator which was used in both preliminary orbit determination techniques. The validity of the assumption regarding the term $\phi(x - x_0)$ was tested empirically, by using various data arc lengths and various magnitudes of error in the initial estimate. In all cases studied (up to 12 hours data arc for $\rho, \dot{\rho}$; 3 hours for ρ, α, δ) this assumption was justified.

4.2 NUMERICAL CONSIDERATIONS

There are several aspects of the preliminary orbit determination program that require consideration of possible numerical difficulties. The most significant of these are the matrix operations in the range and range-rate technique. It is necessary to accumulate and invert matrices of the form $M^T M$ in double precision in order to obtain satisfactory numerical results.

In addition, the calculation of the time from the orbital epoch should be in double precision. Without double precision the accuracy of the solution is decreased if large data arcs (where the effects of time errors are magnified) are being used. It is also important to realize that the quantization of the data may contribute a sizeable error in the ρ, α, δ program. For example, if α and δ are accurate to the nearest 0.001 of a degree, consider the error that occurs in $\bar{\rho}$. Since $\bar{\rho}$ has the components,

$$\bar{\rho} = (x, y, z)$$

$$\begin{aligned}x &= \rho \cos \delta \cos \alpha \\y &= \rho \cos \delta \sin \alpha \\z &= \rho \sin \delta\end{aligned}$$

the deviation in x is

$$\Delta x = -\rho \cos \delta \sin \alpha \Delta \alpha - \rho \sin \delta \cos \alpha \Delta \delta + \cos \delta \cos \alpha \Delta \rho$$

The magnitude of the rms error due to quantization of the angular measurement will be 0.3 (the rms deviation for a sawtooth waveform of unit amplitude) times the quantization interval, or $(0.3)(0.001)/57.295$ radians. The error in x

$$\Delta x = -\rho \sin (\alpha + \delta) \Delta \alpha$$

where we have neglected $\Delta \rho$ (since its standard deviation is only 20 meters), and set $\Delta \alpha = \Delta \delta$. Assuming $\sin (\alpha + \delta)$ to be maximum and evaluating the rms error in Δx provides,

$$\Delta x_{\text{rms}} = -\rho \frac{(1)(0.3)(0.001)}{57.295} \quad (54)$$

If ρ is in meters, then equation (54) gives, for the rms error in x due to angular data quantization, approximately

$$\begin{aligned}\Delta x_{\text{rms}} &= -0.4 \times 10^9 (0.525 \times 10^{-5}) \text{ meters} \\ &= -.21 \times 10^4 \text{ meters}\end{aligned} \quad (8)$$

The only way this error can be reduced is to increase the accuracy of α and δ . For the 0.001 quantization interval used here, the ρ, α, δ , set transformed to selenocentric position vectors (given the ephemeris of the moon) has only five significant figures; the remaining three are noise. The loss of accuracy does not prove to be a serious deterrent to obtaining a good estimate of the orbit.

For those cases in which the data included the nominal noise ($\sigma = 0.06^\circ$), the rms deviation in x is 60 times that due to quantization of the angular data; thus the 10^{-3} quantization of the angular data is

adequate. Again it should be noted that the difficulties associated with the inaccuracy of the angular data were overcome by the use of a least squares operator.

4.3 ORBIT SELECTION AND GENERATION OF DATA

In order to determine the effectiveness of the orbit determination process, data were generated based on two state vectors. One is the nominal state vector for the Lunar Orbiter, while the other is perturbed significantly from the nominal. The elements of the nominal orbit are:

a = 1.6129288 lunar radii
e = 0.29063512
i = 37.288795 degrees
 Ω = 17.143341 degrees
 ω = 19.260395 degrees
M = 3.4008163 degrees
 r_p = 1.1441545 lunar radii = 1988.64 km
 r_a = 2.0904123 lunar radii = 3633.32 km
Period = 221.99267 minutes

The elements of the perturbed orbit are:

a = 3.2930000 lunar radii
e = .63666150
i = 34.080858 degrees
 Ω = 17.604341 degrees
 ω = 19.173341 degrees
M = 359.99984 degrees
 r_p = 1.1964737 lunar radii = 2079.58 km
 r_a = 5.3895263 lunar radii = 9367.48 km
Period = 674.08036 minutes

The above angular quantities are in the selenocentric coordinate system. The epoch in each case is 27 June 1966, 4 hours, 0 minutes,

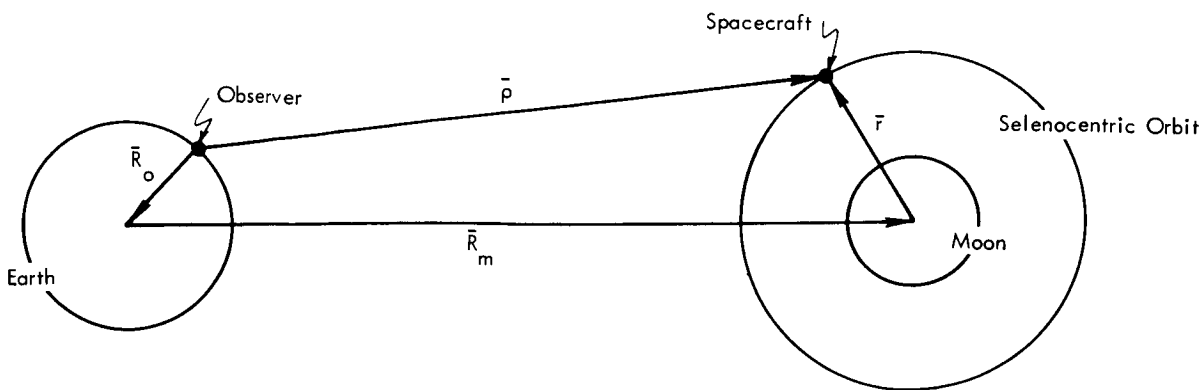
48.00 seconds. These two sets of data were used to examine the numerical characteristics of the preliminary orbit determination processes.

4.4 POSITION FIX TECHNIQUE

4.4.1 Mathematical Formulation

A primary objection to the use of angular data in preliminary orbit determination for a lunar satellite is the low quality of such data. The diameter of the moon is approximately 0.5° , and it is anticipated that a one sigma deviation of 0.06° could occur in the angular data; thus the error in the measurement is potentially only one order of magnitude smaller than the measured quantity. On the other hand, the range data, ρ , have a standard deviation of 20 m; this is more than 6 orders of magnitude smaller than the measured range, and thus should be more than adequate for the purpose proposed here. The problem, then, is to determine a technique which can use the low quality angular data and maintain accuracy.

The ρ, α, δ (position fix) technique is developed using the vector diagram in the sketch below. The vector $\bar{\rho}$ can be determined by the use of range and angular data. Let \bar{R}_o be the vector defining the observer's



position relative to the geocenter, \bar{R}_m the ephemeris of the moon, and \bar{r} the selenocentric position vector of the vehicle. Then it is clear that

$$\bar{r} = \bar{\rho} - (\bar{R}_o + \bar{R}_m)$$

It is also possible to represent the selenocentric position vector as

$$\bar{r} = f\bar{r}_o + g\dot{\bar{r}}_o \quad (55)$$

Equation (55) states that the motion of the satellite lies in a plane and can be represented using a two body gravitational model. The coefficients f and g are scalar functions of time, while \bar{r}_o and $\dot{\bar{r}}_o$ represent the position and velocity vectors of the vehicle at some time t_o .

There are two possible representations of the f and g coefficients. One is a time series expansion and the other is as a closed form coefficient. The advantage of a time series expansion is that it is not necessary to solve Kepler's equation. However, there is the disadvantage that a large number of terms is required to converge to a preassigned degree of accuracy. An additional disadvantage of the time series expansion is that the use of a large number of terms introduces numerical difficulties in the significance of the answer obtained. On the other hand, the closed form f and g coefficients are exact and Kepler's equation can be solved by use of the Newton-Raphson formula, which is quadratically convergent. A complete derivation of the closed form f and g coefficients is in appendix E. Equation (55) can be written as

$$\bar{r} = (f \ g) \begin{pmatrix} \bar{r}_o \\ \dot{\bar{r}}_o \end{pmatrix} \quad (56)$$

In general, if there are n observations, equation (56) becomes (writing out the components for \bar{r} , \bar{r}_0 and $\dot{\bar{r}}_0$),

$$\begin{bmatrix} x_1 \\ y_1 \\ z_1 \\ \hline x_2 \\ y_2 \\ z_2 \\ \hline \cdot \\ \cdot \\ \hline x_n \\ y_n \\ z_n \end{bmatrix} = \begin{bmatrix} f_1 I_{3 \times 3} & g_1 I_{3 \times 3} \\ \hline f_2 I_{3 \times 3} & g_2 I_{3 \times 3} \\ \hline \cdot & \cdot \\ \cdot & \cdot \\ \hline f_n I_{3 \times 3} & g_n I_{3 \times 3} \end{bmatrix} \begin{bmatrix} x_0 \\ y_0 \\ z_0 \\ \hline \dot{x}_0 \\ \dot{y}_0 \\ \dot{z}_0 \end{bmatrix} \quad (57)$$

where $I_{3 \times 3}$ is a 3 x 3 identity matrix. Equation (57) can be represented as

$$y = A(x_i) x_{i+1} \quad (58)$$

where x_{i+1} is $(i+1)^{st}$ value for x , and A is the matrix of f 's and g 's computed using the i^{th} value of x . The least squares solution of equation (58) is

$$x_{i+1} = (A(x_i)^T A(x_i))^{-1} A(x_i)^T y. \quad (59)$$

Formulation of the solution in terms of equation (59) will smooth the random errors associated with the angular data. The operator $(A^T A)^{-1} A^T$ in equation (59) has the effect of smoothing the data by minimizing the sum of the squares of the differences between the observed and computed selenocentric positions.

In order to obtain initial estimates for the values of f and g it is necessary to use an approximation. This is accomplished by selecting a short time interval of data centered about the epoch, averaging the

values of the position vector magnitudes, and assuming the orbit to be circular. Averaging the values of the position vector magnitudes produces a value for a , the semi-major axis. Then for the j^{th} observation,

$$f_j = \cos \Delta M_j$$

$$g_j = \Delta t_j + \frac{a^{3/2}}{\mu} \left[\sin \Delta M_j - \Delta M_j \right]$$

where ΔM_j is the change in the mean anomaly and is obtained from the mean motion and Δt_j . The quantity Δt_j is the time of the j^{th} observation measured from an arbitrary epoch. Since there may be a large number of observations, it is convenient to write equation (59) as

$$\mathbf{x} = \left(\sum_{j=1}^n (\mathbf{A}_j^T \mathbf{A}_j) \right)^{-1} \sum_{j=1}^n \mathbf{A}_j^T \mathbf{Y}_j$$

Once an initial value of \mathbf{x} is obtained, this value is used to generate improved values for the f and g coefficients. The process is repeated until the convergence criteria are satisfied.

4.4.2 Numerical Characteristics

In order to start the ρ, α, δ orbit determination process, it is necessary to obtain a first guess for the value of the state vector. The present technique considers a short arc of data and uses a circular approximation to obtain a state vector. In order to determine the convergence capabilities of the program, this initial approximation was bypassed, and arbitrary state vectors were input including large errors to see if the process would still converge. In one test case it was found that it is possible to input as an initial estimate a state vector whose position and velocity vector components are in error by factors of 10 and whose signs are arbitrarily changed, and still achieve convergence. Table VIII shows the values of \mathbf{x} and $\dot{\mathbf{x}}$ assumed as the first approximation, together with the values computed by the program on successive iterations.

TABLE VIII. ITERATION HISTORY FOR THE ρ, α, δ PROGRAM WITH A POOR INITIAL ESTIMATE

Note: In this test the nominal pre-estimate subroutine was bypassed. The circular approximation in that subroutine would give an initial estimate far superior to that used here.

State vector	x (meters)	\dot{x} (meters/sec)
Actual	$.7898036 \times 10^6$	1.275553×10^3
First guess	-21.336042	-.0050800
First computed value	.7720043	1.255805
Second computed value	.7910757	1.277078
Third computed value	.7897181	1.275440
Fourth computed value	.7897797	1.275554
Fifth computed value	.7898039	1.275546
Sixth computed value	.7898043	1.275546

The quantities x and \dot{x} are representative and were chosen for convenience. On the first iteration, the sign on the x component is reversed (as it should be), and the magnitude is good to two figures. On subsequent iterations, the estimate oscillates with a decreasing amplitude about the actual state vector.

Effect of Angular Data Quality. - There is a definite dependence in the quality of the answer on the quality of the data. Figures 35 through 40 illustrate the effect of a constant bias of $0^\circ.0$ in the angular data, and 1 sigma random components in the angles of $0^\circ.06$, $0^\circ.01$ and $0^\circ.005$, for an eccentricity of 0.29. The same plots are shown in figures 41 through 46 for an eccentricity of 0.63. The independent variable in the above plots is the length of observation arc (in minutes), and the dependent variable is the deviation of the computed values of the osculating orbital elements from the actual values.

It is clear from figures 35 through 40 that if $\sigma = 0.06^\circ$, the time of observation required to achieve a given accuracy estimate is markedly longer than for $\sigma = 0.01^\circ$ or $\sigma = 0.005^\circ$. The minimum time to observe the vehicle for preliminary orbit determination for the nominal angular data noise of $0^\circ.06$ is approximately 40 minutes; for longer observing times, the deviation is reduced. With the nominal σ of $0^\circ.06$, an observation time of 40 minutes will allow recovery of the orientation elements, i , Ω and ω , with less than a 2° error, the eccentricity, e , to one significant figure, the epoch mean anomaly, M_o , with an error of $1/2^\circ$, and the semi-major axis, a , with an error of 30 km.

Increasing the observation span to 60 minutes has very little effect on the quality of the estimates of a and M_o . However, there is substantial improvement in the orientation element recovery, with the error reduced to less than $0^\circ.3$. For the nominal intermediate lunar orbit, about 60 minutes of data can be taken before the first occultation by the moon, so these accuracies should be attainable.

For the highly eccentric orbit ($\rho = 0.63$, figures 7 through 12), 60 minutes of tracking with the $0^\circ.06$ angular data gives significantly poorer estimates than those obtained at the 0.29 eccentricity. The orientation

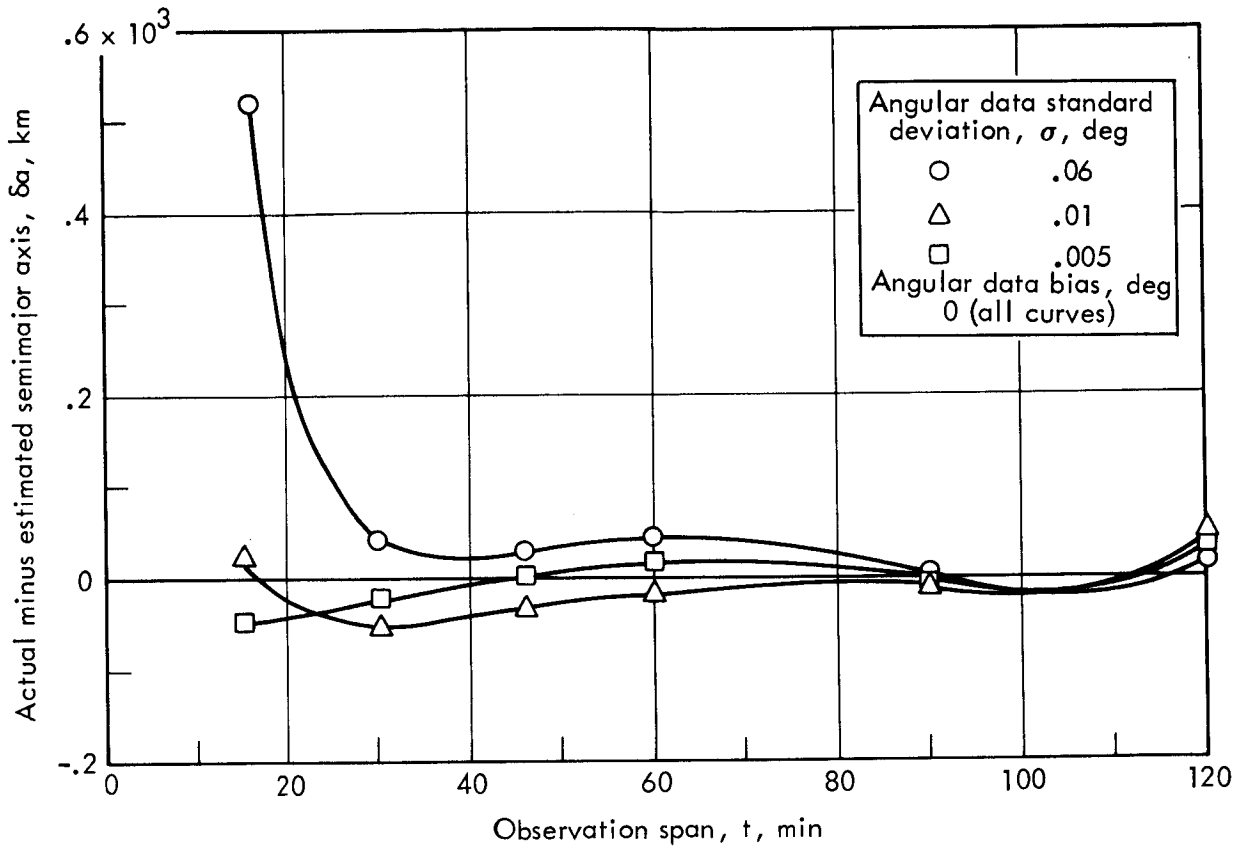


FIGURE 35. — SEMI-MAJOR AXIS ESTIMATE QUALITY VERSUS OBSERVATION SPAN FOR VARIOUS ANGULAR DATA STANDARD DEVIATIONS ($e = 0.29$)

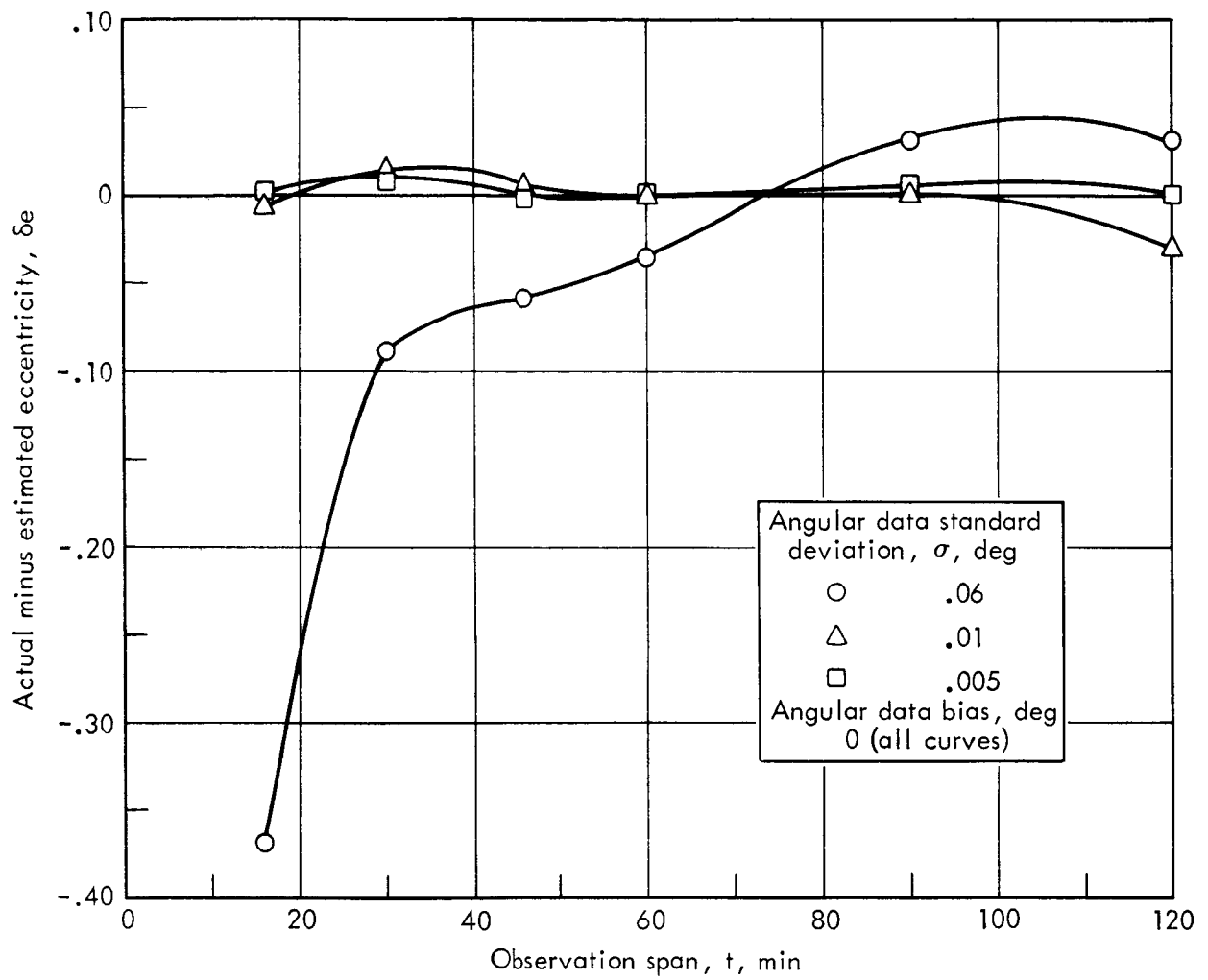


FIGURE 36.— ECCENTRICITY ESTIMATE QUALITY VERSUS OBSERVATION SPAN FOR VARIOUS ANGULAR DATA STANDARD DEVIATIONS ($e = 0.29$)

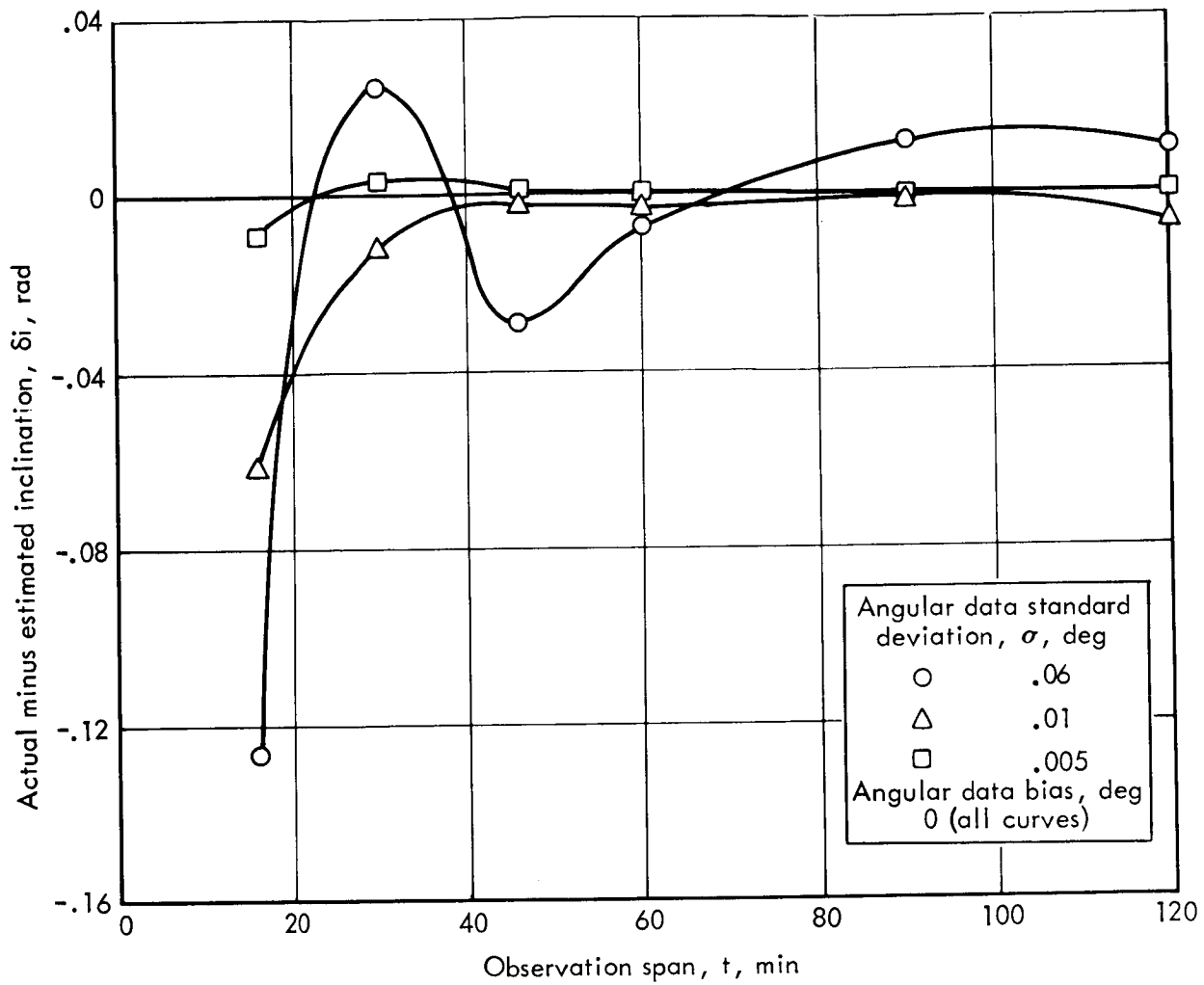


FIGURE 37. — INCLINATION ESTIMATE QUALITY VERSUS OBSERVATION SPAN FOR VARIOUS ANGULAR DATA STANDARD DEVIATIONS ($e = 0.29$)

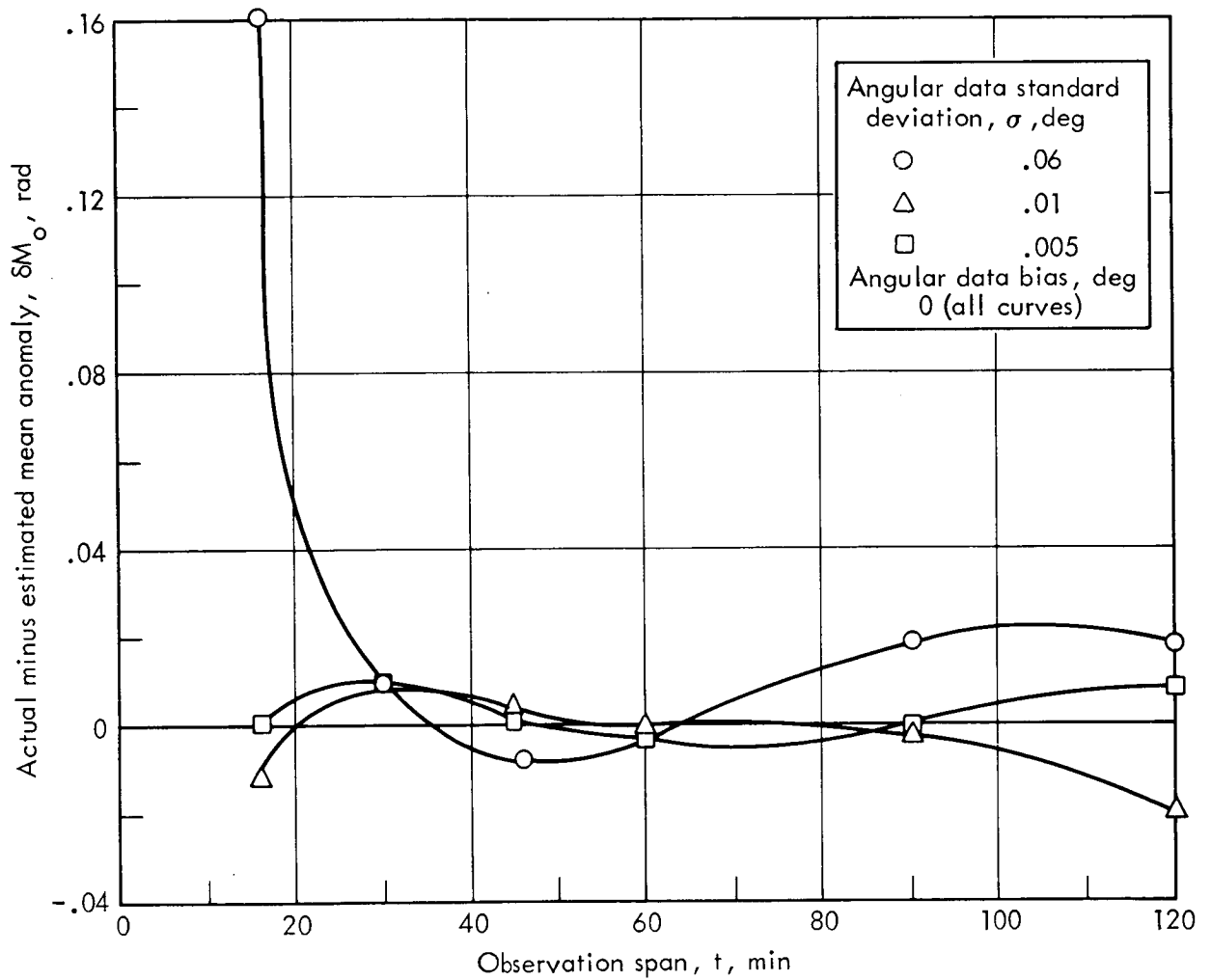


FIGURE 38.—NODAL LONGITUDE ESTIMATE QUALITY VERSUS OBSERVATION SPAN FOR VARIOUS ANGULAR DATA STANDARD DEVIATIONS ($e = 0.29$)

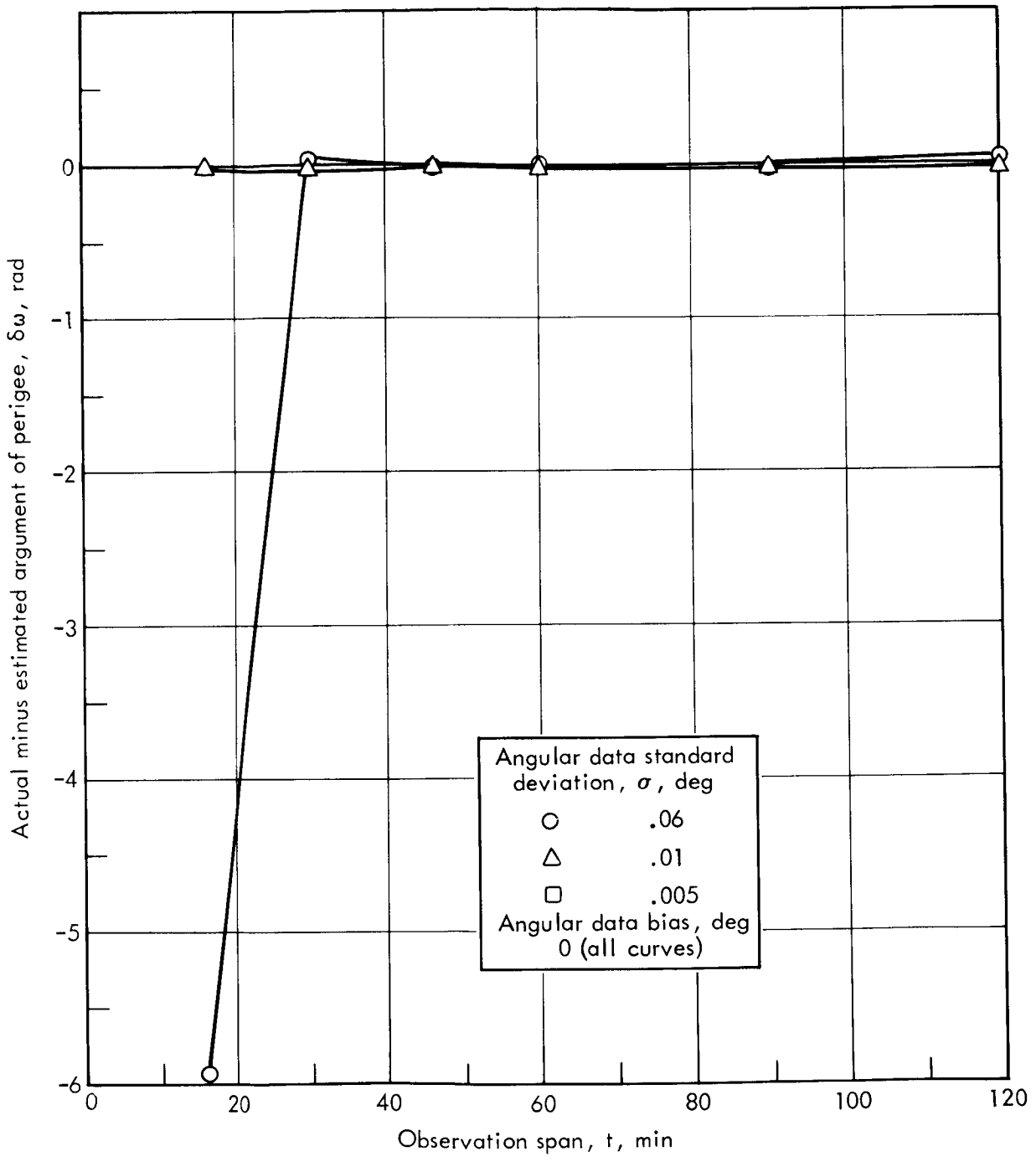


FIGURE 39.—ARGUMENT OF PERIGEE ESTIMATE QUALITY VERSUS OBSERVATION SPAN FOR VARIOUS ANGULAR DATA STANDARD DEVIATIONS ($e = 0.29$)

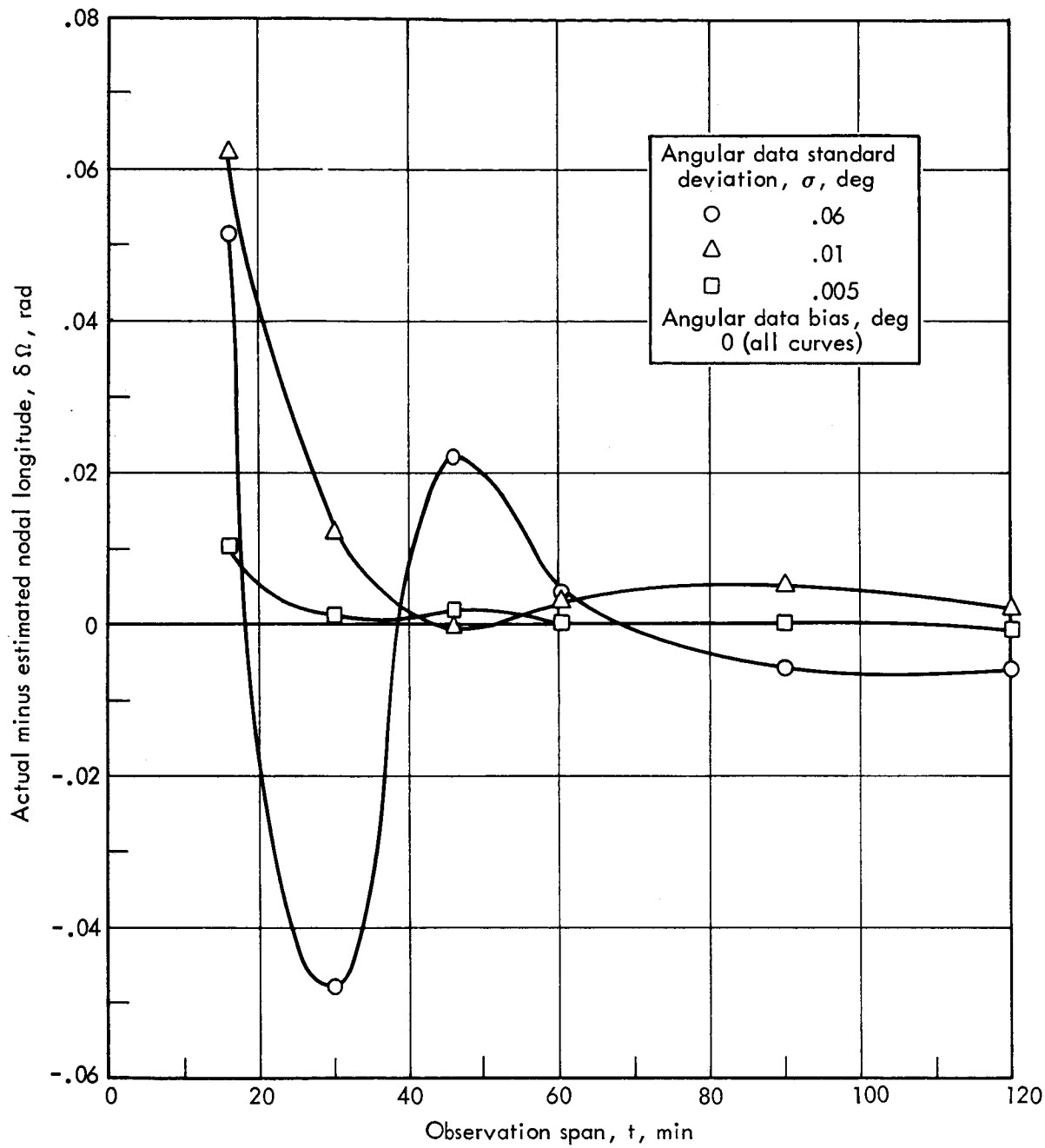


FIGURE 40. — EPOCH MEAN ANOMALY ESTIMATE QUALITY VERSUS OBSERVATION SPAN FOR VARIOUS DATA STANDARD DEVIATIONS ($e = 0.29$)

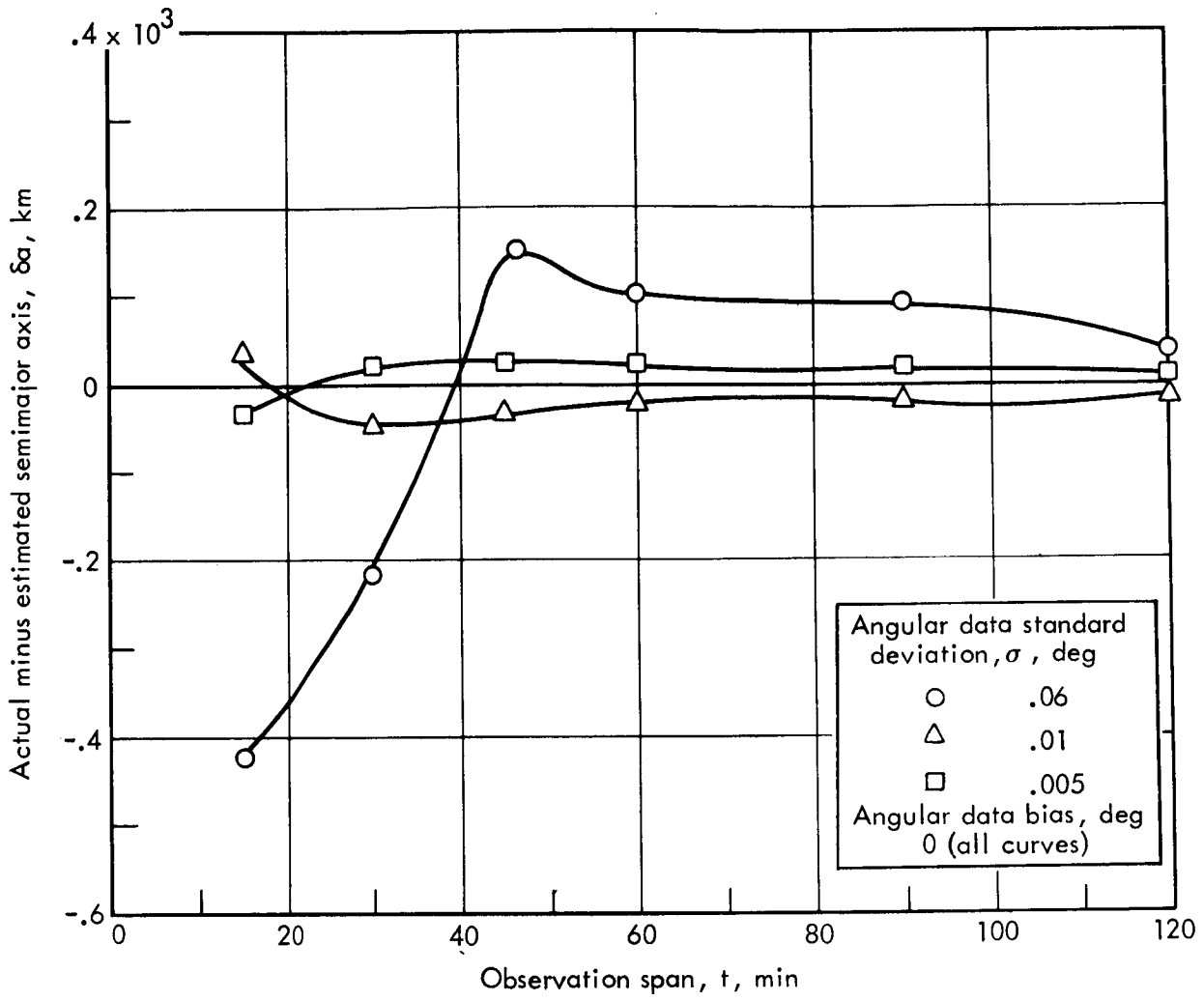


FIGURE 41. — SEMI-MAJOR AXIS ESTIMATE QUALITY VERSUS OBSERVATION SPAN FOR VARIOUS ANGULAR DATA STANDARD DEVIATIONS ($e = 0.63$)

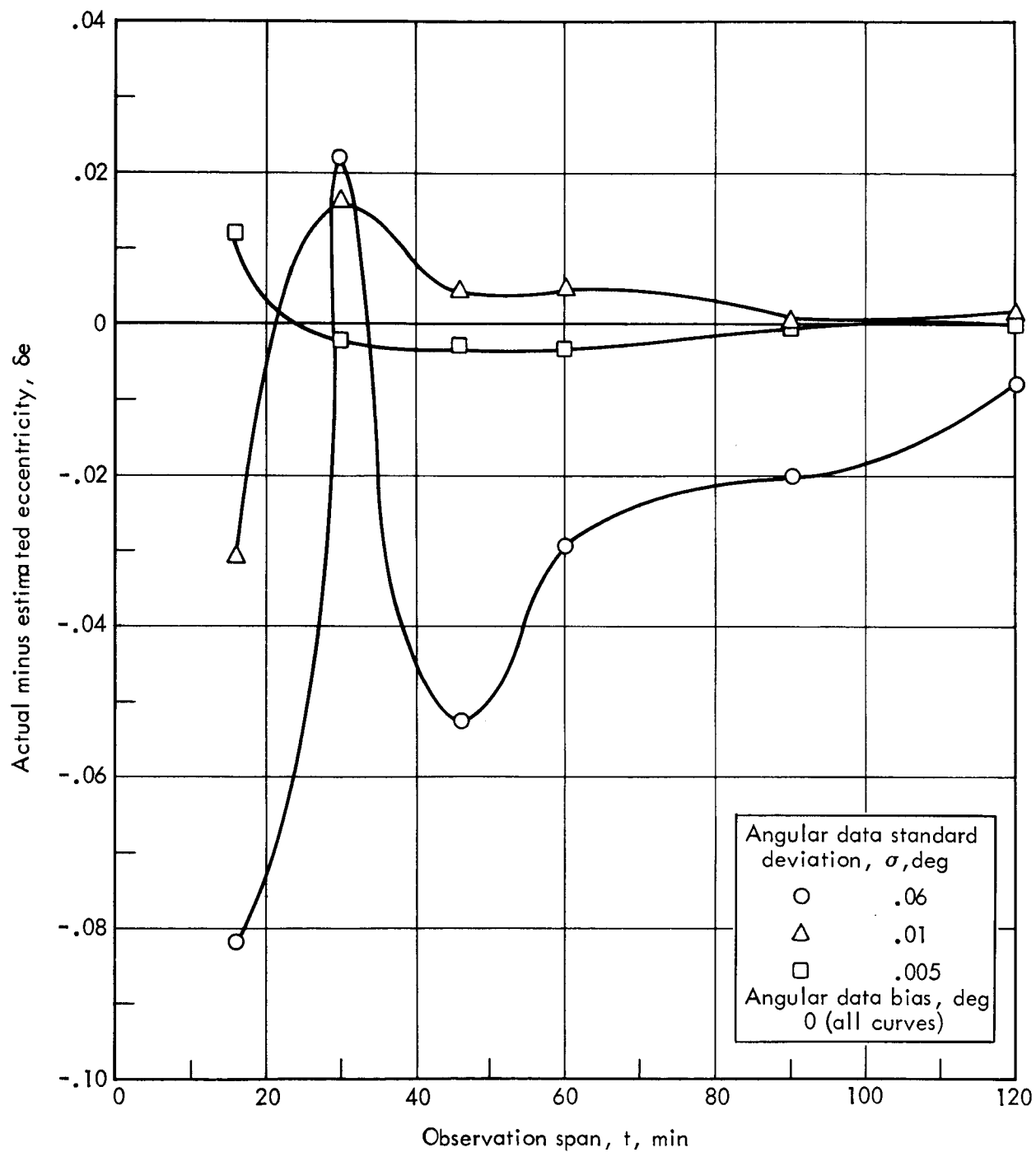


FIGURE 42. — ECCENTRICITY ESTIMATE QUALITY VERSUS OBSERVATION SPAN FOR VARIOUS ANGULAR DATA STANDARD DEVIATIONS ($e = 0.63$)

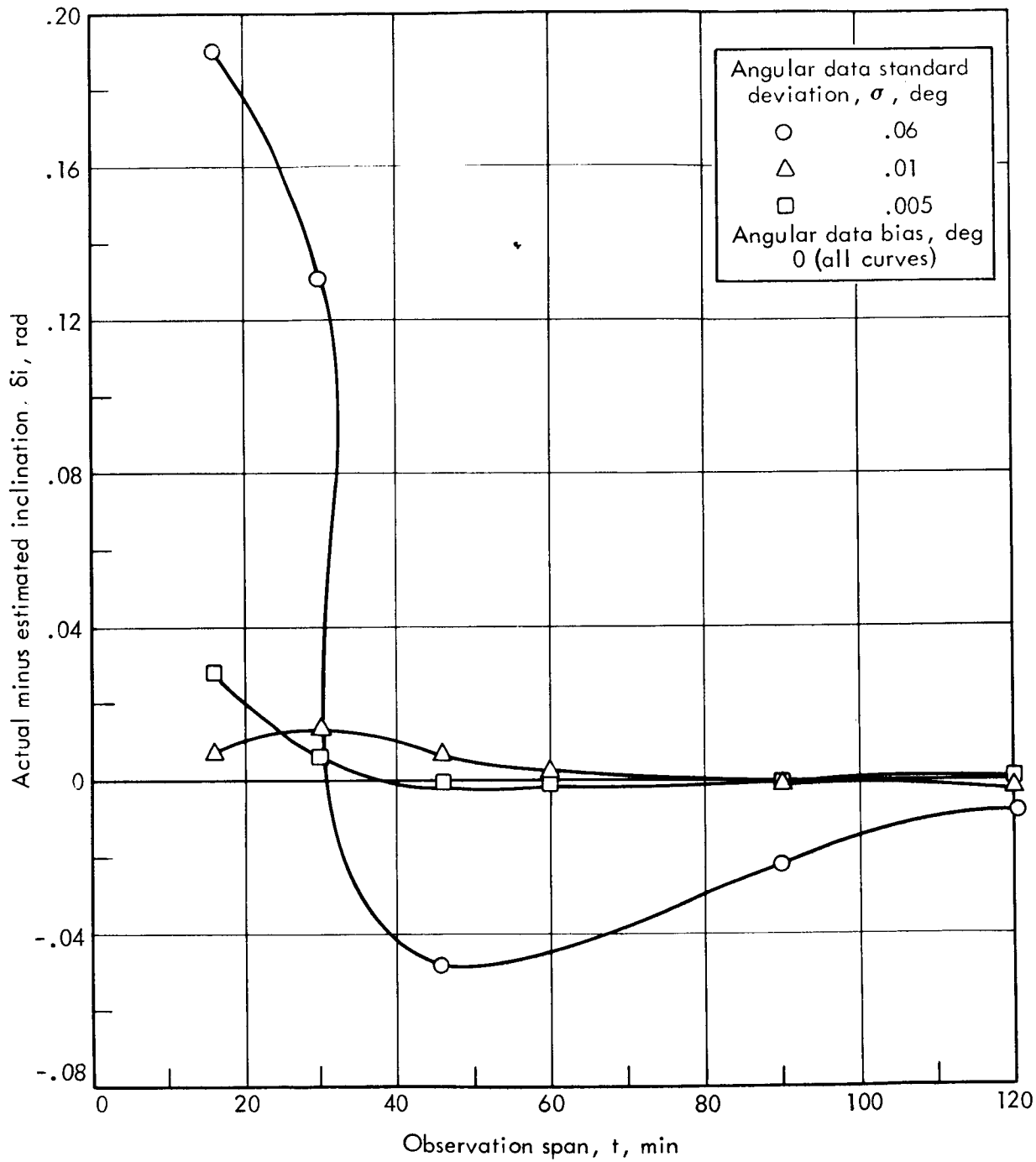


FIGURE 43.—INCLINATION ESTIMATE QUALITY VERSUS OBSERVATION SPAN FOR VARIOUS ANGULAR DATA STANDARD DEVIATIONS ($e = 0.63$)

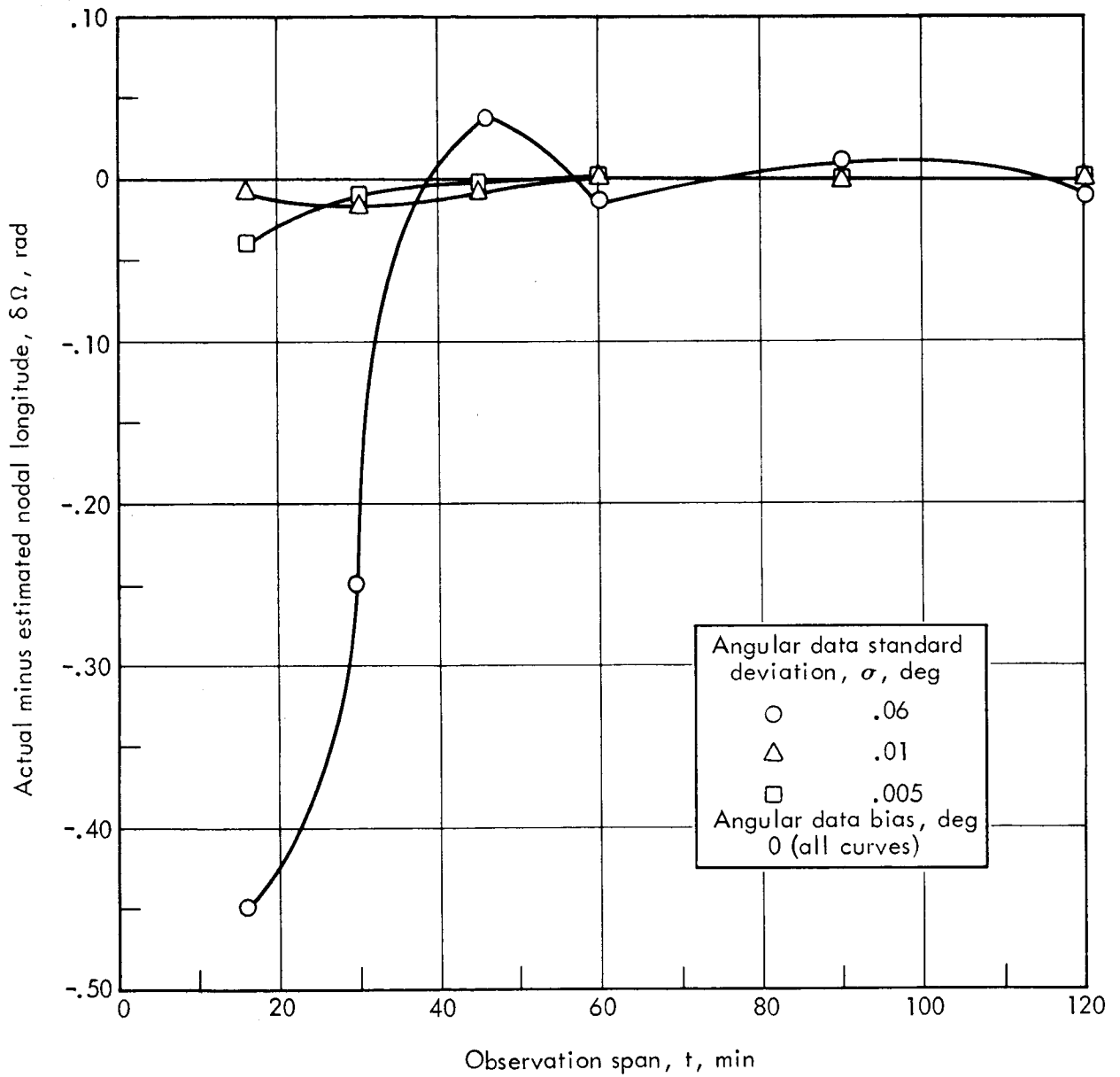


FIGURE 44.—NODAL LONGITUDE ESTIMATE QUALITY VERSUS OBSERVATION SPAN FOR VARIOUS ANGULAR DATA STANDARD DEVIATIONS ($e = 0.63$)

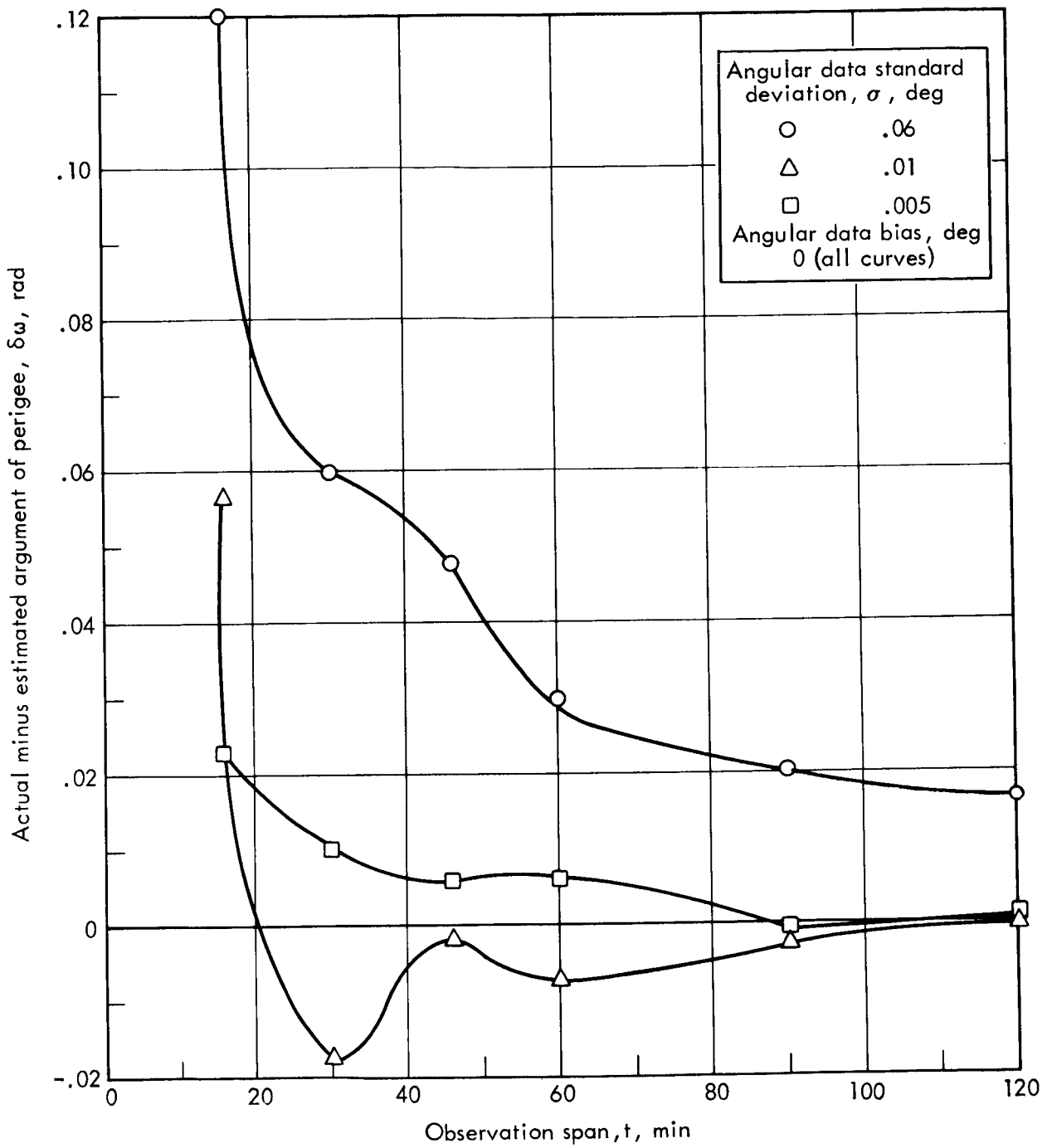


FIGURE 45.—ARGUMENT OF PERIGEE ESTIMATE QUALITY VERSUS OBSERVATION SPAN FOR VARIOUS ANGULAR DATA STANDARD DEVIATIONS ($e = 0.63$)

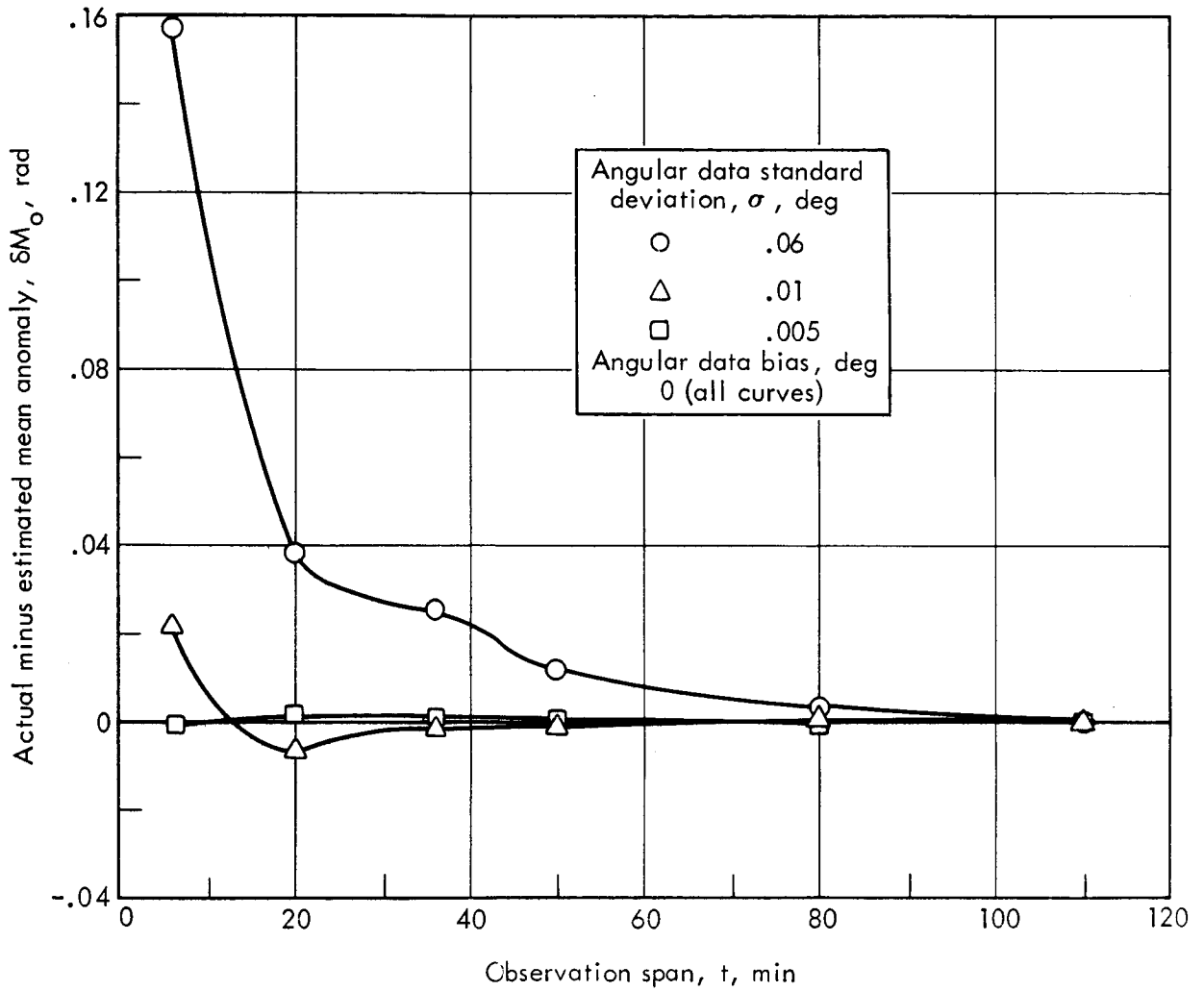


FIGURE 46.— EPOCH MEAN ANOMALY ESTIMATE QUALITY VERSUS OBSERVATION SPAN FOR VARIOUS ANGULAR DATA STANDARD DEVIATIONS ($e = 0.63$)

element errors are up to $2^{\circ}.5$, M_o is in error by $0^{\circ}.6$, a is in error by 100 km and e is good to 1 significant figure. The increase in estimate quality with increasing data span is more pronounced here than it was at the lower eccentricity. Comparison of the estimates ($e = 0.63$ vs. $e = 0.29$) after two hours of tracking reveals no significant degradation for the larger eccentricity; in fact, e itself and M_o are recovered with higher accuracy.

Effect of Angular Data Biases. - Figures 47 through 52 represent the effect of data biases of 0° , $0^{\circ}.001$, $0^{\circ}.01$ and $0^{\circ}.1$ (with σ constant at $0^{\circ}.06$), for an eccentricity equal 0.29. Figures 53 through 58 present the same effect for eccentricity equal 0.63. For the data with $\sigma = 0^{\circ}.06$ ($e = 0.63$) and observation spans greater than 60 minutes, there is a general degradation of estimate quality with increasing angular data bias. The most severe errors occur in the orientation elements, with the bias of $0^{\circ}.1$ giving an error of more than 6° in inclination, 10° in nodal longitude and 10° in argument of perigee; there is also an error of 18° in M_o . In addition, it is clear that as the bias increases it is necessary to observe for a longer time. Again the effect of observing for a longer time than that indicated on the graphs is to reduce the magnitude of the deviation.

Figures 59 through 64 represent the effect of biases of 0.0° , 0.001° , 0.01° , 0.1° (with σ constant at 0.005), for eccentricity equal 0.29.

The effects of biases on a and e are masked by the low quality angular data ($\sigma = 0^{\circ}.06$) in figures 47 and 48. Reducing the σ to $0^{\circ}.005$ (figures 59 through 64) gives a somewhat clearer picture of the bias effect. Figures 59 and 60, in particular, show plainly the increasingly poor estimate quality as the angular data biases are increased.

Effect of the Number of Observing Sensors. - One might expect that if two stations are observing a vehicle, that the results would be better than one station observing because of the triangulation effect. The effect of using two stations is to strengthen the smoothing capability of the least squares operator. In table IX the effect of one station versus

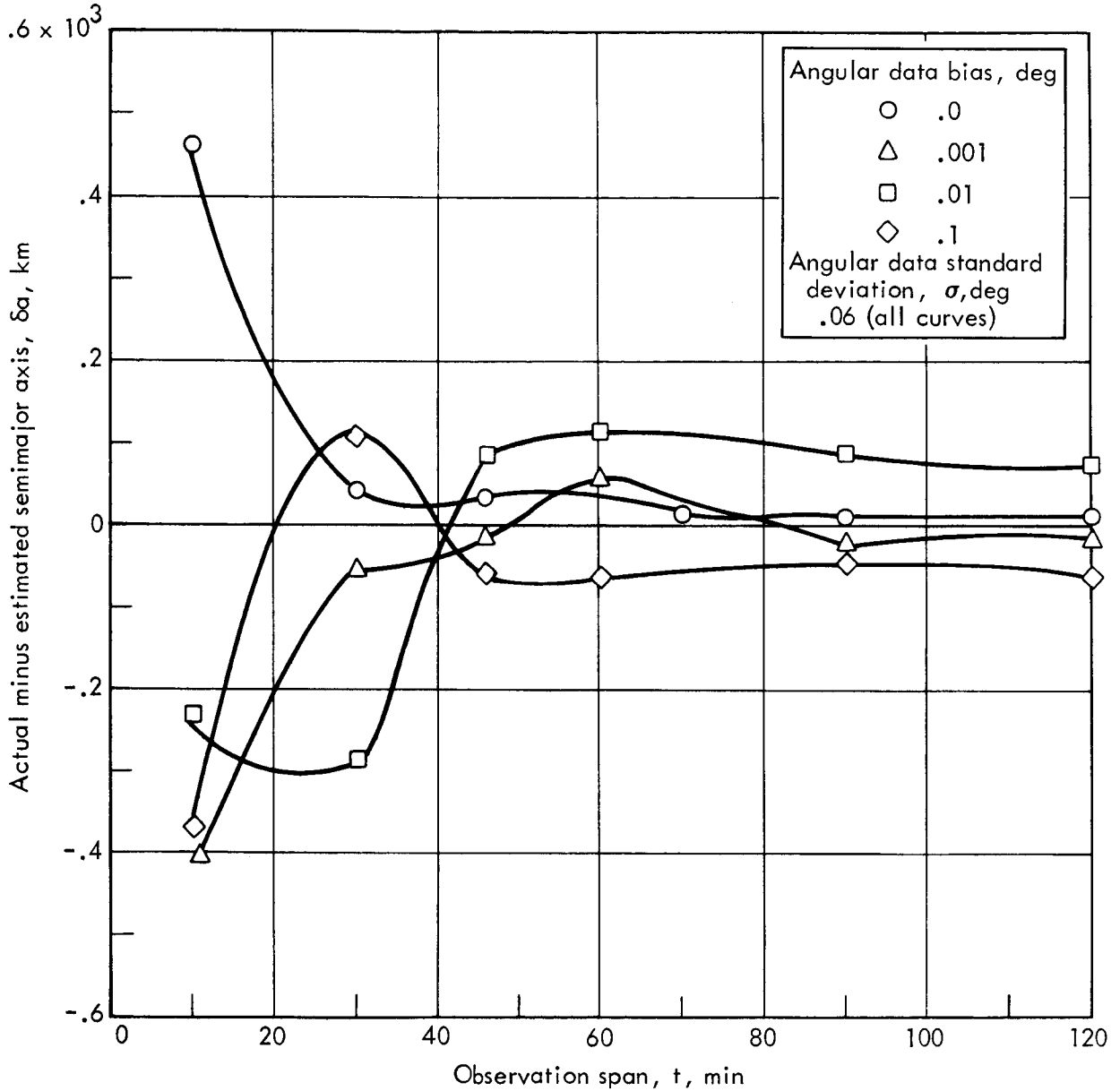


FIGURE 47. — SEMI-MAJOR AXIS ESTIMATE QUALITY VERSUS OBSERVATION SPAN FOR VARIOUS ANGULAR DATA BIASES ($e = 0.29$)

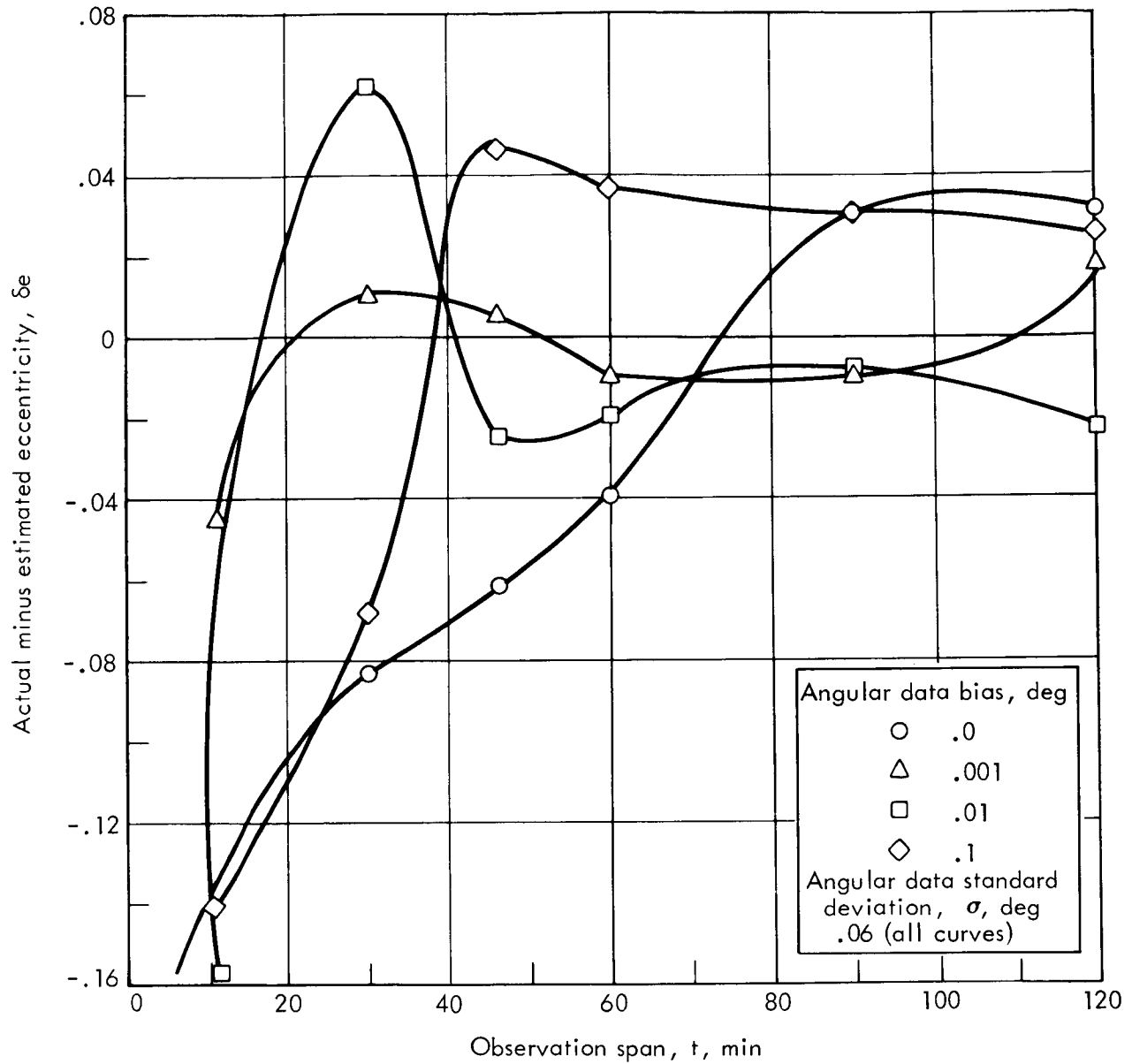


FIGURE 48.— ECCENTRICITY ESTIMATE QUALITY VERSUS OBSERVATION SPAN FOR VARIOUS DATA BIASES ($e = 0.29$)

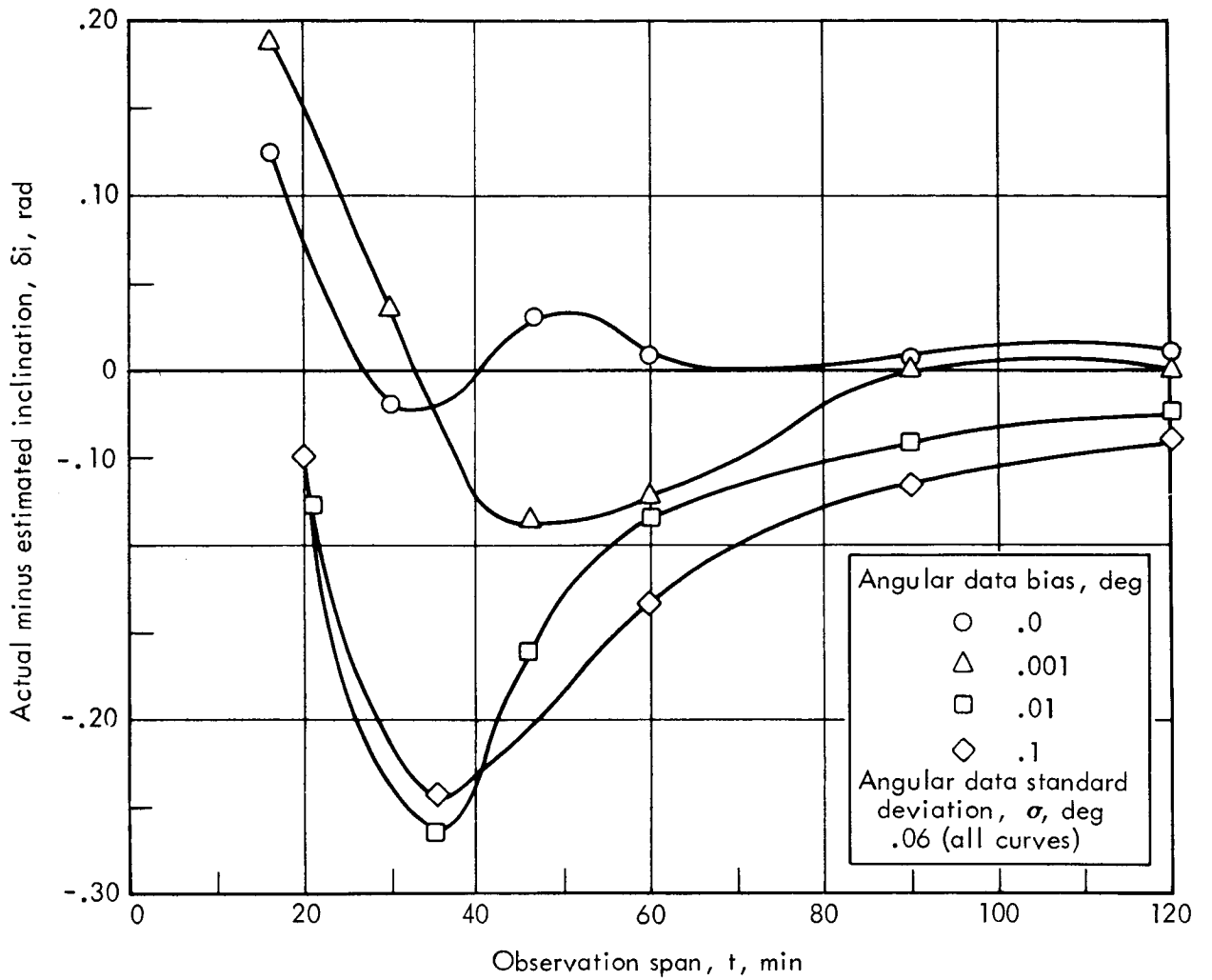


FIGURE 49.—INCLINATION ESTIMATE QUALITY VERSUS OBSERVATION SPAN FOR VARIOUS ANGULAR DATA BIASES ($e = 0.29$)

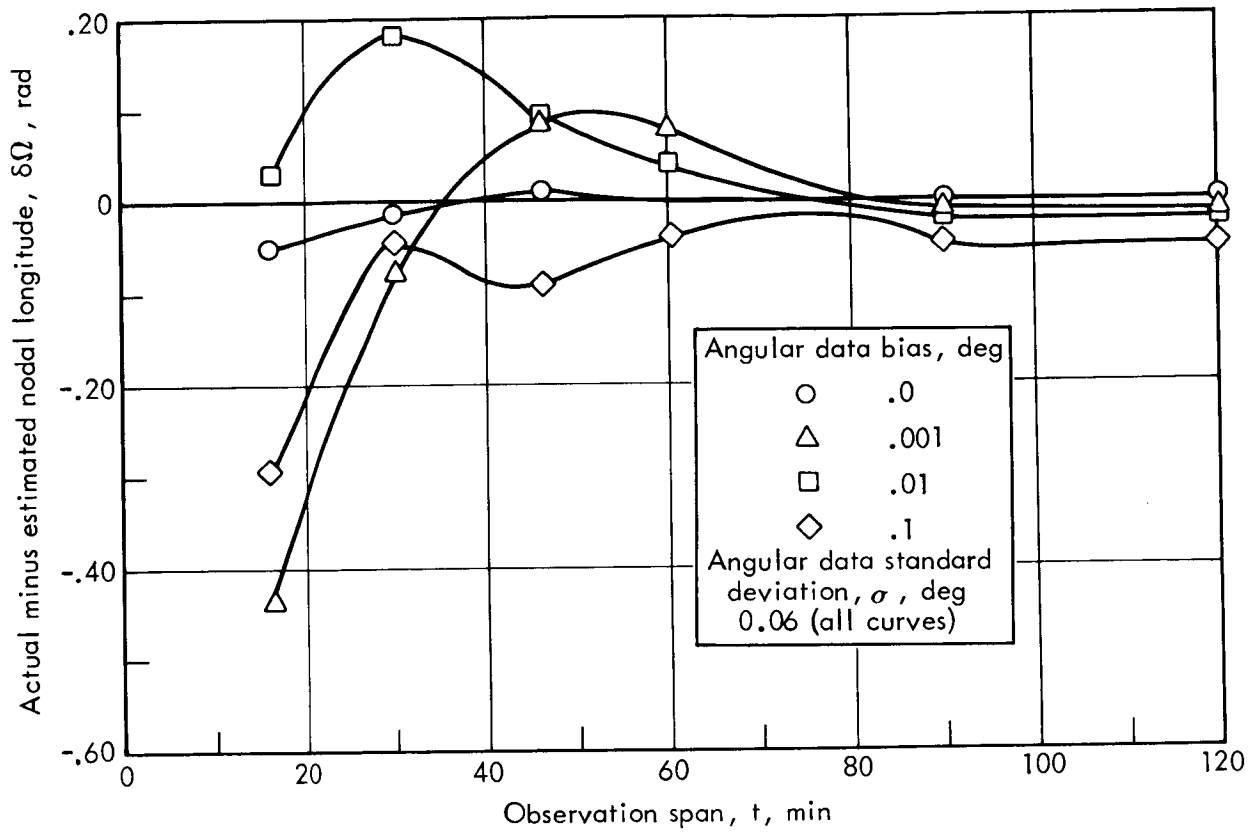


FIGURE 50.—NODAL LONGITUDE ESTIMATE QUALITY VERSUS OBSERVATION SPAN FOR VARIOUS ANGULAR DATA BIASES ($e = 0.29$)

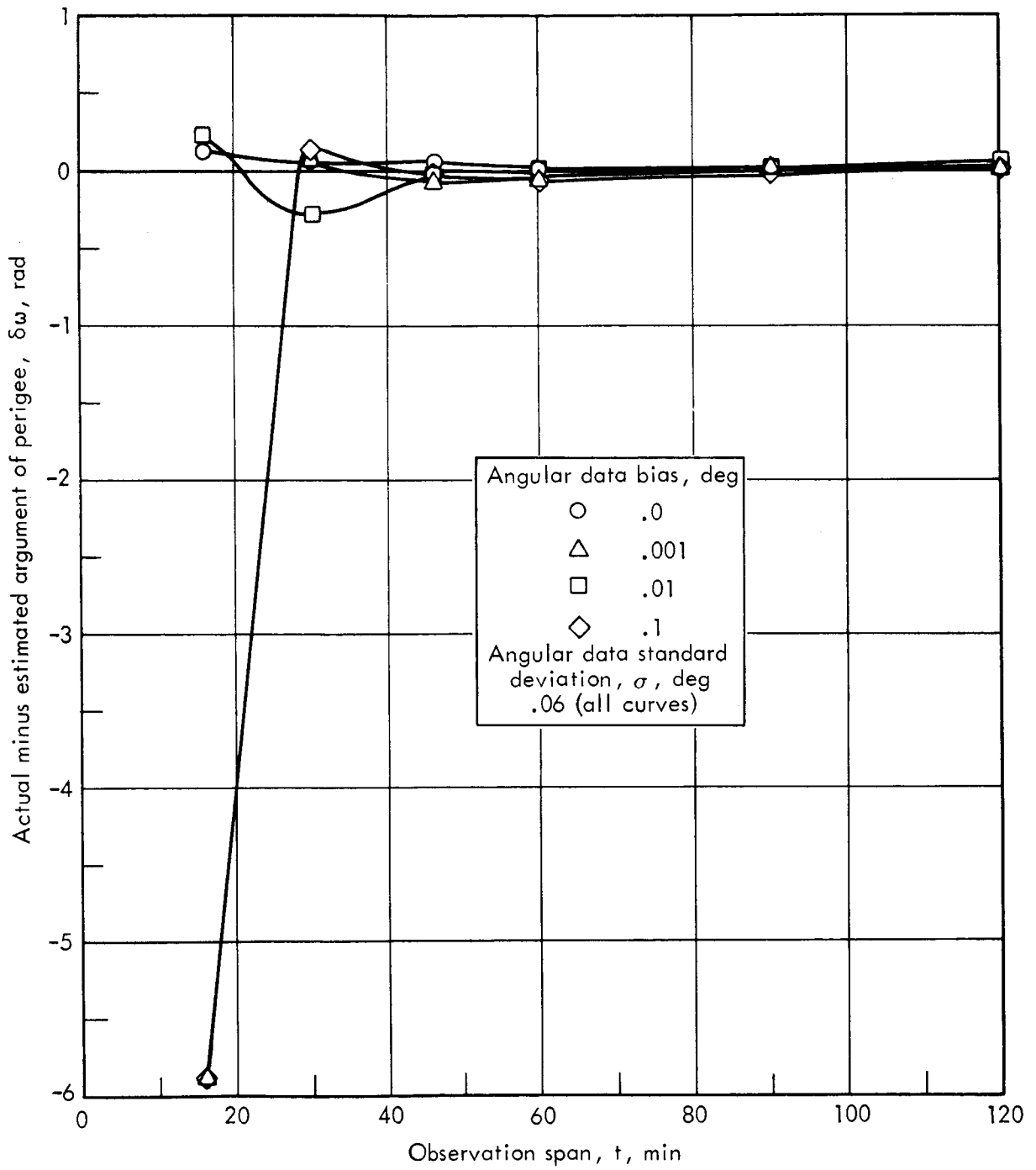


FIGURE 51. — ARGUMENT OF PERIGEE ESTIMATE QUALITY VERSUS OBSERVATION SPAN FOR VARIOUS ANGULAR DATA BIASES ($e = 0.23$)

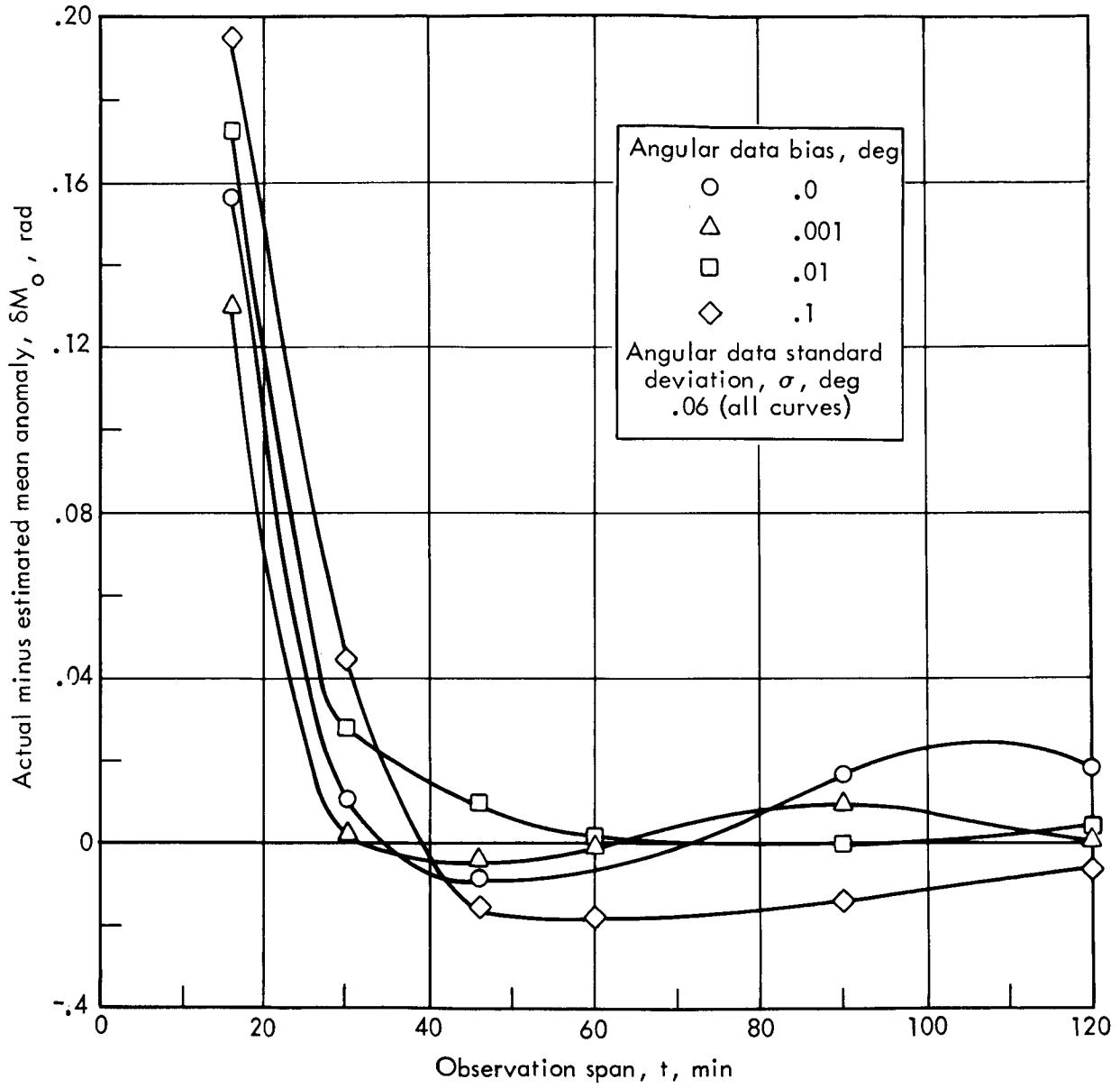


FIGURE 52.— EPOCH MEAN ANOMALY ESTIMATE QUALITY VERSUS OBSERVATION SPAN FOR VARIOUS ANGULAR DATA BIASES ($e = 0.29$)

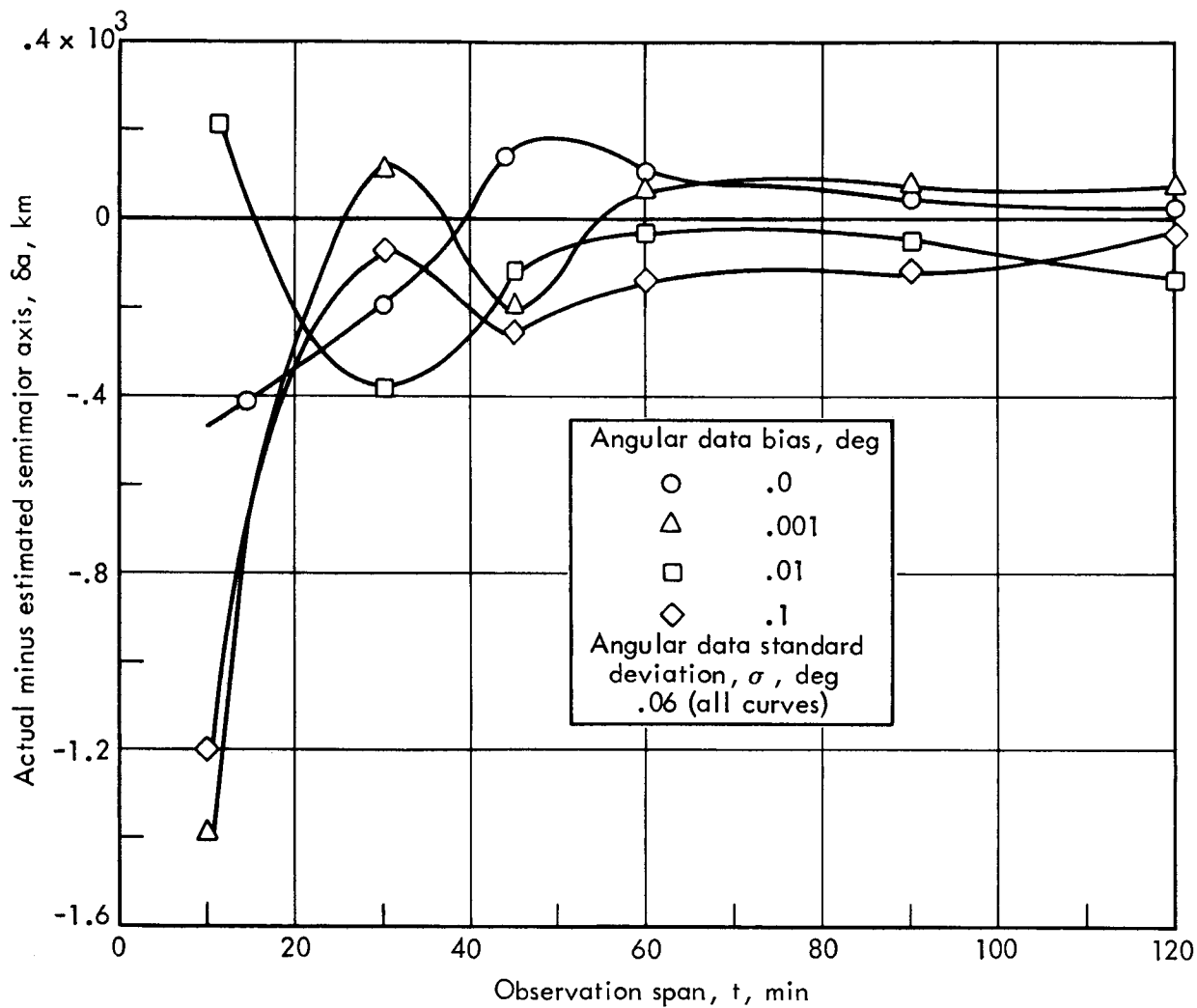


FIGURE 53. — SEMI-MAJOR AXIS ESTIMATE QUALITY VERSUS OBSERVATION SPAN FOR VARIOUS ANGULAR DATA BIASES ($e = 0.63$)

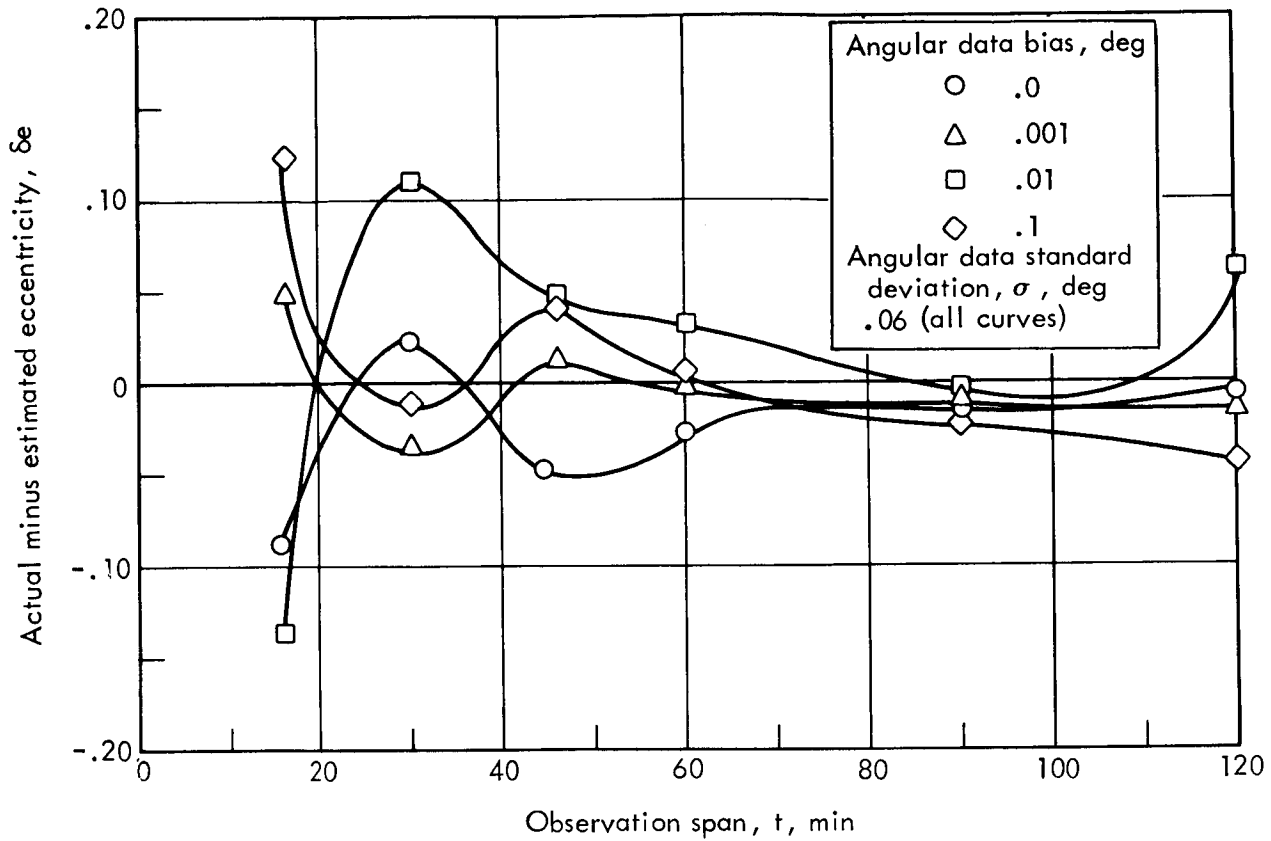


FIGURE 54. — ECCENTRICITY ESTIMATE QUALITY VERSUS OBSERVATION SPAN FOR VARIOUS ANGULAR DATA BIASES ($e = 0.63$)

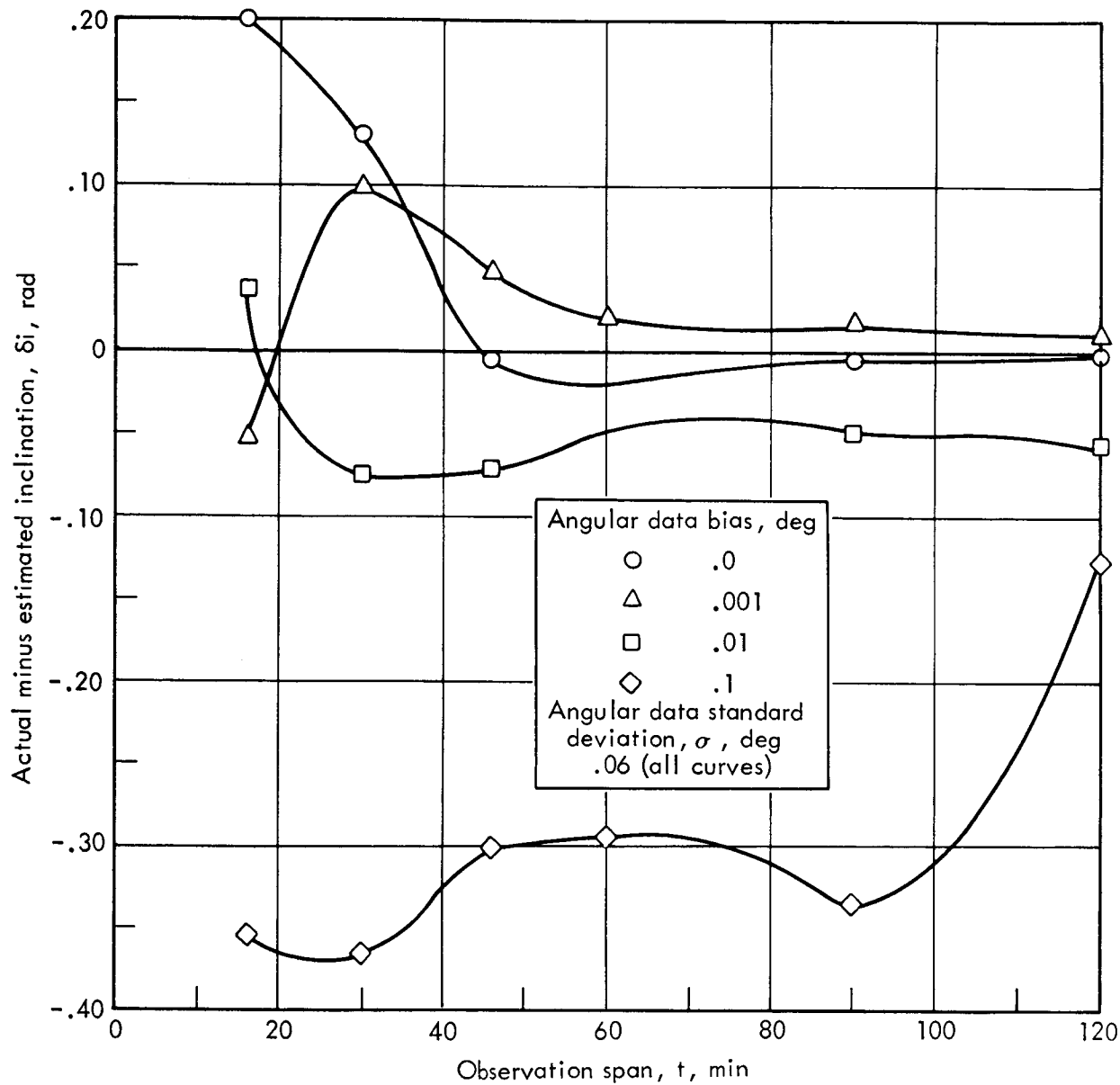


FIGURE 55.—INCLINATION ESTIMATE QUALITY VERSUS OBSERVATION SPAN FOR VARIOUS ANGULAR DATA BIASES ($e = 0.63$)

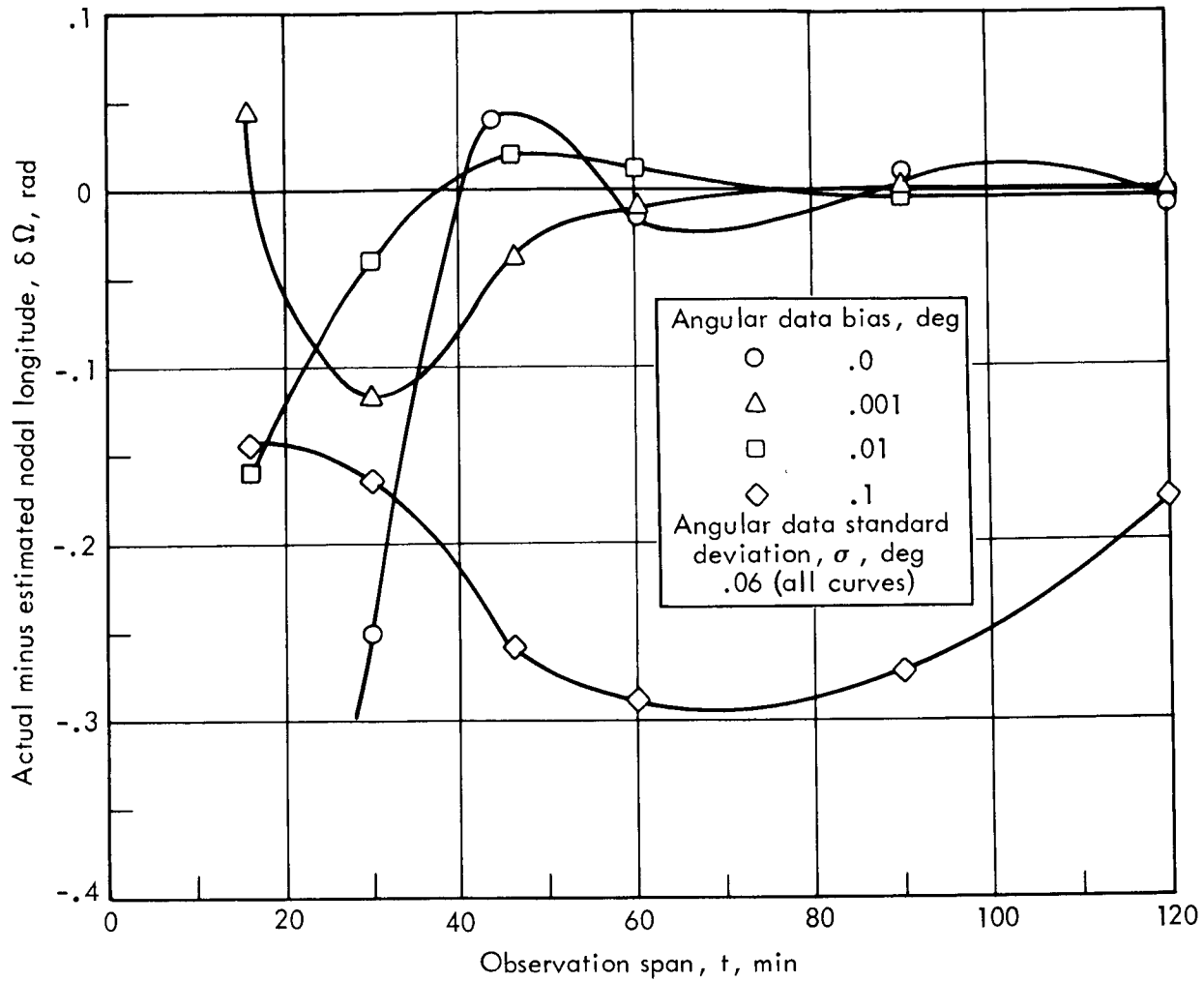


FIGURE 56.—NODAL LONGITUDE ESTIMATE QUALITY VERSUS OBSERVATION SPAN FOR VARIOUS ANGULAR DATA BIASES ($e = 0.63$)

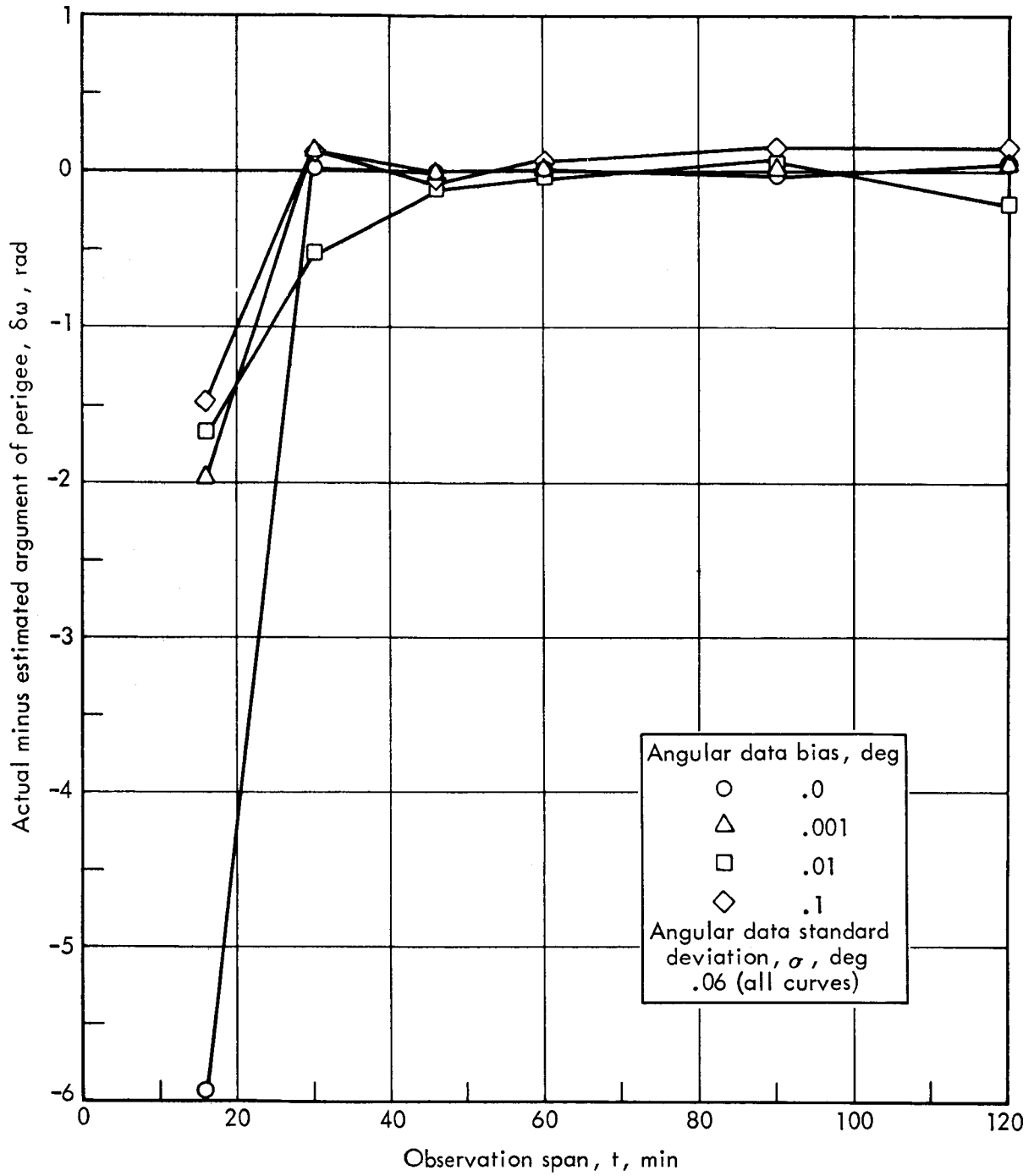


FIGURE 57.—ARGUMENT OF PERIGEE ESTIMATE QUALITY VERSUS OBSERVATION SPAN FOR VARIOUS ANGULAR DATA BIASES ($e = 0.63$)

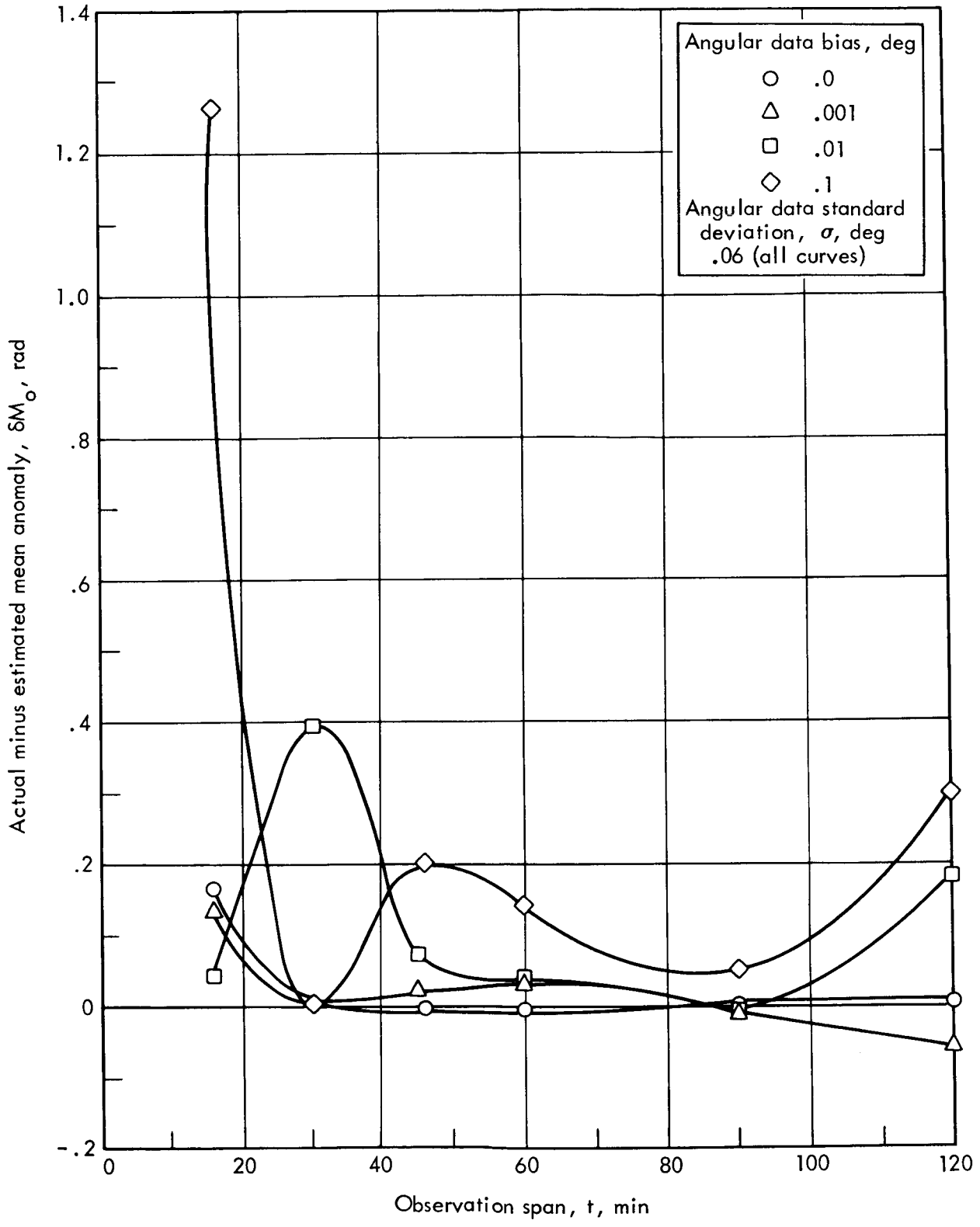


FIGURE 58. — EPOCH MEAN ANOMALY ESTIMATE VERSUS OBSERVATION SPAN FOR VARIOUS ANGULAR DATA BIASES ($e = 0.63$)

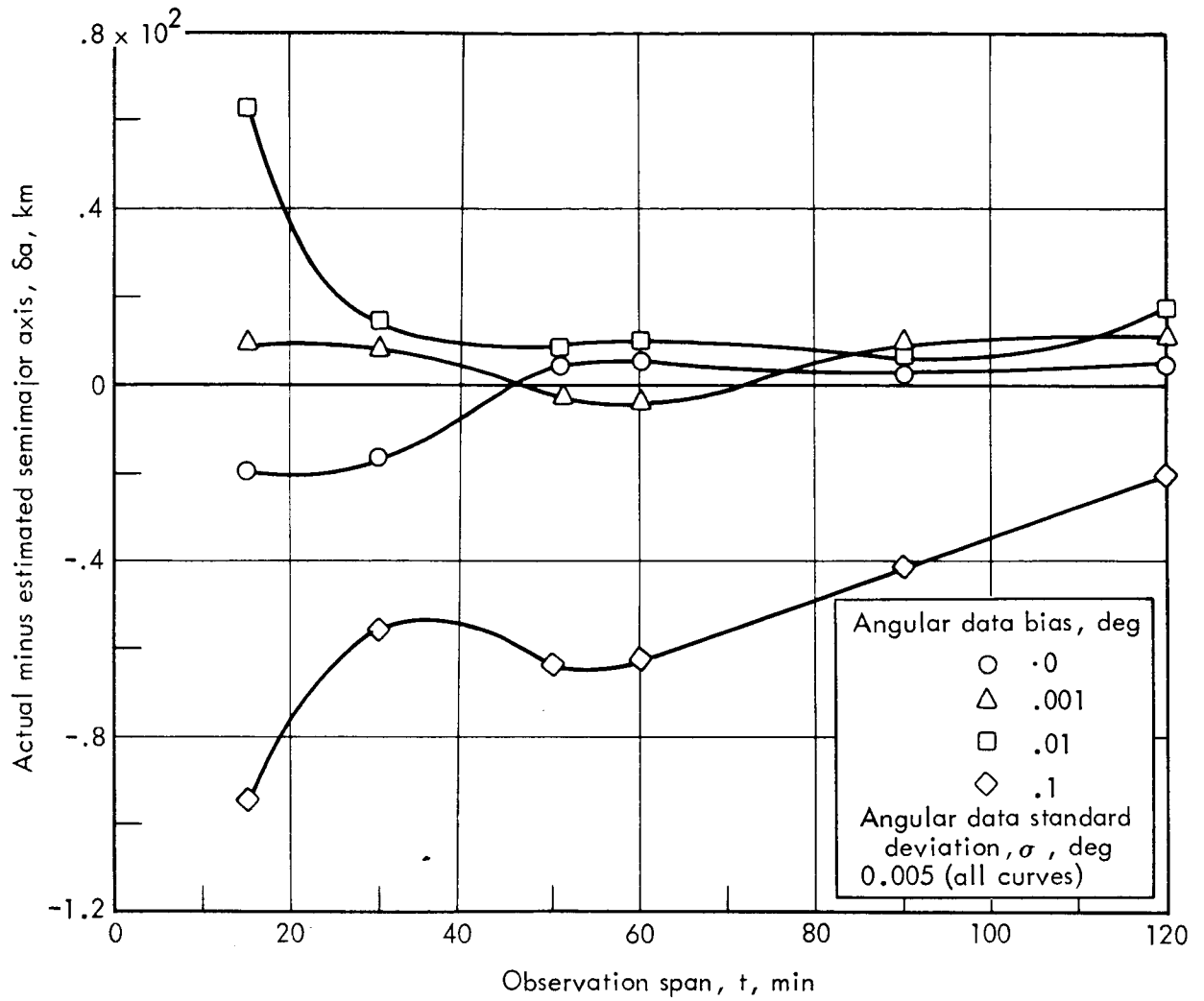


FIGURE 59. — SEMI-MAJOR AXIS ESTIMATE QUALITY VERSUS OBSERVATION SPAN FOR VARIOUS ANGULAR DATA BIASES ($\sigma = 0.005$)

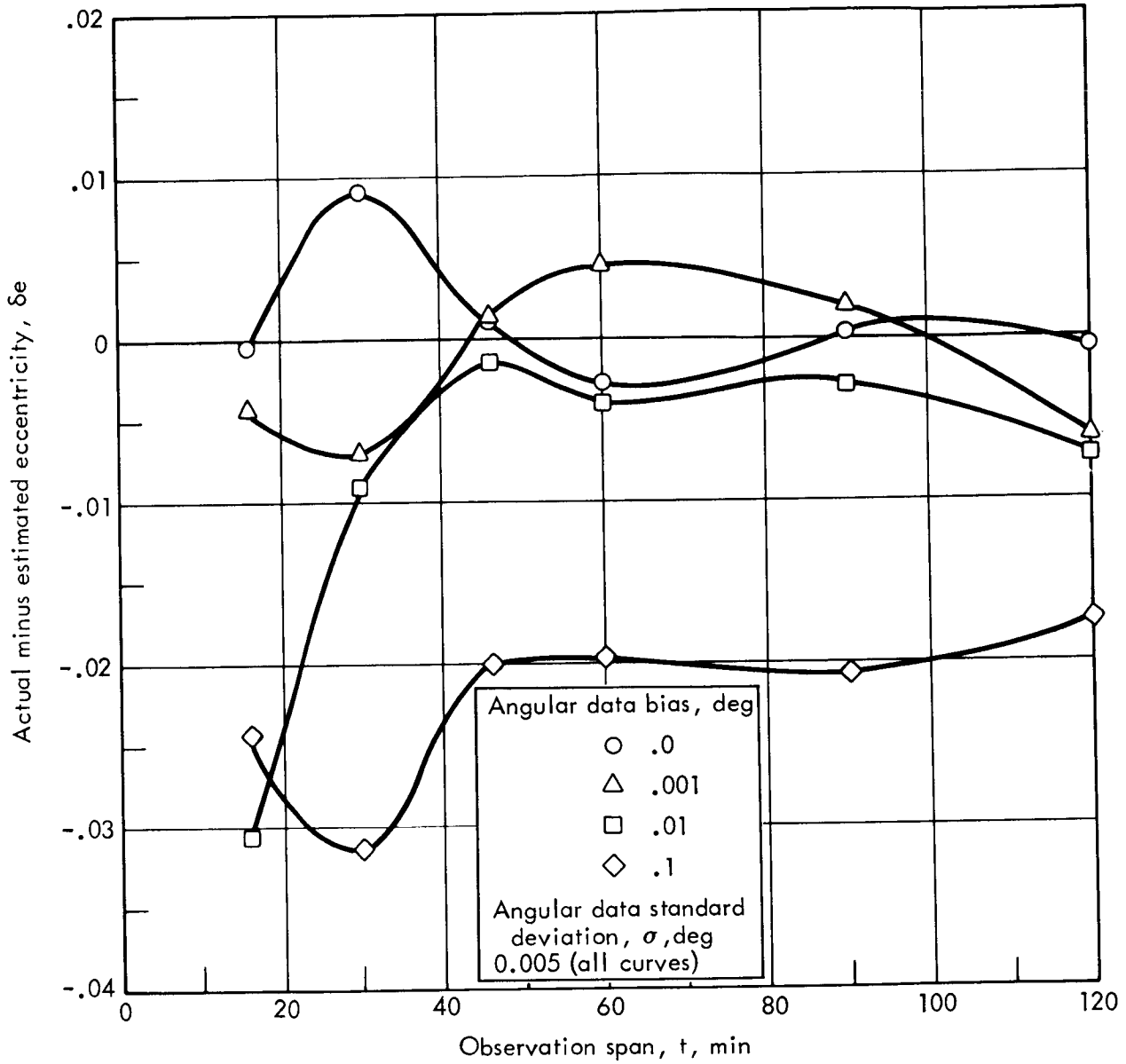


FIGURE 60.—ECCENTRICITY ESTIMATE QUALITY VERSUS OBSERVATION SPAN FOR VARIOUS ANGULAR DATA BIASES ($\sigma = 0.005$)

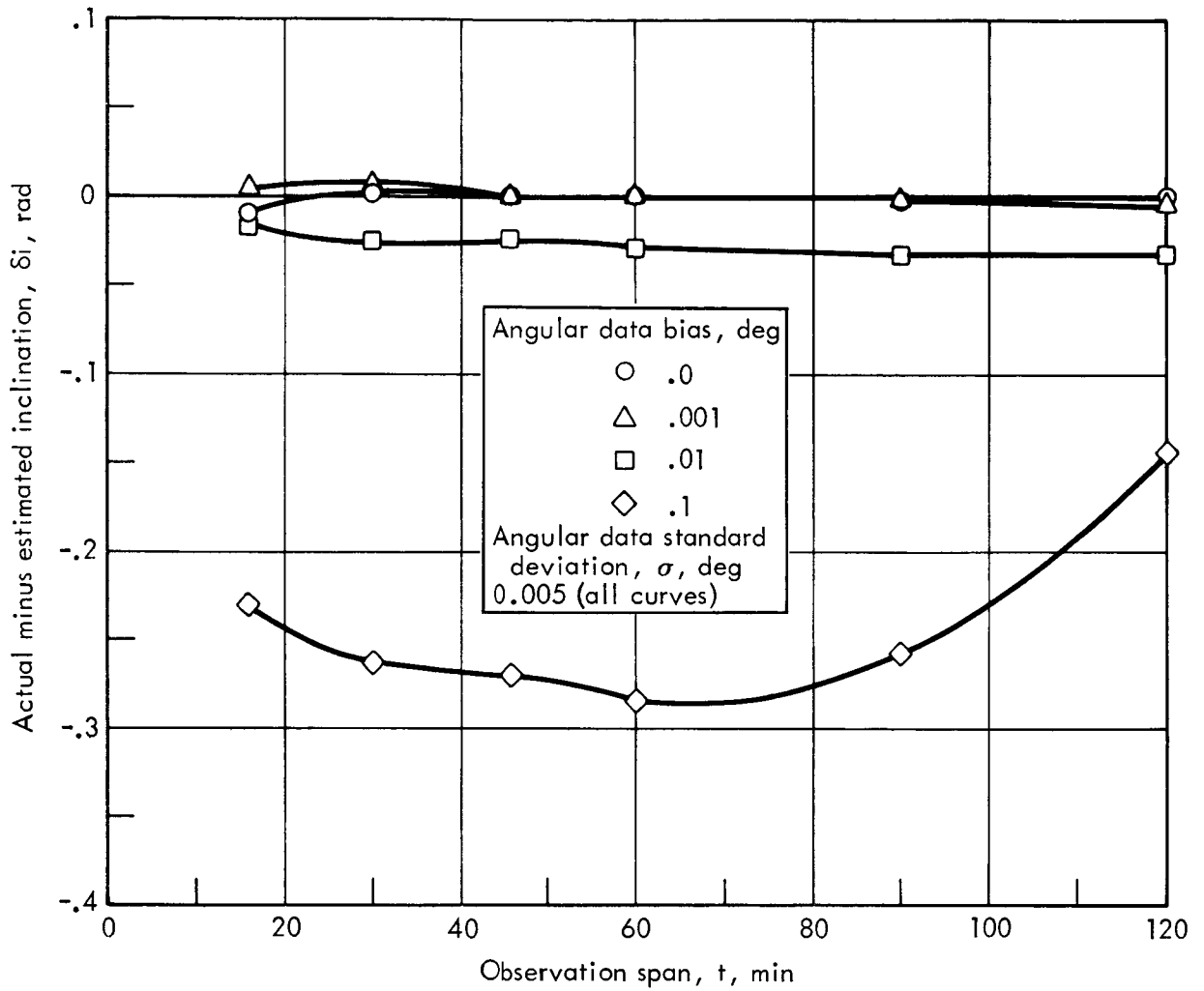


FIGURE 61.—INCLINATION ESTIMATE QUALITY VERSUS OBSERVATION SPAN FOR VARIOUS ANGULAR DATA BIASES ($\sigma = 0.005$)

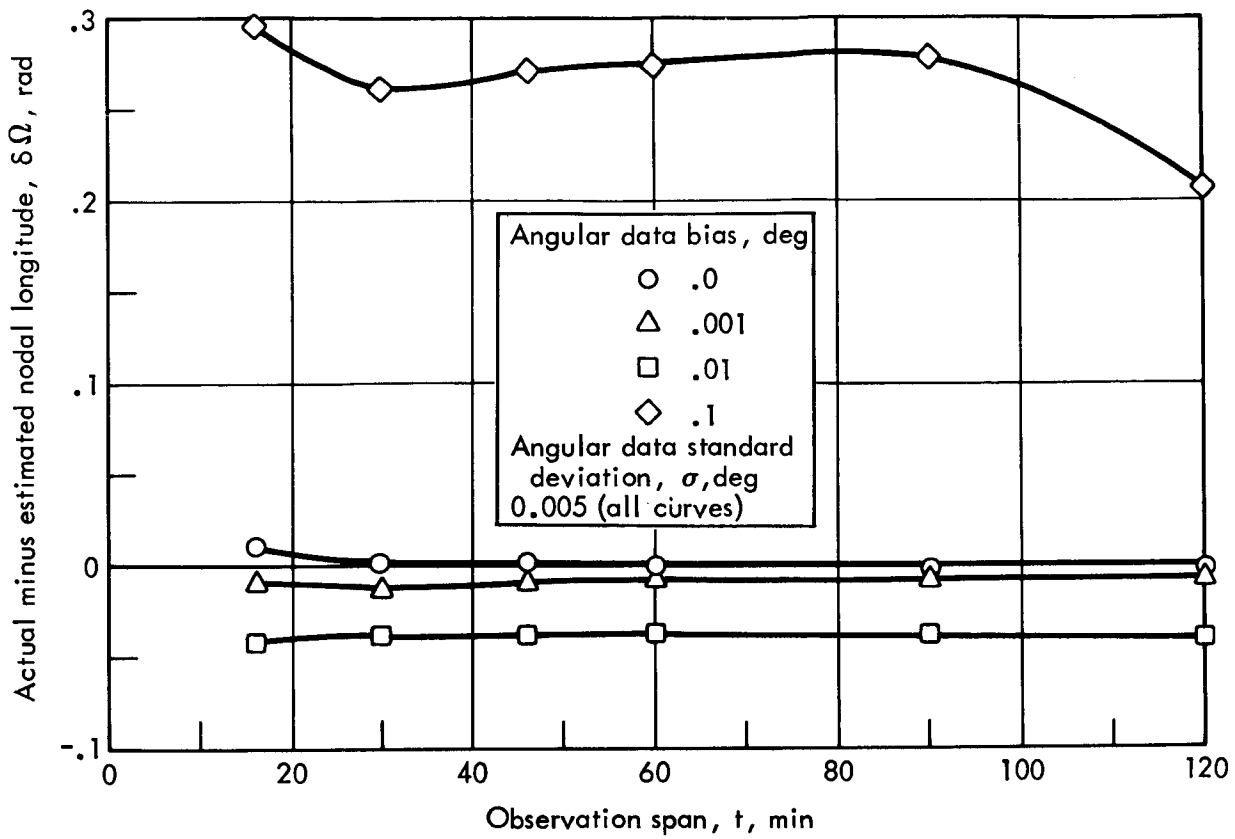


FIGURE 62. — NODAL LONGITUDE ESTIMATE QUALITY VERSUS OBSERVATION SPAN FOR VARIOUS ANGULAR DATA BIASES ($\sigma = 0.005$)

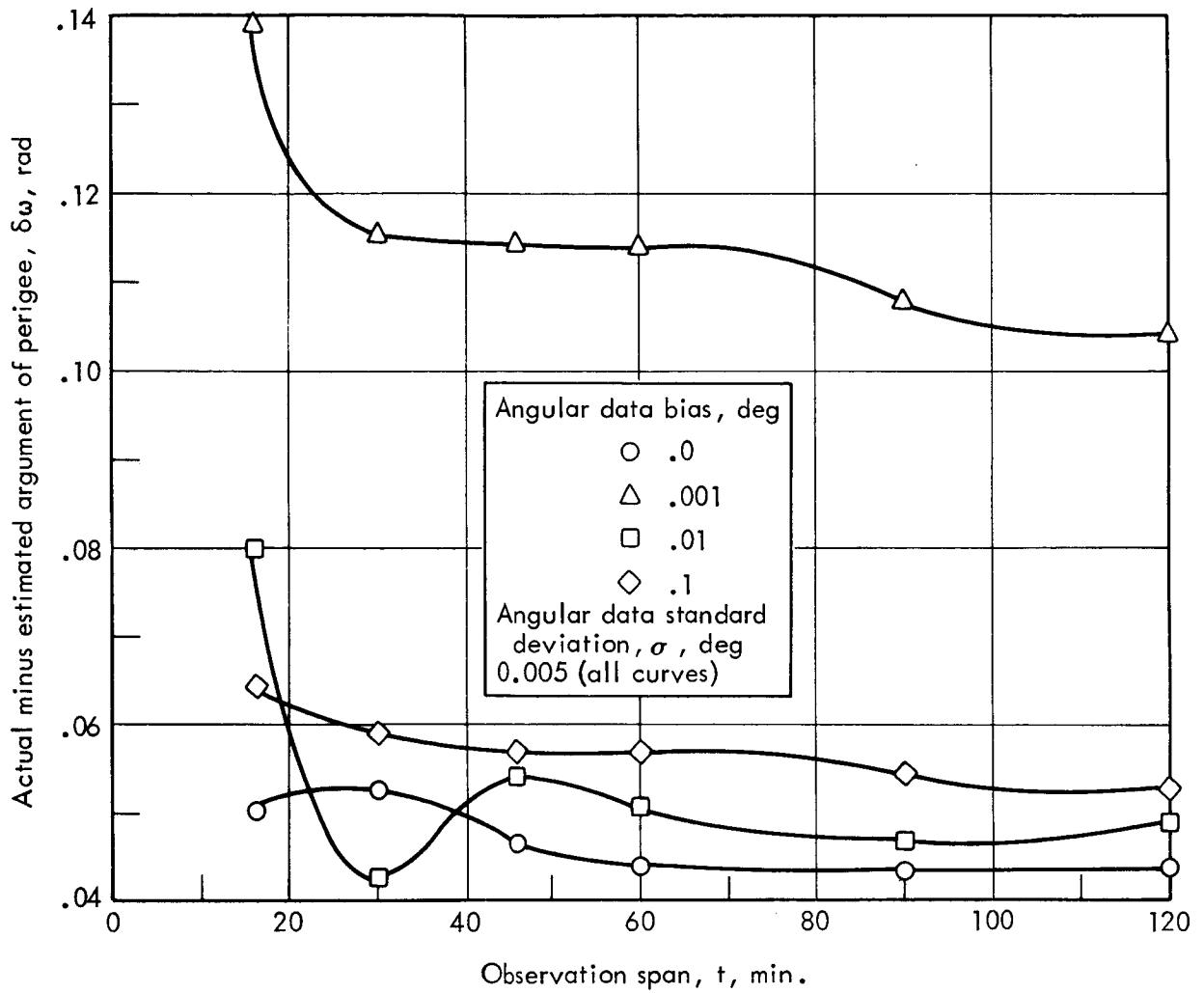


FIGURE 63. — ARGUMENT OF PERIGEE ESTIMATE QUALITY VERSUS OBSERVATION SPAN FOR VARIOUS ANGULAR DATA BIASES ($\sigma = 0.005$)

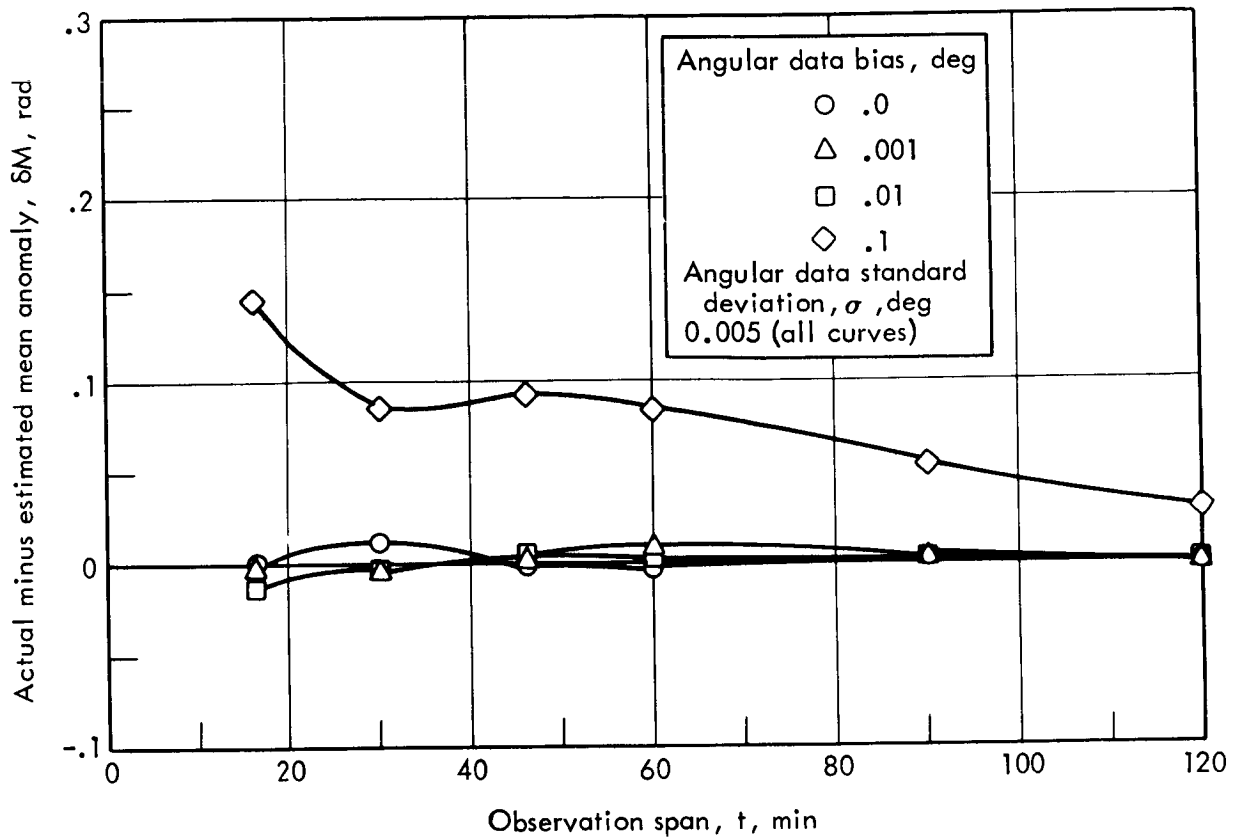


FIGURE 64.— EPOCH MEAN ANOMALY ESTIMATE QUALITY
VERSUS OBSERVATION SPAN FOR VARIOUS
ANGULAR DATA BIASES ($\sigma = 0.005$)

two stations is shown. The data were generated using the state vector whose eccentricity is 0.63, over an arbitrary one hour time period ($\sigma = 0.06^\circ$ and there is a 0° bias).

Effect of Data Quantity. - There is a significant effect due to the quantity of the data used to determine an orbit for a given time span. As the number of data points increases, the magnitude of the deviation decreases. Table X illustrates the deviation of the semi-major axis as a function of the number of position vectors used. The eccentricity is 0.63, $\sigma = 0.06^\circ$, and the bias is 0° . The semi-major axis is picked as a representative element. The observation time is one hour.

4.5 RANGE, RANGE-RATE TECHNIQUE

4.5.1 Mathematical Formulation

The concept of using range in addition to range-rate data to determine a preliminary orbit for a lunar orbiter is enhanced by the high quality of the range data. A disadvantage of the $\dot{\rho}$ only technique is that it is usually necessary to observe for long time periods if a unique set of orbit orientation elements is to be determined. We hope to avoid this delay by using a redundant data set, as well as including range data. If the range and range rate history of a vehicle is available, it is possible to determine the in plane elements a , e and M_0 .

Returning to the vector diagram on page 109, again let \bar{R}_0 be the position vector of the observer with respect to the geocenter, $\bar{\rho}$ the position vector of the vehicle measured from the observer, \bar{r} the selenocentric position vector, and \bar{R}_m the position vector of the moon. Of the above quantities only \bar{R}_0 and \bar{R}_m are known at a particular instant in time. Therefore, let

$$\bar{R} = \bar{R}_0 + \bar{R}_m$$

TABLE IX. EFFECT OF THE NUMBER OF OBSERVING SENSORS
ON THE QUALITY OF ORBITAL ELEMENT ESTIMATES

Element	Actual minus estimated deviation	
	One sensor	Two sensors
a, lunar radii	0.02223	0.00213
e	0.04087	-0.02836
i, rad	-0.00892	-0.00723
Ω , rad	-0.00645	0.00314
ω , rad	0.01279	0.00526
M, rad	-0.05501	-0.00624

TABLE X. EFFECT OF DATA QUANTITY ON THE ESTIMATE OF
ORBITAL ENERGY - ρ , α , δ PROGRAM

<u>Number of ρ, α, δ triads</u>	<u>Actual minus estimated semi-major axis; δa (meters)</u>
3	.92102 x 10 ⁷
6	.66434
12	.47829
24	.26310
60	.06775
120	-.00649

Then it is clear that

$$\bar{\rho} = \bar{R} + \bar{r} \quad (60)$$

Dotting equation (60) with itself and differentiating the result produces

$$\rho\dot{\rho} = \bar{R} \cdot \dot{\bar{R}} + \bar{R} \cdot \dot{\bar{r}} + \bar{r} \cdot \dot{\bar{R}} + \bar{r} \cdot \dot{\bar{r}} \quad (61)$$

The selenocentric position and velocity vectors at a time t can be written as

$$\bar{r} = f\bar{r}_0 + g\dot{\bar{r}}_0 \quad (62)$$

$$\dot{\bar{r}} = \dot{f}\bar{r}_0 + \dot{g}\dot{\bar{r}}_0 \quad (63)$$

where \bar{r}_0 is the position vector at an arbitrary epoch and $\dot{\bar{r}}_0$ is the velocity vector at an arbitrary epoch. The quantities f , g , \dot{f} and \dot{g} are the closed form coefficients (discussed in section 4.4). Define two auxiliary vectors \bar{A} and \bar{B} as

$$\bar{A} = \dot{f}\bar{R} + f\dot{\bar{R}} \quad (64)$$

$$\bar{B} = \dot{g}\bar{R} + g\dot{\bar{R}} \quad (65)$$

Substituting equations (62) through (65) into equation (61) produces

$$\rho\dot{\rho} - \bar{R} \cdot \dot{\bar{R}} - \bar{r} \cdot \dot{\bar{r}} = \bar{r}_0 \cdot \bar{A} + \dot{\bar{r}}_0 \cdot \bar{B} \quad (66)$$

For brevity let

$$F_i = \rho\dot{\rho} - \bar{R} \cdot \dot{\bar{R}} - \bar{r} \cdot \dot{\bar{r}} \quad i = 1, \dots, n$$

At any observation time the quantity F_i can be evaluated as can \bar{A} and \bar{B} . The unknown quantities are \bar{r}_0 and $\dot{\bar{r}}_0$. Equation (66) can be written as

$$y = Mx \quad (67)$$

where

$$y = \begin{bmatrix} F_1 \\ F_2 \\ \cdot \\ \cdot \\ \cdot \\ F_n \end{bmatrix}_{n \times 1}$$

$$M = \begin{bmatrix} A_{1x} & A_{1y} & A_{1z} & B_{1x} & B_{1y} & B_{1z} \\ A_{2x} & A_{2y} & A_{2z} & B_{2x} & B_{2y} & B_{2z} \\ A_{3x} & A_{3y} & A_{3z} & B_{3x} & B_{3y} & B_{3z} \\ \cdot & \cdot & \cdot & \cdot & \cdot & \cdot \\ \cdot & \cdot & \cdot & \cdot & \cdot & \cdot \\ \cdot & \cdot & \cdot & \cdot & \cdot & \cdot \\ A_{nx} & A_{ny} & A_{nz} & B_{nx} & B_{ny} & B_{nz} \end{bmatrix}_{n \times 6}$$

$$x = \begin{bmatrix} x_0 \\ y_0 \\ z_0 \\ x_0' \\ y_0' \\ z_0' \end{bmatrix}_{6 \times 1}$$

The least squares solution of equation (67) is

$$x = (M^T M)^{-1} M^T y \quad (68)$$

In order that each observation may be completely processed as it is read into the program, equation (68) will be written as

$$x = \left(\sum_{i=1}^n (M_i^T M_i) \right)^{-1} \sum_{i=1}^n M_i^T y_i$$

In order to generate the initial values of f , g , \dot{f} and \dot{g} , it is necessary to obtain an estimate for the state vector. It is possible to obtain the values of a , e and M_0 from a harmonic analysis of the range and range-rate curves. The method for obtaining the orientation elements is discussed in the next section. Once a value of the state vector x has been obtained, improved values for the f , \dot{f} , g and \dot{g} coefficients are generated and the process is repeated until a convergence criterion is satisfied.

4.5.2 Numerical Characteristics

The problem of determining an orbit from range and range-rate data is difficult because there may be many orbits which give nearly the same range and range-rate time histories. One of the most significant difficulties is the inversion of the $M^T M$ matrix. It has been observed that the quality of the inverse depends upon the observation time as well as the number of observations. The use of more than a minimal data set will eliminate many of the difficulties in inverting the matrix.

Two techniques for using the ρ , $\dot{\rho}$ program were investigated:

- 1) Assume that the semi-major axis has been precomputed using the $\dot{\rho}$ program, and solve for e , M_0 , i , Ω and ω .
- 2) Assume a , e and M_0 have been precomputed and solve for i , Ω and ω .

These two techniques will be treated separately.

Solution for Orbital Elements Assuming Constant a . - After one revolution of observing the vehicle, it is possible to obtain an accurate value for the semi-major axis using the LRC $\dot{\rho}$ program. The possibility of holding this precomputed semi-major axis, a , constant during

successive iterations was investigated. In order to obtain an approximation of the state vector, the nominal elements for e and M were assumed and perturbations in the orientation elements were introduced. The solution obtained from inverting the matrix the first time helps the orientation elements significantly. However, subsequent iterations show that the solutions diverge from the actual values due to errors which have been introduced in e and M_0 . Table XI illustrates the situation. The orientation elements have been perturbed 20° , and e and M_0 input correct to six figures and allowed to assume whatever values the program called for on iterations after the first.

Solution for Orbital Elements Assuming a , e and M Constant. - If elements a , e and M have been obtained from an analysis of the range-rate curves, they may be input and held constant from iteration to iteration. This eliminates the problem of the solution diverging after several iterations which was observed when only a was held constant. As already demonstrated, the quality (i. e., the deviation from the actual value) of the estimate of the orbital elements to which the iterations converge increases with increasing observation time. However, increased observation times introduced errors because of the increasing difference between the orbital path predicted using a two-body mathematical model, and that actually followed by the vehicle.

As the observation time increases, the accuracy of the orientation elements increases, primarily because the conditioning of the matrix, $M^T M$, is improved. Table XII compares the final values of i , Ω , and ω for a one hour versus a three hour observation time for initial perturbations of 10° , 20° , 40° , and 80° in the orientation elements. Note that the size of the initial error in the orientation elements is relatively unimportant; zeros could have been input as initial estimates with no degradation in the final estimate. For these three hour data spans, only three iterations were found to be necessary, since the errors in the orientation elements were all less than 10^{-2} rad.

However, to investigate the stability of the method, fourteen iterations were computed using a one hour data span. This is the minimum observation span studied (shorter arcs resulted in ill conditioned matrices)

TABLE XI. ITERATION HISTORY FOR THE $\rho\dot{p}$ PROGRAM
 ASSUMING ONLY A PRECOMPUTED SEMI-MAJOR AXIS

Source of element set	a (lunar radii)	e	i (radians)	Ω (radians)	ω (radians)	M (radians)
Actual	1.6129	0.2906	0.6508	0.2992	0.3361	3.9088
Initial estimate	1.6129	0.2906	0.3017	0.6482	0.6852	3.9088
First iteration	1.6129	0.2905	0.6507	0.2989	0.3365	3.9086
Second iteration	1.6129	0.2895	0.6517	0.2974	0.3405	3.9049
Third iteration	1.6129	0.2734	0.6584	0.2838	0.3923	3.8511
Fourth iteration	1.6129	0.1207	0.7728	0.0828	1.4998	2.7849

TABLE XII. EFFECT OF OBSERVING INTERVAL ON THE QUALITY OF THE ORIENTATION ELEMENT ESTIMATES - $\rho\dot{p}$ PROGRAM

Element	Actual minus estimated element, rad	
	One hour observation interval	Three hour observation interval (occulted data removed)
Initial orientation error $\pm 10^\circ$		
i	0.01410159	0.00326998
Ω	-0.02625568	-0.00079189
ω	0.00155586	0.00419935
Initial orientation error $\pm 20^\circ$		
i	-0.00439960	0.00326674
Ω	0.00129179	-0.00082691
ω	-0.05920514	0.00419904
Initial orientation error $\pm 40^\circ$		
i	0.01389854	0.00325781
Ω	-0.02547841	-0.00084762
ω	-0.05360503	0.00380027
Initial orientation error $\pm 80^\circ$		
i	-0.00612827	0.00325060
Ω	-0.02271669	-0.00079632
ω	-0.01149236	0.00419849

and will represent a lower bound on estimate quality. The behavior of the technique for this short arc is perhaps of academic interest only, since the elements a , e , and M_0 , which were assumed to have been precomputed by the LRC \dot{p} program, would not be available until a complete revolution of data had been processed.

The oscillatory nature of the solutions is represented in Figures 65, 66, and 67. The independent variable is the iteration number and the dependent variable is the deviation in the particular orientation element. The observation time is one hour for a , e , and M constant. The initial perturbations in the orientation elements are $\pm 10^\circ$. Note that the ordinate scale has been expanded to facilitate study of the iteration history. The maximum error in inclination is about $1^\circ.5$; in nodal longitude it is about $2^\circ.5$. The largest error occurs in argument of perigee, and may be as much as 7° .

4.6 INFLUENCE OF PERTURBATIONS INTRODUCED BY THE EARTH AND THE MOON'S ASPHERICITY

The preliminary orbit determination techniques that have been developed are based on two-body motion. In order to represent the "real world" as accurately as possible, the data that were used included perturbations due to irregularities in the moon's gravitational field and the earth. In order to determine the effect on estimate accuracy of using a two-body formulation, it is necessary to examine the nature of the perturbations.

The perturbations due to the moon are a result of the primary oblateness term, $J_{2,0}$ and the triaxial effect which is manifested as a $J_{2,2}$ term. The perturbative acceleration due to the $J_{2,0}$ term is 2×10^{-4} , while that due to the $J_{2,2}$ term is 2.3×10^{-5} , when compared to the magnitude of the central force term (Reference 8). There are three orbital elements that have secular variations; that is, they increase linearly with time. These are ω , the argument of perigee, Ω , the right ascension of the ascending node, and M , the osculating mean anomaly.

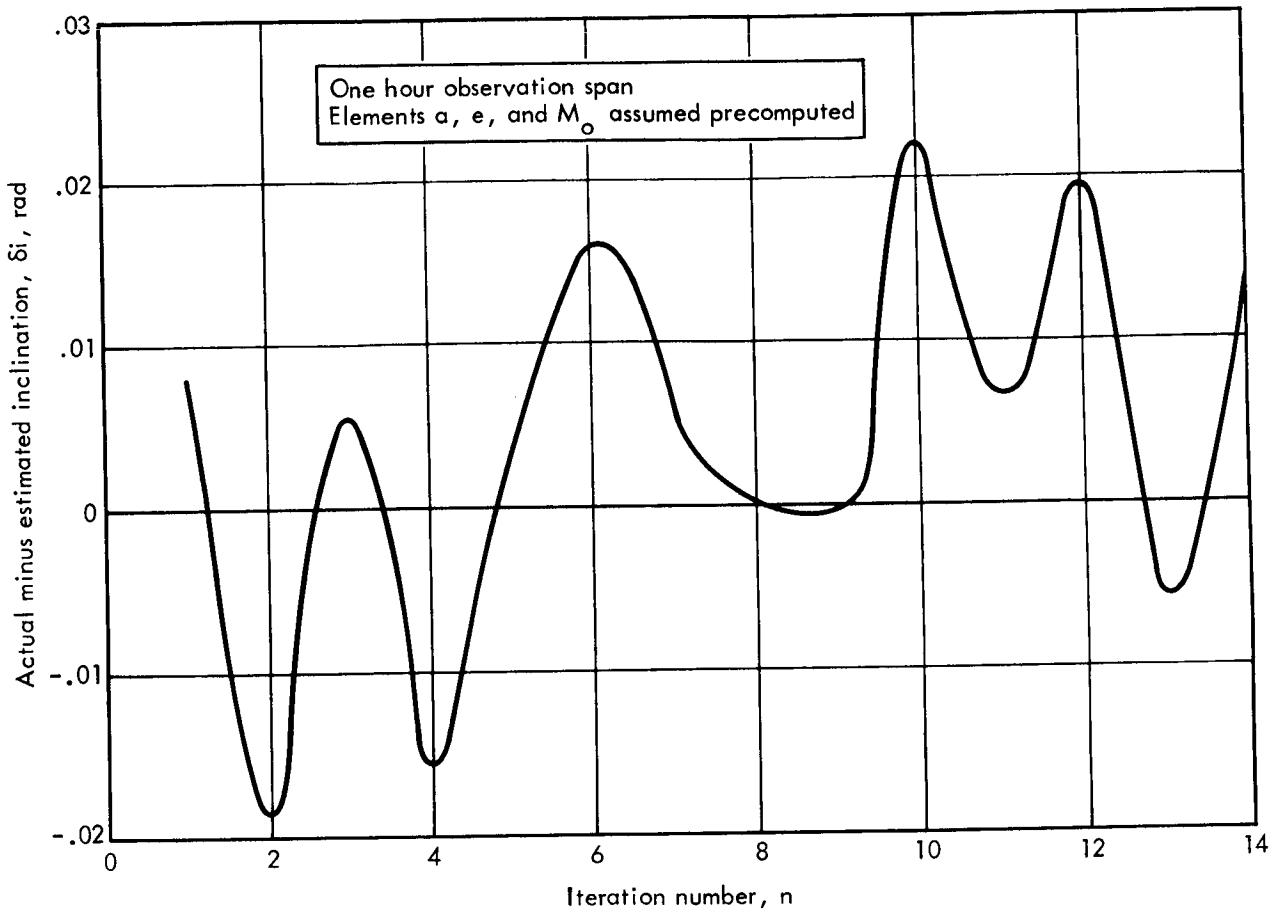


FIGURE 65.—INCLINATION ESTIMATE QUALITY VERSUS ITERATION NUMBER—RANGE, RANGE-RATE PROGRAM

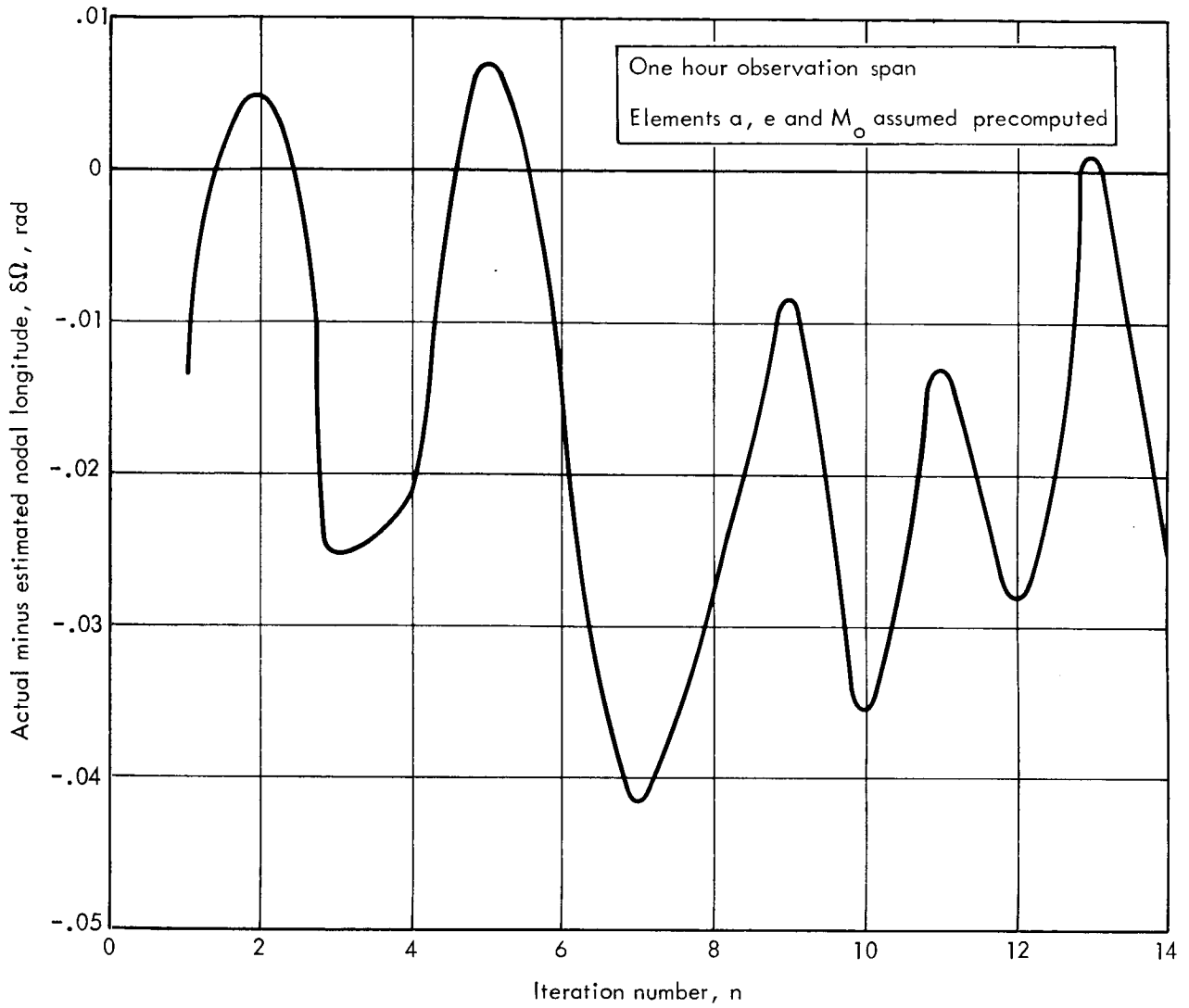


FIGURE 66. — NODAL LONGITUDE ESTIMATE QUALITY VERSUS ITERATION NUMBER — RANGE, RANGE-RATE PROGRAM

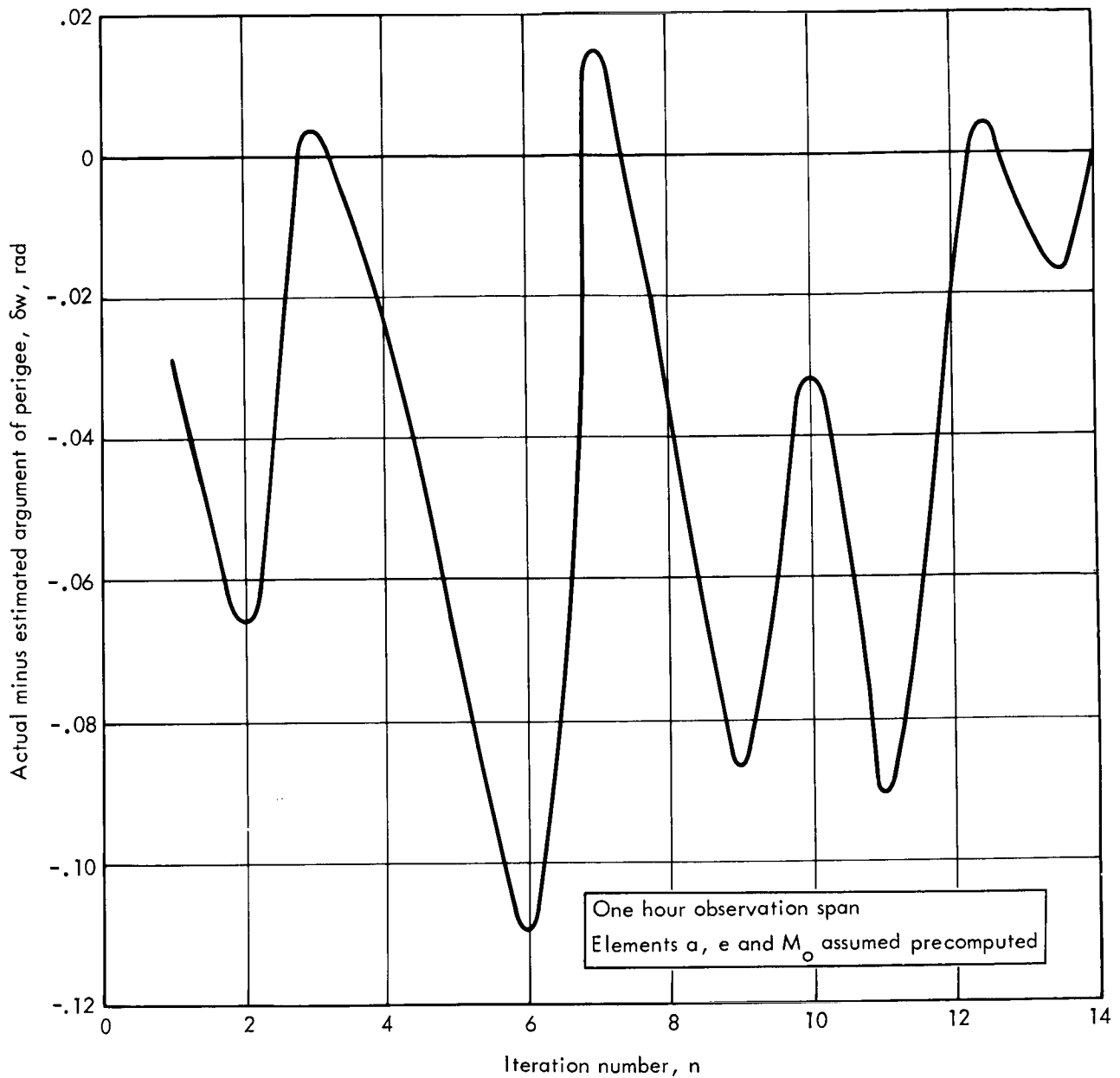


FIGURE 67.—ARGUMENT OF PERIGEE ESTIMATE QUALITY VERSUS ITERATION NUMBER—RANGE, RANGE-RATE PROGRAM

The other elements, a , the semi-major axis, i , the inclination, and e , the eccentricity vary periodically. The maximum value of the periodic variation is of the order $J_{2,0}$.

The magnitude of the perturbations due to the third body effect of the earth depends on the semi-major axis of the lunar satellite. The nature of the perturbations is such that the semi-major axis varies periodically; the other elements have long periodic or secular variations. Over a short time span, the long periodic variations appear secular. For a lunar satellite of approximately 1.9 lunar radii, the perturbations due to the earth are equal in magnitude to those due to the moon's oblateness.

The error committed in using a two-body model to fit "real-world" observations grows rapidly with time. After one hour from an arbitrary epoch, the deviation from two-body motion in the selenocentric position vector is approximately 1500 meters; after five hours, the magnitude of the perturbation is approximately 10,000 meters.

It is possible to minimize the effect of the perturbations by selecting the epoch in the center of any given data arc. The primary effect of the perturbation is to decrease the accuracy of the solution and will be more noticeable for longer time spans. To evaluate the size of the error, two twelve-hour observation spans using range and range-rate data were used to determine an orbit. One span of data was based on a two-body model, and the other included the perturbative effects of the nonspherical moon and the earth. The results are tabulated in table XIII. The two-body data produces deviations from the actual elements in the fourth and fifth significant figure, while the perturbed data produces deviations in the second and third significant figures.

The perturbative effects of the earth, moon and data noise can be minimized by choosing the epoch in the middle of the data span, and by using the shortest time span that produces reasonable answers. It should be emphasized that the perturbative effects only affect the quality of the orbital elements, and do not cause divergence of the orbit determination process.

TABLE XIII. EFFECT OF TWO BODY GRAVITATIONAL MODEL
ON THE QUALITY OF ELEMENT ESTIMATION

Element	Deviation from actual using two body data (radians)	Deviation from actual using per- turbed data (radians)
i	0.00001	0.01275
Ω	0.00030	0.03065
ω	0.00056	0.00790

5. NEW TECHNOLOGY

This section is included to comply with requirements of the "New Technology" clause of the Master Agreement under which this report was prepared. This report describes a study performed using certain orbit determination processes developed by TRW Systems. The most significant new technology resulting from this contract is the position fix preliminary orbit determination technique.

APPENDIX A

State Vectors and Classical Elements Defining the Nominal Orbits and Data Sets

1. REFERENCE ORBITS - INITIAL ESTIMATES

The reference orbits consist of the nominal orbit plus the seven alternate lunar satellite orbits. The state vector representing these orbits served as the initial estimate in the differential corrections. Both the selenographic classical elements and the geocentric cartesian state vectors of these reference orbits are listed below. In addition to the unimproved initial estimates, there is an energy corrected initial estimate for each energy perturbed data set. The energy corrected initial estimate is keyed to its particular data set, as listed in section 2.2 of this appendix. The epoch time associated with all classical elements and state vectors in this appendix is as follows:

$$T = 27 \text{ June } 1966, 4^{\text{h}} 0^{\text{m}} 48.0^{\text{s}}$$

1.1 CLASSICAL ELEMENTS OF INITIAL ESTIMATES

Orbit Code	Classical Elements*		
	a i	e Ω	M ω
A	2788.0 15.0	0.2869 25.47	0.0 -12.46
B1	2788.0 0.0	0.2869 25.47	0.0 -12.46
B2	2788.0 30.0	0.2869 25.47	0.0 -12.46
B3	2788.0 45.0	0.2869 25.47	0.0 -12.46
B4	2788.0 60.0	0.2869 25.47	0.0 -12.46

*i, Ω , ω , M in degrees; a in kilometers

Orbit Code	Classical Elements *		
	a i	e Ω	M ω
B5	2788.0 15.0	0.2869 10.0	0.0 -12.46
B6	2788.0 15.0	0.2869 90.0	0.0 -12.46
B7	2788.0 15.0	0.2869 130.0	0.0 -12.46

*i, Ω , ω , M in degrees; a in kilometers

1.2 GEOCENTRIC CARTESIAN COORDINATES OF INITIAL ESTIMATES

Orbit Code	\dot{x} x	\dot{y} y	\dot{z} z
A	-0.33522130 E6 -0.55498911 E0	-0.15591166 E6 0.31028165 E0	-0.49929099 E5 0.48958576 E0
B1	-0.33521291 E6 -0.58903405 E0	-0.15596344 E6 0.52029433 E0	-0.49830170 E5 0.88413385 E-1
B2	-0.33525053 E6 -0.43643029 E0	-0.15584486 E6 0.39362549 E-1	-0.49989888 E5 0.83418740 E0
B3	-0.33529862 E6 -0.24143719 E0	-0.15576758 E6 -0.27400032 E0	-0.50079314 E5 0.10987342 E1
B4	-0.33536230 E6 0.16701741 E1	-0.15568510 E6 -0.60845176 E0	0.50120364 E5 0.12651979 E1
B5	-0.33497605 E6 -0.13982413 E0	-0.15635212 E6 0.49814116 E0	-0.50106203 E5 0.57683833 E0
B6	-0.33717647 E6 -0.12889087 E1	-0.15514144 E6 -0.12426783 E1	-0.49653804 E5 -0.17088040 E0
B7	-0.33835693 E6 -0.72183550 E0	-0.15575143 E6 -0.22020012 E1	-0.49933339 E5 -0.55587434 E0

1.3 GEOCENTRIC CARTESIAN COORDINATES OF ENERGY
CORRECTED INITIAL ESTIMATES

Orbit Code	$\begin{matrix} x \\ \cdot \\ x \end{matrix}$	$\begin{matrix} y \\ \cdot \\ y \end{matrix}$	$\begin{matrix} z \\ \cdot \\ z \end{matrix}$
AEP1	-0.33522130 E6 -0.57890268 E0	-0.15591166 E6 0.33842679 E0	-0.49929099 E5 0.51262919 E0
AEP2	-0.33522130 E6 -0.59952285 E0	-0.15591166 E6 0.36269578 E0	-0.49929099 E5 0.53249907 E0
AEP3	-0.33522130 E6 -0.62135736 E0	-0.15591166 E6 0.38839396 E0	-0.49929099 E5 0.55353911 E0
AEP6	-0.33522130 E6 -0.68704057 E0	-0.15591166 E6 0.46570062 E0	-0.49929099 E5 0.61683232 E0
B1 EP3	-0.33521291 E6 -0.65771414 E0	-0.15596344 E6 -0.61265343 E0	-0.49830170 E5 0.12516132 E0
B2 EP3	-0.33525053 E6 -0.49476117 E0	-0.15584486 E6 0.99104720 E-1	-0.49989888 E5 0.92151589 E0
B3 EP3	-0.33529862 E6 -0.28654119 E0	-0.15576758 E6 -0.23551289 E0	-0.50079314 E5 0.12040003 E1
B4 EP3	-0.33536230 E6 -0.10895289 E-1	-0.15568510 E6 -0.59264672 E0	-0.50120364 E5 0.13817528 E1
B5 EP3	-0.33497605 E6 -0.17803563 E0	-0.15635212 E6 0.58899201 E0	-0.50106203 E5 0.64277529 E0
B6 EP3	-0.33717647 E6 -0.14050592 E1	-0.15514144 E6 -0.12698850 E1	-0.49653804 E5 -0.15171957 E0
B7 EP3	-0.33835693 E6 -0.79951335 E0	-0.15575143 E6 -0.22942619 E1	-0.49933339 E5 -0.56282225 E0

2. OBSERVED ORBITS - DATA SETS

The observed orbits are perturbations in energy or orientation of the nominal orbits. The state vectors which represent these orbits were derived from the nominal orbits and its associated a priori covariance matrix, as explained in section 3.3.2. The a priori covariance matrix is listed in section 3 of this appendix. Simulated observations were

computed from the trajectories generated by the propagation of each respective state vector.

In addition to the geocentric cartesian coordinates of the observed orbits, the corresponding selenographic classical elements are presented for the purpose of comparing the nominal and perturbed orbits.

2.1 CLASSICAL ELEMENTS OF OBSERVED ORBITS

Orbit Code	Classical Elements*		
	a i	e Ω	M ω
AOP1	2789.6681 15.874985	0.28730842 23.120315	0.0 349.76643
AOP2	2794.8202 16.771925	0.28855734 21.022099	0.0 351.69109
AOP3	2803.4247 17.686780	0.29061875 19.116735	0.0 353.35375
AOP6	2850.6580 20.504861	0.30186997 14.504739	0.0 356.97412
AEP1	3042.4205 15.0	0.34152163 25.461554	0.0 347.54042
AEP2	3350.8584 15.0	0.39758537 25.461361	0.0 347.54039
AEP3	3732.5884 15.0	0.45511172 25.461385	0.0 347.54037
AEP6	5723.5286 15.0	0.63666141 25.470626	0.0 347.55434
B1OP3	2803.4426 3.2191806	0.29063931 348.87001	0.0 23.865239
B2OP3	2803.4418 32.635833	0.29063919 21.902542	0.0 350.31601
B3OP3	2803.4437 47.614969	0.29063956 22.863905	0.0 349.06925

* i, Ω , M in degrees; a in kilometers

Orbit Code	Classical Elements*		
	a i	e Ω	M ω
B4OP3	2803.3755 62.602358	0.29062854 23.301072	0.0 348.31160
B5OP3	2803.4727 17.686188	0.29064468 3.6607669	0.0 353.34686
B6OP3	2803.3951 17.686684	0.29063137 83.665441	0.0 353.34743
B7OP3	2803.4505 17.686675	0.29064085 123.67494	0.0 353.34602
B1EP3	3732.6725 0.00006509	0.45512062 101.65282	0.0 271.34886
B2EP3	3732.6357 30.0	0.45511673 25.461668	0.0 347.53990
B3EP3	3732.6283 45.0	0.45511604 25.461617	0.0 347.54012
B4EP3	3732.5488 60.0	0.45510767 25.461758	0.0 347.53995
B5EP3	3732.5348 15.0	0.45510619 10.001531	0.0 347.55695
B6EP3	3732.6107 15.0	0.45511396 89.992144	0.0 347.53905
B7EP3	3732.5656 15.0	0.45510946 130.00142	0.0 347.55359

*i, Ω , ω , M in degrees; a in kilometers

2.2 GEOCENTRIC CARTESIAN COORDINATES OF OBSERVED ORBITS

Orbit Code	\dot{x} x	\dot{y} y	\dot{z} z
AOP1	-0.33521874 E6 -0.54982336 E0	-0.15588933 E6 -0.29400176 E0	-0.49916474 E5 0.51483076 E0
AOP2	-0.33521614 E6 -0.54465761 E0	-0.15592794 E6 0.27772186 E0	-0.49903852 E5 0.54007576 E0
AOP3	-0.33521355 E6 -0.53949185 E0	-0.15593609 E6 0.26144196 E0	-0.49891231 E5 0.56532076 E0

Orbit Code	$\begin{matrix} x \\ \dot{x} \end{matrix}$	$\begin{matrix} y \\ \dot{y} \end{matrix}$	$\begin{matrix} z \\ \dot{z} \end{matrix}$
AOP6	-0.33520581 E6 -0.52399457 E0	-0.15596050 E6 0.21260224 E0	-0.49853362 E5 0.64105576 E0
AEP1	-0.33520883 E6 -0.57173290 E0	-0.15590337 E6 0.32998831 E0	-0.49926298 E5 0.50572029 E0
AEP2	-0.33519636 E6 -0.58847669 E0	-0.15589507 E6 0.34969500 E0	-0.49923494 E5 0.52185485 E0
AEP3	-0.33518390 E6 -0.60522048 E0	-0.15588677 E6 0.36940163 E0	-0.49920693 E5 0.53798937 E0
AEP6	-0.33514647 E6 -0.65545183 E0	-0.15586186 E6 0.42852158 E0	-0.49912286 E5 0.58639299 E0
B1OP3	-0.33521386 E6 -0.59093755 E0	-0.15598095 E6 0.48527842 E0	-0.49787946 E5 0.17286181 E0
B2OP3	-0.33523462 E6 -0.40458838 E0	-0.15587452 E6 -0.19972590 E-1	-0.49983146 E5 0.89604778 E0
B3OP3	-0.33527561 E6 -0.19542062 E0	-0.15580047 E6 -0.33978732 E0	-0.50057429 E5 0.11425043 E1
B4OP3	-0.33533377 E6 0.73757034 E-1	-0.15571899 E6 -0.67620733 E0	-0.50109016 E5 0.12878948 E1
B5OP3	-0.33497078 E6 -0.12925029 E0	-0.15637838 E6 0.44560742 E0	-0.50068957 E5 0.65093064 E0
B6OP3	-0.33716638 E6 -0.12687538 E1	-0.15515441 E6 -0.12686143 E1	-0.49611135 E5 -0.85543531 E-1
B7OP3	-0.33835223 E6 -0.71243504 E0	-0.15575876 E6 -0.22166757 E1	-0.49888451 E5 -0.46611040 E0
B1EP3	-0.33517530 E6 -0.64101293 E0	-0.15593973 E6 0.59019409 E0	-0.49819490 E5 0.11622517 E0
B2EP3	-0.33521380 E6 -0.48057615 E0	-0.15581841 E6 0.84576468 E-1	-0.50007625 E5 0.90027913 E0
B3EP3	-0.33526299 E6 -0.27557420 E0	-0.15573936 E6 -0.24487105 E0	-0.50074364 E5 0.11784049 E1
B4EP3	-0.33532813 E6 -0.41852122 E-2	-0.15565500 E6 -0.59648964 E0	-0.50116359 E5 0.13534131 E1

Orbit Code	x \dot{x}	y \dot{y}	z \dot{z}
B5EP3	-0.33493302 E6 -0.16874542 E0	-0.15633735 E6 0.56690383 E0	-0.50101872 E5 0.62972055 E0
B6EP3	-0.33718402 E6 -0.13768117 E1	-0.15509822 E6 -0.12632705 E1	-0.49639067 E5 -0.15637795 E0
B7EP3	-0.33839161 E6 -0.78063096 E0	-0.15572284 E6 -0.22718346 E1	-0.49925030 E5 0.56113333 E0

3. A PRIORI COVARIANCE MATRIX

Below is the a priori covariance matrix associated with the nominal orbit for this study. The approximate uncertainties in position and velocity reflected in this covariance matrix were used to generate the perturbed state vectors, which in turn were used to generate the observed orbits. The data simulation was based on these observed orbits.

	x	y	z	\dot{x}	\dot{y}	\dot{z}
x	0.20048468 E3	-0.39872253 E1	-0.27660444 E2	0.37987683 E0	0.41636174 E0	0.40015449 E0
y		0.24084474 E3	-0.27064508 E1	0.41636174 E0	0.45635079 E0	0.43858694 E0
z			0.22245951 E3	0.40015449 E0	0.43858694 E0	0.42151458 E0
x				0.71978769 E-3	-0.14314952 E-4	-0.99307574 E-4
y		SYMMETRIC			0.86468994 E-3	-0.97168017 E-5
z						0.79868285 E-3

APPENDIX B

Compendium of Cases Run in Convergence Study

This is a partial list of runs which were made during the course of the convergence study. The runs are categorically presented, reflecting the approximate sequence in which the study progressed.

In order to keep the comments under the "Remarks Column" at a minimum, the following information is pertinent to all cases unless otherwise specified:

1. Two sensors tracking
2. No a priori information
3. Unrestrained solution
4. Range and range-rate data
5. Six parameter curve fit ($x \ y \ z \ \dot{x} \ \dot{y} \ \dot{z}$)

The four columns, along with the above assumptions, define the various test cases. The energy corrected initial estimates are labelled "EC". The first letter is the reference state vector. The tracking span is in minutes.

<u>Initial estimate</u>	<u>Observed orbit</u>	<u>Tracking span</u>	<u>Remarks</u>
1. <u>ENERGY CORRECTION</u>			
A	AEP3	60	Not energy corrected
A-EC	AEP3	60	Energy corrected
A	AEP3	300	Not energy corrected
A-EC	AEP3	300	Energy corrected
A	AEP3	680	Not energy corrected
A-EC	AEP3	1000	Energy corrected
A	AEP6	45	Large period error
A-EC	AEP6	45	Large period, corrected
A	AOP3	60	Orientation perturbed

<u>Initial estimate</u>	<u>Observed orbit</u>	<u>Tracking span</u>	<u>Remarks</u>
-------------------------	-----------------------	----------------------	----------------

2. A PRIORI INFORMATION

A	AEP3	30	With a priori
A	AEP3	30	No a priori
A	AEP3	15	With a priori
A	AEP3	15	No a priori
A	AEP3	5	With a priori
A	AEP3	5	No a priori
A	AEP3	3	With a priori
A	AEP3	3	No a priori

3. BOUNDS AND NORMAL MATRIX CONDITIONING

A-EC	AEP3	60	Bounded solution
A-EC	AEP3	300	Bounded solution
A	AOP3	300	Bounded solution
A	AEP6	45	Bounded solution
A	AEP3	60	Bounded, one sensor
A-EC	AEP3	300	Unbounded, matrix conditioning
A-EC	AEP3	300	Unbounded, matrix conditioning
A-EC	AEP3	300	Unbounded, matrix conditioning

4. NUMBER OF SENSORS

A	AEP3	15	One sensor
A	AEP3	30	One sensor
A	AEP3	45	One sensor
A	AEP3	60	One sensor
A	AEP3	5	One sensor
A	AEP3	3	One sensor
A	AOP3	15	One sensor
A	AOP3	15	Two sensors
A	AOP3	30	One sensor
A	AOP3	30	Two sensors
A	AOP3	60	One sensor

<u>Initial estimate</u>	<u>Observed orbit</u>	<u>Tracking span</u>	<u>Remarks</u>
5. <u>DATA TYPE</u>			
A-EC	AEP3	300	Range, range-rate, plus angles
A-EC	AEP3	300	Range only
A-EC	AEP3	300	Range-rate only
A-EC	AEP3	60	Range, range-rate, plus angles
A-EC	AEP3	60	Range only
A-EC	AEP3	60	Range-rate only
6. <u>STEP FITS</u>			
STEP	AEP3	300	Initial estimate from 60 minute case
STEP	AEP3	1000	Initial estimate from 300 minute case
STEP	AEP3	3300	Initial estimate from 1000 minute case
7. <u>EPOCH SHIFT</u>			
A	AEP3	60	One minute epoch bias selenocentric fit
A	AEP3	60	Two minute epoch bias selenocentric fit
A	AEP3	60	Ten minute epoch bias selenocentric fit
8. <u>SIX-SIGMA PERTURBATIONS</u>			
A	AEP6	15	Large period error
A-EC	AEP6	300	Energy corrected
A	AOP6	300	Orientation perturbed
9. <u>ALTERNATE LUNAR ORBITS</u>			
B1-EC	B1EP3	60	Nominal conditions
B1	B1OP3	60	Nominal conditions
B2-EC	B2EP3	60	Nominal conditions
B2	B2OP3	60	Nominal conditions

<u>Initial estimate</u>	<u>Observed orbit</u>	<u>Tracking span</u>	<u>Remarks</u>
B3-EC	B3EP3	60	Nominal conditions
B3	B3OP3	60	Nominal conditions
B4-EC	B4EP3	60	Nominal conditions
B4	B4OP3	60	Nominal conditions
B5-EC	B5EP3	60	Nominal conditions
B5	B5OP3	60	Nominal conditions
B6-EC	B6EP3	60	Nominal conditions
B6	B6OP3	60	Nominal conditions
B7-EC	B7EP3	60	Nominal conditions
B7	B7OP3	60	Nominal conditions

APPENDIX C

AT-85 Program Description

1. GENERAL

AT-85 is the latest revision of a general orbit determination program which has been in use at TRW Systems for over 5 years. The program, known as "ESPOD", was originally developed for the SPACETRACK/SPADATS Center, Ent Air Force Base, Colorado Springs, Colorado. (AT-85 is the current version of "ESPOD", and it has been improved and expanded considerably since it has been an operational program at TRW Systems.)

The primary purpose of the program is to determine the elements of a satellite orbit and a covariance matrix of uncertainty in the determination, given some initial estimate of the orbit. Orbit determination is not limited to earth satellites; given earth-based observations, trajectories of vehicles orbiting about the moon or sun can also be handled. From the best elements obtained, the program predicts the future position and velocity of the satellite. The program includes a sophisticated collection of mathematical, statistical, and operational techniques to make it operate rapidly, and produce high precision in the results.

2. GENERAL ORBIT MODEL

AT-85 utilizes a Cowell method of special perturbations for propagating the satellite position and velocity. The process is initiated with a Range-Kutta starter which sets up the finite differences from which the Cowell integration proceeds. At each given time the influences of all the forces acting on the satellite are calculated and summed. These forces are dependent entirely upon the position and velocity of the satellite at a given time; that is, they are special for the moment. The integration step size is automatically controlled to keep seventh-order differences in acceleration within a certain numerical range. This technique guarantees a certain accuracy but permits the step size to be as large as possible.

The AT-85 Program provides a recursive computation technique for calculating the perturbative acceleration of a satellite resulting from the fact that the earth is not a homogeneous sphere. Nominally, only the first three zonal harmonics are used; however, the first nine zonal harmonics and all sectorial and tesseral harmonics through order and degree four may be used. Whether or not the integration uses the earth as the dynamic center, a triaxial potential configuration is available for the moon.

Atmospheric drag is derived as a force tangent to the direction of travel of the satellite, jointly proportional to a drag parameter and the density of the atmosphere. The drag parameter can assume one of the three following forms:

1. Simple ballistic drag, $C_D A / 2m$
2. Ballistic drag plus a secular variation
3. Ballistic drag plus a periodic variation

The atmosphere, on option, may assume any of the four models listed below.

1. ARDC Model Atmosphere, 1959
2. ARDC 59/Paetzold 62 Dynamic Model
3. U. S. Standard Atmosphere, 1962 (COESA 62 Static)
4. U. S. Standard Atmosphere, 1962, including correction for top-atmospheric temperatures (COESA 62 Dynamic)

The program has the ability to change dynamic center. Normally, the earth is the central body; at a specified time to epoch, a phase shift to either the moon or the sun can be effected. The perturbing effects of the sun, moon, and earth can be selectively included in any potential model, though the effects of the other planets are not included.

3. DIFFERENTIAL CORRECTION

Since no set of observations obtained from a tracking system can be fit to a trajectory perfectly, only an estimate of the actual trajectory can

be made. Like most curve fitting programs, AT-85 uses a weighted least squares method of forming the best estimate from the observations available. AT-85 can compute the corrections to the initial estimate in either polar/spherical elements or in cartesian coordinates. Also, corrections can be applied in either a geocentric or a selenocentric coordinate system. The latter makes it possible to resolve some unorthodox tracking situations of lunar orbiters. In the simplest case, only the position and velocity components are to be computed; all other parameters and constants are assumed to be known exactly. In addition to solving for six components of position and velocity, AT-85 may include other non-orbital parameters, such as drag parameters, observation biases, and station location coordinates. The final elements are achieved by iterating on the differential correction procedure. Convergence is obtained when the sum of the squares of the weighted residuals changes by less than 0.1 percent due to the last computed correction.

Since the differential correction process depends upon the appropriateness of a linear approximation to a nonlinear function, linear theory may fail if finite corrections become too large. In order to keep the corrections within a linear region, bounds are used on the individual solution components. This is a desirable technique which is automated in AT-85, increasing its ability to converge to correct elements. The bounds are adjusted automatically to compensate either for diverging corrections or for too slow convergence. Whenever a "correction" results in a divergence, i. e., the new orbital elements yield a larger sum of squares of weighted residuals than the previous elements, the bounds are halved and a new, more constrained solution is attempted. If this fails to achieve a convergent iteration, the bounds are halved again until one-eighth bounds have been tried. At this point, the program exits. On the other hand, if a correction yields a new sum of squares of weighted residuals which actually is less than the previous sum, the bounds are doubled, permitting larger corrections. However, when the actual sum of squares is not within 10 percent of a previously predicted sum, the bounds remain unchanged. When the actual sum and the predicted sum are not in close agreement, nonlinearity is indicated.

The covariance matrix associated with an initial estimate can be handled in the solution of the normal equation to properly weigh the tracking estimate. Actually, AT-85 accepts an a priori normal matrix (the inverse of the covariance matrix). The normal equation is modified to "iterate" with the a priori information; that is, a priori information usefulness is not limited to a one iteration correction.

It is also possible to condition the accumulated tracking normal matrix with a "conditioning normal matrix."

This conditioning matrix is a collection of numbers, with no particular physical significance, which is added to the normal matrix. The solution is normally very sensitive to the size of the elements (usually diagonal) so that a great deal of experience is required in their selection. In the bounds technique previously discussed, the program searches for the matrix which will result in the desired solution vector magnitude. The bounds technique is essentially a refined, automated version of normal matrix conditioning. The final converged answer is unaffected by the conditioning matrix, although the statistical significance of the tracking estimate is lost.

AT-85 can also accept both an a priori normal matrix and a conditioning matrix. As before, the use of the conditioning matrix destroys the statistical interpretation.

The input and output equinoxes as well as the iteration summary can be handled in seven different systems. They are:

1. Mean of 1950.0
2. Mean 0^{hr}, day of epoch
3. Mean of epoch
4. Mean of date
5. True of 0^{hr}, day of epoch
6. True of epoch
7. True of date

The input, output, and iteration summary need not be in the same equinox. Astronomically reduced observations of right ascension and declination in mean of 1950.0 coordinates can also be handled, although observations are usually true of date.

4. RESEARCH CAPABILITY

AT-85 is primarily an operational program. The program structure permits the analyst to change any constants defining the mathematical models, to change the weights applied to residuals, to change other sensor parameters, to weight a priori estimates, to force the integration to particular step sizes, to change any physical constants, etc. With this convenience, AT-85 can be used as a research tool. The effect of varying the potential model, the solution of observation biases, and fitting lunar orbiters in selenocentric coordinates, can be studied for general or particular influence on many types of satellites.

APPENDIX D

AT-14 Program Description

The AT-14 Program is a data simulation routine which has been in use at TRW Systems for several years. The routine computes observations from a reference trajectory for a given tracking station, and considering its particular noise model.

The reference trajectory for which observations are to be simulated is supplied to the AT-14 Program on an ephemeris tape which contains the position and velocity components at some time interval. The time interval of the ephemeris tape determines the sample rate of the station. The ephemeris tape can be generated on the AT-85 Program. A nice feature of the data simulation is that the observations used in the differential corrections with the AT-85 Program were generated with the same program. Hence the mathematical model has no inconsistencies. This fact was insured by checking the compatibility of the physical constants for the two programs.

A tracking station is specified by its geodetic latitude, longitude, and height above a reference ellipsoid. The noise model is specified by the standard deviations and biases of each observation type. And, finally, a tracking interval, constrained to the time span of the ephemeris tape, is assigned.

The routine computes any of the following topocentric observations: range, azimuth, elevation, range-rate, right ascension, and declination. The output of the AT-14 Program is in the form of punched cards which are in the standard observations card format of the AT-85 Program.

APPENDIX E

Derivation of Closed Form f and g Coefficients

Assume that a position vector at an arbitrary time, t , can be expressed as a linear function of the position and velocity vectors at a time t_0 , i. e.,

$$\bar{r}(t) = f\bar{r}(t_0) + g\dot{\bar{r}}(t_0). \quad (\text{E1})$$

Since $\bar{r}(t_0)$ and $\dot{\bar{r}}(t_0)$ are constant, the f and g coefficients must be functions of time, and equation (E1) can be rewritten as

$$\bar{r}(t) = f(t)\bar{r}(t_0) + \dot{\bar{r}}(t_0)g(t) \quad (\text{E2})$$

The functions $f(t)$ and $g(t)$ may be written in terms of time series expansions or as closed form expressions. The time series (which avoid use of Kepler's equation) have the disadvantage that the number of terms required to achieve a preassigned level of accuracy increases as the time span, $t-t_0$, increases. Alternatively, the closed form expressions require solution of Kepler's equation, but give a precise two body representation regardless of the time span. For the preliminary orbit determination applications of the f and g coefficients, the time span, $t-t_0$, may be equivalent to several revolutions; for this reason the closed form coefficients are used.

Assuming two-body motion,

$$\bar{r}(t) \times \dot{\bar{r}}(t) = \sqrt{\mu a(1-e^2)} \bar{W}, \quad (\text{E3})$$

where a is the semimajor axis, e is the eccentricity, μ is the gravitational constant, and \bar{W} is a vector perpendicular to the plane formed by $\bar{r}(t)$ and $\dot{\bar{r}}(t)$. Consider the following,

$$\bar{r}(t) \times \dot{\bar{r}}(t_0) = f(t)\bar{r}(t_0) \times \dot{\bar{r}}(t_0) = f(t)\sqrt{\mu a(1-e^2)} \bar{W}. \quad (\text{E4})$$

In order to evaluate equation (E4), it is necessary to introduce some auxiliary relationships. For elliptic motion there exist the following geometric relationships,

$$x(t) = a(\cos E(t) - e) \quad (E5)$$

$$y(t) = a\sqrt{1-e^2} \sin E(t) \quad (E6)$$

where E is the eccentric anomaly, and x and y are the components of \bar{r} in the orbit plane \bar{P} , \bar{Q} system. Differentiating equations (E5) and (E6) results in

$$\dot{x}(t) = -a\dot{E}(t) \sin E(t) \quad (E7)$$

$$\dot{y}(t) = a\sqrt{1-e^2} \dot{E}(t) \cos E(t) \quad (E8)$$

The quantity $\dot{E}(t)$ is evaluated by using Kepler's equation,

$$M(t) = E(t) - e \sin E(t) \quad (E9)$$

$$\dot{M}(t) = \dot{E}(t) - e \cos E(t) \dot{E}(t) \quad (E10)$$

$$\dot{M}(t) = \dot{E}(t) (1 - e \cos E(t)) \quad (E11)$$

$$\dot{E}(t) = \dot{M}(t) (1 - e \cos E(t))^{-1} = \frac{a\dot{M}(t)}{r(t)} \quad (E12)$$

Substituting equations (E5) through (E8) into equation (E4) yields

$$\bar{r}(t) \times \dot{\bar{r}}_O(t_0) = \begin{vmatrix} i & j & k \\ x(t) & y(t) & 0 \\ \dot{x}(t_0) & \dot{y}(t_0) & 0 \end{vmatrix} \quad (E13)$$

Equating coefficients produces

$$x(t) \dot{y}(t_0) - \dot{x}(t_0) y(t) = f(t) \sqrt{\mu a (1 - e^2)}$$

or

$$f(t) = \frac{x(t) \dot{y}(t_0) - \dot{x}(t_0) y(t)}{\sqrt{\mu \rho}} \quad (E14)$$

Writing

$$\bar{r}(t_0) \times \bar{r}(t) = g(t) \sqrt{\mu a (1 - e^2)} \bar{W}$$

and evaluating the cross product as in equation (E13) gives

$$g(t) = \frac{x(t_0) y(t) - x(t) y(t_0)}{\sqrt{\mu a (1 - e^2)}} \quad (\text{E15})$$

Using the relationships of equations (E12) through (E15), and

$$\dot{M}(t) = n = \frac{\sqrt{\mu}}{a^{3/2}}$$

allows rewriting equations (E14) and E(15) in the form

$$f(t) = \frac{a (\cos E - e) \sqrt{\mu \rho} \cos E_0 + a \sqrt{\mu \rho} \sin E \sin E_0}{r_0 \sqrt{\mu \rho}} \quad (\text{E16})$$

and

$$g(t) = \frac{a^2 \sqrt{1 - e^2} (\cos E_0 - e) \sin E - a^2 \sqrt{1 - e^2} (\cos E - e) \sin E_0}{\sqrt{\mu \rho}} \quad (\text{E17})$$

which can be simplified to

$$f(t) = 1 - \frac{a}{r_0} \left[1 - \cos (E - E_0) \right] \quad (\text{E18})$$

$$g(t) = (t - t_0) + \frac{a^{3/2}}{\sqrt{\mu}} \left[\sin (E - E_0) - (E - E_0) \right] \quad (\text{E19})$$

by noting that

$$\sin E = \sin (E - E_0 + E_0)$$

and using Kepler's equation. The time rate of change of the f and g coefficients are found by differentiating equations (E18) and (E19).

APPENDIX F

Range, Right Ascension, Declination Orbit Determination Technique

This appendix provides a description of the preliminary orbit determination program, which uses range ρ , right ascension α , and declination δ , data. A block diagram of the ρ , α , δ program is presented in figure F1.

The computational algorithm for the block diagram (figure F1) is as follows:

1) Input:

Program Constants

- μ , gravitational constant; (earth radii)³/min²
- f , oblateness of the earth
- ω , rotation rate of earth; rad/min
- RE, radius of earth; ft

Sensor Data

- ϕ , latitudes of observing stations; degrees
- λ , longitudes of observing stations; degrees
- H, altitudes of observing stations; feet above mean sea level

Observations

- ρ , range; feet
- α , right ascension; degrees
- δ , declination; degrees

Reference Times

- OE, orbital epoch; year, month, days, hours, minutes, seconds
- LE, lunar ephemeris epoch; year, month, days, hours, minutes, seconds

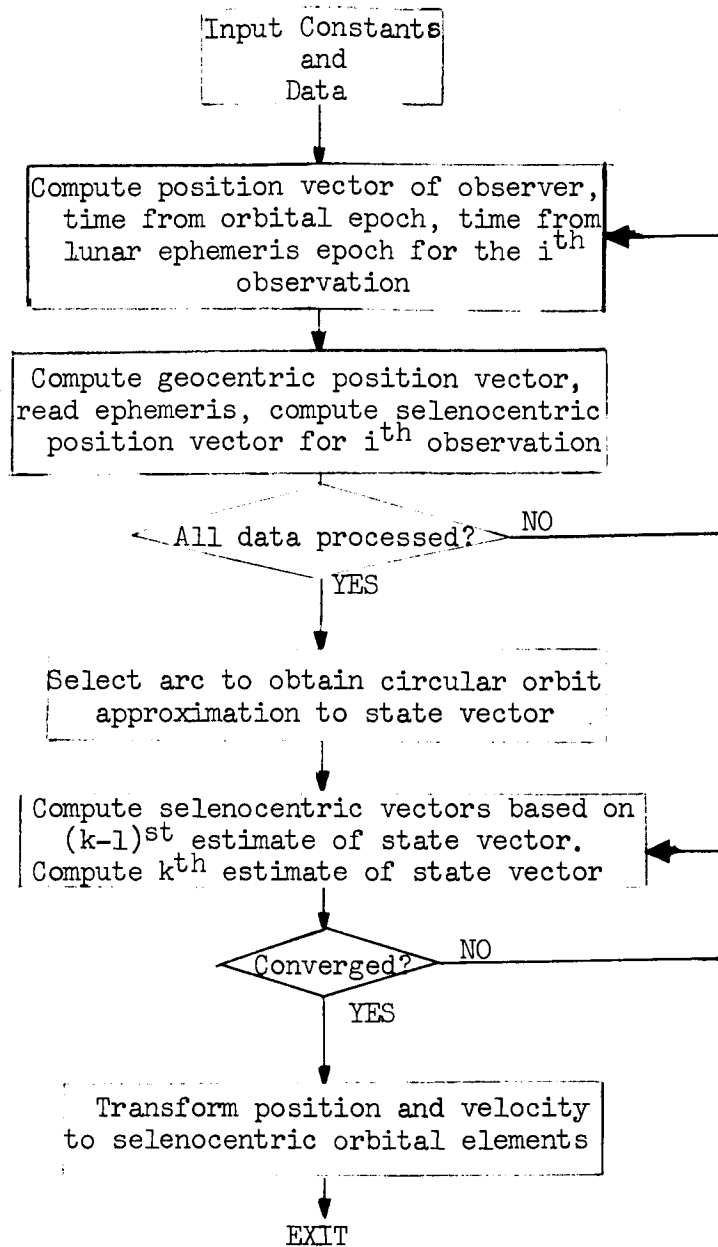


FIGURE F1.—BLOCK DIAGRAM FOR RANGE, RIGHT ASCENSION, DECLINATION PROGRAM

2) Compute Position Vector of Observer:

$$C = \left[1 - (2f - f^2) \sin^2 \phi \right]^{-1/2}$$

$$S = C(1-f)^2$$

$\bar{R}_O = (x, y, z)$, Geocentric Vector of Observer

$$x = -(C + H) \cos \phi \sin \lambda_g \cdot RE + \rho \cos \delta \cos \alpha$$

$$y = -(C + H) \cos \phi \sin \lambda_g \cdot RE + \rho \cos \delta \sin \alpha$$

$$z = -(S + H) \sin \phi \cdot RE + \rho \sin \delta$$

Convert the lunar ephemeris to days and day fractions:

$$DPDNL = DYSL + HRSL/24 + XMNL/1440 + SECL/86400$$

Convert the orbital epoch to days and day fractions:

$$DPDNO = DYSO + HRSO/24 + XMNO/1440 + SECO/86400$$

Convert the time tag read from i^{th} data card to days and day fractions ($i = 1, \dots, n$, where n is the number of observations):

$$DPDN_i = DYS_i + HRS_i/24 + XMN_i/1440 + SEC_i/86400$$

Compute Δt_i from the orbital epoch for the i^{th} observation (to be used in finding E_i from Kepler's equation):

$$DTEE_i = (DPDN_i - DPDNO) 1440 \text{ (minutes)}$$

$$\lambda_g = \lambda + \alpha_{g0} + \omega \cdot DTEE$$

Compute Δt_i from the lunar ephemeris epoch for the i^{th} observation (to be used in interpolating in the lunar ephemeris):

$$DTEE_i = (DPDN_i - DPDNL) 1440 \text{ (minutes)}$$

Read ρ, α, δ corresponding to a particular time, t_i

3) Compute Selenocentric Vector:

Interpolate in the lunar ephemeris to obtain $\bar{R}_m = (x_m, y_m, z_m)$,

The lunar ephemeris, which is input on cards, uses the true of date position and velocity of the moon at 5-minute intervals. Position is in feet, and velocity is in feet per second. For computational purposes, the position and velocity are obtained by linear interpolation. The right ascension of the Greenwich meridian at zero hours, ephemeris epoch day, α_{go} , is also input with the lunar ephemeris.

$$\text{Selenocentric Vector } \bar{r} = (x_r, y_r, z_r)$$

$$x_r = x + x_m$$

$$y_r = y + y_m$$

$$z_r = z + z_m$$

This is done for each ordered triplet of ρ, α, δ (i. e., loop to step 2) until all observations have been processed).

4) Compute state vector based on circular approximation (or input any approximation). See section 4.4.

5) Given a state vector estimate, compute the corresponding selenocentric position vector for each observation time. For a given $\text{DTE}_i = \Delta t_i$, solve Kepler's Equation to obtain ΔE_i . Then

$$M_i = \frac{\sqrt{\mu}}{a^{3/2}} \Delta t_i$$

$$\Delta M_i = \Delta E_i - e \cos E_o \sin \Delta E_i + e \sin E_o (1 - \cos \Delta E_i)$$

$$f_i = 1 - \frac{a}{r_o} [1 - \cos \Delta E_i]$$

$$g_i = \frac{a^{3/2}}{\sqrt{\mu}} [\Delta M_i - \Delta E_i + \sin \Delta E_i]$$

$$r_i = a [1 - e \cos E_o \cos \Delta E_i + e \sin E_o \sin \Delta E_i]$$

$$e \cos E_o = 1 - \frac{r_o}{a}$$

$$e \sin E_o = \frac{\bar{r} \cdot \dot{\bar{r}}}{\sqrt{\mu a}}$$

After selenocentric position vectors have been represented for all observation times, compute the k^{th} estimate of the state vector,

$$x_k = \begin{pmatrix} x \\ y \\ z \\ \dot{x} \\ \dot{y} \\ \dot{z} \end{pmatrix} = \left(\sum_{i=1}^n (A_i^T A_i) \right)^{-1} \sum_{i=1}^n A_i^T Y$$

where $A_i = (f_i : g_i)$, computed using the $(k-1)^{\text{st}}$ estimate of the state vector, and Y is the vector of selenocentric position vectors computed from the observations.

The solution vector x is an improved estimate of the state vector. Loop to step 5) until the convergence criterion is satisfied.

APPENDIX G

Range and Range Rate Orbit Determination Technique

This appendix presents an outline of the program used to determine preliminary orbits for a lunar orbiter using ρ and $\dot{\rho}$ data. A block diagram of the program is presented in figure G1.

The computational algorithm is as follows:

1) Input:

Program Constants

μ , gravitational constant; (earth radii)³/min²
 f , oblateness coefficient
 ω , rotation rate of earth, radians/min
RE, radius of earth; feet

Sensor Data

ϕ , latitudes of observing stations; degrees
 λ , longitudes of observing stations; degrees
H, altitudes of observing sensors, feet

Initial Estimate

a , semi-major axis; lunar radii
 e , eccentricity
 i , inclination; degrees
 Ω , right ascension of ascending node; degrees
 ω , argument of perigee; degrees
M, mean anomaly; degrees

Observations

ρ , range; feet
 $\dot{\rho}$, range rate; ft/sec

Reference Times

LE, lunar epoch; year, month, days, hours, minutes, seconds
OE, orbital epoch; year, month, days, hours, minutes, seconds

2) Transform orbital elements to selenocentric rectangular components of position and velocity:

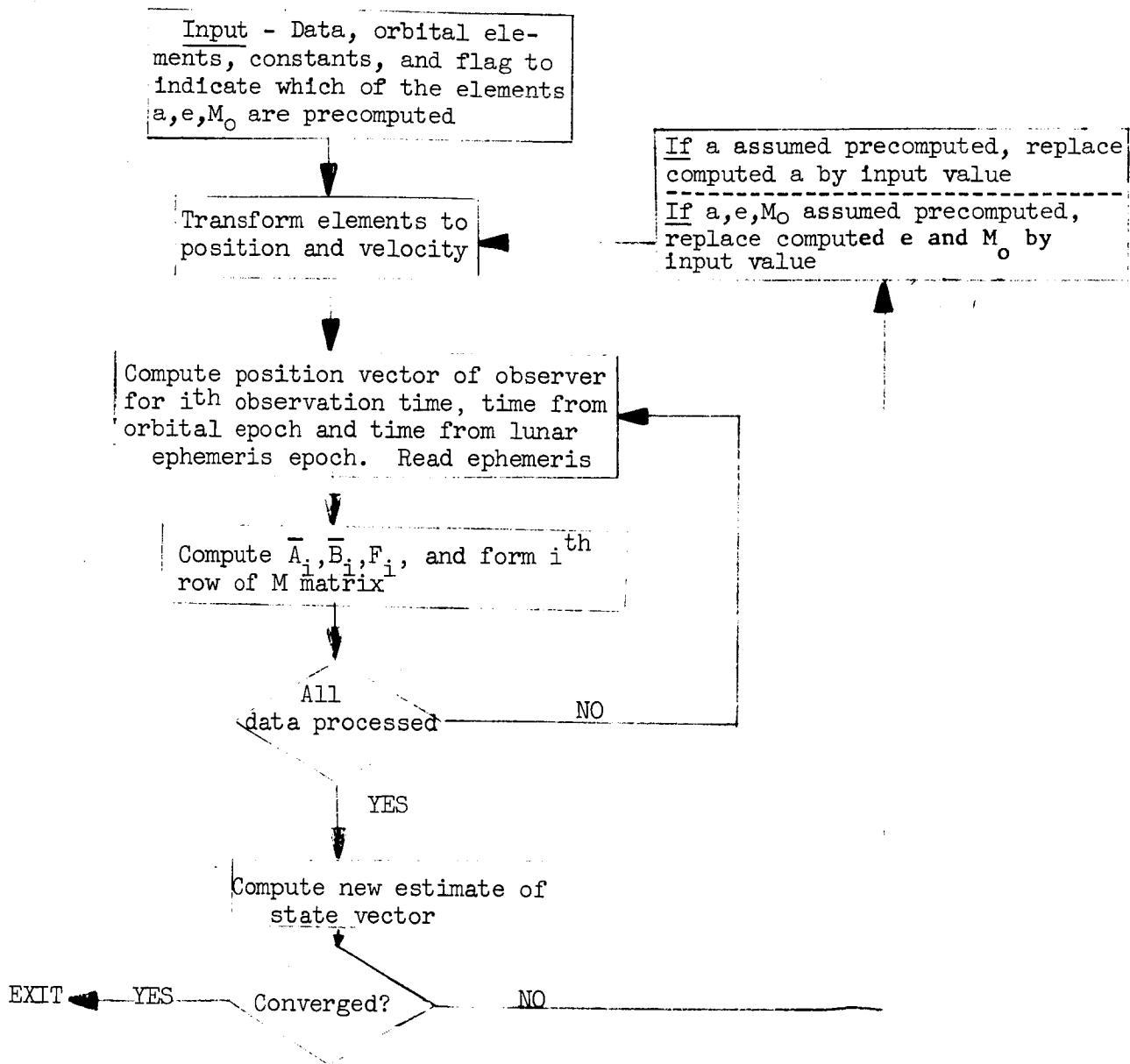


FIGURE G1. — BLOCK DIAGRAM FOR RANGE AND RANGE-RATE PROGRAM

$$x = x_{\omega} P_x + y_{\omega} Q_x$$

$$y = x_{\omega} P_y + y_{\omega} Q_y$$

$$z = x_{\omega} P_z + y_{\omega} Q_z$$

$$\dot{x} = \dot{x}_{\omega} P_x + \dot{y}_{\omega} Q_x, \text{ etc.}$$

where:

$$P_x = \cos \Omega \cos \omega - \sin \Omega \sin \omega \cos i$$

$$P_y = \sin \Omega \cos \omega + \cos \Omega \sin \omega \cos i$$

$$P_z = \sin \omega \sin i$$

$$Q_x = -\cos \Omega \sin \omega - \sin \Omega \cos \omega \cos i$$

$$Q_y = -\sin \Omega \sin \omega + \cos \Omega \cos \omega \cos i$$

$$Q_z = \cos \omega \sin i$$

$$p = a(1 - e^2), \text{ (semi-latus rectum)}$$

$$M_0 = \text{mean anomaly at epoch}$$

$$E = \text{solution of } (M_0 = E - e \sin E) = \text{eccentric anomaly}$$

$$r_{\omega} = a(1 - e \cos E)$$

$$x_{\omega} = a(\cos E - e)$$

$$y_{\omega} = \sqrt{|ap|} \sin E$$

$$\dot{x}_\omega = - \frac{\sqrt{|\mu a|}}{r_\omega} \sin E$$

$$\dot{y}_\omega = \frac{\sqrt{\mu p}}{r_\omega} \cos E$$

3) Compute position vector of observer:

$$C = \left[1 - (2f - f^2) \sin^2 \phi \right]^{1/2}$$

$$S = C(1 - f)^2$$

$$\bar{R}_o = (x, y, z), \text{ Position Vector of Observer}$$

$$x = (C+H) \cos \phi \cos \lambda_g \cdot RE$$

$$y = (C+H) \cos \phi \sin \lambda_g \cdot RE$$

$$z = (S+H) \sin \phi \cdot RE$$

Convert the lunar ephemeris to days and day fractions:

$$DPDNL = DYSL + HRSL/24 + XMNL/1440 + SECL/86400$$

Convert the orbital epoch to days and day fractions:

$$DPDNO = DYSO + HRSO/24 + XMNO/1440 + SECO/86400$$

Convert the time tag read from i^{th} data card to days and day fractions ($i = 1, \dots, n$, where n is the number of observations):

$$DPDN_i = DYS + HRS/24 + XMN/1440 + SEC/86400$$

Compute Δt_i from the orbital epoch for the i^{th} observation (to be used in finding E_i from Kepler's equation)

$$DTEO_i = (DPDN_i - DPDNO) 1440 \text{ (minutes)}$$

Compute Δt_i from the lunar ephemeris epoch for the i^{th} observation (to be used in interpolating in the lunar ephemeris):

$$DTEE_i = (DPDN_i - DPDNL) 1440 \text{ (minutes)}$$

$$\lambda_g = \lambda + \alpha_{g0} + \omega \cdot DTEE_i$$

Read ephemeris $\bar{R}_m = (x_m, y_m, z_m)$, $\dot{\bar{R}}_m = (\dot{x}_m, \dot{y}_m, \dot{z}_m)$

The lunar ephemeris, which is input on cards, used the true of date position and velocity of the moon at 5-minute intervals. Position is in feet, and velocity is in feet per second. For computational purposes, the position and velocity are obtained by linear interpolation. The right ascension of the Greenwich meridian at zero hours, ephemeris epoch day, α_{g_0} , is also input with the lunar ephemeris.

$$\bar{R}_i = \bar{R}_m + \bar{R}_o$$

$$\dot{\bar{R}}_i = \dot{\bar{R}}_m + \bar{\omega} \times \bar{R}_o$$

- 4) Given the selenocentric position and velocity, \bar{r}_o and $\dot{\bar{r}}_o$, generate f , \dot{f} , g and \dot{g} for the i^{th} observation time. Having these quantities, form the auxiliary quantities

$$\bar{A}_i = \dot{f}_i \bar{R}_i + f_i \dot{\bar{R}}_i$$

$$\bar{B}_i = \dot{g}_i \bar{R}_i + g_i \dot{\bar{R}}_i$$

$$(r\dot{r})_i = \sqrt{\mu a} \left[e \cos E_o \sin \Delta E_i + e \sin E_o \cos \Delta E_i \right]$$

$$F_i = \rho_i \dot{\rho}_i - \bar{R}_i \cdot \dot{\bar{R}}_i - r_i \dot{r}_i$$

and the i^{th} row of the M matrix

$$M_i = (A_{ix} \ A_{iy} \ A_{iz} \ B_{ix} \ B_{iy} \ B_{iz})$$

Continue until all observations have been processed.

- 5) The new solution vector is obtained by:

$$x = \left(\sum_{i=1}^n (M_i^T M_i) \right)^{-1} \sum_{i=1}^n M_i^T F_i$$

Loop to step 2) until convergence criterion has been satisfied.

REFERENCES

1. Lewis, D. H. : Lunar Satellite Orbit Determination Convergence Problems. Memo 7883.6-31, TRW Systems Group, TRW Inc., June 1, 1965.
2. Morrison, D. D. : Methods for Nonlinear Least Squares Problems and Convergence Proofs. Proceedings of the JPL Seminar on Tracking Programs and Orbit Determination, Feb. 23, 1960.
3. Morrison, D. D. : Tracking with Poor Nominal Conditions. TRW/CDRC Problem Note PA 2027-01/6, TRW Systems Group, TRW Inc., May 18, 1959.
4. Anderson, J. D. : Theory of Orbit Estimation—Part II Estimation Formulas. Rep. 32-498, Jet Propulsion Laboratory, California Institute of Technology, Oct. 1, 1963.
5. Douglas, B. C. ; Lemmon, W. W. ; and Magness, T. A. : Numerical Aspects of Orbit Determination. Rep. 8408-6048-RU000, TRW Systems Group, TRW Inc., June 10, 1964.
6. Magness, T. A. ; and McGuire, J. B. : Statistics of Orbit Determination—Correlated Observations. Rep. 8976-6001-RU000, TRW Systems Group, TRW Inc., Dec. 15, 1961.
7. Owen, D. B. : Handbook of Statistical Tables. Addison-Wesley Publishing Co., 1962.
8. Fitchett, L. W. : Attachment to NAS 1-4605 (RRM). June 23, 1965.

BIBLIOGRAPHY

- Battin, R.: Astronautical Guidance. McGraw-Hill Book Co., Inc., c1964, pp. 31-87.
- Brouwer and Clemence: Methods of Celestial Mechanics. Addison-Wesley Publishing Co. (Reading, Mass.), c1963, pp. 70-91.
- Cohen, P.; and Deutsch, A.: Error Analysis for Doppler Determined Satellite Orbits of Other Planets. ARS J., vol. 31, no. 12, Dec. 1961.
- Danby, J. M. A.: Fundamentals of Celestial Mechanics. The Mac Millan Co., c1962, pp. 164-183.
- Deutsch, A.: Orbits for Planetary Satellites from Doppler Data Alone. ARS J., vol. 3, no. 60, June 1960.
- Deutsch, R.: Orbital Dynamics of Space Vehicles. Prentice Hall, c1963, pp. 58-132.
- Douglas, B. C.; and Ingram, D. S.: Lunar Orbiter Preliminary Orbit Determination. Memo 9883.5-62, TRW Systems Group, TRW Inc.
- Escobal, P. R.: Methods of Orbit Determination. John Wiley and Sons, Inc., chapters 6, 7, and 8.
- Gates, C. R.: The Behavior of Lunar Satellites and the Determination of Their Orbits: A Preliminary Investigation. NASA Contract NAS7-100, Jet Propulsion Laboratory, California Institute of Technology, Sept. 18, 1962, chapters II and V.
- Gersten, Robert H., and Schwarzbein, Z. E.: Self-Contained Orbit Determination Techniques. Paper 63-431 presented at the Astrodynamics Conference (New Haven, Conn.), Amr. Inst. Aeron. and Astro., Aug. 1963.
- Gersten, Robert H., and Schwarzbein, Z. E.: Preliminary Orbit Determination for a Moon Satellite from Range-Rate Data. AIAA J., vol. 1, Feb. 1963, pp. 467-469.
- Golton, E.: The Use of the Doppler Effect to Deduce an Accurate Position for an Artificial Earth Satellite. Planetary and Space Science, vol. 9, Oct. 1962, pp. 607-623.
- Herget, Paul: The Computation of Orbits. Edwards Brothers (Ann Arbor, Mich.), 1948, pp. 40-73.
- Huang, Su-Shu: Periodic Orbits for Moon Probes. Paper 2603-62 presented at the 17th Annual Meeting and Space Flight Exposition (Los Angeles, Calif.), Am. Roc. Soc., Nov. 1962.

- Koelle, H. H. : Handbook of Astronautical Engineering. McGraw-Hill Book Co., Inc., 1961.
- Koskela, P. : Determination of the Preliminary Orbits of Artificial Lunar and Planetary Satellites. AIAA J., vol. 2, no. 5, May 1964.
- Kovalevsky, J. : Determination of Artificial Earth Satellite Orbits. Space Science Reviews, vol. 1, Oct. 1962, pp. 313-330.
- Leach, Richard: The Prediction of a Radar Range and Range Rate Tracking System for Use on Elliptical Orbits. Paper 63-430 presented at the Astrodynamics Conference (New Haven, Conn.), Am. Inst. Aeron. and Astro., Aug. 1963.
- Lorell, J. : Orbit Determination for a Lunar Satellite. J. Astro. Sc., vol. XI, no. 1, Spring 1964, pp. 1-7.
- McCuskey, S. W. : Introduction to Celestial Mechanics, Addison-Wesley Publishing Co. (Reading, Mass.), 1963, pp. 70-91.
- Merill, Grayson: Handbook of Satellites and Space Vehicles, D. Van Nostrand (Princeton, N. J.), pp. 147-159.
- Message, P. J. : Dynamical Astronomy and Artificial Members of the Solar System. International Symposium on Space Age Astronomy (Pasadena, Calif.), International Astronomical Union, Aug. 1961.
- Moulton, F. R. : An Introduction to Celestial Mechanics. The Mac Millan Co., 1962, pp. 191-250.
- Siry, Joseph W. : Progress in Orbit Determination. International Symposium on Space Age Astronomy (Pasadena, Calif.), International Astronomical Union, Aug. 1961.
- Smart, W. M. : Spherical Astronomy. Cambridge University Press (Great Britain), 1949, pp. 98-160.
- Szebehely, Victor G. : Astrodynamics. Astronautics, vol. 7, Nov. 1962, pp. 52-55.